

# **Star-shaped Polyelectrolytes**

## DISSERTATION

zur Erlangung des akademischen Grades eines  
Doktors der Naturwissenschaften (Dr. rer. nat.)  
im Fach Chemie der Fakultät für Biologie, Chemie und Geowissenschaften  
der Universität Bayreuth

Vorgelegt von

**Felix Plamper**

Geboren in Weiden i. d. Opf.,

Bayreuth, 2007

Die vorliegende Arbeit wurde in der Zeit von Februar 2004 bis Juli 2007 in Bayreuth am Lehrstuhl Makromolekulare Chemie II unter Betreuung von Herrn Prof. Dr. Axel H. E. Müller angefertigt.

Prüfungsausschuss:

Prof. Dr. Helmut Alt

Prof. Dr. Matthias Ballauff (Zweitgutachter)

Prof. Dr. Alexander Böker (Vorsitzender)

Prof. Dr. Axel H. E. Müller (Erstgutachter)

Tag der Einreichung: 13. Juli 2007

Tag des wissenschaftliches Kolloquiums: 20. Dezember 2007

Amtierender Dekan: Prof. Dr. Axel H. E. Müller

Vollständiger Abdruck der von der Fakultät für Biologie, Chemie und Geowissenschaften der Universität Bayreuth genehmigten Dissertation zur Erlangung des Grades eines Doktor der Naturwissenschaften (Dr. rer. nat.).

*And when they saw the star,  
they rejoiced exceedingly with great joy.*

Bible, Mt 2.10

*dedicated to my family*

---

# Table of Contents

<b>1. Introduction</b> .....	1
<b>1.1. Star-shaped Polymers</b> .....	1
<b>1.1.1. Classification and Properties</b> .....	1
<b>1.1.2. Synthesis of Star-Shaped Polymers</b> .....	3
<b>1.2. Polyelectrolytes – Introduction</b> .....	8
<b>1.2.1. Classification</b> .....	8
<b>1.2.2. Theory of Linear Polyelectrolytes</b> .....	9
<b>1.2.3. Theory of Star-Shaped Polyelectrolytes</b> .....	12
<b>1.3. Phase Separation in Polymer Solutions</b> .....	17
<b>1.4. Experimental Methods of Determining the Solution Behavior of Star-shaped Polyelectrolytes</b> .....	20
<b>1.4.1. Potentiometric Titration</b> .....	20
<b>1.4.2. Osmotic Pressure and Osmotic Coefficient</b> .....	21
<b>1.4.3. Dynamic Light Scattering</b> .....	23
<b>1.4.4. Common Techniques for the Determination of Molecular Weight</b> .....	25
<b>1.5. Objective of this Thesis</b> .....	30
<b>1.6. References</b> .....	31
<b>2. Overview of thesis – Results</b> .....	36
<b>2.1. Synthesis of Star-Shaped Polyelectrolytes</b> .....	37
<b>2.2. Titration Behavior of Star-Shaped Weak Polyelectrolytes</b> .....	38
<b>2.3. Counterion Distribution of Star-Shaped Polyelectrolytes</b> .....	40
<b>2.4. Conformational Changes in Polycation Stars Induced by the Presence of Salt and the Use of Light-Sensitive Salt</b> .....	41
<b>2.5. Temperature-Induced Phase Separation in Solutions of Star-Shaped and Linear PDMAEMA</b> .....	44
<b>2.6. Individual Contributions to Joint Publications</b> .....	45
<b>2.7. References</b> .....	47
<b>3. Synthesis, Characterization and Aqueous Solution Behaviour of Star-shaped Poly(acrylic acid)</b> .....	49
<b>3.1. Introduction</b> .....	50
<b>3.2. Experimental Part</b> .....	51
<b>3.3. Results and Discussion</b> .....	57
<b>3.3.1. Synthesis and Characterization of Oligoinitiators</b> .....	57
<b>3.3.2. Synthesis and Characterization of Poly(acrylic acid) stars</b> .....	59
<b>3.3.3. Potentiometric Titration</b> .....	66
<b>3.3.4. Osmometry – Determination of Osmotic Coefficient</b> .....	67

3.4. Conclusion	69
3.5. References	70
<b>4. Synthesis and Characterization of Star-Shaped Poly(<i>N,N</i>-dimethylaminoethyl methacrylate) and Its Quaternized Ammonium Salts</b>	<b>73</b>
4.1. Introduction	74
4.2. Experimental Section	76
4.3. Results and Discussion	80
4.3.1 Synthesis of Star-Shaped Poly( <i>N,N</i> -dimethylaminoethyl methacrylate)	80
4.3.2. Quaternization of PDMAEMA Stars	84
4.3.3. Determination of Initiation Site Efficiency	84
4.3.4. Hydrodynamic Behavior	88
4.3.5. Cryogenic Transmission Electron Microscopy	90
4.3.6. Osmotic Coefficients	91
4.4. Conclusions	92
4.5. Supporting Information	93
4.6. References	100
<b>5. Nanoblossoms: Light-Induced Conformational Changes of Cationic Polyelectrolyte Stars in Presence of Multivalent Counterions</b>	<b>103</b>
5.1. Introduction	104
5.2. Experimental Section	105
5.3. Results and Discussion	107
5.3.1. Collapse of Polyelectrolyte Stars Induced by Multivalent Counterions	107
5.3.2. Photostretching of Polyelectrolyte Stars	110
5.3.3. Photodissolution of Polyelectrolyte Stars	111
5.4. Conclusion	112
5.5. References	113
<b>6. Tuning the Thermoresponsive Properties of Weak Polyelectrolytes: Aqueous Solutions of Star-Shaped and Linear Poly(<i>N,N</i>-dimethylaminoethyl methacrylate)</b>	<b>114</b>
6.1. Introduction	115
6.2. Experimental Section	117
6.3. Results and Discussion	119
6.3.1. Titration Behavior of Star-Shaped PDMAEMA	120
6.3.2. Thermoresponsive Properties of Star-Shaped PDMAEMA	121
6.4. Conclusions	126
6.5. Supporting Information	127
6.6. References	128
7.1. Results and Discussion	132
7.2. Supporting Information – Experimental Details	136
<b>8. Summary</b>	<b>139</b>

---

<b>9. List of Publications</b> .....	143
<b>10. Appendix</b> .....	144
<b>10.1. Appendix to Chapter 2.1, Chapter 3 and Chapter 4 – Preparation of Star-Shaped Polyelectrolytes with Higher Arm Numbers</b> .....	144
<b>10.2. Appendix to Chapter 2.2, Chapter 3 and Chapter 6 – Titration Behavior of Weak Polyelectrolytes</b> .....	145
<b>10.3. Appendix to Chapter 2.3, Chapter 3 and Chapter 4 – Counterion Distribution of Star-Shaped Polyelectrolytes</b> .....	147
<b>10.4. Appendix to Chapter 2.4, and Chapter 5 – Interaction of Multivalent Counterions with Polyelectrolyte Stars</b> .....	152
<b>10.5. Appendix to Chapter 2.5, Chapter 6 and Chapter 7 – Thermoresponsive Properties of PDMAEMA</b> .....	156
<b>10.6. References</b> .....	163
<b>Glossary</b> .....	165
<b>Acknowledgement</b> .....	167



# 1. Introduction

## 1.1. Star-shaped Polymers

### 1.1.1. Classification and Properties

Star-shaped polymers belong to the class of non-linear or branched polymers. The classification of simple, branched architectures is completed by brush-like/comb-shaped,<sup>1-3</sup> hyperbranched<sup>4-6</sup> or dendrimeric polymers<sup>5,7</sup> (Figure 1. 1). Star polymers do ideally have one branching point, whereas the degree of branching approaches unity for dendrimers.

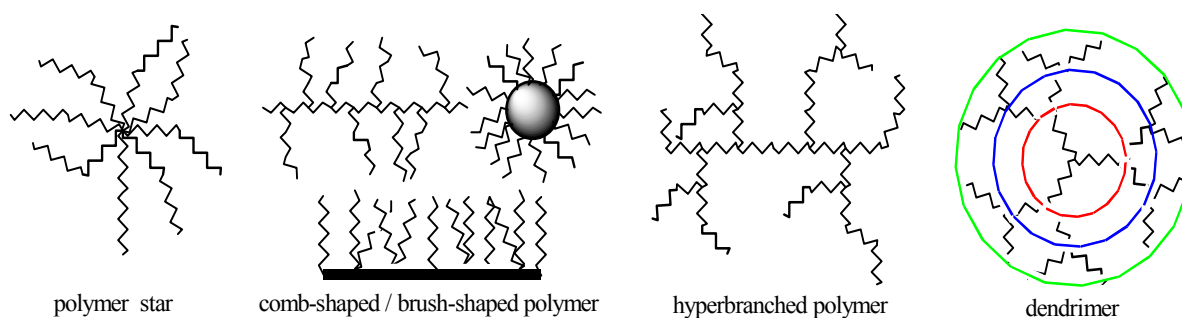


**Figure 1. 1: Types of branched polymers**

The finite size of the stars leads to a finite size of the core of the star, which means that typically more than one branching point is present in real star polymers. As long as the core is small compared to the dimensions of the star (e.g. one order of magnitude smaller), the core is believed not to influence the behavior of the stars. In contrast spherical polymer brushes do have a core, whose size is in the order of magnitude of the chains or even larger. The outer limit is given by a core which is much larger than the polymer chains. Those brushes resemble already planar brushes, as the curvature is small compared to the dimensions of the chains. After all, a star polymer can be regarded as a limiting case of a spherical polymer brush.

Two parameters are important for the characterization of those stars. The length of the star's arms, i.e. the degree of polymerization per polymeric arm,  $DP_{arm}$ , and the number of arms,  $f_{star}$ . In the ideal case the number of arms would be constant throughout the sample as the arm length would be the same for all arms. It is rather hard to obtain the ideal case during synthesis of star shaped systems for higher arm numbers and therefore only rare examples are given for polymers with almost no polydispersity in arm number and arm length.<sup>8</sup> Practically there are deviations from the ideal case, seen in an arm length distribution and/or arm number distribution. Therefore it is necessary to determine the distribution in both arm number and arm length for full characterization of the star-shaped polymers. The polydispersity in molecular weight can be easily obtained by standard characterization methods (e.g. light

scattering and osmometry). According to Schulz' coupling theorem it resembles mainly the polydispersity in arm number, when the average arm number is considerably high.<sup>9</sup>

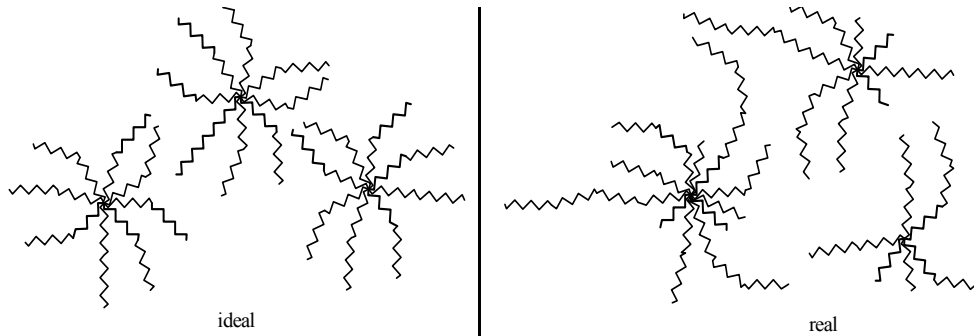


**Figure 1. 2: Comparison between a sample with uniform molecules and a sample with an arm number and arm length distribution**

When comparing with linear polymers, branched polymers show several properties of their linear analogues, whereas other properties are influenced by the architecture. For example some characteristics of the monomers are also inherited to the polymer like the chemical reactivity and the spectral properties of the side groups, as well as principal trends in hydrophobicity. Thermal and mechanical behavior and solution properties<sup>10</sup> are often altered, since the dimensions of branched polymers are considerably smaller than the dimensions of linear polymers at the same molecular weight. The strain at stress failure and the stiffness of bulk polymer samples often decreases for branched molecules due to the lack of entanglements. The topology can also change crystallization behavior, as the branches prevent a regular array of the monomeric units.<sup>11</sup>

As already mentioned the dimensions of star-shaped polymers are smaller compared to linear ones. This is also valid in solution. The dimension of a polymer is reflected in its hydrodynamic radius,  $V_h$ , which is related to the molecular weight,  $M$ , by the Kuhn-Mark-Houwink-Sakurada equation<sup>12-14</sup> ( $[\eta] = K \cdot M^\alpha$ ;  $[\eta]$  is the intrinsic viscosity,  $K$  and  $\alpha$  are polymer-, topology- and solvent-specific constants valid for a certain temperature,  $T$ ) and Einstein equation<sup>15, 16</sup> ( $[\eta] = 2.5 \cdot N_A \frac{V_h}{M}$ ,  $N_A$  is Avogadro's constant):

$$V_h = \frac{K}{2.5 \cdot N_A} \cdot M^{\alpha+1} \quad \mathbf{1.1.}$$

The molecular weight of star polymers can be changed by two ways: varying the arm number or the arm length. Therefore equation 1. 1. needs to be modified by the help of the theory of Daoud and Cotton<sup>17</sup> ( $R_g \propto DP_{arm}^{0,6} \cdot f_{star}^{0,2}$ ;  $R_g$  assigns the radius of gyration) and the

Flory-Fox relationship<sup>18</sup> ( $[\eta] = \Phi \cdot \left(\frac{R_g^3}{M}\right)$ ;  $\Phi$  is again a polymer- and solvent-specific constant).

$$V_h \propto DP_{arm}^{9/5} \cdot f_{star}^{3/5} \quad 1.2.$$

We see directly that increasing the arm number leads only to small change in hydrodynamic volume. In contrast,  $V_h$  scales typically with  $DP^{1.8}$  for linear polymers. Therefore the segment density within those stars increases rapidly with increasing arm number, whereas the segment density even decreases with increasing arm length.

This scaling law needs to be modified for star-shaped, charged polymers (polyelectrolytes) as seen in chapter 1.2. Other differences between linear and branched polyelectrolytes will be discussed in the same chapter.

### 1.1.2. Synthesis of Star-Shaped Polymers

There are two principal strategies for the synthesis of star-shaped polymers: core-first or arm-first method. Both require controlled / living polymerizations in order to obtain well defined products. Throughout this thesis Atom Transfer Radical Polymerization (ATRP) was utilized.

#### 1.1.2.1. Controlled Radical Polymerization

Atom Transfer Radical Polymerisation (ATRP)<sup>19-21</sup> has become one of the most prominent polymerizations techniques for synthesis of advanced polymer architectures. The reason is the insensitivity of this polymerization towards other functional groups, since radicals are mainly prone to attack its own species or to attack unsaturated groups (e.g. vinyl groups) to produce new radicals. This advantage is inherent in all controlled radical polymerizations like Nitroxide Mediated Polymerization (NMP),<sup>22</sup> Reversible Addition-Fragmentation Chain Transfer (RAFT)<sup>23</sup> or other Degenerative Transfer<sup>24</sup> (DT) polymerizations.<sup>21</sup> The main advantage of ATRP over those other polymerization techniques is the rather easy way to obtain suitable initiators. Especially the preparation of multifunctional initiators is rather simple e.g. by esterification of the initiating units (which are usually stock products like the  $\alpha$ -bromobutyrate) to an oligoalcohol. In contrast, transfer agent synthesis for RAFT requires often a more tedious procedure.

The principle of all those polymerization methods is the reduction of the radical's concentration in the polymerization mixture compared to concentrations used in conventional radical polymerization. The majority of radicals are masked in NMP or ATRP. Therefore the probability for the encounter of two radicals, which leads to termination

reactions like recombination or disproportionation, is reduced compared to the likelihood of the propagation reaction. We want to compare shortly those polymerizations by their mechanism (Figure 1. 3).

NMP utilizes nitroxides, which are comparatively stable radicals (like TEMPO), to mask the active radical. There is an equilibrium between the masked species and the free radicals, which is usually far on the side of the masked species. The few radicals, who are in equilibrium, allow the polymerization at a slow rate of propagation.

ATRP utilizes an exchange of halogen radicals, between a metal complex and the propagating chain end. Those halogen atoms protect the propagating chain ends during most of the time of the polymerization.

RAFT procedure superimposes a degenerative transfer on the free radical polymerization processes taking place during RAFT polymerization. Intermediate, non-propagating radicals are involved, which are generated by addition of the propagating chains onto dithiocompounds like dithioesters, xanthates, trithiocarbonates or dithiocarbamates (chain transfer agent). Those radicals can lead to a retardation of the polymerization compared to conventional radical polymerization.<sup>25</sup> Hence, the number of propagating radicals is also here reduced in addition to fact that only a small amount of initiator is needed to create multiple amounts of chains due to the transfer mechanism.

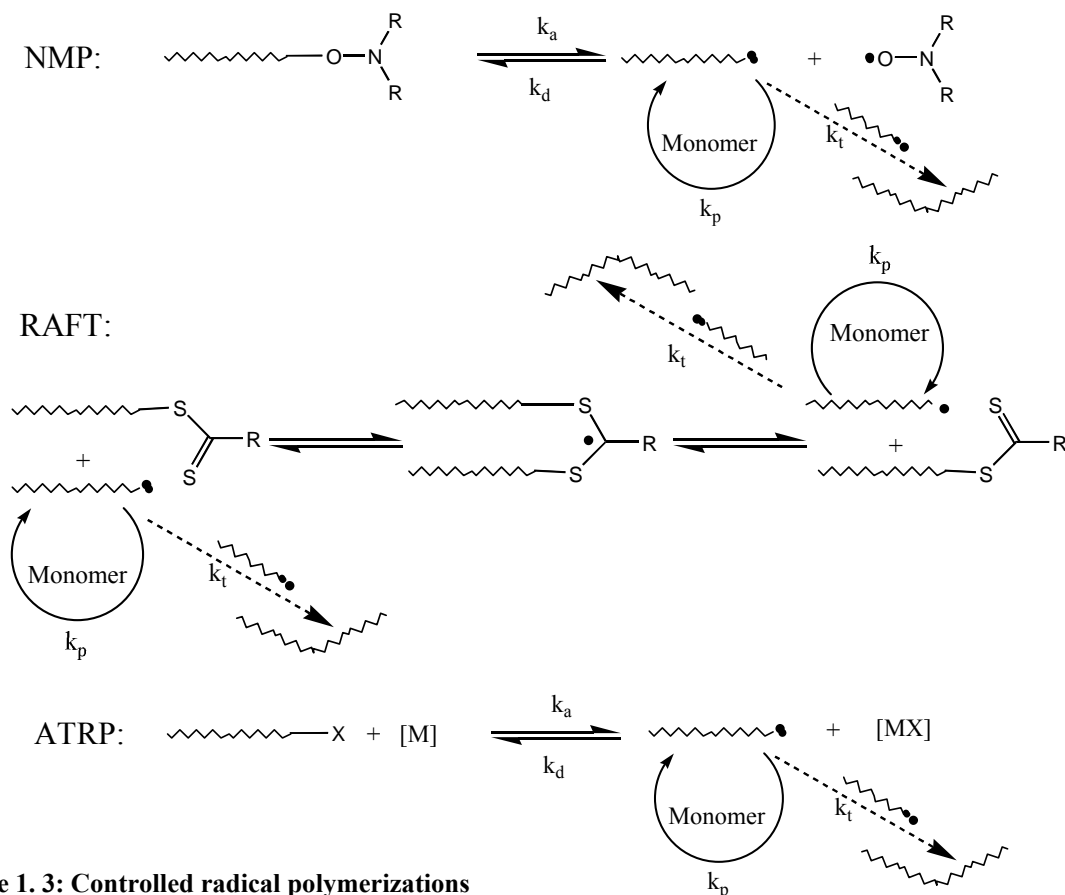


Figure 1. 3: Controlled radical polymerizations

We want to introduce ATRP<sup>26-28</sup> in more detail. The important reaction is the homolysis of the carbon-halogen bond, catalyzed by a metal complex, which can take up a halogen radical. As a prerequisite a free coordination site needs to be available on the catalyst, which can be easily oxidized. The fine-tuning of the catalyst's orbitals can be achieved by ligands, which also can give rise to better solubility of the metal complex in the respective solvents. The most prominent catalyst systems are copper(I) halides, Cu(I)X, which are partly oxidized to copper(II) halides under reduction of the chain ends. Different ligands can be used like 2,2'-bipyridine or phenanthroline. Especially multidendate ligands are powerful in complexing the metal even in presence of huge excess of complexing monomers (vinylpyridine, monomers with amine-sidegroups). For this reason *N,N,N',N'',N'''*-pentamethyldiethylenetriamine (PMDETA), 1,1,4,7,10,10-hexamethyltriethylene-tetraamine (HMTETA) and tris[2-(dimethylamino)ethyl]amine (Me<sub>6</sub>-TREN) are widely used ligands.<sup>26</sup>

The range of catalysts is not limited to copper compounds (e.g. ruthenium compounds)<sup>26</sup>, but its cheapness makes copper catalyst systems often to the systems of choice.

Typical initiating moieties comprise benzyl halides, tosyl halides,  $\alpha$ -haloketones,  $\alpha$ -halonitriles and  $\alpha$ -haloesters. In all cases, good initiating systems are characterized by having a rate of initiation comparable to propagation or even faster.

Most of the monomers, which can be polymerized radically, can be used for ATRP. Special catalyst systems need to be applied for radical chain ends with high energy (e.g. for vinyl acetate<sup>29</sup>). However the monomer must not interfere with the catalyst system. Therefore it is hard to perform ATRP on acidic monomers, since the protons might oxidize the catalyst and protonate the ligand. This is the reason why suitable monomers for polyelectrolytes like acrylic acid are not polymerized directly by ATRP but protected monomers are used (e.g. *tert*-butyl acrylate – *t*-BA). After their polymerization they can be easily transformed to the desired polymer (here elimination of isobutylene gives poly(acrylic acid), PAA).<sup>30</sup> Besides acrylic acid *N,N*-dimethylaminoethyl methacrylate (DMAEMA) was used in this thesis.<sup>31</sup> Since it is a complexing monomer, the commonly used ligand PMDETA, which was used for the polymerization of *t*-BA, was exchanged by HMTETA, which is a ligand with better complexing abilities. The used monomers, which were employed during this thesis, are listed in Figure 1. 4 along with the polymer-analogous reactions exerted to yield the final polyelectrolytes (e.g. quaternized PDMAEMA: poly{[2-(methacryloyloxy)ethyl]trimethylammonium iodide}: PMETAI)

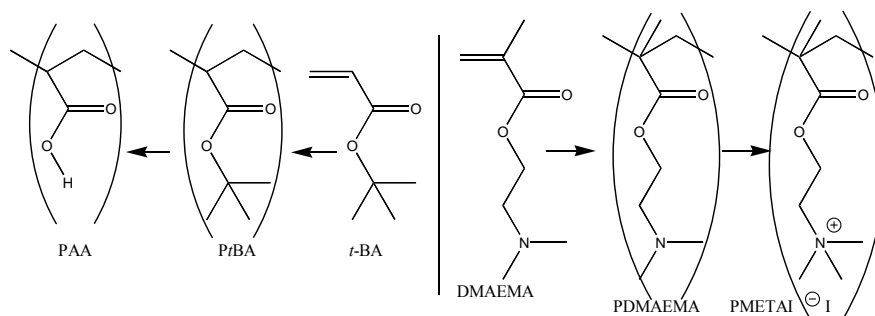


Figure 1. 4: Monomers and Polymers used

### 1.1.2.2. Synthesis of Star-Shaped Polymers

The core-first method for preparation of star-shaped polymers<sup>11</sup> uses multifunctional initiators. The maximum arm number is determined by the number of initiating moieties attached to the initiator molecule. If the initiation site efficiency is close to unity and if the initiator is a single component with a constant number of initiation sites throughout the sample, then well defined polymers will be obtained with a precise number of arms (Figure 1. 5).

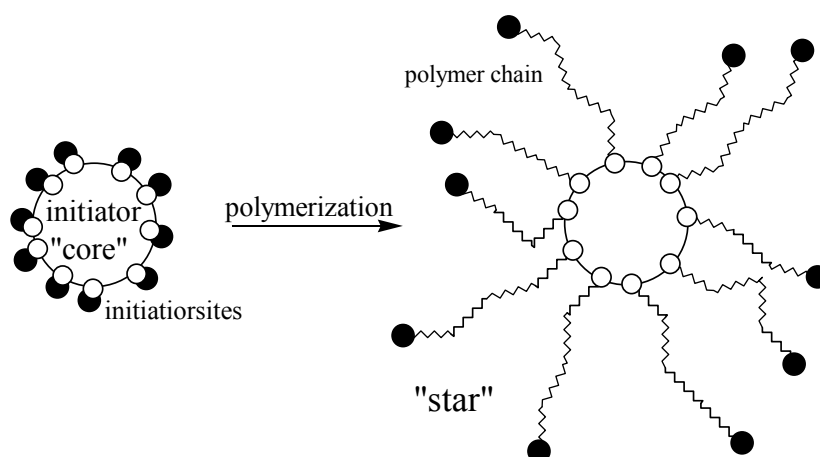


Figure 1. 5: Core-first Method

One drawback of this attempt is the sometimes tedious synthesis of well defined initiators when comparing to the arm-first method (see page 7). It is rather difficult to construct well defined multifunctional initiators for ionic polymerizations. In addition the solubility is often poor in the required solvents. Therefore we want to concentrate on the multifunctional initiators for radical polymerization. The variety of possible multifunctional transfer agents for the star synthesis by RAFT (e.g. dendrimer based<sup>32</sup>) can be principally divided into two types (R or Z approach).<sup>33, 34</sup> The use of multifunctional NMP-initiators is less common.<sup>35, 36</sup> In contrast many scaffolds were used for preparation of ATRP initiators. For example calixarenes<sup>37-39</sup> or sugars like glucose, saccharose or cyclodextrines were used due to their

defined number of hydroxy functions.<sup>40-42</sup> During this thesis sugar-based initiators were utilized and a novel initiator was introduced originating from a small inorganic nanoparticle (see chapter 10.1). The easiest way to obtain suitable initiators is given by the esterification of a small molecule with multiple hydroxy groups with an initiating moiety. In this context initiation sites for ATRP (like the esters of  $\alpha$ -bromocarboxylic acids) are rather easily attached onto the multifunctional scaffold. Therefore the polymerization method of choice is ATRP for the aims of this thesis. However one drawback is the possibility of star-star coupling during recombination of two propagating radicals of two different stars when performing core-first synthesis with controlled radical polymerization. Intramolecular recombination would lead to cyclic chains attached to core. Star-star coupling can become a problem especially for polymerizations originating from an initiator with many initiation sites. The probability of star-star-coupling should be proportional to the expected arm number. Therefore special care needs to be taken for the core-first synthesis aiming for many arms. Usually the conversion should be limited to moderate values so that propagation is much more likely than termination. Dilution and the manipulation of the equilibrium toward the dormant species by addition of copper(II) salts can help to diminish the concentration of active radicals.

In the scope of this thesis we only make use of the core-first attempt. We introduce shortly the arm-first method to complete the most typical methods for preparation of star-shaped molecules.

During the procedure of the arm-first method linear polymer chains are prepared, which are crosslinked afterwards (Figure 1. 6).

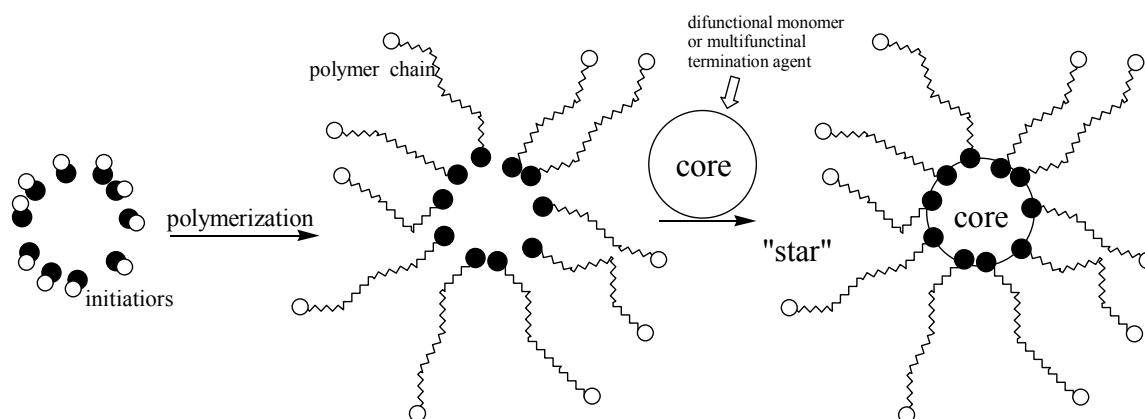


**Figure 1. 6: Arm-first method**

Coupling agents are often small organic or inorganic molecules. For example stepwise addition of a difunctional monomer (e.g. divinyl benzene) can lead to the formation of a second block with functional groups. Active chain ends can attack also neighbouring polymer

chains and finally a microgel forms the centre of the star.<sup>43-45</sup> Therefore the synthetic efforts are limited using difunctional monomers during the arm-first approach. Even high average arm numbers can be obtained easily<sup>46</sup> and principally all common living / controlled polymerization techniques can be employed. The drawback of this attempt is the rather broad distribution in arm number, though the polydispersity of the arms is just limited to the quality of the precursor polymers. Often some arms remain unattached to the core and sometimes they need to be separated from the star-shaped molecules by tedious purification steps.

To achieve polymers with a uniform arm number, multifunctional termination agents have been developed for anionic polymerization.<sup>8, 47</sup>

Quite recently a new arm first approach with help of macromonomers was introduced, yielding narrow distributed stars.<sup>48</sup>

## **1.2. Polyelectrolytes – Introduction**

### **1.2.1. Classification**

Polyelectrolytes are charged polymers.<sup>49</sup> Usually every repeating unit is capable of bearing a charge. It is reasonable to introduce two different classifications. Above all the polyelectrolyte belongs either to the group of cationic or to the group of anionic polyelectrolytes depending whether the polyelectrolyte carries positive or negative charges. Mixed architectures with both negative and positive monomeric units belong therefore to the class of polyampholytes. A special case of polyampholytes is given by polybetaines (positive and negative charges on each repeating unit). Irrespective to the sign of charge one should distinguish between two other types of polyelectrolytes: strong (quenched) or weak (annealed) polyelectrolytes. The number of nominal charges is irrespective to changes in *pH* for strong polyelectrolytes, whereas the number of nominal charges can be easily adjusted by *pH* for weak polyelectrolytes. Polymers made of monomers, which are strong acids or bases or which are the salts of strong acids or bases, belong usually to the class of strong polyelectrolytes. Therefore the charged groups are fully deprotonated for anionic polyelectrolytes. Monomers, which are weak bases or acids themselves, form usually weak polyelectrolytes.

The polyion's counterions are an integral part of the polyelectrolyte. The polymeric backbone bears charges, whereas compensation of all polymeric charges by counterions is required due to electroneutrality. Monovalent counterions are the imminent companions of most synthetic polyelectrolytes resulting in 1-1 polyelectrolytes.

Polyelectrolytes are ubiquitous in nature. Most of the proteins are polyampholytes, though a regular array of charges along the biopolymers is hardly found in nature.<sup>50</sup> Another prominent

example with a regular array of charged units is given by the ribonucleic acid (RNA) or desoxyribonucleic acid (DNA), the polymer carrying the genetic code. Hyaluronic acid is a charged polysaccharide, which acts as a natural lubricant.<sup>50</sup>

Man-made polyelectrolytes are usually prepared in the same way like normal polymers. Sometimes special precautions need to be taken due to interference of the charged, basic or acidic monomers with e.g. catalysts. Therefore protected polymers are sometimes the precursors for the desired product (see chapter 1.1.2.).

## 1.2.2. Theory of Linear Polyelectrolytes

As said, counterions are an integral part of the polyelectrolyte. Before other properties can be derived, it is crucial to understand the counterion distribution around the polyelectrolyte. Especially the strong correlation of the counterions with the polyion leads to a behaviour termed counterion condensation: a part of counterions are not active in bulk solution but attached to the backbone. Therefore the osmotic pressure of a polyelectrolyte solution or its electrophoretic mobility is a direct consequence of the counterion distribution. The counterion distribution around linear polymers is only well understood for stiff polyelectrolytes. Flexible polyelectrolytes exert a strongly coupled behaviour, as changes in counterion distribution lead to changes in conformation and vice versa. Therefore only two simple models for stiff, infinitely long polyelectrolytes are introduced.

### 1.2.2.1. Two-Phase Model

The two-phase model is rather simple model to describe the distribution of monovalent counterions around a stiff, linear polyelectrolyte (infinitely long).<sup>49</sup> It was introduced by Oosawa.<sup>51</sup> The surrounding space around such a polyion was divided into two cylindrical shells with two different potentials  $\psi_1$  and  $\psi_2$ . Within each cylindrical shell the potentials are regarded as spatially constant potentials (Figure 1. 7).  $n_1$  denominates the counterion's concentration in region 1 (shell with polyion) and  $n_2$  assigns the concentration of counterions in shell 2 (shell with free counterions). The counterions in shell 1 are condensed on the polyion and do not contribute to the counterion's activity. The ratio  $n_2 \cdot V_2 / (n_1 \cdot V_1 + n_2 \cdot V_2)$  gives the fraction  $\phi$  of free counterions, which is the theoretical equivalent to the experimental quantity osmotic coefficient  $\phi$ .

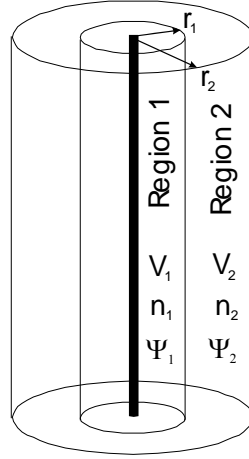


**Figure 1. 7: Two-phase model**

As  $V_1$  and  $V_2$  is the volume of shell 1 and 2, respectively, and  $\phi$  assigns the volume fraction of region 1. We observe two different concentrations in both regions according to Boltzmann's law as a consequence of the difference in the electrostatic potentials in both regions (as implied by the differences in chemical potential):

$$n_1 = n_2 \cdot e^{-\frac{e(\psi_2 - \psi_1)}{kT}} \quad \left( \text{in general: } n(r) = n(R_0) \cdot e^{-\frac{e\psi(r)}{kT}} \right) \quad 1.3.$$

$$\Rightarrow \ln\left(\frac{n_1}{n_2}\right) = \ln\left(\frac{n_1 \cdot V_1}{n_2 \cdot V_2}\right) - \ln\left(\frac{V_1}{V_2}\right) = \ln\left(\frac{1-\phi}{\phi}\right) - \ln\left(\frac{\phi}{1-\phi}\right) = -\frac{e(\psi_2 - \psi_1)}{kT} \quad 1.4.$$

The charge density  $q_0 = e/b$  along the polymer backbone is given by the ratio of unity charge,  $e$ , and the distance between the charges along the chain  $b$ . The charge density is reduced by the counterion condensation yielding an effective charge density  $q$  ( $q = \phi \cdot q_0$ ).

Onsager derived the radial dependence of the electrostatic potential around a homogeneously charged, infinitely long, stiff rod. We obtain following formula with  $R_0$ , which assigns an arbitrary distance, at which the potential vanishes.<sup>52</sup>

$$\psi(r) = -\frac{q}{2\pi\epsilon_0\epsilon} \ln\left(\frac{r}{R_0}\right) \quad 1.5.$$

The difference in potential  $\Delta\psi = \psi_2 - \psi_1$  along the shells with radius  $r_1, r_2$  ( $\phi$  respectively) can now be assigned to both  $\phi$  and  $b$ .

$$\Delta\psi = -\frac{\phi e}{2\pi\epsilon_0\epsilon b} \ln\left(\frac{r_2}{r_1}\right) = \frac{\phi e}{4\pi\epsilon_0\epsilon b} \ln \phi \quad 1.6.$$

equation 1. 4. and 1. 6. results in

$$\ln\left(\frac{1-\phi}{\phi}\right) = \ln\left(\frac{\varphi}{1-\varphi}\right) - \frac{e\Delta\psi}{kT} = \ln\left(\frac{\varphi}{1-\varphi}\right) - \frac{\phi e^2}{4\pi\epsilon_0\epsilon b \cdot kT} \ln\varphi$$

$$\Rightarrow \quad \ln\left(\frac{1-\phi}{\phi}\right) = \ln\left(\frac{\varphi}{1-\varphi}\right) - \phi\xi_M \ln\varphi \quad 1. 7.$$

$$\text{with Manning parameter} \quad \xi_M = \frac{l_B}{b} \quad 1. 8.$$

$$\text{and Bjerrum length} \quad l_B = \frac{e^2}{4\pi\epsilon_0\epsilon \cdot kT} \quad 1. 9.$$

According to this theory the fraction of free counterions  $\phi$  depending on the Manning parameter  $\xi_M$  can be derived from 1. 7. for vanishing concentrations.

$$0 \leq \xi_M < 1 \quad \Rightarrow \quad \phi = 1 \quad 1. 10.$$

$$\xi_M \geq 1 \quad \Rightarrow \quad \phi = 1/\xi_M \quad 1. 11.$$

The Bjerrum length equals the distance of two elemental charges, where their electrostatic energy is compensated by the thermal energy. It is a constant for a given temperature and for a given solvent, in water and at room temperature  $l_B = 715$  pm. This quantity has a decisive effect on the counterion condensation. If distance  $b$  between the charge carrying units is larger than  $l_B$ , i.e.  $\xi_M < 1$ , then all counterions are released and are present in bulk solution. If Bjerrum length  $l_B$  exceeds  $b$ , i.e.  $\xi_M > 1$ , counterions condense on the backbone until the maximum charge density  $q_{max} = e/l_B$  has been reached again. This is the illustrative background of equation 1. 10. and 1. 11.

### 1.2.2.2. Poisson-Boltzmann Cell Model and Manning Limit

A more precise theory could be obtained by solving analytically the nonlinearized Poisson-Boltzmann equation (PB equation) for infinitely long, homogenously charged, stiff rods.<sup>53-55</sup> The solution's volume is divided into parallel cylindrical cells, with radius  $R$  and the polyion in the center with radius  $a$ . By definition the electrostatic potential and the electrical field is zero at the rim of the cell (at radius  $R$ ).

The Poisson equation is adapted for the cylindrical geometry. The Boltzmann factor (1. 3.) is introduced for the counterion's concentration  $n(r)$ , which yields

$$\left( \frac{d^2}{dr^2} + \frac{1}{r} \frac{d}{dr} \right) \psi(r) = -\frac{en(r)}{\epsilon_0\epsilon} \quad 1. 12.$$

The condition of electroneutrality yields finally with integration parameter  $\gamma$  and  $R_M$

$$\psi(r) = \frac{2kT}{e} \ln \left( \frac{r}{R} \sqrt{1 + \gamma^2} \cos \left( \gamma \ln \frac{r}{R_M} \right) \right) \quad \mathbf{1.13.}$$

Both parameters are coupled according to the following equations, which can be solved numerically

$$\gamma \ln \left( \frac{a}{R_M} \right) = \arctan \frac{1 - \xi_M}{\gamma} \quad \mathbf{1.14.}$$

$$\gamma \ln \left( \frac{R}{R_M} \right) = \arctan \frac{1}{\gamma} \quad \mathbf{1.15.}$$

As a result the ratio of free counterions  $\phi$  can be derived for infinite dilution<sup>56</sup>. For  $\xi_M > 1$   $\phi$  is given by

$$\phi = \frac{1}{2\xi_M} \quad \mathbf{1.16.}$$

This equation is also known as one of Manning limiting laws. Therefore counterion condensation is often referred as Manning condensation. However Manning used a different approach. By analysis of the electrostatic free excess energy the Debye-Hückel theory of simple ionic solutions was modified leading to the same result.<sup>57</sup>

### 1.2.3. Theory of Star-Shaped Polyelectrolytes

In contrast to linear polyelectrolytes the theoretical description needs to be expanded to a three phase model for star-shaped polyelectrolytes. Besides counterions, which are directly condensed on the backbone, there are also noncondensed counterions to be encountered within the star. Those counterions do not contribute to the free counterions in bulk solution, which are supposed to be responsible for e.g. the osmotic pressure of such systems. Likos et al.<sup>58</sup> performed molecular dynamics simulations and compared the results with an analytical theory of those polyelectrolyte systems. They varied the degree of polymerisation per arm  $DP_{\text{arm}}$ , the number of arms per star  $f_{\text{star}}$  and the fraction of charged monomeric units ( $\alpha'$ ).

The solution volume  $V$  was divided into  $N_{st}$  spherical cells, so called Wigner-Seitz cells.  $N_{st}$  is the number of stars in volume  $V$ . The core of star is placed in the center of this cell, which has a radius  $R_w$  (Figure 1. 8).

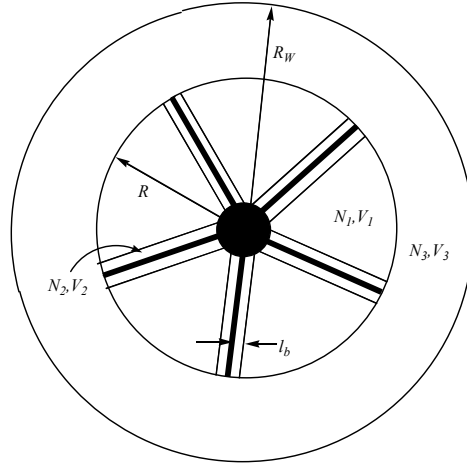


**Figure 1. 8: Polyelectrolyte star within an adapted Wigner-Seitz cell**

Geometrical considerations give following formula:

$$\frac{4\pi}{3} R_w^3 = \frac{V}{N_{st}} = \frac{1}{\rho_{st}} \quad 1.17.$$

$\rho_{st}$  is the number density of stars. The arm's distance between core and chain end is given by the variable length  $R$ . According to the model,  $R$  is dependent on the chains conformation, though the arms are always located within a cylinder, which emanates from the core with radius  $l_B$  (Bjerrum length). The whole cell is divided into three regions. Volume  $V_3 = 4\pi(R_w^3 - R^3)/3$  assigns the volume outside the star, which is accessible by  $N_3$  free ions. As said, a cylinder with volume  $V_1$  and radius  $l_B$  around the polymer chains is assigned to the number  $N_1$  of condensed counterions. The chain's volume  $V_\sigma$  is not included in  $V_1$ . To obtain  $V_1$  one needs to subtract the monomer's radius  $\sigma_{LJ}$  from  $l_B$  yielding  $V_1 = f_{star} \pi(l_B^2 - \sigma_{LJ}^2)R$ . Volume  $V_2$  with  $N_2$  ions is given by the difference between the volume of the star  $V_{star} = 4\pi R^3/3$  and  $V_1 + V_\sigma$ , since  $V_{star} = V_1 + V_2 + V_\sigma$ .

For derivation of the fraction of free ions the free energy  $F$  needs to be minimized. The free energy is given by the following formula:

$$F(R, N_1, N_2, N_3) = U_H + U_C + F_{el} + F_{Fl} + \sum_{i=1}^3 S_i \quad 1.18.$$

$U_H$  is the averaged electrostatic energy of the whole star. It is given by the spatial integral over all pairs of local charge densities  $\zeta(r)$  at spot  $r$ . The local charge densities are averaged over time (mean-field approach). Since each pair has been regarded twice, the obtained electrostatic energy needs to be multiplied by a factor  $1/2$ . This yields:

$$U_H = \frac{1}{2\varepsilon} \iint \frac{\zeta(r)\zeta(r')}{|r-r'|} d^3r \cdot d^3r' \quad 1.19.$$

The radial charge density can be derived by a simple consideration.  $Q^*$  is the effective charge of the star, which is given by the charge of the sum of all free counterions ( $N_3$ ). For a spherical charge distribution within a radius  $R$  and an effective charge  $Q^*$  it is given for the integration limits  $0 < r < R$ :

$$Q^* = \int_0^R Q^* \frac{1}{R} dr = \int_0^R \zeta(r) \cdot 4\pi r^2 \cdot dr \quad \Rightarrow \quad \zeta(r) = Q^* \frac{1}{4\pi r^2 R} \quad 1.20.$$

By use of the Heaviside step-function  $\Theta$  ( $\Theta(x) = 0$  for  $x < 0$ ;  $\Theta(x) = 1$  for  $x \geq 0$ ) one can extend equation 1.20. over the whole Wigner-Seitz cell:

$$\zeta(r) = Q^* \frac{\Theta(R-r)}{4\pi r^2 R} - Q^* \frac{\Theta(r-R) \cdot \Theta(R_W - r)}{V_3} \quad 1.21.$$

Equation 1.19. can be solved analytically by use of equation 1.21.

$U_H$  does not take into account direct interactions between the chains and the counterions. Those interactions are included in the term for the electrostatical correlation energy,  $U_C$ . The averaged distance,  $z_m$ , of the counterions in volume  $V_l$  to the charged monomeric units are related to the Bjerrum length,  $l_B$ , and compared to the thermal energy,  $k_B T$ . Taking into account the number of interactions,  $N_1$ , gives:

$$U_C = -k_B T \frac{l_B}{z_m} N_1 \quad 1.22.$$

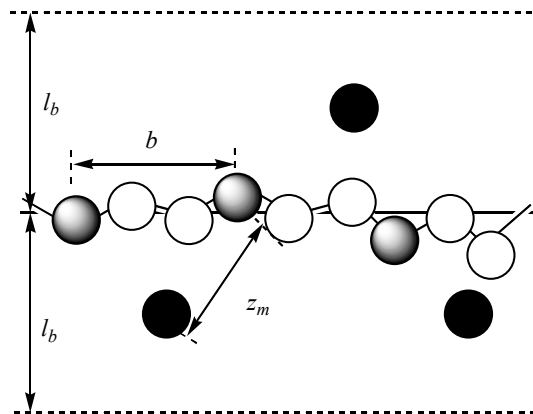


**Figure 1.9: Averaged geometry of the condensed counterions (black) towards the charged monomer units (grey) (white: uncharged monomers)**

$z_m$  is approximated by  $z_M = 0.5(l_B^2 + b^2)^{0.5}$ , since  $b$  is the average distance between two charges along the polymer (Figure 1. 9).

Equation 1. 18. has further terms, which specify the entropic contributions of the chains and the counterions. Following equation is given for the elastic properties of the polymeric backbone due to Gaussian statistics:<sup>59</sup>

$$F_{el} = k_B T \frac{3 \cdot f_{star} \cdot R^2}{2 \cdot DP_{arm} \cdot \sigma_{LJ}^2} \quad 1. 23.$$

Besides that the free energy caused by the mutual exclusion of two chains needs to be taken into account according to Flory's formula:<sup>60</sup>

$$F_{Fl} = k_B T \frac{3\nu(f_{star} \cdot DP_{arm})^2}{2\pi R^3} \quad 1. 24.$$

$\nu$  is the Flory-parameter for the excluded volume. Likos et al. have discussed  $\nu$  and they used as approximation  $\nu = 30\sigma_{LJ}^3$ .

Finally the entropic contribution of the counterions needs to be taken into account for each region. One can write:

$$S_i = k_B T \int_{V_i} \rho_i(r) \left[ \ln(\rho_i(r) \sigma_{LJ}^3) - 1 \right] d^3r + 3N_i \ln\left(\frac{\Lambda}{\sigma_{LJ}}\right) \quad 1. 25.$$

$\Lambda$  is the thermal de Broglie wave-length of the counterions. For further considerations the Broglie term is neglected.  $\rho_i(r)$  is the number density of the ions. Within the cylinder around the polymeric backbone and within the bulk volume outside the star a uniform distribution of counterions is expected:  $\rho_1(r) = N_1/V_1$ ;  $\rho_3(r) = N_3/V_3$ . For all  $N_2$  confined counterions in  $V_2$  one needs to introduce a sphere with the same volume  $V_2$ , but with radius  $R'$ , since not the whole star's space ( $4\pi R^3/3$ ) is accessible. Therefore the counterion density is given by:

$$\rho_2(r) = \frac{N_2}{4\pi R'} \cdot \frac{\Theta(r-R)}{r^2} \quad 1. 26.$$

$$\text{with } R' = R \left[ 1 - \frac{3}{4} f_{star} \left( \frac{l_B}{R} \right)^2 \right]^{1/3} \quad 1. 27.$$

After these considerations each entropic contribution to the free energy can be calculated.

As we are interested in the fraction of free counterions, analytical expressions for  $N_3$ ,  $N_1$  and  $R$  can be found ( $N_2$  is given by  $N_3$ ,  $N_1$ ).

$$R^3 = \frac{N}{3f_{star}} \cdot \left\{ \frac{l_B \sigma_{LJ}^2 N_3^2}{2} \left( \mathcal{G}\left(\frac{R}{R_w}\right) - \frac{R}{R_w} \mathcal{G}'\left(\frac{R}{R_w}\right) \right) + \right. \\ \left. + 3R\sigma_{LJ}^2 \left( N_2 \left( 1 + \frac{2\pi f_{star} l_B^2 R}{3V_2} \right) - N_3 \frac{V}{V_3} \right) + N_1 R \sigma_{LJ}^2 \left( 1 - \left( \frac{f_{star}}{N_c} \right)^2 \frac{l_B R^2}{4z_m^3} \right) + \frac{9v}{8\pi} \left( \frac{f_{star} \cdot DP_{arm} \cdot \sigma_{LJ}}{R} \right)^2 \right\}$$

1. 28.

$$N_3 = \frac{R}{l_B \mathcal{G}(R/R_w)} \left\{ 2 + \ln \left[ \left( \frac{N_c - N_1}{N_3} - 1 \right) \frac{V_3}{3V_2} \right] \right\} \quad 1. 29.$$

$$N_1 = (N_c - N_3) \left\{ 1 + \frac{3V_2}{V_1} \exp \left( -2 - \frac{l_B}{z_m} \right) \right\}^{-1} \quad 1. 30.$$

$$\text{with } \mathcal{G}(x) = 1 + \frac{5 - 9x + 5x^3 - x^6}{5(1 - x^3)^2} \quad \text{and} \quad \mathcal{G}'(x) = \frac{d\mathcal{G}}{dx}$$

Some examples concerning the counterion distribution can be taken from reference <sup>58</sup>.

**Table 1. 1: Dependence of the counterion distribution for different arm numbers  $f_{star}$  and different fractions of charged monomeric units  $\alpha'$ . Arm length  $DP_{arm} = 50$ , cell radius  $R_w = 55,83 \cdot \sigma_{LJ}$  (except for  $f_{star} = 40$ :  $R_w = 62,04 \cdot \sigma_{LJ}$ ;  $f_{star} = 50$ :  $R_w = 74,44 \cdot \sigma_{LJ}$ ); in bracket: results of molecular dynamics (MD) simulations**

$f_{star}$	$\alpha'$	$R/\sigma_{LJ}$	$N_1$	$N_2$	$N_3$	$N_3/\sum N_i = \phi$
5	1/3	26,1 (26,8)	25 (27)	32 (20)	23 (33)	0,29 (0,41)
10	1/6	23,7 (23,4)	38 (22)	21 (20)	21 (38)	0,26 (0,48)
10	1/4	25,2 (25,3)	61 (46)	36 (31)	23 (43)	0,19 (0,36)
10	1/3	26,9 (27,4)	81 (72)	53 (38)	26 (50)	0,16 (0,31)
18	1/6	25,8 (24,2)	90 (60)	31 (31)	23 (53)	0,16 (0,37)
18	1/4	26,9 (26,6)	141 (107)	49 (49)	26 (60)	0,12 (0,28)
18	1/3	28,1 (28,3)	190 (159)	70 (58)	28 (71)	0,10 (0,25)
30	1/4	28,8 (27,2)	272 (213)	60 (65)	28 (82)	0,08 (0,23)
30	1/3	29,7 (28,6)	366 (309)	83 (75)	31 (96)	0,06 (0,20)
40	1/3	30,9 (29,2)	517 (392)	90 (139)	33 (109)	0,05 (0,17)
50	1/3	32,0 (29,8)	670 (514)	93 (154)	37 (132)	0,05 (0,17)

**Table 1. 2: Dependence of the counterion distribution for different arm lengths  $DP_{arm}$ . Arm number  $f_{star} = 10$ , fraction of charged monomeric units  $\alpha' = 1/3$ , cell radius  $R_w = 136,48 \cdot \sigma_{LJ}$  (except for  $N = 50$ :  $R_w = 55,83 \sigma_{LJ}$ ); in bracket: results of molecular dynamics (MD) simulations**

$DP_{arm}$	$R/\sigma_{LJ}$	$N_1$	$N_2$	$N_3$	$N_3/\Sigma N_i = \phi$
50	26,9 (27,4)	81 (72)	53 (38)	26 (50)	0,16 (0,31)
100	54,0 (57,3)	103 (96)	166 (140)	61 (94)	0,18 (0,28)
150	78,8 (84,2)	133 (131)	287 (251)	80 (118)	0,16 (0,24)
200	100,4 (106,7)	162 (169)	410 (384)	88 (107)	0,13 (0,16)

We can discern that the counterion confinement of star-shaped polyelectrolytes is expected to be of intermediate nature compared to linear (e.g. PAA with  $\alpha' \sim 0.25$ :  $\phi \sim 0.4$ )<sup>61</sup> and densely grafted brush-like polyelectrolytes.<sup>62</sup>

A further look at equation 1. 28. reveals that the scaling of the radius  $R$  (here: radius of the star's enclosing sphere) is approximated by following formula for rather highly charged stars ( $\alpha = 0.33$ ):

$$R \propto DP_{arm}^1 \cdot f_{star}^0 \quad \mathbf{1. 31.}$$

This is a result of the strong stretching of the chains and is in contrast to the uncharged star polymers ( $R \propto DP_{arm}^{0.6} f_{star}^{0.2}$ ; see equation 1. 2.)

### 1.3. Phase Separation in Polymer Solutions

Linear PDMAEMA is only miscible in pure water within a certain temperature region. Above a certain temperature, called cloud point, it starts to form two phases. This phase separation depends also on concentration. The minimum temperature at which phase separation can occur at all is called lower critical solution temperature (LCST).<sup>50</sup>

Polymers are at least partly miscible with solvents as long as the change in free enthalpy upon mixing is negative  $\Delta G_{mix} = \Delta H_{mix} - T \Delta S_{mix} < 0$  ( $\Delta H_{mix}$ : change in enthalpy;  $\Delta S_{mix}$ : change in entropy). The *Flory-Huggins* theory<sup>63-65</sup> specifies both terms for concentrated solutions. Using a lattice model  $\Delta S_{mix}$  was determined by use of the *Boltzmann* law:

$$\Delta S_{mix} = -R(n_1 \ln \varphi_1 + n_2 \ln \varphi_2) \quad \mathbf{1. 32.}$$

$n_i$  assigns the molar amount and  $\varphi_i$  assigns the volume fraction of component  $i$ . The equation strongly resembles the equation for small molecules, where just the volume fraction is replaced by the molar fraction  $x_i$ . We assume that the polymer segments and the solvent molecules possess always the same volume. That means that upon mixing no overall volume

change takes place and  $\Delta H_{\text{mix}}$  is directly obtained by the change in free energy  $\Delta U_{\text{mix}}$ . Contributions to the free energy of solvent-solvent interactions, solvent-polymer segment interactions and polymer-polymer segment interactions are accounted by  $\varepsilon_{11}$ ,  $\varepsilon_{12}$  and  $\varepsilon_{22}$  respectively. Each segment or solvent molecule is surrounded by  $q$  other segments. For a segment, which is embedded in a polymer chain, two next neighbors are polymer segments. The interactions of those with the segment are similar to the interactions in bulk polymer, therefore those interactions do not contribute to  $\Delta G_{\text{mix}}$ . Those considerations lead to the final expression of  $\Delta U_{\text{mix}}$ :

$$\Delta U_{\text{mix}} = RT\varphi_2 n_1 \chi \quad \mathbf{1.33.}$$

$\varphi_2$  assigns here the volume fraction of the polymer.  $\chi$  is the *Flory-Huggins* interaction parameter and is defined as:

$$\chi = -\frac{q\Delta\varepsilon}{2k_B T} \quad \mathbf{1.34.} \quad \text{with} \quad \Delta\varepsilon = \varepsilon_{11} + \varepsilon_{22} - 2\varepsilon_{12}$$

If  $\chi$  is negative, the polymer-solvent interactions prevail. The solvent is a good solvent for the polymer.

We summarize ( $DP$  is the degree of polymerization):

$$\Delta G_{\text{mix}} = RT(\varphi_2 n_1 \chi + n_1 \ln \varphi_1 + n_2 \ln \varphi_2) = RT \left( \frac{n_2 DP}{n_1 + n_2 DP} n_1 \chi + n_1 \ln \frac{n_1}{n_1 + n_2 DP} + n_2 \ln \frac{n_2 DP}{n_1 + n_2 DP} \right) \quad \mathbf{1.35.}$$

With this expression it can be shown that for  $\chi = 0.5$  the solution is in the  $\theta$ -state, which means that the second virial coefficient of the osmotic pressure becomes zero. The polymer molecules act like unperturbed chains. For  $\chi > 0.5$  the solvent turns to be a bad solvent for the polymer, finally leading to phase separation.

Those considerations do not account for any rotational or vibrational movements of the polymer segment. Also the contact entropy of the solvent towards (preferred orientation!) the polymer is not taken into account. Therefore  $\chi$  is expanded into an enthalpic,  $\chi_H$ , and an entropic term,  $\chi_S$ , to include additional contributions to  $\Delta G_{\text{mix}}$ . It is also convenient to introduce  $\psi$  and  $\theta$ , which gives a simple expression for the temperature dependence of the corrected *Flory-Huggins* parameter:

$$\chi = \chi_H + \chi_S \quad \mathbf{1.36.} \quad \text{with} \quad \chi_S = 0.5 - \psi \quad \text{and} \quad \chi_H = \frac{\theta\psi}{T}$$

$$\chi = 0.5 - \psi \left( 1 - \frac{\theta}{T} \right) \quad 1.37.$$

For  $T = \theta$  the *Flory-Huggins* parameter becomes 0.5, which means that the polymer is in its theta state.  $\theta$  is here the theta temperature and  $\psi$  accounts for the extent of the temperature dependence of  $\chi$ .

With this background we now want to turn to phase separation phenomena in polymer solutions. Phase separation occurs, when the chemical potential of both components are identical in the two phases obtained at two different compositions. Additionally both phases should be located at compositions along the  $\Delta G_{\text{mix}}$  profile, which are close to the minima of  $\Delta G_{\text{mix}}$ . Therefore a tangent needs to touch  $\Delta G_{\text{mix}}$  at two spots. In principle three different shapes of  $\Delta G_{\text{mix}}$  with  $\varphi_2$  can be obtained:

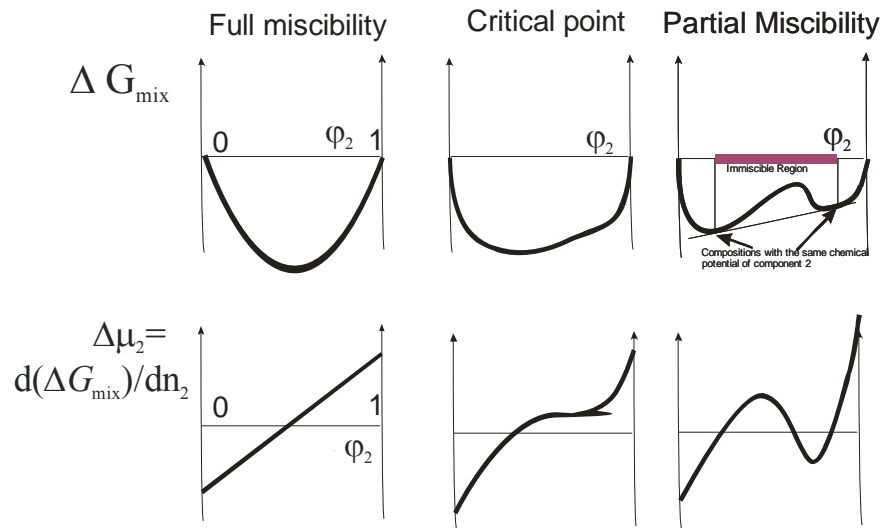


**Figure 1. 10: Different types of the free enthalpy of mixing  $\Delta G_{\text{mix}}$  and chemical potential  $\Delta\mu$  in dependence of composition resulting in partial immiscibility (right hand side)**

At a certain critical *Flory-Huggins* parameter  ${}^k\chi$  phase separation takes place for the first time (at a certain critical volume fraction  ${}^k\varphi_2$ ). We discern for the critical shape of  $\Delta G_{\text{mix}}$  (equation 1. 35.) that the chemical potential of the polymer  $\Delta\mu_2$  (derivative of  $\Delta G_{\text{mix}}$  with  $\varphi_2$ ,  $d(\Delta G_{\text{mix}})/d\varphi_2 = \Delta\mu_2$ ) needs to have saddle point. This condition is fulfilled, when

$${}^k\varphi_2 = \frac{1}{1 + \sqrt{DP}} \quad 1.38$$

$$\text{and} \quad {}^k\chi = 0.5 + \frac{1}{2DP} + \frac{1}{\sqrt{DP}} \quad 1.39$$

or by use of equation 1. 37:<sup>66</sup>

$$\frac{1}{{}^kT} = \frac{1}{\theta} + \frac{1}{\psi\theta} \left( \frac{1}{2DP} + \frac{1}{\sqrt{DP}} \right) \quad 1.40.$$

${}^kT$  is the critical temperature, at which  $\chi$  becomes critical. In our terms it is either the upper critical solution temperature (UCST) or the lower critical solution temperature (LCST). There

are some systems, which show both UCST and LCST.<sup>67-69</sup> Here the dependence of  $\chi$  with temperature is even more complicated and  $\chi(T)$  can adopt  $^k\chi$  at different temperatures.

## 1.4. Experimental Methods of Determining the Solution Behavior of Star-shaped Polyelectrolytes

### 1.4.1. Potentiometric Titration

The degree of ionization of weak polyelectrolytes depends directly on the degree of neutralization and therefore on the  $pH$ . Often it is necessary to know the degree of charging  $\alpha'$  at a certain  $pH$  (e.g. for the determination of the osmotic coefficient; see chapter 1.4.2). Thus, to elucidate the protonation or deprotonation behavior in dependence with  $pH$  one measures the  $pH$  of the pure polymer solution in dependence of added strong acid or base. The amount of added acid or base can be put into correlation with the amount of ionizable groups present in the mixture and gives directly the degree of neutralization  $\alpha$ . Since we are regarding solutions ( $\sim 1-10$  mmol/L of monomeric units) of weak polyelectrolytes with  $pK_{a/b}$  values larger than 4, the self-(de)protonation is only relevant at the outer limits of the titration curve (at the very low or very high  $pH$  values).  $pK_{a/b}$  is the negative decadic logarithm of equilibrium constant of deprotonation or protonation for acids or bases, respectively (for definition of  $pK_{a/b,0}$  and  $pK_{a/b,app}$  see appendix 10.2). On the other hand the  $pK_{a/b}$  values are not larger than 10. Therefore principally complete (de)protonation can be achieved within the standard  $pH$  range ( $0 < pH < 14$ ) by addition of strong base / acid. Thus, the degree of neutralization,  $\alpha$ , is identical to the degree of ionization (degree of charging),  $\alpha'$ , at intermediate degrees of neutralization in very good approximation.

The easiest way to measure the  $pH$  is the use of a  $pH$  glass electrode.<sup>50</sup> It is an ion-selective electrode, sensitive to oxonium ions ( $H_3O^+$ ). It consists of a thin glass membrane, whose surface is swollen by water. Protons can be exchanged depending on the  $pH$  and this leads to a change in membrane potential. To compare the potentials, it needs to be measured against a known potential given by a reference electrode (see Figure 1. 11). The reference electrode (e.g. AgCl/Ag) can be located in the same electrode (combined electrode), which produces a potential irrespective to the  $H^+$  concentration. It is filled with KCl solution, as KCl generates almost no diffusion potential  $U_5$  across the diaphragm of the reference electrode due to similar mobility of potassium and chloride ions.

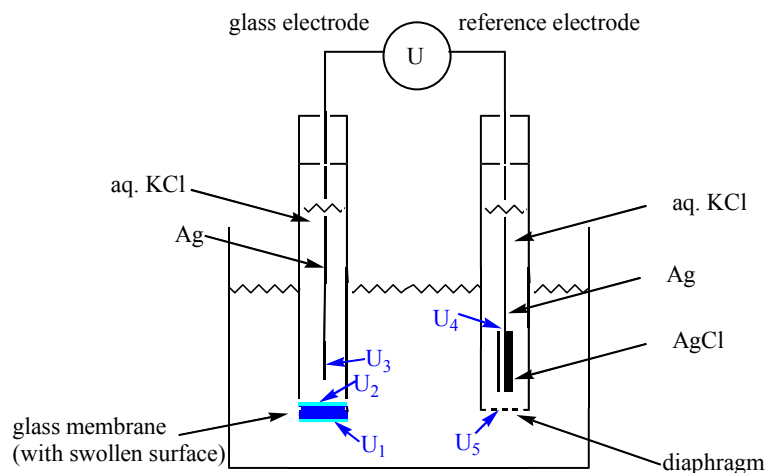


**Figure 1. 11: setup to measure  $pH$  by potentiometry (glass electrode)**

The other potentials involved in the measurement chain are  $U_1$  (Galvani potential of outer glass membrane surface),  $U_2$  (Galvani potential of inner glass membrane – usually constant),  $U_3$  (Galvani potential between the inner electrolyte and inner electrode – usually constant) and  $U_4$  (Galvani potential of reference electrode – usually constant). One needs to calibrate the electrode with solutions of known  $pH$  to address e.g. changes of the membrane. The principle to transform the measured potentials into the activity of the oxonium ions is given by the Nernst equation:<sup>70</sup>

$$U = U_0 + \frac{RT}{nF} \ln a_{H_3O^+} \approx U_0 - \frac{\ln 10 RT}{nF} pH \quad 1.41.$$

Current temperature needs to be entered into the equation to obtain meaningful results. The Nernst equation can be also used for other ion-selective electrodes. For example polymer membrane electrodes can be designed by incorporation of a selective ligand for the ion of choice. The higher the concentration, the more ions will be adsorbed on the membrane and the membrane potential will change.

### 1.4.2. Osmotic Pressure and Osmotic Coefficient

The osmotic pressure,  $\Pi$ , belongs to the class of colligative properties, i.e. the measured quantity is (only) dependent on the molar concentrations of distinct particles,  $[P]$ . By use of a semipermeable membrane one can easily measure the osmotic pressure. The membrane separates two regions: the pure solvent is in one chamber, whereas the other halfcell is filled with the polymer solution.

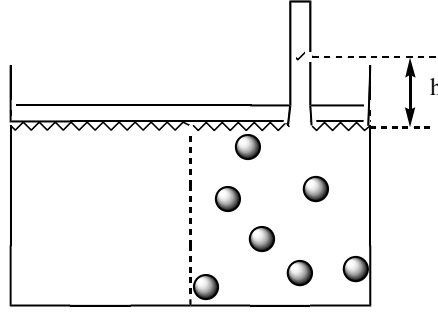


**Figure 1. 12: Principal setup to measure the osmotic pressure**

The polymer cannot pass the membrane. The chemical potential of the solvent is lowered on the side of the solution due to the dissolved particles. Therefore solvent, which passes through the membrane, dilutes the solution and exerts a pressure. This pressure difference can lead to a column of solvent, exerting hydrostatic pressure on the sample. The height of the column,  $h$ , is directly proportional to the osmotic pressure ( $\Pi = g \cdot h \cdot \rho$ ;  $\rho$  is the density of the solution and  $g$  is the earth's gravitational acceleration). The van't Hoff equation<sup>71, 72</sup> describes the ideal osmotic pressure  $\Pi_{\text{van'tHoff}}$  at infinite dilution:

$$\Pi_{\text{van'tHoff}} = [P]RT \quad 1. 42.$$

The van't Hoff equation is also used to determine the number-average molecular weight,  $M_n$ , of uncharged polymers. Knowing the mass concentration  $c_{m,p}$  of the polymer, osmometry gives the molar concentration of the polymer (osmometry counts the number of molecules). The ratio of both concentrations gives directly  $M_n$ . Non-ideal behavior is accounted by extrapolating  $\Pi/c_{m,p}$  to zero concentration. The intercept on the y-axis equals  $RT/M_n$ . The terminological description of the non ideal behavior is given by a virial development, introducing the second virial coefficient  $A_2$ :

$$\Pi = c_{m,p}RT(1/M_n + A_2c_{m,p} + \dots) \quad 1. 43.$$

Van't Hoff equation can be derived from considerations regarding the chemical potential,  $\mu_S$ , of the solvent on both sides of the membrane. In equilibrium the chemical potential needs to be the same on both sides:

$$\mu_{S,\text{leftside}} = \mu_S^*(p) = \mu_{S,\text{rightside}} = \mu_S(x_S, p + \Pi) = \mu_S^*(p + \Pi) + RT \ln x_S = \mu_S^*(p) + \int_p^{p+\Pi} V_m \cdot dp + RT \ln x_S$$

**1. 44.**

$\mu_S^*(p)$  assigns the chemical potential of the pure solvent at an external pressure  $p$ .  $\mu_S(x_S, p + \Pi)$  assigns the chemical potential of the solvent in presence of a solute (molar fraction  $x_S$ ) at pressure  $p + \Pi$ . The pressure dependence of the chemical potential is given by

the integral over the molar volume  $V_m$  of the solvent. For small concentrations following approximation can be made:

$$-RT \cdot \ln x_s = -RT \cdot \ln(1 - x_p) \approx R \cdot T \cdot x_p = \int_p^{p+\Pi} V_m \cdot dp = V_m \cdot \Pi \quad 1.45.$$

By approximating the molar fraction  $x_p$  by  $n_p / n_s$  ( $n_X$  assign the molar amount of component X) and taking into account that  $n_s \cdot V_m = V$  one can easily derive the van't Hoff equation.

We already know that polyelectrolytes contain a huge number of counterions. In principle each particle contributes equally to the osmotic pressure, but not all counterions are freely available in bulk solution. Therefore one can compare the expected osmotic pressure of a polyelectrolyte according to van't Hoff law with the measured osmotic pressure. Each counterion is taken into account for the theoretical calculation, as though all counterions would contribute equally to the osmotic pressure:

$$\Pi_{\text{van'tHoff}} = RT \left( \frac{c_{m,P}}{M_m} (\alpha' + 1 / DP_n) \right) \approx RT \alpha' \frac{c_{m,P}}{M_m} \quad 1.46.$$

$c_{m,P}$  is the mass concentration of the polyelectrolyte,  $DP_n$  is the number-average degree of polymerization,  $\alpha'$  is the degree of ionization, whereas  $M_m$  is the average molar mass of the monomeric unit of the polymer.  $\alpha'$  equals unity for strong polyelectrolytes. The right side of the last equation holds true, as the number of polymeric backbones is negligible compared to the number of counterions.

To account for the non ideal behavior of the polyelectrolytes, we can introduce a correction factor  $\phi$ .

$$\Pi_{\text{real}} \approx RT \phi \alpha' \frac{c_{m,P}}{M_m} \quad \text{and} \quad \phi = \frac{\Pi_{\text{real}}}{\Pi_{\text{van'tHoff}}} \quad 1.47.$$

This correction factor  $\phi$  is called osmotic coefficient<sup>73</sup> and it is a measure of the fraction of free, non confined counterions. It is comparable to an activity coefficient.<sup>74-77</sup> We can conclude that osmometry is a valuable method to investigate the counterion distribution of polyelectrolytes.

### 1.4.3. Dynamic Light Scattering

Intensity fluctuations of the scattered light are recorded during Dynamic Light Scattering (DLS) measurements.<sup>78,79</sup> Other terms for this technique are Photon Correlation Spectroscopy (PCS) or Quasi-Elastic Light Scattering (QELS). Those fluctuations can be correlated to

motions of the dissolved particles. E.g. translational movements will continuously change the arrangement of the scatterers with time, simultaneously changing the dynamic structure factor. This leads to changes in the detected intensity. Also rotational motions or segment relaxations can lead to fluctuations in the intensity of the scattered light. The standard procedure to illustrate and average the temporal fluctuations is to introduce an intensity time autocorrelation function  $g^{(2)}(\tau)$ .  $g^{(2)}(\tau, q)$  can be measured depending on the length of scattering vector  $q$  ( $q = (4 \pi \cdot n / \lambda) \cdot \sin(\theta / 2)$ ;  $\lambda$ : wavelength of the incident light;  $n$ : refractive index of medium used;  $\theta$ : scattering angle) by help of a sensitive avalanche diode, connected to a correlator (homodyne mode):

$$g^{(2)}(\tau) = \frac{\langle I(t) \cdot I(t + \tau) \rangle}{\langle I \rangle^2} \quad 1.48.$$

The brackets assign the temporal average over all times.  $I(t)$  is the scattered intensity at time  $t$ , whereas  $I(t + \tau)$  is the intensity after the lag time  $\tau$ . The autocorrelation function  $g^{(2)}(\tau)$  becomes unity after long lag times  $\tau$ , since the expression is normalized with the square of the average intensity  $\langle I \rangle$ . This means no correlation is present for long  $\tau$ . At short  $\tau$  the autocorrelation function is considerably larger than unity, indicating correlations of the detected intensity at short time scales. Those correlations correspond to temporal correlations in the structure of the solution. The larger the scatterers in the solution the larger are the temporal correlations. This is due to their slow movement of large particles according to the Stokes-Einstein relation:<sup>16</sup>

$$D = \frac{kT}{6\pi\eta R_h} \quad 1.49.$$

$D$  assigns here the collective diffusion coefficient,  $\eta$  assigns the viscosity of the solvent and the hydrodynamic radius  $R_h$  assigns the radius of a sphere with the same hydrodynamic properties compared to the investigated particles.

$g^{(2)}(\tau)$  contains the diffusion coefficient indirectly. Motion and therefore the diffusion coefficient are direct parameters in the electrical field autocorrelation function  $g^{(1)}(\tau)$  which is connected physically to the intensity correlation function  $g^{(2)}(\tau)$  for motions of independent particles by the so-called Siegert relation,<sup>80</sup>

$$g^{(2)}(\tau) = 1 + \gamma \cdot (g^{(1)}(\tau))^2 \quad 1.50.$$

with  $\gamma$  being an efficiency factor ( $0 < \gamma < 1$ ; depending e.g. on the illuminated area). For monodisperse spherical particles  $g^{(1)}(\tau)$  is given by a single exponential decay:

$$g^{(1)}(\tau, \theta) = e^{-D \cdot q^2 \cdot \tau} = e^{-\Gamma \cdot \tau} \quad 1.51.$$

$\Gamma = D \cdot q^2$  is the decay rate ( $\Gamma = 1 / \tau_0$ ). Again, the obtained diffusion coefficient can be expressed in terms of hydrodynamic radius according to the Stokes-Einstein equation. Therefore DLS is a powerful method to investigate changes in the size of particles like aggregation. For non-spherical particles other processes may contribute to the decay in the correlation function. For example  $\Gamma$  needs to be modified for rotational diffusion (coefficient  $D_R$ ):

$$\Gamma = q^2 \cdot D + 6 \cdot D_R \quad 1.52.$$

Here we see that translational diffusion leads to a linear increase of the decay rates with  $q^2$ , whereas the contribution of rotational motion is irrespective to the scattering angle. At small scattering angles large distances within the sample are probed. Therefore time correlations are present for longer lag times  $\tau$ , since the particles need more time to rearrange within the probed dimensions. In contrast internal motions are irrespective to the probed distances.

For polydisperse systems the analysis can be modified, since the decay in the autocorrelation function is a superposition of single exponential decays from different species:

$$g^{(1)}(\tau, \theta) = \int_0^{\infty} G(\Gamma) \cdot e^{-\Gamma \cdot \tau} d\Gamma \quad 1.53.$$

$G(\Gamma)$  is a probability density function. There are two established procedures for its analysis: Cumulant and CONTIN. CONTIN is a modified Laplace transformation of  $g^{(1)}(\tau)$  and is therefore a suitable method to determine multimodal size distributions. The primary distributions are intensity weighted distributions. The cumulant method is a polynomial fitting procedure of  $\ln(g^{(1)}(\tau)) = A + B \cdot \tau + C \cdot \tau^2 + D \cdot \tau^3$ , which gives the average hydrodynamic radius along with its polydispersity (A, B, C and D are fitting parameters).

#### 1.4.4. Common Techniques for the Determination of Molecular Weight

Characterization in terms of molecular weight is a prerequisite before starting investigations of other physical properties. A structure-behavior relationship can only be obtained after careful characterization of the prepared macromolecules. Therefore a short, schematic description is given for the most common methods used in this thesis.<sup>50</sup>

### 1.4.4.1. Gel Permeation Chromatography

Size Exclusion Chromatography (SEC or GPC, which stands for Gel Permeation Chromatography) is a suitable relative method to determine the molecular weight distribution and therefore molecular weight averages.

The SEC column separates different macromolecules with regard to their size and therefore regarding their hydrodynamic volume,  $V_H$ .  $V_H$  is dependent on molecular weight  $M$ , so the elution-times correlate with the molecular weight (see equation 1. 55.).

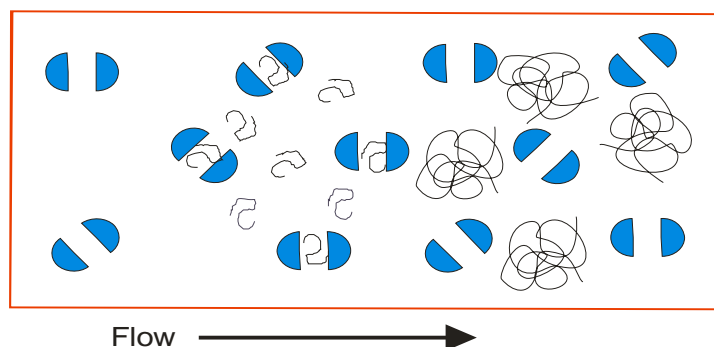


Figure 1. 13: Principle of separation inside a GPC column

Smaller molecules spend more time in the pores of the separating column-gel than larger sized particles. Therefore the elution-volumes  $V_e$  are smaller for expanded molecules. If the molecules are too large, none of them will fit into the pores. They can only use the space between the resin-beads  $V_v$ . Small molecules can however occupy both  $V_v$  and  $V_i$  (space in the pores). So every fraction has its separation constant  $K_{SEC}$ :

$$V_e = V_v + K_{SEC} V_i \quad 1. 54.$$

The exact elution volume of a polymer is dependent on the chemical nature of the polymer, the solvent and the polymer's topology. A prerequisite for meaningful results is the good solubility of the polymer in the solvent and the absence of adsorption of the polymer on the column. Other parameters are the length, width of the column, flow rate and temperature. The flow rate needs to be optimized, aiming for best separation and low amount of axial dispersion (diffusion along the column axis). Due to the many parameters it is crucial to calibrate the setup with polymers of known molecular weight, keeping all other parameters constant. The elution times of almost monodisperse samples are recorded to arrange a semi-logarithmic calibration plot. This is suitable as within certain limits a logarithmic equation has been found empirically.

$$\log M = K' - k' V_e \quad 1. 55.$$

We mentioned that  $V_H$  is the separation parameter and according to Einstein equation  $V_H$  is proportional to  $[\eta] M$ .<sup>15, 16</sup> This gives the opportunity for universal calibration:

$$\log V_H \sim \log ([\eta] M) = \log (K \cdot M^{\alpha+1}) = K^* - k^* V_e \quad 1. 56.$$

During calibration with polymers, whose Kuhn-Mark-Houwink parameters  $K$  and  $\alpha$  are known,<sup>14</sup> each elution volume  $V_e$  can be assigned a certain hydrodynamic volume  $V_h$ . Once a universal calibration is established, one need to know only the Kuhn-Mark-Houwink parameters  $K$  and  $\alpha$  of another polymer, to obtain the real molecular weight distribution of that polymer without performing a new calibration. The only drawback: Kuhn-Mark-Houwink equation<sup>14</sup> holds only true for polymers larger than 20000 g/mol. The most elegant way making use of the universal calibration is the use of a viscosity detector, which detects the specific viscosity  $\eta_{sp}$  of any fraction. Knowing the mass concentration  $c$  in each fraction by use of concentration sensitive detectors (UV or RI), the intrinsic viscosity  $[\eta]$  is approximated with the reduced viscosity  $\eta_{red} = \eta_{sp}/c$ .

Other useful GPC setups include GPC-light-scattering or GPC-MALDI-ToF coupling. Both give directly molecular weight distributions without any calibration, as long as the column guarantees effective separation of different species.

#### 1.4.4.2. Osmometry

Number averaged molecular weights  $M_n$  are obtained by osmometry. The result is irrespective to the shape of the polymer, since osmometry simply counts the number of molecules and is therefore an absolute method. Only the choice of solvent and membrane requires careful considerations. The solvent needs to be chosen in a way that the polymer is not charged up by reactions involving the solvent (e.g. avoid protic solvents for PDMAEMA). Also aggregation must not occur in order to obtain the molecular weight of the single chains. The molecular weight cut-off, MWCO, of the membrane should be considerably smaller than the molecular weight at the onset of the molecular weight distribution. For details on the theory please refer to chapter 1.4.2.

#### 1.4.4.3. Static Light Scattering

Static light scattering (SLS) gives the weight-average molecular weight,  $M_w$ , besides the second virial coefficient,  $A_2$ , of the osmotic pressure (see chapter 1. 4. 2.) and the radius of gyration,  $R_g$ . The oscillating electric field of light polarizes the illuminated medium. The electrons of the molecules are shifted compared to the nuclei. This results in a dipole,

oscillating with the same frequency than the incident beam. On the other hand the dipoles themselves act as transmitter of light with the same frequency. For polarized light the transmitter transmits light perpendicular to the dipole axis, irrespective to the orientation of the incident beam. This behaviour is called scattering. The scattered intensity is irrespective to the scattering angle  $\theta$ , when the detection plane is perpendicular to the field vector of polarized light. This holds strictly true for scatterers, which are much smaller than the wavelength of light. For larger scatterers, the angular dependence of the scattered light is altered. Destructive interference leads to lower intensities at higher scattering angles. This can give information on the dimensions of the scatterer.

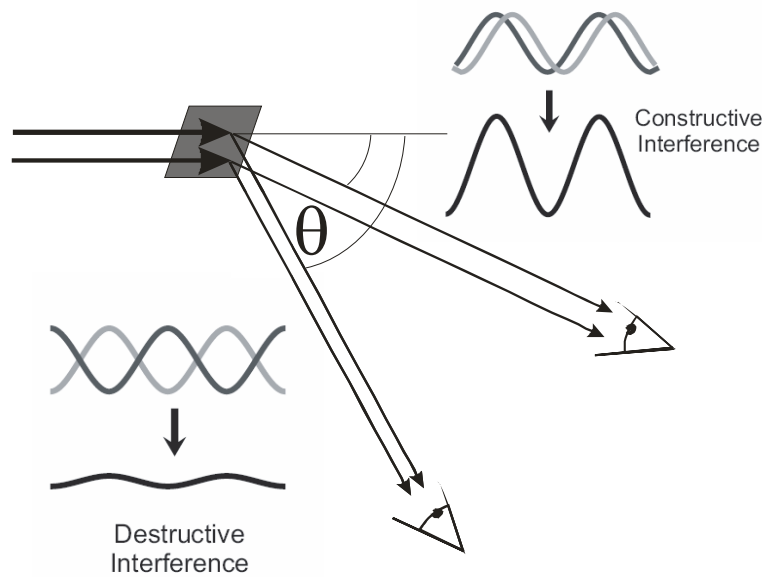


**Figure 1. 14: Principle of light scattering on nano-scaled objects**

The more single scatterers are combined in one object the higher is its contribution to the total scattered intensity especially at low scattering angles. Therefore the molecules are weighed by light scattering, which leads to the weight-average molecular weight  $M_w$ .

The theoretical background of the scattering is given by the terminological description of the radiation characteristics of an oscillating dipole, which leads to the Rayleigh ratio  $R(\theta)$  for non polarized light.<sup>81</sup>

$$R(\theta) = \frac{I_s r^2}{I_0 (1 + \cos^2 \theta)} = 8\pi^4 \alpha^2 / \lambda_0^4 \quad \mathbf{1. 57.}$$

$I_0$  is the intensity of the incident beam.  $I_s$  assigns the intensity of the scattered light, detected at a distance  $r$  from the sample under a scattering angle  $\theta$ .  $\alpha$  assigns the polarizability of the scatterer for the wavelength  $\lambda_0$ .

In the frequency-averaged light scattering theory of Einstein,<sup>82</sup> the sample solution is divided into many small volumes, to account for fluctuation in polarizability of those volumes. Those fluctuations are vital to obtain a net scattering, since a microscopically homogenous solution cannot yield any net scattering due to destructive interference of the scattered light (a scattered beam always encounters another beam with the necessary phase-shift to obtain destructive interference). The fluctuations of the polarizability of those small volumes are caused by concentration fluctuations. Pressure or temperature fluctuations are canceled out, when the excess intensity  $I_S^{\text{excess}}$  ( $= I_S^{\text{solution}} - I_S^{\text{solvent}}$ ) instead of  $I_S$  enters the scattering equations. Those fluctuations obey Boltzmann statistics and the extent of those fluctuations are coupled to the extent of the change of the solvent's chemical potential with polymer's concentration ( $\delta\mu/\delta c_{m,p}$ ) compared to thermal energy  $kT$ . Non-ideal behavior of the chemical potential is accounted with the introduction of the second virial coefficient  $A_2$ . This yields following equation:

$$\frac{Kc_{m,p}}{R(\theta)} = \frac{1}{M_w} + 2A_2c_{m,p} \quad \mathbf{1.58.} \quad \text{with} \quad K = \frac{2\pi^2 n_0^2 \left( \frac{\partial n}{\partial c_{m,p}} \right)_{p,T}^2}{N_A \lambda_0^4}$$

$K$  is a constant, which includes the refractive index of the solvent and the refractive index increment,  $\partial n/\partial c_{m,p}$ . To account for  $I_0$  (which can not be measured easily), the scattered intensity of a standard (toluene) is also recorded during SLS measurement.

Until now only interparticle interactions and the arrangement of particles have been addressed by introducing  $A_2$ . As the intensity of the scattered radiation can be expressed by the product of form factor  $P(\theta)$  (addresses the shape of a single molecule) and structure factor  $S(\theta)$  (addresses the arrangement of molecules), we need to define  $P(\theta)$ .

As already explained, destructive interference leads to decreased intensity for large scattering angles, when particles are examined, which are larger than  $\lambda_0/20$ . Debye<sup>83-85</sup> and Guinier<sup>86,87</sup> derived an equation for the form factor in dependence of the radius of gyration  $R_g$  by use of geometrical considerations.

$$P(q) = 1 - q^2 \langle R_g^2 \rangle_z / 3 \quad \mathbf{1.59.}$$

Here the length of the scattering vector  $q$  ( $q = (4\pi \cdot n / \lambda) \cdot \sin(\theta/2)$ ;  $\lambda$ : wavelength of the incident light;  $n$ : refractive index of medium used;  $\theta$ : scattering angle) is introduced to give the final Zimm equation:<sup>88</sup>

$$\frac{Kc_{m,P}}{R(q)} = \frac{1}{P(q)} \frac{1}{M_w} + 2A_2c_{m,P} \quad \mathbf{1.60.}$$

By help of this equation a special evaluation method (Zimm plot) can be applied, which gives  $M_w$ ,  $A_2$  and  $R_g$ .

#### **1.4.4.4. MALDI-ToF Mass Spectrometry**

Matrix-Assisted Laser Desorption Ionization – Time of Flight (MALDI-ToF) mass spectrometry (MS) is an absolute method to determine molecular weight distributions. In contrast to standard MS the macromolecules are embedded in a light-sensitive matrix. A laser pulse evaporates the matrix taking the macromolecule into the gas phase. Certain additives enable the ionization of the macromolecules. The ions are accelerated in an electrical field with the potential difference  $U$  towards the detector, before it enters a field-free drift region of the length  $x$ . The time between the laser pulse and the detection is measured and transferred into the ratio mass to charge  $m/z$ :

$$t = \frac{x}{\sqrt{2}} \sqrt{\frac{m/z}{U}} \quad \mathbf{1.61.}$$

Assuming only single ionization per molecule yields a number-average molecular weight distribution.

For samples with a broad molecular weight distribution the measured averages should be taken with care, since equal probability of transfer into the vacuum (or of ionization) of different molecules with different molecular weight cannot be ensured (the higher the molecular weight the less likely is the transfer into the vacuum but the more likely is the ionization as more ionization sites are available per molecule).

### **1.5. Objective of this Thesis**

The aim of the thesis can be divided into two parts. First the synthesis and characterization of star-shaped polyelectrolytes should deliver well-defined polymers. As illustrated before, ATRP was chosen in combination with a core-first approach. This attempt was believed to yield high arm numbers with narrow distribution in molecular weight. The first system to synthesize was star-shaped poly(acrylic acid) (PAA) as a member of the group of weak anionic polyelectrolytes. Since some investigations were hampered by the variable degree of neutralization we turned to strong polyelectrolytes. The cationic system of quaternized

poly(*N,N*-dimethylaminoethyl methacrylate) (PDMAEMA) was chosen as a suitable candidate. PDMAEMA is an interesting polymer, since it can exhibit LCST behavior.

The second part deals with the investigation of the solution behavior of the stars. The origin of understanding polyelectrolytes is the knowledge of the counterion distribution as mentioned during the theoretical description of star-shaped polyelectrolytes. Therefore we concentrated on the determination of the osmotic coefficient of polyelectrolyte stars and compared it to theory. The osmotic coefficient is a direct measure of the counterion confinement. The experiments should confirm the strong counterion confinement within the stars, which is the prerequisite for further properties encountered e.g. in presence of salt. For example the high net osmotic pressure inside the stars can be relieved by an increase in bulk ionic strength or by incorporation of multivalent counterions. Another consequence of the counterion confinement within the star-shaped architecture is an ultrasoft pair interaction potential as predicted by theory.<sup>89, 90</sup> The theoretical prediction of a rich phase behavior of ordered structures in concentrated aqueous solutions was a direct result of the ultrasoft pair interactions.<sup>91</sup>

Therefore the long-term objective of this thesis was the discovery of those liquid-crystalline phases by X-ray scattering. As we did not obtain any ordered structures in solutions, the search for ordered structures will not be covered in this thesis. This will remain a future objective. However the LCST behavior of star-shaped thermoresponsive polymers was believed to be dependent on the polyelectrolyte character of the system (i.e. hampered for low *pH*).<sup>92</sup> This was shown in the last section of this thesis.

## 1.6. References

1. Zhang, M.; Müller, A. H. E. *Journal of Polymer Science, Part A: Polymer Chemistry* **2005**, *43*, 3461.
2. Rühle, J.; Ballauff, M.; Biesalski, M.; Dziezok, P.; Gröhn, F.; Johannsmann, D.; Houbenov, N.; Hugenberg, N.; Konradi, R.; Minko, S.; Motornov, M.; Netz, R. R.; Schmidt, M.; Seidel, C.; Stamm, M.; Stephan, T.; Usov, D.; Zhang, H. *Advances in Polymer Science* **2004**, *165*, (Polyelectrolytes with Defined Molecular Architecture I), 79.
3. Minko, S. *Polymer Reviews* **2006**, *46*, 397.
4. Turner, S. R. *Polymeric Materials Science and Engineering* **1995**, *73*, 77.
5. Hawker, C. J.; Piotti, M. *ACS Symposium Series* **2000**, *755*, (Specialty Monomers and Polymers), 107.

6. Simon, P. F. W.; Radke, W.; Müller, A. H. E. *Macromolecular Rapid Communications* **1997**, *18*, 865.
7. Tomalia, D. A. *Scientific American* **1995**, *272*, 62.
8. Roovers, J.; Zhou, L. L.; Toporowski, P. M.; van der Zwan, M.; Iatrou, H.; Hadjichristidis, N. *Macromolecules* **1993**, *26*, 4324.
9. Schulz, G. V. *Z. Phys. Chem. (Leipzig)* **1939**, *B43*, 25.
10. Roovers, J., *Star and hyperbranched polymers*. Marcel Dekker: New York, 1999; p 285.
11. Quirk, R. P.; Lee, Y.; Kim, J., *Star and hyperbranched polymers*. Marcel Dekker, Inc.: New York, 1999; p 1.
12. Flory, P. J. *Journal of the American Chemical Society* **1943**, *65*, 372.
13. Bartovics, A.; Mark, H. *Journal of the American Chemical Society* **1943**, *65*, 1901.
14. Houwink, R. *Journal fuer Praktische Chemie* **1940**, *157*, 15.
15. Einstein, A. *Annalen der Physik* **1906**, *19*, 289.
16. Einstein, A. *Annalen der Physik* **1905**, *17*, 549.
17. Daoud, M.; Cotton, J. P. *Journal de Physique* **1982**, *43*, 531.
18. Flory, P. J.; Fox, T. G., Jr. *Journal of the American Chemical Society* **1951**, *73*, 1904.
19. Wang, J.-S.; Matyjaszewski, K. *Macromolecules* **1995**, *28*, 7572.
20. Wang, J.-S.; Greszta, D.; Matyjaszewski, K. *Polymeric Materials Science and Engineering* **1995**, *73*, 416.
21. Braunecker, W. A.; Matyjaszewski, K. *Progress in Polymer Science* **2007**, *32*, 93.
22. Zilliox, J. G.; Rempp, P.; Parrod, J. *Journal of Polymer Science, Polymer Symposia* **1968**, *22*, 145.
23. Chiefari, J.; Chong, Y. K. B.; Ercole, F.; Kristina, J.; Jeffery, J.; Le, T. P. T.; Mayadunne, R. T. A.; Meijs, G. F.; Moad, C. L.; Moad, G.; Rizzardo, E.; Thang, S. H. *Macromolecules* **1998**, *31*, 5559.
24. Greszta, D.; Mardare, D.; Matyjaszewski, K. *Macromolecules* **1994**, *27*, 638.
25. Barner-Kowollik, C.; Buback, M.; Charleux, B.; Coote, M. L.; Drache, M.; Fukuda, T.; Goto, A.; Klumperman, B.; Lowe, A. B.; McLeary, J. B.; Moad, G.; Monteiro, M. J.; Sanderson, R. D.; Tonge, M. P.; Vana, P. *Journal of Polymer Science, Part A: Polymer Chemistry* **2006**, *44*, 5809.
26. Matyjaszewski, K.; Xia, J. *Chemical Reviews* **2001**, *101*, 2921.
27. Wang, J.-S.; Matyjaszewski, K. *J. Am. Chem. Soc.* **1995**, *117*, 5614.
28. Sawamoto, M.; Kamigaito, M. *Trends Polym, Sci*, **1996**, *4*, 371.

29. Ando, T.; Kamigaito, M.; Sawamoto, M. *Polymer Preprints (American Chemical Society, Division of Polymer Chemistry)* **2002**, *43*, 179.
30. Davis, K. A.; Matyjaszewski, K. *Macromolecules* **2000**, *33*, 4039.
31. Zeng, F.; Shen, Y.; Zhu, S.; Pelton, R. *Macromolecules* **2000**, *33*, 1628.
32. Zheng, Q.; Pan, C.-y. *Macromolecules* **2005**, *38*, 6841.
33. Barner-Kowollik, C.; Davis, T. P.; Stenzel, M. H. *Australian Journal of Chemistry* **2006**, *59*, 719.
34. Mayadunne, R. T. A.; Jeffery, J.; Moad, G.; Rizzardo, E. *Macromolecules* **2003**, *36*, 1505.
35. Dufils, P.-E.; Gigmes, D.; Guerret, O.; Bertin, D.; Tordo, P. *Polymer Preprints (American Chemical Society, Division of Polymer Chemistry)* **2005**, *46*, 328.
36. Erdogan, T.; Gungor, E.; Durmaz, H.; Hizal, G.; Tunca, U. *Journal of Polymer Science, Part A: Polymer Chemistry* **2006**, *44*, 1396.
37. Ueda, J.; Kamigaito, M.; Sawamoto, M. *Macromolecules* **1998**, *31*, 6762.
38. Angot, S.; Murthy, K. S.; Taton, D.; Gnanou, Y. *Macromolecules* **1998**, *31*, 7218.
39. Taton, D.; Saule, M.; Logan, J.; Duran, R.; Hou, S.; Chaikof, E. L.; Gnanou, Y. *Journal of Polymer Science, Part A: Polymer Chemistry* **2003**, *41*, 1669.
40. Haddleton, D. M.; Edmonds, R.; Heming, A. M.; Kelly, E. J.; Kukulj, D. *New Journal of Chemistry* **1999**, *23*, 477.
41. Edmonds, R.; Bon, S. A. F.; Haddleton, D. M. *Polymer Preprints (American Chemical Society, Division of Polymer Chemistry)* **2000**, *41*, 444.
42. Kakuchi, T.; Narumi, A.; Matsuda, T.; Miura, Y.; Sugimoto, N.; Satoh, T.; Kaga, H. *Macromolecules* **2003**, *36*, 3914.
43. Held, D. Universität Mainz, Mainz, 2000.
44. Baek, K.-Y.; Kamigaito, M.; Sawamoto, M. *Journal of Polymer Science, Part A: Polymer Chemistry* **2002**, *40*, 1972.
45. Baek, K.-Y.; Kamigaito, M.; Sawamoto, M. *Journal of Polymer Science, Part A: Polymer Chemistry* **2002**, *40*, 2245.
46. Furukawa, T.; Ishizu, K. *Macromolecules* **2005**, *38*, 2911.
47. Buchard, W.; Lang, P.; Wolfe, M. S.; Spinelli, H. J.; Page, L. *Macromolecules* **1991**, *24*, 1306.
48. Gao, H.; Ohno, S.; Matyjaszewski, K. *Journal of the American Chemical Society* **2006**, *128*, 15111.

49. Dautzenberg, H.; Jaeger, W.; Kötz, J.; Philipp, B.; Seidel, C.; Stscherbina, D., *Polyelectrolytes: Formation, Characterization and Application*. Carl Hanser Verlag: Munich, 1994; p 104.
50. see, textbooks of polymer chemistry / physical chemistry / biochemistry.
51. Oosawa, F., *Polyelectrolytes*. Marcel Dekker: New York, 1971.
52. Onsager, L. *Ann. N. Y. Acad. Sci.* **1949**, *51*, 627.
53. Fuoss, R.; Katchalsky, A.; Lifson, S. S. *Proc. Natl. Acad. Sci. U.S.A.* **1951**, *37*, 579.
54. Alfrey, T.; Berg, P. W.; Morawetz, H. *J. Polym. Sci.* **1951**, *7*, 543.
55. Blaul, J. Osmotischer Koeffizient kettensteifer Polyelektrolyte auf der Basis von Poly(para-phenylen) in fremdsalzfreier Lösung. Universität Karlsruhe (TH), Karlsruhe, 2001.
56. Lifson, S.; Katchalsky, A. *J. Polym. Sci.* **1954**, *13*, 43.
57. Manning, G. S. *J. Chem. Phys.* **1969**, *51*, 924.
58. Jusufi, A.; Likos, C. N.; Löwen, H. *Journal of Chemical Physics* **2002**, *116*, 11011.
59. Flory, P. J. *Brookhaven Symposia in Biology* **1960**, *13*, 89.
60. Flory, P. J.; Fisk, S. *Journal of Chemical Physics* **1966**, *44*, 2243.
61. Katchalsky, A. *Pure and Applied Chemistry* **1971**, *26*, 327.
62. Das, B.; Guo, X.; Ballauff, M. *Progress in Colloid & Polymer Science* **2002**, *121*, 34.
63. Flory, P. J. *Journal of Chemical Physics* **1941**, *9*, 660.
64. Huggins, M. L. *Journal of Chemical Physics* **1941**, *9*, 440.
65. Flory, P. J. *Journal of Chemical Physics* **1942**, *10*, 51.
66. Shultz, A. R.; Flory, P. J. *Journal of the American Chemical Society* **1952**, *74*, 4760.
67. Ougizawa, T.; Inoue, T.; Kammer, H. W. *Macromolecules* **1985**, *18*, 2089.
68. Pfohl, O.; Hino, T.; Prausnitz, J. M. *Polymer* **1995**, *36*, 2065.
69. Halacheva, S.; Rangelov, S.; Tsvetanov, C. *Macromolecules* **2006**, *39*, 6845.
70. Nernst, W.; Bose, E. *Zeitschrift fuer Elektrochemie und Angewandte Physikalische Chemie* **1898**, *5*, 233.
71. van't Hoff, J. H. *Zeitschrift fuer Physikalische Chemie, Stöchiometrie und Verwandtschaftslehre* *5*, 174.
72. van 't Hoff, J. H. *Journal of Membrane Science* **1995**, *100*, 39.
73. Traube, J. *Berichte der Deutschen Chemischen Gesellschaft* *24*, 1321.
74. Schreiner, E. *Z. physik. Chem.* **1924**, *111*, 415.
75. Bjerrum, N. *Zeitschrift fuer Elektrochemie und Angewandte Physikalische Chemie* **1918**, *24*, 321.

76. Bjerrum, N. *Z. physik. Chem.* **1923**, *104*, 406.
77. Cantelo, R. C. *Journal of Physical Chemistry* **1929**, *33*, 627.
78. Schmitz, K., *An introduction to dynamic light scattering by macromolecules*. Acad. Press: Boston, 1990.
79. Brown, W., *Light scattering - principles and development*. Clarendon Press: Oxford, 1996.
80. Siegert, A. J. F. *MIT Rad Lab Rep No 465* **1943**.
81. Rayleigh, L. *Nature (London, United Kingdom)* **1920**, *104*, 276.
82. Einstein, A. *Annalen der Physik (Weinheim, Germany)* **1910**, *33*, 1275.
83. Debye, P. *Journal of Applied Physics* **1944**, *15*, 338.
84. Debye, P. *Journal of Physical and Colloid Chemistry* **1947**, *51*, 18.
85. Debye, P.; Chu, B.; Woermann, D. *Journal of Chemical Physics* **1962**, *36*, 1803.
86. Guinier, A. *Physics Today* **1969**, *22*, 25.
87. Williams, C. E.; May, R. P.; Guinier, A. *Mater. Sci. Technol.* **1994**, *2B*, 611.
88. Doty, P. M.; Zimm, B. H.; Mark, H. *Journal of Chemical Physics* **1944**, *12*, 144.
89. Jusufi, A.; Likos, C. N.; Löwen, H. *Physical review letters* **2002**, *88*, 018301.
90. Likos, C. N.; Hoffmann, N.; Jusufi, A.; Löwen, H. *Journal of Physics: Condensed Matter* **2003**, *15*, S233.
91. Hoffmann, N.; Likos, C. N.; Löwen, H. *Journal of Chemical Physics* **2004**, *121*, 7009.
92. Kudlay, A. N.; Erukhimovich, I. Y.; Khokhlov, A. R. *Macromolecules* **2000**, *33*, 5644.

## 2. Overview of thesis – Results

This thesis includes five publications, which are presented in Chapters 3 to 7.

We synthesized star-shaped poly(*tert*-butylacrylate) (PtBA) and the corresponding poly(acrylic acid) in the first publication (chapter 3). The number of functionalities, generated by the multifunctional sugar-initiators used, ranged between 5 and 21. Titration behavior was investigated in context with the determination of the osmotic coefficient. To obtain higher arm numbers, a novel silsesquioxane-based initiator was developed, which carries on average 58 initiation sites on a nanoparticle (see appendix 10.1).

Next, star-shaped poly(*N,N*-dimethylaminoethyl methacrylate) (PDMAEMA) with 3 to 24 arms was synthesized. The quaternization of PDMAEMA yields the corresponding quaternized PDMAEMA stars (poly[2-(methacryloyloxy)ethyl trimethylammonium iodide], PMETAI). The conformation of those strong polyelectrolyte stars was investigated in dependence of ionic strength and type of counterions. The osmotic coefficient was extracted and compared to theory (publication 2; chapter 4).

Strongly related, we investigated the conformation of the PMETAI stars in presence of multivalent counterions. The increasing valency of the counterions leads to a collapse of the star. By using photosensitive counterions the collapse is reversed by illumination as illustrated in publication 3 (chapter 5).

Finally, we investigated the thermoresponsive behavior of the PDMAEMA stars, synthesized in chapter 4. The differences in the occurrence of cloud points compared to linear PDMAEMA were extracted. The results are listed in publication 4 (chapter 6), whereas the discovery of an unexpected UCST-behavior of PDMAEMA is reported in publication 5 (chapter 7).

In the following, a summary of the main results is presented. We refer to the respective publication for experimental details.

## 2.1. Synthesis of Star-Shaped Polyelectrolytes

Star-shaped poly(acrylic acid) (PAA) was prepared by a two-step strategy (chapter 3). First *tert*-butyl acrylate (tBA) was polymerized by controlled radical polymerization using multifunctional initiators. Throughout this thesis modified glucose, saccharose and  $\beta$ -cyclodextrin have been used aiming for stars with 5, 8 and 21 arms. Those initiators were prepared and carefully characterized by means of mass spectrometry and NMR. By choosing different molar ratios of monomer to initiation sites and varying the conversion different arm lengths could be obtained. The PtBA stars were analyzed in terms of their molecular weight distribution by gel permeation chromatography (GPC) with viscosity detection. The obtained number averaged molecular weights  $M_n$  do coincide with the expected  $M_n(\text{theo})$  obtained by conversion and monomer to initiator ratio. The star-shaped PtBA was transformed to PAA by treatment with trifluoroacetic acid. The rather mild conditions provide almost quantitative elimination of isobutylene, yielding PAA. The ester groups used to attach the arms to the core stay almost completely intact (aqueous GPC). Those PAA stars could be methylated and again the molecular weights, obtained by mass spectrometry (matrix assisted laser desorption ionization – time of flight mass spectrometry; MALDI-ToF), do correlate with the theoretical molecular weights. After having obtained the star-shaped PAA, we could detach the arms by alkaline treatment for analysis of the arm length and arm length distribution. The experimentally determined arm lengths ( $DP_{\text{arm}}$ ) obtained after alkaline cleavage do coincide with the expected arm lengths. This was verified by both endgroup determination (by NMR) and mass spectrometry (MALDI-ToF of the methylated PAA arms). This indicates that the initiation site efficiency is close to unity and our stars carry the maximum arm number, given by the initiator molecule.

To increase the number of arms per star, a new initiator with a high number of initiation sites was required. Novel silsesquioxane nanoparticles bearing a high number of hydroxyl functions were prepared (see appendix 10.1).<sup>1</sup> Those particles, which are moderately polydisperse in terms of molecular weight ( $PDI \sim 1.2$ ), were used to prepare initiators with on average 58 initiation sites per molecule.

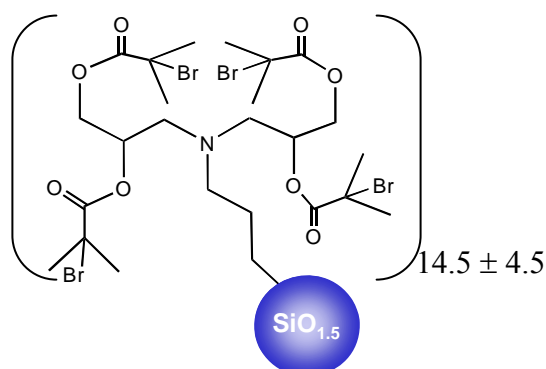


**Figure 2. 1: Structure of ATRP initiator with 58 functions**

Besides their use in preparation of glycopolymer stars,<sup>1</sup> they can be used for the synthesis of PtBA with arm number up to 40. We refer to the appendix (Chapter 10.1) for details on the preparation of PtBA / PAA stars using the silsesquioxane based initiators and difficulties encountered hereby (destruction of the core).

In contrast to those difficulties, the corresponding star-shaped poly(*N,N*-dimethylaminoethyl methacrylate) (PDMAEMA) could be easily quaternized to obtain strong polyelectrolytes (poly{[2-(methacryloyloxy)ethyl] trimethylammonium iodide; PMETAI; see chapter 4). The silsesquioxane core remains intact as seen by Asymmetric Field Flow Fractionation (AFFF). The preparation of star-shaped PDMAEMA followed in principle the method for synthesis of PtBA. The initiation site efficiency was considerably lowered (0.3 to 0.7) especially for the initiators with a high number of functionalities. The initiation site efficiency could be extracted by both conventional cleavage of the arms and by a statistical method: star-like fragments were detached from the core by HF and analyzed by GPC.

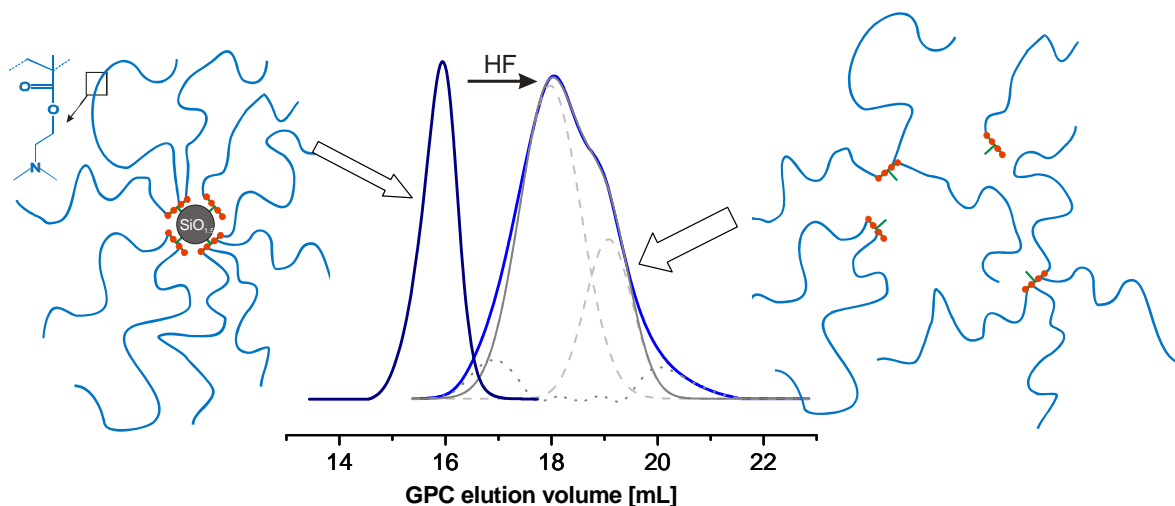
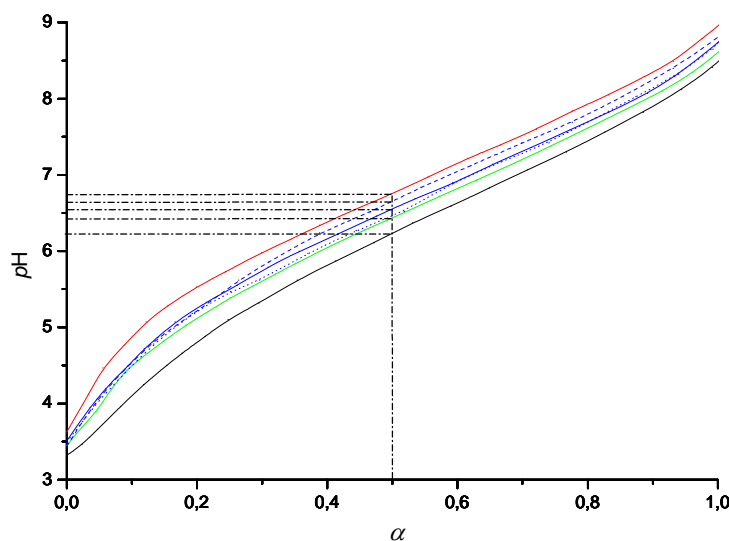


Figure 2. 2: Comparison of eluograms of (PDMAEMA<sub>170</sub>)<sub>18</sub> and the star-like PDMAEMA fragments obtained after treatment of (PDMAEMA<sub>170</sub>)<sub>18</sub> with HF

## 2.2. Titration Behavior of Star-Shaped Weak Polyelectrolytes

We now turn to some solution properties. We investigated the potentiometric titration behavior of the stars (chapter 3 and chapter 6). The degree of neutralization at a given *pH* was needed for the determination of the osmotic coefficient of PAA stars. We performed the titrations of the weak polyacid with NaOH in absence of additional salt, to compare directly to the conditions present during the determination of the osmotic coefficient (see chapter 2.3.). The segment density has a discernable influence on the position of the titration curves. The higher the arm number and the shorter the arms, the more basic the solution became for the

same polymer concentration. This was explained by the high osmotic pressure inside the star, which was also confirmed by the osmotic coefficients obtained by osmometry (chapter 2.3.). The high osmotic pressure from the  $\text{Na}^+$  ions inside the star hampers the deprotonation of the carboxy groups. This is possible since we investigated a weak polyelectrolyte. The equilibrium of the deprotonation of the acid can be altered by the osmotic pressure and at higher osmotic pressure less NaOH reacts with carboxy groups leading to an increased pH in the solution (see also change of acid-base equilibrium upon dialysis in appendix 10.3). For a more detailed investigation on the extraction of protonation equilibrium constants  $pK_{a,app}$  and  $pK_{a,0}$  we refer to appendix 10.2.



**Figure 2. 3:** Potentiometric titration curves for stars  $(\text{PAA}_{100})_{21}$  (—),  $(\text{PAA}_{100})_8$  (—),  $(\text{PAA}_{100})_5$  (—),  $(\text{PAA}_{75})_8$  (---),  $(\text{PAA}_{160})_8$  (⋯) and linear  $\text{PAA}_{100}$  (—);  $c \sim 0.6$  g/L; titrated with 0.048 n NaOH

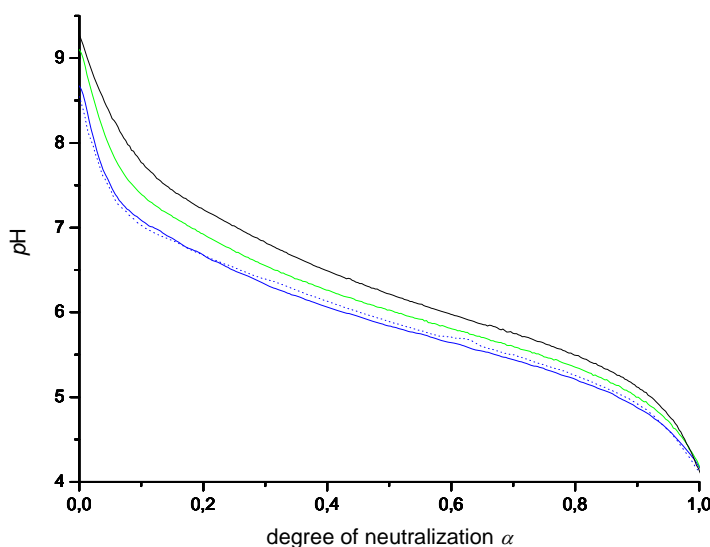


**Figure 2. 4:** Titration behavior of star-shaped PDMAEMA in Millipore water with 0.1 n HCl (1.0 g/L; 24 °C; —  $(\text{PDMAEMA}_{108})_1$ , —  $(\text{PDMAEMA}_{110})_{5.4}$ , —  $(\text{PDMAEMA}_{170})_{18}$ , ⋯  $(\text{PDMAEMA}_{240})_{24}$ )

PDMAEMA was titrated with HCl. The influence of the arm number on the  $pK_{b,app}$  was analogous: The higher the arm number the higher the  $pK_{b,app}$ . However the arm length

dependence could not undoubtedly be extracted due to lack of stars with the same arm number and different arm lengths (chapter 6).

### **2.3. Counterion Distribution of Star-Shaped Polyelectrolytes**

One foundation of polyelectrolyte physics, i.e. the counterion distribution, was compared to theoretical predictions before more complicated properties were extracted. Different means are available for determination of the counterion distribution. In the scope of this thesis mainly osmometry was applied, which delivers the osmotic coefficient,  $\phi$ . It is defined as the ratio of the experimental osmotic pressure to that expected according to van't Hoff's law,<sup>2-4</sup> while van't Hoff's law regards all counterions as equally osmotically active. Those results were also compared to results obtained by potentiometry for PAA stars (see appendix 10.3). Some stars were also investigated by Anomalous Small Angle X-Ray Scattering (ASAXS),<sup>5</sup> which can be used to extract the scattering contribution of solely the counterions (see appendix 10.3).

A strong counterion confinement could be seen by osmometry for the strong, star-shaped polyelectrolyte PMETAI (quaternized PDMAEMA) and for PAA at intermediate degrees of neutralization.

In contrast to problems in the stability of the signal for PAA with high degree of neutralization (see appendix 10.3), the osmotic pressure became constant after the initial rise due to injection of the sample into the osmometer for PAA with a low degree of neutralization.

The osmotic coefficient of  $(\text{PAA}_{100})_{21}$  ( $\alpha = 0.24$ ) can be compared to a strong polyelectrolyte star with similar arm number and comparable arm length,  $(\text{PMETAI}_{170})_{18}$ . As expected, the osmotic coefficient is decreased when increasing the ratio of charged units along the polymer chain.

The higher the arm number, the more counterions are confined, as shown for different PMETAI stars. This is in full agreement with theory.<sup>6</sup> The osmotic coefficient increases for longer arms at constant arm number, as expected by theory for a moderate increase in arm length (see Table 1. 1 and 1. 2).<sup>6</sup> However, the observed concentration dependence is not rendered by theory. Though the same order of magnitude is found by theory, the osmotic coefficient increases with increasing concentration. Possible reasons are discussed in chapter 3 and chapter 4.

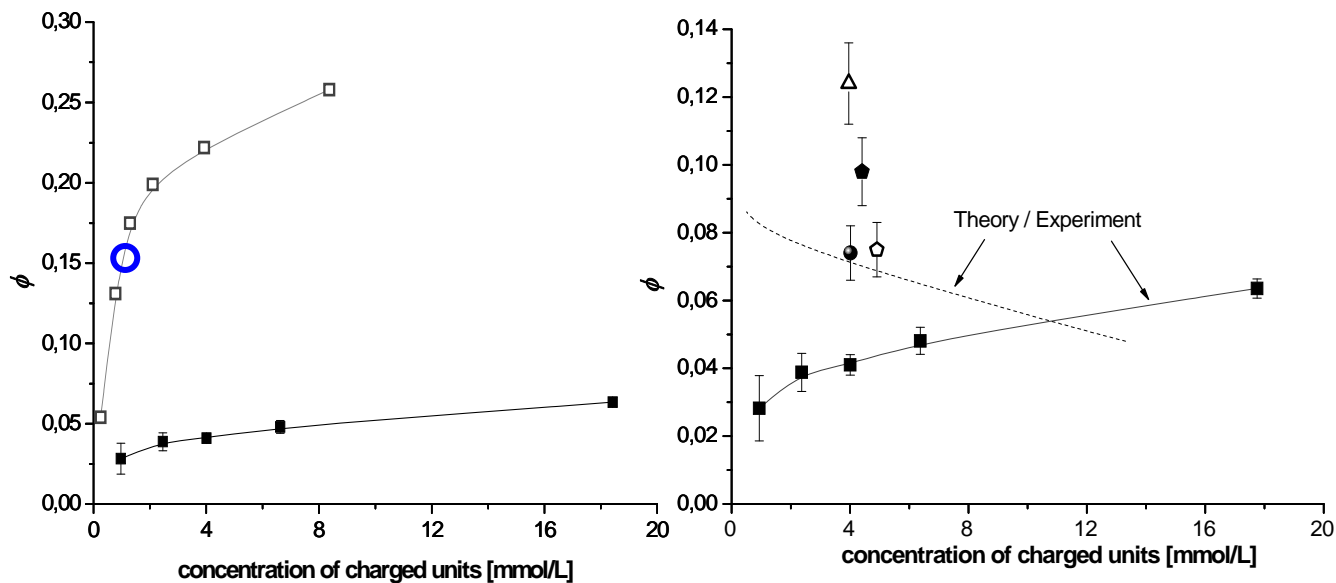


Figure 2. 5: Left hand side: osmotic coefficient  $\phi$  of  $(\text{PAA}_{100})_{21}$  ( $\alpha = 0.24$ ) compared to  $(\text{PMETA}_{170})_{18}$  in dependence of concentration; right hand side: osmotic coefficients,  $\Phi$ , of  $(\text{PMETA}_{170})_{18}$  (■),  $(\text{PMETA}_{170})_{9.5}$  (●),  $(\text{PMETA}_{110})_{5.4}$  (◊),  $(\text{PMETA}_{170})_{5.6}$  (◆), and  $(\text{PMETA}_{100})_{3.1}$  (△). Dashed line: theoretical dependence for a fully ionized star with 18 arms and  $DP_{\text{arm}} = 170$ ; blue symbol helps to compare with data from potentiometry in the appendix 10.3.

Those results show that the majority of the counterions (90% at full charge) is located inside the polyelectrolyte stars. This leads to a pronounced osmotic pressure inside the stars, which is compensated by a stretching of their arms (see chapter 2.4). Finally we can conclude that the counterion confinement of polyelectrolyte stars is of intermediate behavior compared to linear (e.g. PAA with  $\alpha' \sim 0.25$ :  $\phi \sim 0.4$ )<sup>7</sup> and densely grafted brush-like polyelectrolytes.<sup>8</sup> This is in full accordance to theory.<sup>6</sup>

## 2.4. Conformational Changes in Polycation Stars Induced by the Presence of Salt and the Use of Light-Sensitive Salt

After having investigated the counterion distribution in the salt-free case, we want to turn to the behavior of the stars in presence of salt. The hydrodynamic radius  $R_h$  was determined in dependence of the ionic strength (chapter 4).

The high osmotic pressure inside the stars is responsible for the stretching of the arms in the absence of salt (hydrodynamic radius  $R_H$  is ca. 50 % of their contour length). As expected, NaCl leads to a shrinkage (Figure 2. 6). Electrostatic and osmotic screening (net osmotic pressure inside the star is lowered upon salt addition) leads to a retraction of the arms. However the use of NaI leads to a more pronounced collapse of the star and the solution enters a two-phase region. This is explained by ion-specific interactions between the polycation and the counterions. At higher iodide concentrations salting-in occurs, which

might be induced by charge reversal of the star polymer.

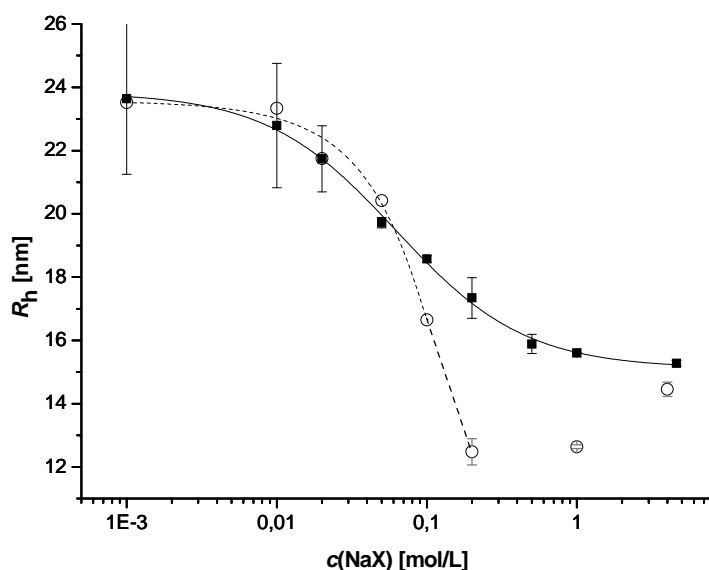


Figure 2. 6: Dependence of the hydrodynamic radius of star-shaped quaternized PDMAEMA, (PMETA<sub>170</sub>)<sub>18</sub>, with ionic strength; squares: NaCl; circles: NaI. The lines are guides for the eye.

But not only ionic strength determines the hydrodynamic radius. Presence of multivalent counterions can also lead to a collapse and finally to a phase separation of the stars even at constant ionic strength (chapter 5). This was shown by turbidimetric titrations, cryo-TEM (for both see appendix 10.4) and DLS of (PMETA<sub>170</sub>)<sub>18</sub> solutions with hexacyanocobaltate(III) ([Co(CN)<sub>6</sub>]<sup>3-</sup>) and tetracyanonickelate(II) ([Ni(CN)<sub>4</sub>]<sup>2-</sup>). The lower the valency of the counterions, the more counterions are needed to obtain the same collapse (Figure 2. 7).

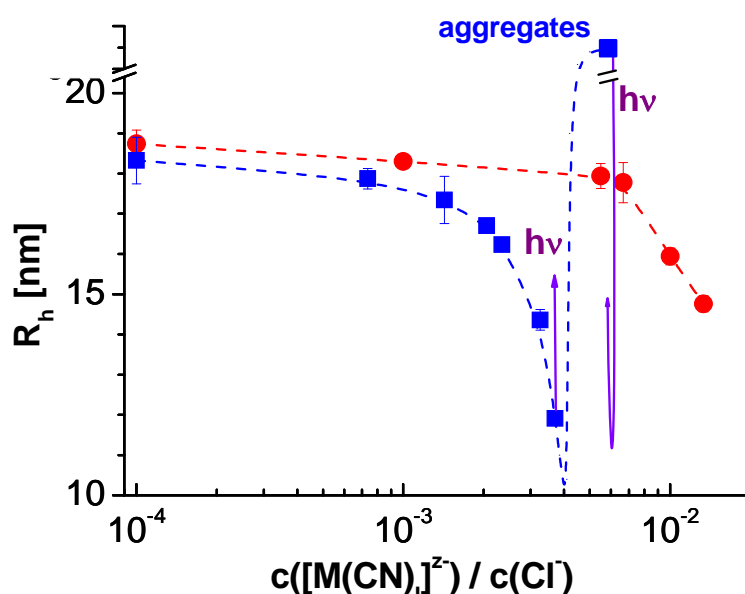
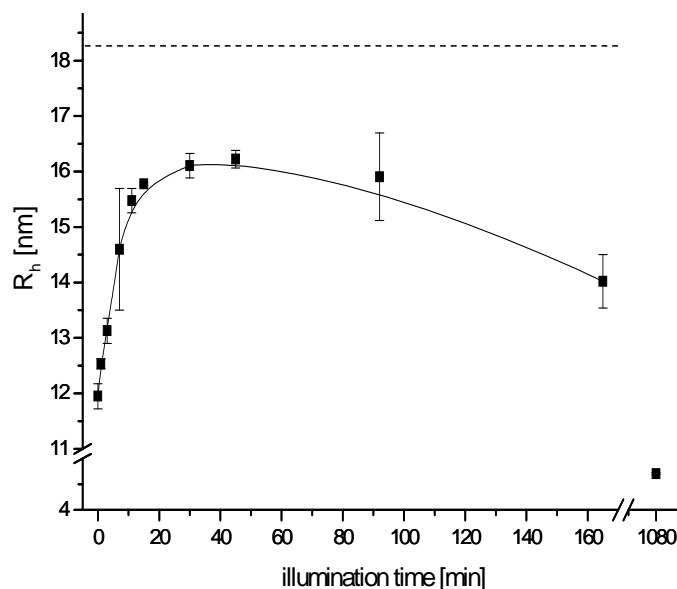


Figure 2. 7: Change of the hydrodynamic radius of the cationic star polyelectrolyte (0.5 g/L of (PMETA<sub>180</sub>)<sub>17</sub>) in dilute aqueous solutions with same ionic strength (0.1 M NaCl) but different ratios of mono- to multivalent salt; circles: titrated with 0.033 n divalent K<sub>2</sub>[Ni(CN)<sub>4</sub>]; squares: titrated with 0.0167 n trivalent K<sub>3</sub>[Co(CN)<sub>6</sub>]; the arrows indicate the principle of photostretching or photodissolution; the dashed lines are a guide to the eye

By use of  $[\text{Co}(\text{CN})_6]^{3-}$ , we can reverse this contraction by UV irradiation (chapter 5).<sup>9, 10</sup> Light exchanges one cyano ligand with water and the charge of the counterion is reduced (photoaquation). One counterion is decomposed into two counterions. This leads again to an increase in osmotic pressure inside the star and the star's arms stretch. We called those stars "nanoblossoms" due to the resemblance to real flowers.



**Figure 2. 8:** Photoinduced stretching measured by DLS of 0.5 g/L  $(\text{PMETA}_{170})_{18}$  in 0.1 N NaCl in presence of  $3.7 \cdot 10^{-4}$  mol/L  $\text{K}_3[\text{Co}(\text{CN})_6]$  in dependence of illumination time; the dotted line depicts the hydrodynamic radius of  $(\text{PMETA}_{170})_{18}$  in 0.1 N NaCl with  $3.7 \cdot 10^{-4}$  mol/L divalent  $[\text{Ni}(\text{CN})_4]^{2-}$ .

At extended illumination the hydrodynamic radius decreases again since  $\text{OH}^-$  is produced which can cause a cleavage of arms. Therefore the expected radius for a divalent cation (Figure 2. 7) is never reached. Only single arms can be detected after several hours. However  $R_h$  decreases only slightly in the same time period of 18 h when the sample was stored in darkness after intermediate irradiation. Again a parallel can be drawn to a flower, as too much light might cause the petals to wither. A countercheck was performed with a polyelectrolyte star solution without any trivalent counterions. Within several hours of irradiation no change of hydrodynamic radius was detected. For differences in the size distribution for interrupted and uninterrupted illumination see the appendix 10.4.

Chapter 5 also describes a way of dissolving the polymer-counterion complex by UV-irradiation (see Chapter 5 and appendix 10.4 for details).

By improving this method, the same principle may be used for the easy modification of a huge variety of branched polyelectrolytes into light-sensitive materials.

## 2.5. Temperature-Induced Phase Separation in Solutions of Star-Shaped and Linear PDMAEMA

We investigated the thermoresponsive behavior of the weak star-shaped polyelectrolyte PDMAEMA. PDMAEMA belongs to the class of polymers that exhibit a lower critical solution temperature (LCST), i.e. the polymer becomes insoluble in water at elevated temperatures. The question, how far the observed cloud points depend on the architecture, should be answered. To assure constant  $pH$  for all samples, the polymers were investigated in buffer.

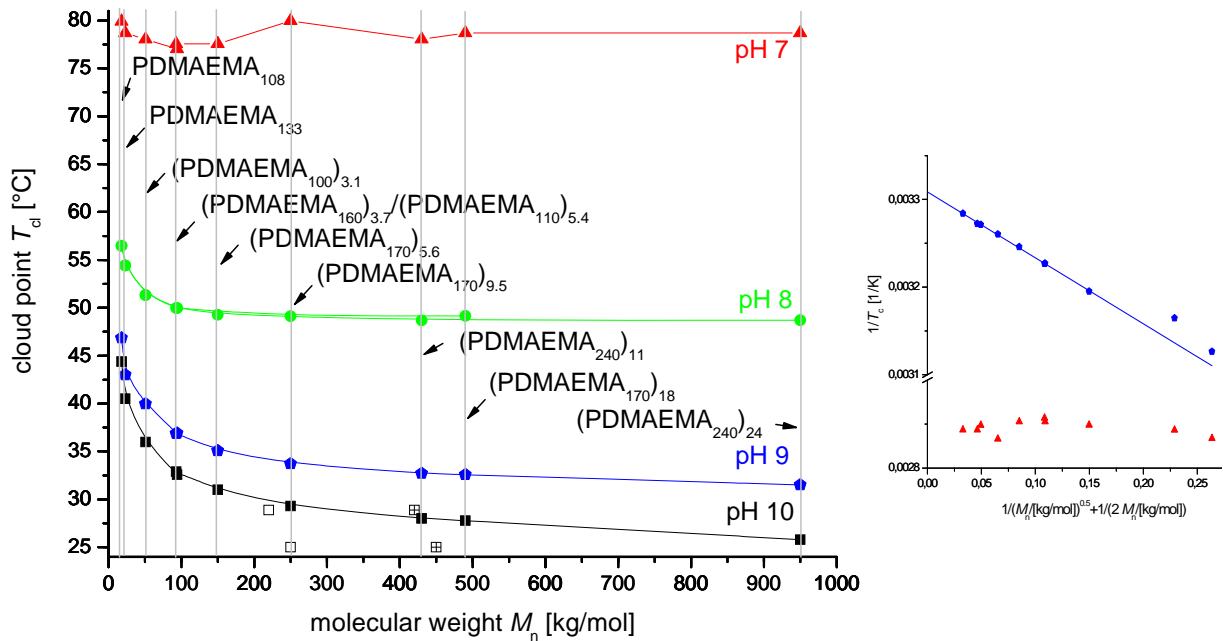


Figure 2. 9: Left hand side: cloud points  $T_{cl}$  at 0.1 g/L of star-shaped PDMAEMA in dependence of number averaged molecular weight and  $pH$  (black:  $pH = 10$ ; blue:  $pH = 9$ , green:  $pH = 8$ ; red:  $pH = 7$ ; hollow symbols: linear PDMAEMA prepared by free radical polymerization;  $\boxtimes$ : same polymers plotted against weight average molecular weight  $M_w$  obtained by GPC in THF); right hand side: plot of inverse  $T_c$  in dependence of modified inverse of molecular weight at  $pH = 9$  and  $pH = 7$ ; the solid lines are a guide to the eye

At high  $pH$  the observed cloud points show only dependence on the molecular weight (Flory-Huggins behavior). Architecture does not play a role. But for lower  $pH$  a slight modulation is observed: in addition to the shift of the whole cloud point curve to elevated temperatures,<sup>11</sup> the cloud points of stars with higher segment densities are shifted to slightly higher temperatures compared to stars with lower segment density. That means that charge density gains importance for lower  $pH$ . It was shown that the effect of charging on the cloud points is captured in a semiquantitative way by introducing the effective degree of polymerization  $DP_{eff}$  ( $1/DP_{eff} = 1/DP + \alpha'$ ;  $\alpha'$  equals the degree of ionization).

In contrast, the charge density has a major influence when regarding PDMAEMA solutions with pure Millipore water, where macroscopic phase separation is prevented for higher arm numbers (see appendix 10.5).

Addition of multivalent counterions leads in buffered solutions of PDMAEMA even to the appearance of an upper critical solution temperature (UCST: insoluble at low temperatures; see chapter 7 and appendix 10.5). The UCST-type miscibility gap shifts to higher temperatures when adding trivalent counterions, whereas the LCST-type cloud points hardly change (Figure 2. 10). Therefore a new facile system has been invented: The LCST-type transition can be adjusted by  $pH$ , whereas the UCST-type cloud points can be adjusted by the concentration of trivalent counterions. The light-sensitivity of hexacyanocobaltate(III) can be employed to an UV-light induced switching of the UCST-behavior. The UCST-behavior disappears upon illumination. This photoinduced dissolution is related to the one described in Chapter 2.4.

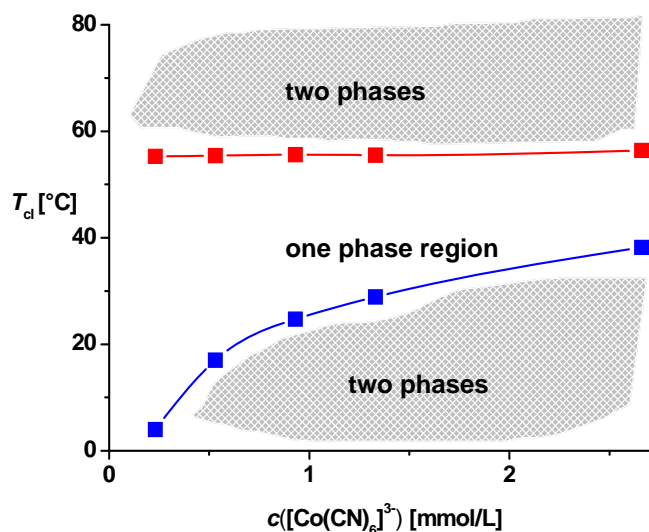


Figure 2. 10: Dependence of the cloud points  $T_{cl}$  of aqueous (PDMAEMA<sub>170</sub>)<sub>18</sub> solutions (0.1 g/L in buffer of  $pH$  8 + 0.1 n NaCl) on the  $[Co(CN)_6]^{3-}$  concentration (red symbols assign LCST-type cloud points, blue ones refer to cloud points of the UCST-behavior)

## 2.6. Individual Contributions to Joint Publications

The results presented in this thesis were obtained in collaboration with others and published as indicated below. In the following, the contributions of all the coauthors to the different publications are specified. The asterisk denotes the corresponding author.

### Chapter 3

This work is published in *Macromolecular Chemistry and Physics* **2005**, 206, p.1813, under the title “**Synthesis, characterization and behavior in aqueous solution of star-shaped**

**poly(acrylic acid)**” F. A. Plamper, H. Becker, M. Lanzendörfer, M. Patel, A. Wittemann, M. Ballauff, A. H. E Müller\*.

The publication was written by me and I have performed most of the experiments. Exceptions are stated in the following.

H. Becker was involved in preparation of saccharose-based initiator.

M. Lanzendörfer performed most of the MALDI-ToF measurements.

M. Patel and A. Wittemann introduced me to Osmometry.

M. Ballauff and A. Müller were involved in corrections of the manuscript and scientific discussions.

#### **Chapter 4**

This work is published in *Macromolecules* **2007**, *40*, p. 5689, under the title “**Synthesis and Characterization of Star-Shaped Poly(*N,N*-dimethylaminoethyl methacrylate) and Its Quaternized Ammonium Salts**” F. A. Plamper, A. Schmalz, E. Penott-Chang, M. Drechsler, A. Jusufi, M. Ballauff, A. H. E Müller\*.

The publication was written by me and I have performed most of the experiments. Exceptions are stated in the following.

A. Schmalz was involved in the preparation and characterization of sugar-based stars within the scope of his Hauptpraktikum under my guidance.

E. Penott-Chang performed the AFFF and some of the SLS measurements.

M. Drechsler measured cryo-TEM.

A. Jusufi established a theory for the osmotic coefficient of the PMETA<sub>I</sub> star.

M. Ballauff and A. Müller were involved in corrections of the manuscript and scientific discussions.

#### **Chapter 5**

This work is published in *Nano Letters* **2007**, *7*, p. 167, under the title “**Nanoblossoms: Light-Induced Conformational Changes of Cationic Polyelectrolyte Stars in the Presence of Multivalent Counterions**” F. A. Plamper, A. Walther, A. H. E Müller, M. Ballauff\*.

The publication was written by me and I have performed most of the experiments. Exceptions are stated in the following.

A. Walther performed the AFM measurements.

M. Ballauff and A. Müller were involved in corrections of the manuscript and scientific discussions.

## Chapter 6

This work is published in *Macromolecules* **2007**, *40*, p. 8361, under the title “**Tuning the Thermoresponsive Properties of Weak Polyelectrolytes: Aqueous Solutions of Star-Shaped and Linear Poly(dimethylaminoethyl methacrylate)**” F. A. Plamper, M. Ruppel, A. Schmalz, O. Borisov, M. Ballauff, A. H. E Müller\*.

The publication was written by me and I have performed most of the experiments. Exceptions are stated in the following.

M. Ruppel set up the titration equipment used for the turbidity measurements and he was involved in scientific discussions.

A. Schmalz prepared and characterized some of the PDMAEMA samples during his Hauptpraktikum under my supervision.

O. Borisov, M. Ballauff and A. Müller were involved in corrections of the manuscript and scientific discussions.

## Chapter 7

This work is published in *Journal of the American Chemical Society* **2007**, *129*, p. 14538, under the title “**Tuning the Thermoresponsiveness of Weak Polyelectrolytes by pH and Light: Lower and Upper Critical-Solution Temperature of Poly(*N,N*-dimethylaminoethyl methacrylate)**” F. A. Plamper, A. Schmalz, M. Ballauff, A. H. E Müller\*.

The publication was written by me and I have performed most of the experiments.

A. Schmalz was involved in some cloud point measurements.

M. Ballauff and A. Müller were involved in corrections of the manuscript and scientific discussions.

## 2.7. References

1. Muthukrishnan, S.; Plamper, F.; Mori, H.; Müller, A. H. E. *Macromolecules* **2005**, *38*, 10631.
2. van't Hoff, J. H. *Zeitschrift fuer Physikalische Chemie, Stöchiometrie und Verwandtschaftslehre* **5**, 174.
3. van 't Hoff, J. H. *Journal of Membrane Science* **1995**, *100*, 39.
4. Traube, J. *Berichte der Deutschen Chemischen Gesellschaft* **24**, 1321.
5. Ballauff, M.; Patel, M.; Rosenfeldt, S.; Dingenouts, N.; Narayanan, T.; Mueller, A.; Plamper, F. *PMSE Preprints* **2005**, *93*, 232.
6. Jusufi, A.; Likos, C. N.; Löwen, H. *Journal of Chemical Physics* **2002**, *116*, 11011.

7. Katchalsky, A. *Pure and Applied Chemistry* **1971**, 26, 327.
8. Das, B.; Guo, X.; Ballauff, M. *Progress in Colloid & Polymer Science* **2002**, 121, 34.
9. MacDiarmid, A. G.; Hall, N. F. *Journal of the American Chemical Society* **1953**, 75, 5204.
10. Wrighton, M.; Hammond, G. S.; Gray, H. B. *Journal of the American Chemical Society* **1971**, 93, 5254.
11. Kudlay, A. N.; Erukhimovich, I. Y.; Khokhlov, A. R. *Macromolecules* **2000**, 33, 5644.

### 3. Synthesis, Characterization and Aqueous Solution Behaviour of Star-shaped Poly(acrylic acid)

*Felix A. Plamper<sup>a</sup>, Harald Becker<sup>a</sup>, Michael Lanzendörfer<sup>a</sup>,*

*Mushtaq Patel<sup>b</sup>, Alexander Wittemann<sup>b</sup>, Matthias Ballauff<sup>b</sup>, Axel H. E. Müller<sup>\*a</sup>,*

<sup>a</sup>Makromolekulare Chemie II, <sup>b</sup>Physikalische Chemie I, and Bayreuther Zentrum für Kolloide und Grenzflächen, Universität Bayreuth, D-95440 Bayreuth, Germany ; Fax +49-921-553393,

**Published in *Macromolecular Chemistry and Physics* 2005, 206, p.1813.**

**ABSTRACT:** We report the synthesis of star-shaped poly(*tert*-butyl acrylate) (PtBA) by atom transfer radical polymerization. We employ the core-first approach using glucose, saccharose and cyclodextrin based initiators leading to stars bearing five, eight and twenty one arms. Subsequent acidic treatment of PtBA leads to star-shaped poly(acrylic acid) (PAA). Alkaline cleavage of the arms enabled us to determine the initiation site efficiency. The PAA stars and arms were esterified to poly(methyl acrylate) (PMA). Molecular weight determination by means of GPC/viscosity, MALDI-ToF MS and NMR endgroup determination showed that initiation site efficiency is close to unity. Potentiometric titration of PAA arms and stars results increasing apparent  $pK_a$  values with increasing arm number, which is a direct result of increasing segment density. Osmometry measurements of aqueous solutions of the PAA stars result in osmotic coefficients between 0.05 and 0.38, indicating that most of the counterions are confined within the star. The confinement increases with arm number.

### 3.1. Introduction

Polyelectrolytes with non-linear topologies have attracted considerable interest in recent years. Rod-like polyelectrolytes<sup>1, 2</sup> have proven to be a good model for the experimental verification of Fuoss',<sup>3</sup> Osawa's<sup>4</sup> and Manning's<sup>5</sup> predictions about the counterion condensation, i.e. the reduction of osmotically active counterions due to electrostatical attraction to the highly charged polyelectrolyte backbone. The situation is more complicated for branched polyelectrolytes with hyperbranched,<sup>6, 7</sup> star-, comb-, or brush-like structures.<sup>8, 9</sup> Planar,<sup>9, 10</sup> spherical<sup>11</sup> and cylindrical<sup>12, 13</sup> polyelectrolyte brushes have been prepared. The swelling behaviour of spherical brushes depending on  $pH$ ,<sup>14</sup> ionic strength<sup>14</sup> and counterions<sup>15</sup> was investigated. The osmotic coefficient  $\phi$ , which is a measure for counterion condensation, is defined as the ratio of measured osmotic pressure and theoretical osmotic pressure according to van't Hoff's law.<sup>16</sup> The osmotic coefficient of spherical brushes<sup>17</sup> was seen to be reduced by one order of magnitude compared to linear polyelectrolytes.<sup>18-21</sup> Intermediate effects on counterion condensation are expected for star-shaped polyelectrolytes as predicted by previous work.<sup>22</sup> Scaling theory together with self-consistent field calculations of polyelectrolyte stars were given by Klein Wolterink et al.<sup>23, 24</sup> and Borisov and Zhulina.<sup>25, 26</sup> Ordered, crystalline phases are expected at higher concentrations and arm numbers.<sup>27, 28</sup> The first experimental proof of such phases was given by Furukawa and Ishizu.<sup>29</sup>

Potentiometric titrations of linear polyacids and polybases were performed and discussed.<sup>18, 30-32</sup> In contrast to low molecular acids, where distinct deprotonation equilibrium constants due to distinct ionization processes can be observed, only average equilibrium constants depending on ionization degree can be extracted for polyacids. Polymer's architecture changes titration behaviour,<sup>24, 33</sup> as was shown for hyperbranched polyacids<sup>6</sup> and predicted by Klein Wolterink et al. for star-shaped weak polyacids by self-consistent field calculations.<sup>24</sup>

Star-shaped polyelectrolytes have been synthesized by different approaches. The arm-first strategy was used by Mays et al., linking polystyryl lithium arms with divinylbenzene, followed by sulfonation to yield poly(styrene sulfonate) stars.<sup>34, 35</sup> Similarly, living anionic poly(*tert*-butyl acrylate) (PtBA) arms were coupled by ethyleneglycol dimethacrylate,<sup>36</sup> followed by elimination of isobutylene to form poly(acrylic acid) (PAA) stars.<sup>8</sup> Later, the same attempt was taken up using atom transfer radical polymerization (ATRP).<sup>29</sup> The arm-first method with difunctional monomers leads to large arm numbers, however, with a rather broad distributions of arm numbers. In contrast, defined multifunctional terminating agents

circumvent this problem. Thus, poly(methacrylic acid) (PMAA) and PAA stars with three, four, and eight arms<sup>37, 38</sup> were obtained.

In the core-first approach polymerization is conducted from an oligofunctional initiator, leading to well-defined stars with a precisely defined arm number. This approach was applied to the synthesis of PAA stars using the ATRP of tBA. Schnitter et al.<sup>39</sup> used an initiator with six  $\alpha$ -bromoester functions esterified with a dendritic core, whereas Moinard et al.<sup>40</sup> used a core carrying four benzyl bromide functions.

In this paper we describe the synthesis and characterization of star-shaped poly(acrylic acid) with five, eight, and 21 arms. In contrast to Schnitter's core-first attempt<sup>39</sup> we attached 2-bromoisobutyrate initiator functions to sugars, namely  $\alpha$ -D-glucose, saccharose and  $\beta$ -cyclodextrin.<sup>41-44</sup> ATRP of tBA lead to the corresponding poly(*tert*-butyl acrylate) stars. These were transformed to poly(acrylic acid) stars by acidic isobutylene elimination. The PAA stars were used to investigate the aqueous solution behaviour of star-shaped weak polyelectrolytes, in particular counterion condensation by means of osmometry. For this purpose potentiometric titrations were also performed.

This paper is organized as follows: First we describe the synthesis of PAA stars and the molecular characterization of both stars and single arms. Then we show first potentiometric titrations and osmometry performed on these stars. Those measurements show that star-shaped PAA differs significantly from their linear analogues. A detailed discussion of those effects will be given in a separate paper.

## 3.2. Experimental Part

**Materials.** 2-Bromoisobutyryl bromide,  $N,N,N',N',N''$ -pentamethyldiethylenetriamine (PMDETA), CuBr, 4-( $N,N$ -dimethylamino)pyridine,  $CF_3COOH$ , 1,4-dioxane, trans-3-indolacrylic acid (IAA), 2,5-dihydroxybenzoic acid (DHB), trimethylsilyldiazomethane and acidic ion-exchange resin (Dowex Marathon) were purchased from Aldrich,  $\alpha$ -D-glucose, pyridine,  $CH_2Cl_2$ , THF, silica gel 60, methanol (MeOH) and  $CHCl_3$  from Merck, saccharose from Aldi-Süd.  $\beta$ -Cyclodextrin was supplied by Avocado, Heysham, UK. These chemicals were taken as delivered (except PMDETA, which was also distilled and degassed, and CuBr, which was treated with pure acetic acid and filtered to remove traces of Cu(II) compounds). *tert*-Butyl acrylate was donated by BASF. It was distilled and the first and last fractions were discarded to remove low molecular mass inhibitor. Irganox 1010 stabilizer (Ciba) was added before the monomer was condensed on the vacuum line to finally degas it by help of three

freeze-thawing cycles. Chemicals needed for polymerization were transferred into the glove box.

**Synthesis of Oligoinitiators.** A typical preparation procedure is described for heptakis[2,3,6-tri-*O*-(2-bromoisobutyryl)]- $\beta$ -cyclodextrin.<sup>[41,42]</sup>  $\beta$ -Cyclodextrin (21.4 g; 0.019 mol) was dehydrated in a vacuum oven at 80 °C for 1 h. Then it was suspended in 120 mL pyridine and 250 mL chloroform. One tip of spatula of 4-(*N,N*-dimethylamino)pyridine was added as a catalyst before the mixture was cooled with ice. By use of a dropping funnel 2-bromoisobutyryl bromide (184 g; 0.8 mol) was added within 4 h to the suspension. The mixture was stirred for one day at room temperature and then it was refluxed for 3 h. The pyridinium bromide was removed by filtration. The liquid was carefully washed two times with 1 N HCl, once with concentrated NaHCO<sub>3</sub> solution, once with 1 N NaCl solution and finally with water. The organic phase was dried with Na<sub>2</sub>SO<sub>4</sub> and concentrated on the rotational evaporator. The yellow-brownish residue was chromatographed over a silica column (toluene:ethyl acetate = 3:1 by vol.) which resulted a yellow solid (28.3g; 35 % yield). The product was further purified to an almost colourless solid by recrystallization from warm *n*-hexane (15.17g; 19 % yield). Full esterification was confirmed by MALDI-ToF mass spectrometry (matrix DHB; mass ratio DHB:LiCl:initiator 10:1:1; reflection mode and linear mode;  $M(+Li^+) = 4267$  g/mol). <sup>1</sup>H-NMR (CDCl<sub>3</sub>): 1.8 (broad s, 126H, CH<sub>3</sub>), 3.5 - 5.4 (49 H, sugar protons)

Analogous procedures were used for the preparation of 2,3,4,6,1',3',4',6'-octa-*O*-(2-bromoisobutyryl)-saccharose and 1,2,3,4,6-penta-*O*-(2-bromoisobutyryl)- $\alpha$ -D-glucose using saccharose or  $\alpha$ -D-glucose as scaffold<sup>[42-44]</sup>. The workup changed so far as pyridinium bromide was not filtered but it was removed by repeated extraction with cold water after the mixture was diluted with ~ 100 mL diethylether. The organic phase was concentrated after it was extracted with concentrated NaHCO<sub>3</sub> solution. The solid was washed with cold methanol. Drying in vacuum oven yielded a white powder (yield: 73 % for glucose-based initiator and 72 % for saccharose-based initiator). Saccharose-based initiator:  $M(+Li^+) = 1541$  g/mol by MALDI-ToF MS (DHB:LiCl:initiator 10:1:1). Glucose-based initiator:  $M(+Li^+) = 931$  g/mol.

**Synthesis of poly(*tert*-butyl acrylate) stars.** A typical polymerization procedure proceeds as follows:<sup>[39]</sup> In a glove box CuBr (14.6 mg; 0.102 mmol) and initiator (e.g. cyclodextrin-based initiator: 50 mg;  $1.17 \cdot 10^{-5}$  mol) were weighed in into a 50 mL round bottom flask which was tightly closed with a seal bearing a septum. *tert*-Butyl acrylate (tBA) (10.4 g; 81 mmol)

and ligand PMDETA (21.3 mg; 0.123 mmol) were added. The molar ratio [initiation site]:[PMDETA]:[CuBr] was about 1:0.50:0.42 and should to be readjusted when heading for different arm lengths. The initially heterogeneous mixture was stirred outside the glovebox at 60 °C to 65 °C in an oil bath. The monomer conversion  $x_p$  was traced by taking samples through the septum under nitrogen counter flow and comparing the NMR signals of the monomer (vinylic protons at 6.3 ppm) and the polymer (methine protons at 2.2 ppm). The conversion was used to calculate the theoretical degree of polymerization per arm

$$DP_{n,theo,arm} = x_p \cdot [tBA]_0/[inisite]_0 \quad 3.1.$$

were  $[tBA]_0$  and  $[inisite]_0$  are the initial monomer and initiation site concentrations, respectively. After 9 h the monomer conversion was 38.4 % and the reaction was stopped by diluting the yellow-green, viscous mixture with acetone (or THF) in presence of oxygen. The solution was then filtered over silica gel to remove copper compounds. The obtained poly(*tert*-butyl acrylate) (PtBA) was freeze-dried from dioxane, which yields 3.1 g polymer after drying in vacuum oven at 40 °C.

**Table 3. 1: Experimental conditions for the synthesis of PtBA stars<sup>a</sup>**

parameter	(PtBA <sub>90</sub> ) <sub>5</sub>	(PtBA <sub>75</sub> ) <sub>8</sub>	(PtBA <sub>100</sub> ) <sub>8</sub>	(PtBA <sub>160</sub> ) <sub>8</sub>	(PtBA <sub>60</sub> ) <sub>21</sub>	(PtBA <sub>100</sub> ) <sub>21</sub>	(PtBA <sub>125</sub> ) <sub>21</sub>
[tBA] <sub>0</sub> (mol/L)	5.4 <sup>b</sup>	6.8 (bulk)	5.4 <sup>b</sup>	bulk	bulk	5.4 <sup>b</sup>	bulk
[Inisite] <sub>0</sub> (mmol/L)	35	34	30	21	24	29	21
[CuBr] (mmol/L)	35	10	30	21	7	29	9
<i>t</i> (min)	145	270	125	180	140	285	540
conversion, $x_p$ <sup>c</sup>	0.56	0.37	0.56	0.48	0.22	0.53	0.38

<sup>a</sup> T ≈ 65 °C, [PMDETA]/[CuBr] ≈ 1, <sup>b</sup> solvent: ethylacetate, <sup>c</sup> measured by NMR

**Transformation to poly(acrylic acid):**<sup>6, 13</sup> PtBA (2.3 g) was dissolved in about 20 mL dichloromethane which results in a slightly yellow solution. After addition of trifluoroacetic acid (10.5 g) the colour of the mixture turned darker and after one night with stirring at room temperature the PAA had precipitated. The white precipitate was dissolved in 20 mL dioxane and 4 mL methanol and freeze-dried to remove trifluoroacetic acid, which gave 1.3 g of PAA star.

**Cleavage of arms by alkaline hydrolysis.** 0.1 g (PAA) stars and about 0.2 g NaOH were dissolved in about 2 mL water (in polyethylene vials) and heated for 5 days at 80 °C. Then the pure linear PAA was recovered by use of a sufficient amount (~ 5 g) of acidic ion exchange resin until reaching  $pH \sim 3$ . The resin was removed and the aqueous solution was freeze-dried. Full cleavage was proven by comparison of the elution volumes of the star-shaped PAA and the linear PAA by means of aqueous GPC.

**Methylation of PAA:**<sup>45</sup> Star-shaped and linear PAA were methylated with trimethylsilyldiazomethane. Typically a solution of 0.1 g PAA in about 1 mL water and 3 mL THF was prepared. Then roughly 1 mL trimethylsilyldiazomethane (2 M in diethylether) was added drop wise under vigorous stirring. When the mixture became cloudy during methylation additional THF was added. The addition was stopped when the yellow colour did not vanish within typically 1 h. The solvent was slowly evaporated. Then the crude mixture was dissolved in a small amount of acetone and the polymer was precipitated into cold methanol (-30 °C). The viscous polymer was finally freeze dried from dioxane. <sup>1</sup>H NMR (CDCl<sub>3</sub>): 1.4 (s, t-butyl if present), 1.5 - 2.0 (methylene protons from backbone), 2.1 - 2.5 (methine protons), 3.32 (s, CH<sub>3</sub>-O-CH<sub>2</sub>CO), 3.35 - 3.45 (not assigned), 3.64 (s, CH<sub>3</sub>-OCO), 3.9 - 4.2 (s, CH<sub>3</sub>-O-CH<sub>2</sub>CO). <sup>13</sup>C NMR (CDCl<sub>3</sub>): 25.7, 26.4, 28.3 (CH<sub>3</sub>-C, residual *tert*-butyl, initiator?), 35.4 (CH<sub>2</sub>-backbone), 41.7 (methine carbons), 52.1 (CH<sub>3</sub>-OCO), 58.9 (CH<sub>3</sub>-O-CH<sub>2</sub>-CO), 64.4 ((CH<sub>3</sub>)<sub>3</sub>C-O), 72.4 (CH<sub>3</sub>-O-CH<sub>2</sub>-CO), 174.8, 175.2 (both carbonyl).

**Purification:** *Purification of PAA by dialysis:* 1 g of (PAA<sub>n</sub>)<sub>x</sub> was dissolved in about 25 mL of water and dialysed against Millipore water for typically 5 days (spectrapore cellulose ester membrane, MWCO 6 kDa). The purified aqueous solution was finally freeze-dried and then dried in vacuum oven at 40 °C.

*Purification of PAA by ultrafiltration:* 15 g of (PAA)<sub>x</sub> were dissolved in 300 mL water. These solutions were ultrafiltrated (polyethersulfone membrane MWCO 10 and 30 kDa; Millipore) with approximately 10 L Millipore™ water. To prevent any potential harm to the stars like cleavage, the process was interrupted after about 3 days. The purified aqueous solution was finally freeze-dried and then dried in vacuum oven at 40 °C.

*Purification of sodium salt of PAA by dialysis:* Dialysis against Millipore™ water was used as purification method to prevent germs and dust being concentrated within the sample solution. About 200 mg of PAA stars and 70 mg NaOH were dissolved in 30 mL Millipore™ water and filled into dialysis tubes (Spectra Pore™; regenerated cellulose membrane; Ø ~ 2 cm; MWCO: 6 - 8 kDa), which was stirred in 5 L of Millipore™ water. The water was

exchanged almost daily. After two weeks the purification process was stopped and the solid contents of the resulting mother solutions were determined by freeze-drying. pH measurement of a 0.7 g/L solution was used for determination of the degree of neutralization (see Potentiometric Titration).

To verify stability of all stars during purification we performed GPC in aqueous buffer solution of samples before and after purification.

**Polymer characterization.** *<sup>1</sup>H and <sup>13</sup>C NMR spectroscopies.* A Bruker Avance (250 MHz) spectrometer was used. The concentrations in solutions were around 10 mg/mL each whereas solvent was either D<sub>2</sub>O or CDCl<sub>3</sub>. Simulations were performed with ACD/HNMR and ACD/CNMR Predictor Ver.3.00.

*FT-IR spectroscopy* (Bruker Equinox 55/S): Poly(methyl acrylate) (PMA) and Poly(acrylic acid) (PAA) was dissolved in acetone and methanol respectively and applied on a KBr plate and dried at 80°C for several minutes.

*MALDI-ToF mass spectrometry* was performed on a Bruker Daltonics Reflex 3 with N<sub>2</sub> laser (337 nm) at 20 kV acceleration voltage. We used trans-3-indolacrylic acid (IAA) as matrix (mass ratio IAA : polymer = 10 : 1) for molecular weight determination of PtBA and PMA polymers. Most measurements were performed in linear mode, except for polymers with  $M_n < 10,000$  g/mol, where reflection mode was used. In case of detection of doubly charged species, a double Gaussian fit was used to extract  $M_n$  and *PDI* of the desired species. Overlap with signals of matrix or low molecular compounds was resolved – if necessary – by Gaussian fit in the undisturbed region. Assuming initiation efficiency,  $f_i$ , close to unity, star's  $M_n$  was taken to determine  $DP_{n,arm}$  by dividing  $M_n$  with the molecular weight of the repeating unit  $M_r$  and the initiation sites per initiator molecule. For PMA stars  $M_r$  was assessed to 90 g/mol to reflect residual *tert*-butyl groups and methylene insertion into the methyl ester moieties according to NMR-spectra (see Figure 3. 6). The molecular mass of the initiator core was taken into account for stars. For linear PMA only double methylation and the residual initiation moiety was taken into account ( $M_r = 88$  g/mol). For simulation of the mass distribution of single molecules due to isotopical statistics we used Bruker Xtof 5.1.1 software.

*Gel Permeation Chromatography (GPC)*: Molecular weight distributions and averages were characterized by conventional GPC and GPC/viscosity using THF as eluent at a flow rate of 1.0 mL/min at room temperature. A conventional THF-phase GPC system was used to obtain apparent molecular weights. GPC system I: column set: 5  $\mu$ m PSS SDV gel, 10<sup>2</sup>, 10<sup>3</sup>, 10<sup>4</sup>, 10<sup>5</sup> Å, 30 cm each; injection volume 20  $\mu$ L of a 2 mg/mL solution; detectors: Waters 410

differential refractometer and Waters photodiode array detector. Narrow PS standards (PSS, Mainz) were used for the calibration of the column set I. Molecular weights of the star-shaped polymers were determined by the universal calibration principle<sup>[46]</sup> using the viscosity module of the PSS WinGPC scientific V 6.1 software package on GPC system II. Linear PMMA standards (PSS, Mainz) were used to construct the universal calibration curve. GPC system II: column set: 5  $\mu\text{m}$  PSS SDV gel, 10<sup>3</sup> Å, 10<sup>5</sup> Å and 10<sup>6</sup> Å, 30 cm each; detectors: Shodex RI-71 refractive index detector, Jasco Uvidec-100-III UV detector ( $\lambda = 254$  nm), Viscotek viscosity detector H 502B, which needs to be purged extensively before every measurement. The extracted number average molecular mass  $M_n$  was used to determine the degree of polymerization  $DP_{n,\text{arm}}$  of one arm by dividing  $M_n$  by the molar mass of the polymer's repeating unit and – for stars – by the initiation sites per initiator molecule (assumption  $f_i = 1$ ). The initiator was taken into account. The third setup was an aqueous GPC (internal standard ethylene glycol; additives: 0.1 M  $\text{NaN}_3$ , 0.01 M  $\text{NaH}_2\text{PO}_4$ ), which validated the intactness of our PAA stars before and after purification steps. Column set: two 8mm PL Aquagel-OH columns (mixed and 30 Å), operated at 35°C. Detector: Bischoff RI-Detector 8110.

*Potentiometric Titration:* In order to determine the degree of neutralization at ambient temperatures we carried out potentiometric titrations of PAA stars at crude mass concentrations of 0.6 g/L ((PAA<sub>75</sub>)<sub>8</sub> and (PAA<sub>160</sub>)<sub>8</sub>) to 0.7 g/L (for all other stars), which is within the concentration range of our osmotic pressure measurements. Adsorbed water and residual *tert*-butyl can reduce the molar carboxy concentration by up to 20 % ([COOH]  $\approx$  8 mmol/L]). To complete the series, we also titrated linear PAA, which was cleaved from (PAA<sub>100</sub>)<sub>21</sub>. We used pH-Meter CG 840 (Schott), which was calibrated by buffer solutions. The titration was carried out with 0.048 N NaOH, i.e. the volume change does not exceed 20 %. The equivalence point of the titration is set as the point of intersection of the inflection tangents of the titration curve at high *pH*. The steep increase of *pH* at the end of titration is caused by excess NaOH. The equivalence point which is theoretically determined by knowledge of the added masses is only insufficiently precise as PAA is hardly to obtain totally water free. When measuring titration curves on different days, an already measured system was again investigated for comparison to shift the whole new data set to the old values to obtain relative correctness. The shift in *pH* (due to changes in temperature and calibration solutions) of the same system at different times is small, being within 0.08 *pH* units.

*Osmometry:* A membrane osmometer Gonotec Osmomat 090 was used for the determination of the osmotic coefficient. The cell was kept at 30 °C. We used a Sartorius

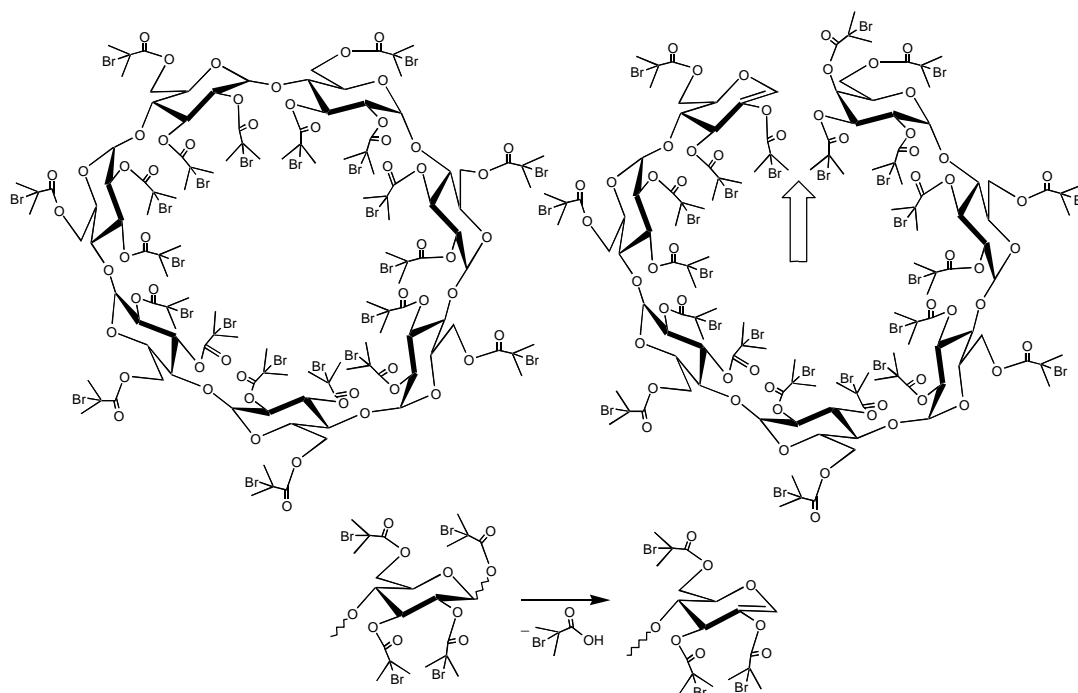
cellulose triacetate membrane (nominal molecular weight cutoff of 5 kDa). Directly after purification of the partially neutralized PAA stars the obtained mother solutions were used to prepare a concentration series by dilution with Millipore water. To rinse the measurement cell with a new sample, about five times 1 mL of sample solution was injected. In case of purified salts of  $(PAA_n)_x$  the osmotic pressure is constant after the rise due to injection. Therefore no rinsing with pure water is necessary between injections of different samples. The osmotic pressure was taken to determine the osmotic coefficient.

### 3.3. Results and Discussion

#### 3.3.1. Synthesis and Characterization of Oligoinitiators

The ATRP oligoinitiators based on  $\alpha$ -glucose and saccharose (1,2,3,4,6-penta-*O*-(2-bromoisobutyryl)- $\alpha$ -glucose and 2,3,4,6,1',3',4',6'-octa-*O*-(2-bromoisobutyryl)-saccharose) were synthesized similar to procedures described by Haddleton et al.<sup>41, 43, 44</sup> and modified by Stenzel-Rosenbaum et al.<sup>42</sup> The synthesis of the initiator based on  $\beta$ -cyclodextrin (heptakis[2,3,6-tri-*O*-(2-bromoisobutyryl)]- $\beta$ -cyclodextrin,<sup>41</sup> Scheme 3. 1) was conducted according to the synthesis based on  $\alpha$ -cyclodextrin.<sup>41, 42</sup>

**Scheme 3. 1:** left: Full 2-bromoisobutyryl ester of  $\beta$ -cyclodextrin; right: possible species assigned to signal in MALDI-ToF MS spectra; bottom: possible pathway to the formation of the detected species.



As shown in Figure 3. 1, full esterification could be proven by MALDI-ToF mass spectrometry ( $M(+Li^+) = 4267$  g/mol,  $C_{126}H_{175}O_{56}Br_{21}Li^+$ ). The MALDI-TOF spectra also show a series of peaks attributed to HBr elimination during the ionization process. In reflector mode an additional superposition of badly resolved peaks is observed, which are not seen in linear mode (e.g. inset e in Figure 3. 1). Thus, it is very likely that we see in linear mode fragments which are developed during flight and detected simultaneously with the originating ions. However the reflector can not refocus incoming fragments with same velocity but different masses, which results in shifted peak location. This confirms our assumption of consecutive HBr elimination during the MALDI ionization procedure.

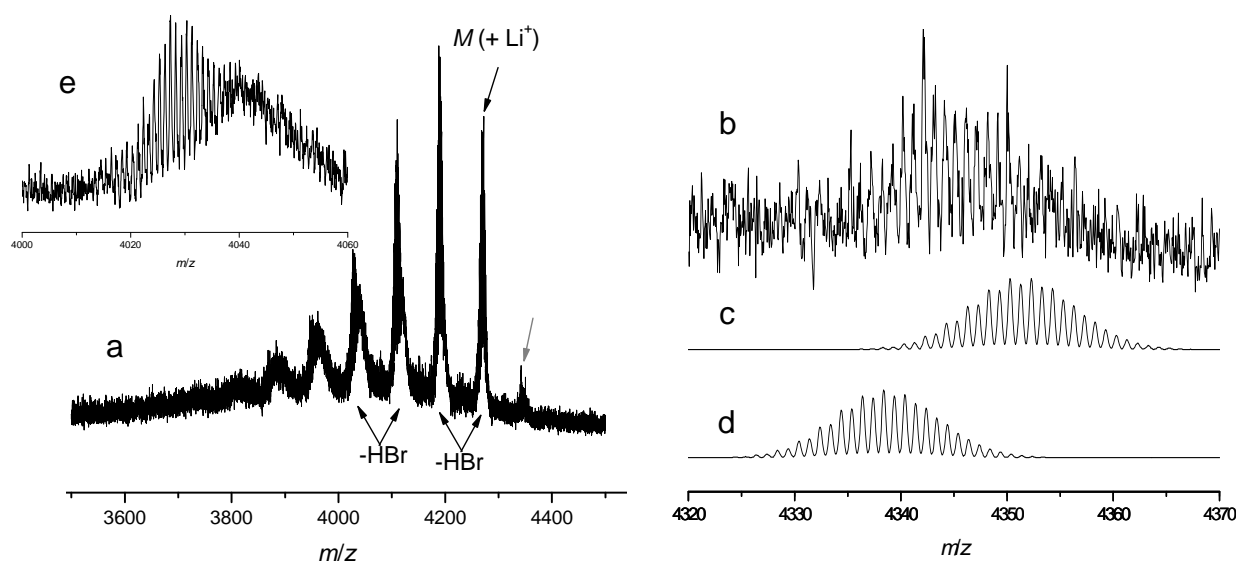


**Figure 3. 1:** a: MALDI-ToF-MS of cyclodextrin-based ATRP oligoinitiator (reflector mode); the peak at  $m/z = 4340$  is assigned to HBr adduct or possible side product (see Scheme 3. 1); b: cutout of peak at  $m/z$  4340 and comparison with simulated spectrum of side product (d) and with simulated spectrum of HBr adduct (c); e: cutout of spectrum at 4030 g/mol; matrix DHB, LiCl

The poorly resolved peak at 4340 g/mol may either originate from an HBr adduct of  $M(+Li^+)$  ( $C_{126}H_{176}O_{56}Br_{22}Li^+$ ) or give evidence of an open structure depicted on the right-hand side of Scheme 3. 1 after single HBr elimination ( $C_{130}H_{179}O_{57}Br_{21}Li^+$ ). Comparison of measured and simulated spectra in Figure 3. 1 suggests an overlap of both possibilities. The open structure formation can be assumed by a ring opening of the  $\beta$ -cyclodextrin scaffold either leading directly to an unsaturated species, or leading to a saturated glucose terminus. Then the anomeric hydroxyl group could have been esterified as well (initiator with 23 initiation sites; structure on the bottom left in Scheme 3. 1), followed by elimination of a whole ester moiety (reaction in Scheme 3. 1). The latter can be explained by the outstanding

reactivity of the ester group attached to the anomeric C-atom, which easily enables elimination especially under MALDI-ToF conditions.

MALDI-ToF MS was also performed with the glucose- and saccharose-based initiators (Figure 3. 2). In case of the saccharose-based initiator we could detect a small fraction initiator with only seven initiation sites (13 mol-%), whereas glucose was fully esterificated. In both cases HBr eliminations occur, but in addition we find peaks corresponding to HBr adducts.

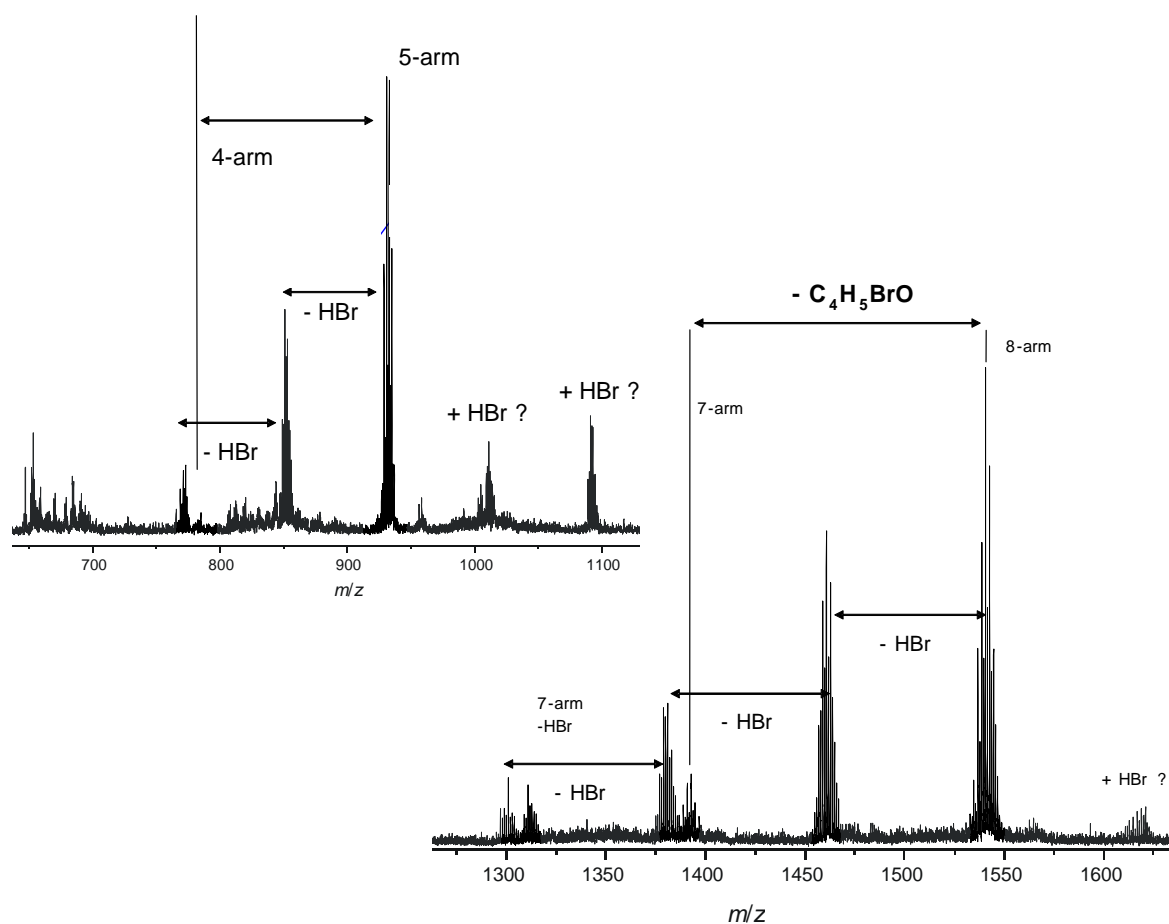


Figure 3. 2: MALDI-TOF-MS reflectron mode spectra of saccharose-based initiator (right) and glucose-based initiator (left); matrix DHB, LiCl

### 3.3.2. Synthesis and Characterization of Poly(acrylic acid) stars

The procedure for the synthesis and complete analysis of the PAA stars consists of the following steps:

1. synthesis of PtBA stars and determination of total  $M_n$  by GPC/viscosity,
2. transformation of PtBA stars to star-shaped PAA and analysis using  $^1\text{H}$  NMR and aqueous GPC,

3. alkaline cleavage of PAA arms from the initiator core and analysis by  $^1\text{H}$  NMR and aqueous GPC,
4. reesterification of PAA stars and cleaved-off PAA arms to poly(methyl acrylate) (PMA) and analysis by  $^1\text{H}$  and  $^{13}\text{C}$  NMR, GPC/viscosity and MALDI-ToF MS,

The synthesis of star-shaped poly(*tert*-butyl acrylate),  $(\text{PtBA}_n)_x$  ( $x$  equals arm number,  $n$  equals degree of polymerization of arms,  $DP_{n,\text{arm}}$ ), by ATRP was conducted analogously to the preparation by Schnitter et al.,<sup>39</sup> who used dendritic initiators. For this study we prepared samples with 21, 8 and 5 arms and differing arm lengths by use of the sugar-based initiators described above. The arm lengths and initiation site efficiencies were determined by means of molecular weight determinations. The typical key steps of characterization will be explained in the following for stars with 21 arms. For the stars with different arm numbers the characterization was conducted analogously. All results of molecular weight determinations and the comparison with the expected values are summed up in Table 3. 2.

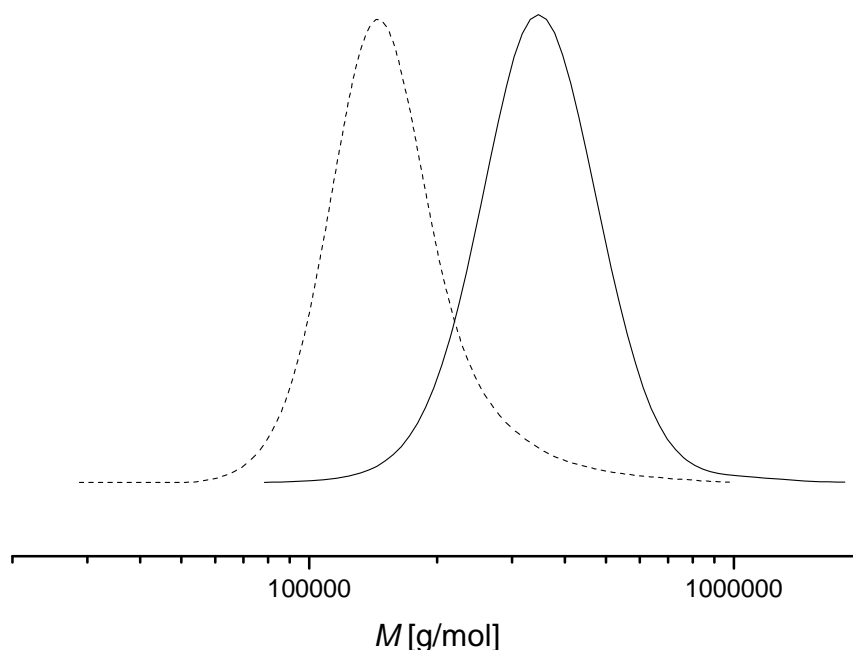


**Figure 3. 3: Molecular weight distributions of  $(\text{PtBA}_{60})_{21}$  (---) and  $(\text{PtBA}_{125})_{21}$  (—) determined by THF-GPC with viscosity detection (RI-traces).**

Absolute molecular weights were determined by GPC with viscosity detection (Figure 3. 3). The  $(\text{PtBA}_n)_x$  stars showed always a discrimination of higher molecular weights in MALDI-ToF MS, thus no reliable MS data could be obtained. We believe that this is due to elimination of isobutylene during the ionization/desorption process. Even for low molecular weight PtBA standards single species could not be resolved and no sequence of elimination processes could be detected in reflectron mode. This can also be explained by considerable

decomposition during the MALDI process.

Elimination of isobutylene catalyzed by trifluoroacetic acid resulted in poly(acrylic acid) stars, which were assigned as  $(PAA_n)_x$ . According to  $^1\text{H}$  NMR, elimination yields were  $\geq 95\%$  in all cases (see Figure 3. 4). Aqueous GPC revealed that the vast majority of arms remain attached to the core during elimination as the amount of linear polymer was found to be  $\leq 5\%$  wt. % (see Figure 3. 5).

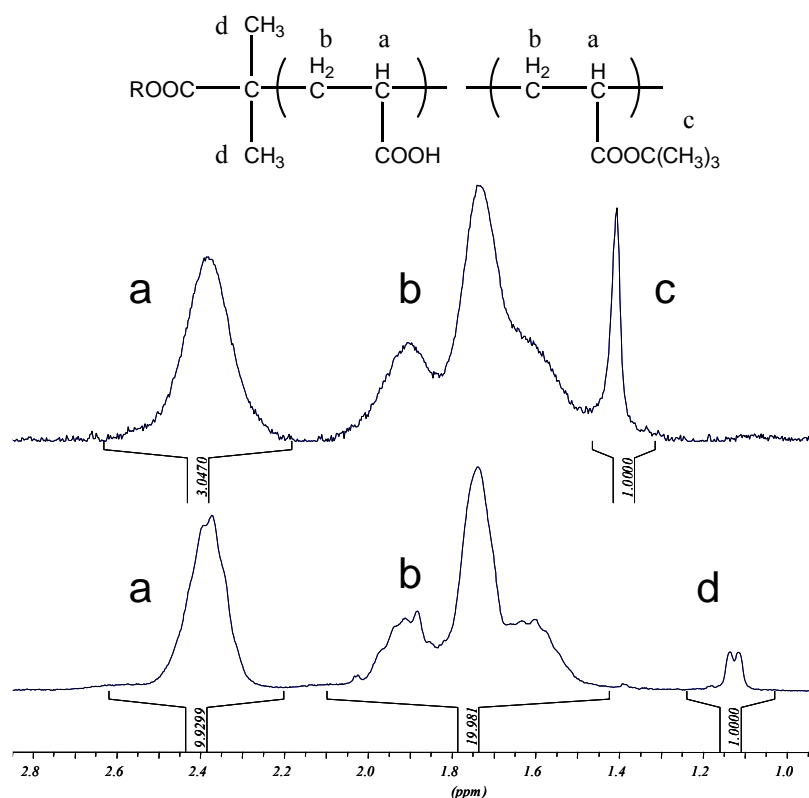


**Figure 3. 4:**  $^1\text{H}$ -NMR spectra of  $(PAA_{60})_{21}$  in  $\text{D}_2\text{O}$  after dialysis (top); the peak at 1.4 ppm originates from 4 % residual tert-butyl groups. Bottom: linear  $PAA_{60}$  obtained from alkaline cleavage of arms; the pseudo-doublet at 1.1 ppm stems from the two methyl groups of the isobutyric acid initiator fragment

In order to determine the lengths of the arms of the  $(PAA_n)_x$  stars, these were cleaved off the core by alkaline hydrolysis. The resulting linear PAA shows  $^1\text{H}$ -NMR signals from the methyl protons of the isobutyric acid initiator moiety (1.1 ppm), which were not seen in the PAA star due to low mobility of segments near the core (Figure 3. 4). They appear as a pseudo-doublet due to their vicinity to the chiral C-atom in the first monomer unit of the polymer. Almost full cleavage was obtained by a fourfold excess of NaOH compared to carboxylic groups. Cleavage was again verified by aqueous GPC (see Figure 3. 5), whereas NMR showed that also the residual tert-butyl groups were hydrolyzed under these conditions (Figure 3. 4). MALDI-ToF MS of pure PAA was not successful. According to the controlled character of

ATRP, every polymer chain should have one initiation site moiety, as chain transfer to solvent or monomer and termination by recombination can be neglected with respect to our GPC analysis. Additionally the length of our arms is still in the range, where endgroup analysis is feasible. Therefore the  $DP_n$  of the PAA arms was determined by  $^1\text{H}$  NMR analysis, comparing the integrals  $I_{\text{endgroup}}$  over the methyl signals of the isobutyric acid endgroup (1.1 ppm) with those  $I_{\text{methine}}$  of the methine protons on the polymer backbone (2.4 ppm) by equation 3. 2.

$$DP_n = 6 \cdot I_{\text{methine}} / I_{\text{endgroup}} \quad 3. 2.$$

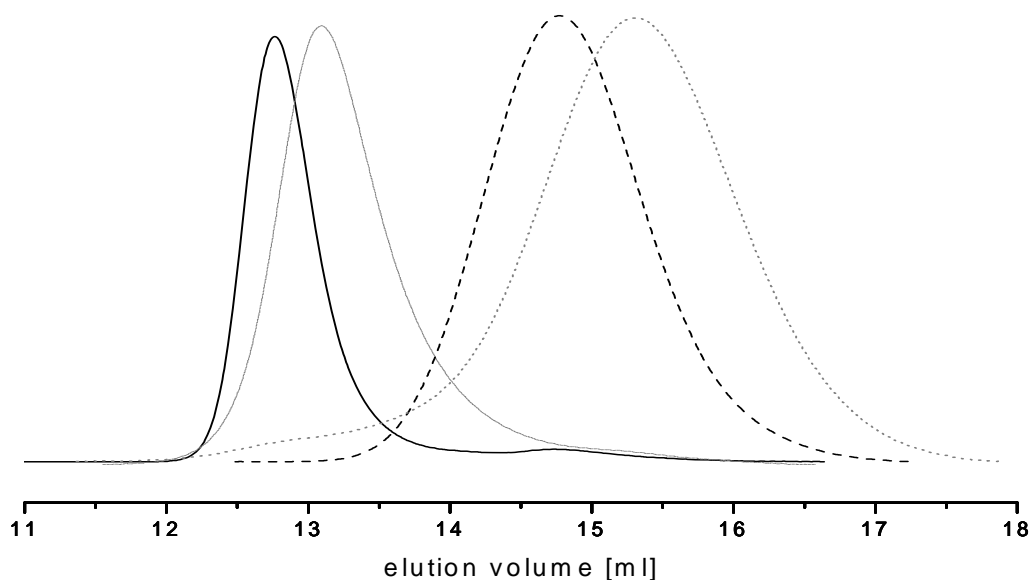


**Figure 3. 5:** Aqueous GPC elution curves of  $(\text{PAA}_{125})_{21}$  (—),  $(\text{PAA}_{60})_{21}$  (---) and of the cleaved-off arms  $\text{PAA}_{125}$  (- - -) and  $\text{PAA}_{60}$  (···)

Some PAA stars were stored as rubidium salts (70% neutralization) at  $pH \sim 7$  in aqueous solution at  $5\text{ }^\circ\text{C}$  for six months. Their SEC elution curves (in phosphate-buffered water) completely coincide with those obtained before, indicating that the stars are stable at neutral conditions in aqueous solution.

Since it is difficult to obtain absolute molecular weights in aqueous GPC, methylation was performed on the PAA stars and their cleaved-off arms. The  $^1\text{H}$  and  $^{13}\text{C}$  NMR spectra (Figure 3. 6) of the methylated PAA showed additional signals at 3.3, 4.1 ppm and 52.1, 58.9 ppm respectively, which may originate from methylene insertion into the C-O ester bond (similar to the generation of  $\alpha$ -chloroketones from alkanoyl chlorides<sup>47, 48</sup>). The only indication of the ketone carbonyl in  $^{13}\text{C}$  NMR spectrum was seen in small peak at 174.8 ppm, which is rather upfield shifted compared to typical  $^{13}\text{C}$  ketone signals (190 – 220 ppm). Additionally, we always find a triplet or pseudo-triplet at 3.4 ppm, which could not be assigned without doubt.

According to NMR, conversion to methyl ester was always around 80 % and the majority of the residual acid groups were transformed to ketones; thus almost no free acid groups remained and hydrophobization was complete. This was confirmed by the disappearance of the H-O vibration in the IR spectra.  $DP_{n,arm}$  determined by  $^1\text{H-NMR}$  endgroup analysis of PMA arms were in good agreement with those obtained from PAA arms.

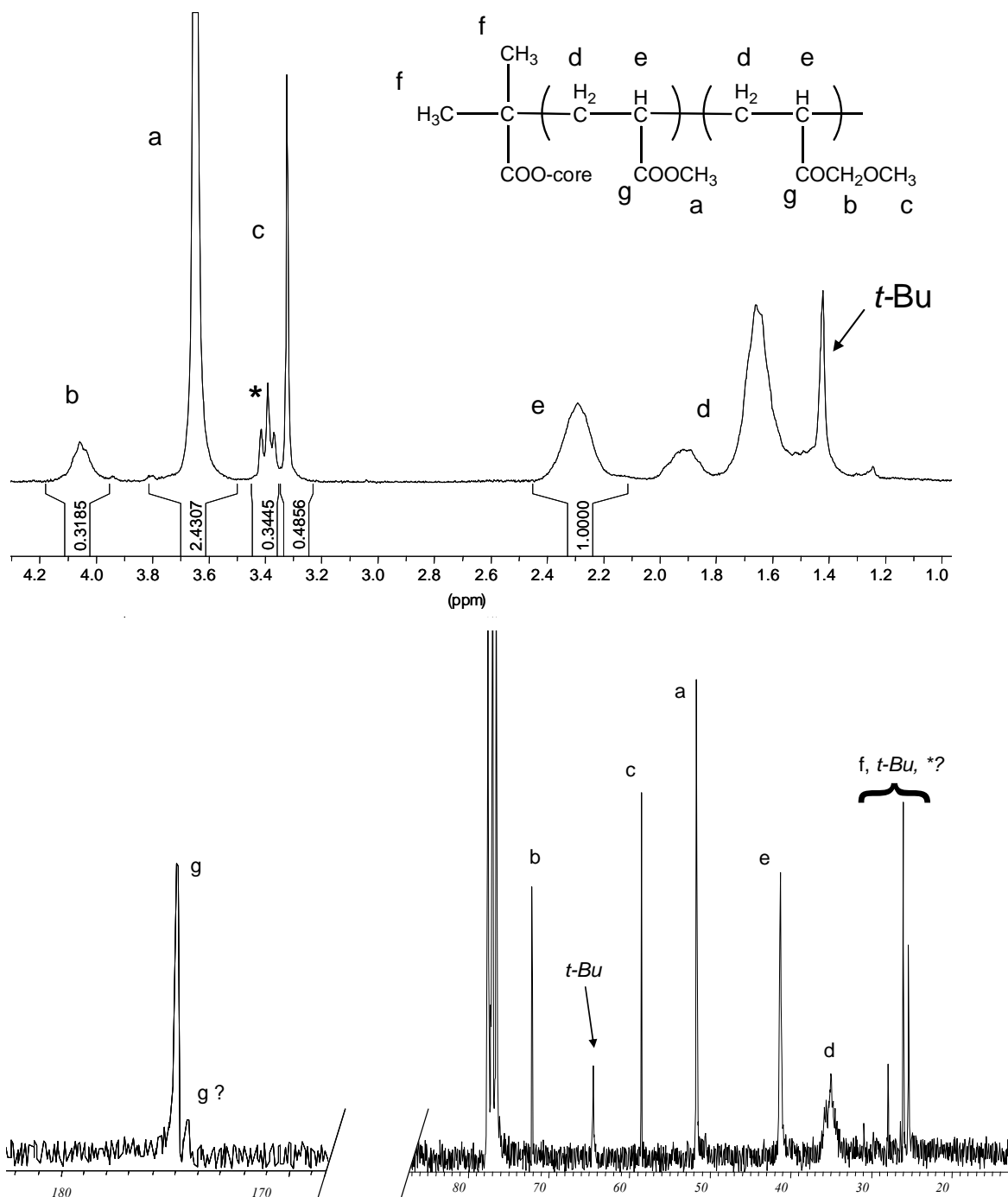


Figure 3. 6:  $^1\text{H-NMR}$  (top) and  $^{13}\text{C-NMR}$  (bottom) spectrum of a methylated PAA star in  $\text{CDCl}_3$ ; the most probable assignment of structures to the signals is shown; the asterisk designs a signal which cannot be completely assigned

The star shaped poly(methyl acrylate)s (PMA) and their linear equivalents gave MALDI-ToF MS spectra in the expected molecular mass range (see experimental section, Figure 3. 7). They appear, however, often noisy due to limited statistics (PMA did not fly deliberately). For results see Table 3. 2 and for details of evaluation see experimental section.

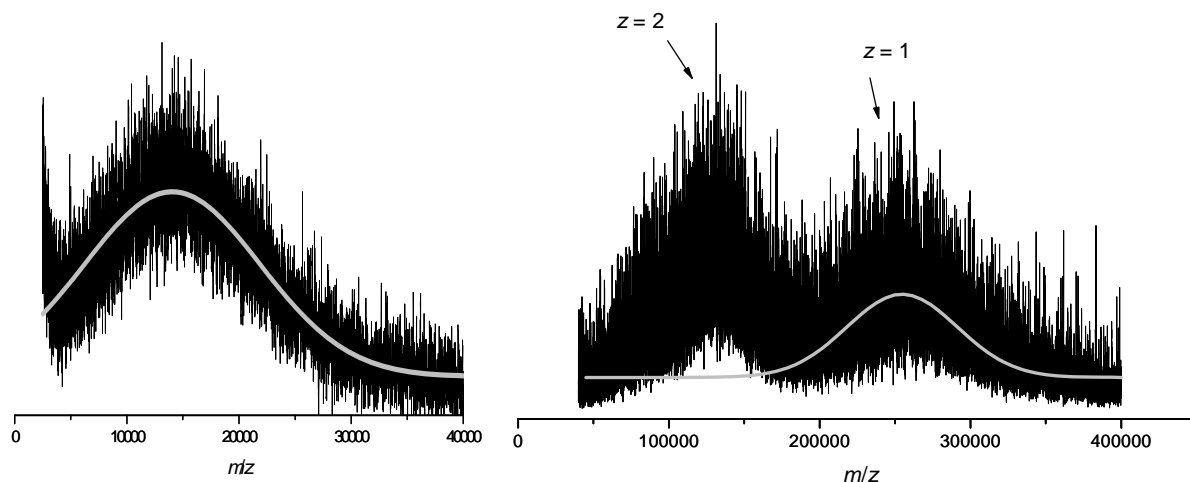


Figure 3. 7: MALDI-ToF spectra of  $(PMA_{125})_{21}$  (right) and of its linear arm,  $PMA_{125}$ , (left) with Gaussian fits of the species of interest.

Table 3. 2: Number-average degrees of polymerization of the arms in the poly(acrylic acid) stars  $(PAA_n)_x$  and polydispersity indices (in brackets) of respective stars (*italics*) and arms (normal style) measured by different methods and efficiencies of initiation sites derived there from

Method	$(PAA_{90})_5$	$(PAA_{75})_8$	$(PAA_{100})_8$	$(PAA_{160})_8$	$(PAA_{60})_{21}$	$(PAA_{100})_{21}$	$(PAA_{125})_{21}$
Expected <sup>a</sup>	86	73	101	155	60	97	125
GPC of PtBA stars <sup>b</sup> (linear PS calibration)	70 (1.05)	60 (1.08)	64 (1.06)	94 (1.09)	35 (1.11)	40 (1.03)	53 (1.03)
GPC of PtBA stars by (universal calibration) <sup>b</sup>	-	76 (1.18)	-	160 (1.12)	54 (1.13)	-	122 (1.12)
MALDI-ToF of PMA stars <sup>b</sup>	100 (1.04)	65 (1.04)	114 (1.05)	153 (1.06)	61 (1.06)	104 (1.02)	133 (1.03)
MALDI-ToF of PMA arms	107 (1.13)	88 (1.32)	130 (1.20)	186 (1.28)	-	120 (1.13)	150 (1.26)
$f_{i,conversion}$ <sup>c</sup>	0.80	0.83	0.78	0.83	-	0.81	0.83
$f_{i,Univ.cal}$ <sup>d</sup>	-	0.86	-	0.86	-	-	0.81
$f_{i,MALDI}$ <sup>e</sup>	0.93	0.74	0.88	0.82	-	0.87	0.89
NMR of PAA arms	83	67	120	180	64	118	120
$f_{i,conversion}$ <sup>c</sup>	1.04	1.09	0.84	0.86	0.94	0.82	1.04
$f_{i,Univ.cal}$ <sup>d</sup>	-	1.13	-	0.89	0.84	-	1.02
$f_{i,MALDI}$ <sup>e</sup>	1.20	0.97	0.95	0.85	0.95	0.88	1.11

<sup>a</sup> from monomer to initiation site ratio and monomer conversion. <sup>b</sup>  $DP_{n,arm} = DP_{n,star}$  divided by the number of initiation sites per initiator molecule. <sup>c</sup> efficiency of initiation sites,  $f_i$ , determined as  $f_i = DP_{n,expected}/DP_{n,arm,experimental}$ , <sup>d</sup> determined as  $f_i = DP_{n,PtBA-star}/DP_{n,arm,experimental}$ , <sup>e</sup> determined as  $f_i = DP_{n,PMA-star}/DP_{n,arm,experimental}$

Table 3. 2 sums up the molecular weight characterization for all polymers synthesized. The arm lengths of the PtBA and PMA stars are calculated by dividing the  $DP_n$  of the stars by the respective number of initiation sites per oligoinitiator. As expected, the arm lengths determined from GPC of the PtBA stars using calibration with linear polystyrene standards are lower than those obtained with viscosity detector and using universal calibration; this is due to the well-known fact that stars have a lower hydrodynamic volume than linear polymers of the same molecular weight. Thus the former values have to be taken as apparent ones only.

Using the reasonable assumption that at least one initiating site in each oligoinitiator was active in initiating polymer chains, the determined molecular weights of the PtBA or PMA stars should be equal to those expected from the monomer/initiation site ratio and monomer conversion. The deviations between these data typically are in the range of  $\pm 5\%$ , in some cases up to  $\pm 12\%$ , showing the possible errors of the determination of monomer conversion, GPC of PtBA with universal calibration, and MALDI-TOF MS of PMA.

If not all initiating sites in a oligoinitiator are active this will result in a star with a smaller number of arms (and an arm number distribution), where each arm is longer than expected. This cannot be detected by analyzing the molecular weight of the star but we have to determine the molecular weight of the arms separately. This is why we cleaved the arms by alkaline hydrolysis and analyzed them using different methods. The initiation site efficiency can then be determined by comparing the arm's molecular weight with that calculated from conversion or from the star molecular weight.

Table 3. 2 shows that the initiation site efficiencies,  $f_i = DP_{n,theo,arm} / DP_{n,exp,arm}$ , differ between those determined by MALDI-TOF MS of PMA arms and those from NMR of PAA arms. Whereas the average initiator functionality is 0.97 as determined by NMR, it is only 0.84 as determined by MALDI-TOF. Since we already determined the expected arm lengths by NMR we rather trust NMR for the experimental determination. Taking into account that the error in the overall functionality was between 5 and 12 % and that some initiation efficiencies apparently are larger than unity we conclude that the initiation site efficiency is close to unity, i.e.  $\geq 95\%$ . At present we can only speculate on the reasons, why the MALDI-TOF determined chain lengths of the PMA arms are higher (on average by ca. 15%) than the ones determined by NMR of PAA arms.

Having shown that we have obtained well defined star-shaped poly(acrylic acid), we now want to present some preliminary investigations of their properties.

### 3.3.3. Potentiometric Titration

We performed potentiometric titrations of our stars as well as of linear PAA obtained by alkaline cleavage of  $(\text{PAA}_{100})_{21}$ . In all cases the PAA was purified before titration either by ultrafiltration or dialysis.

The  $pH$  dependence on the degree of neutralization,  $\alpha = [\text{Na}^+]/[\text{COOH}]_0$ , where  $[\text{COOH}]_0$  is the total concentration of carboxyl and carboxylate groups and  $[\text{Na}^+]$  assigns the amount of added NaOH, are presented in Figure 3. 8.

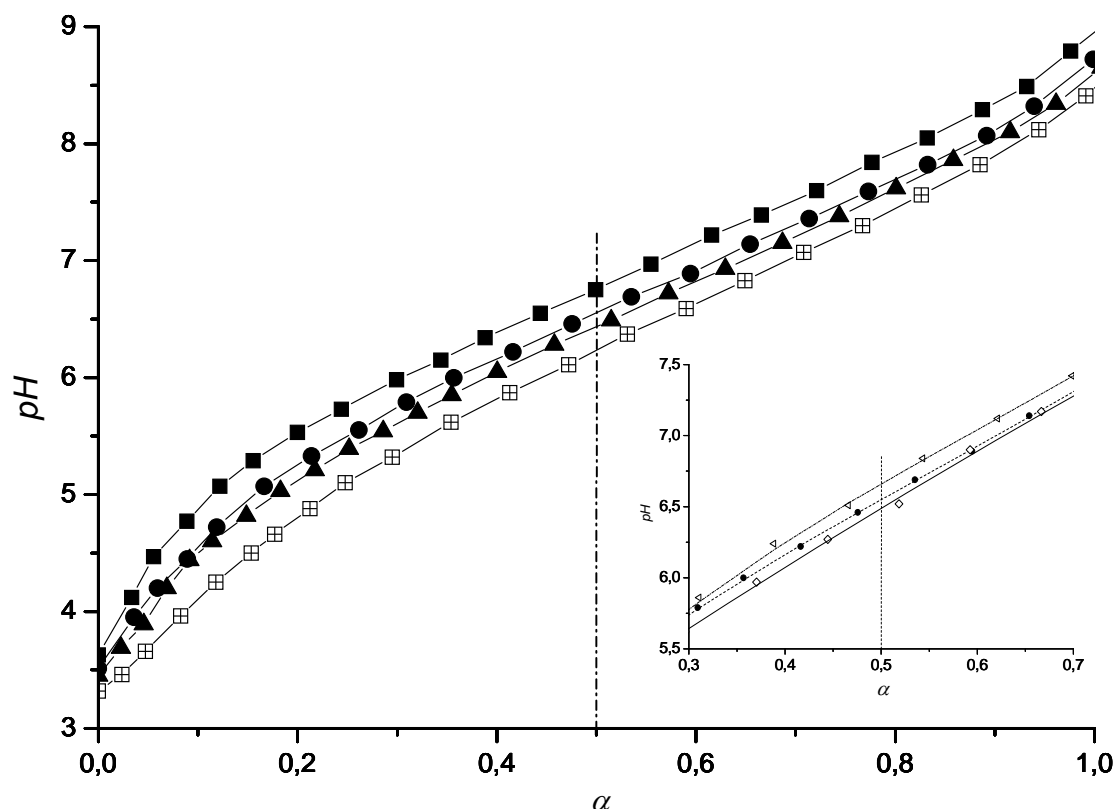


**Figure 3. 8:** Potentiometric titration curves for stars  $(\text{PAA}_{100})_{21}$  (■),  $(\text{PAA}_{100})_8$  (●),  $(\text{PAA}_{100})_5$  (▲), and linear  $\text{PAA}_{100}$  (◻). Inset: cutout of titration of  $(\text{PAA}_{75})_8$  (◁),  $(\text{PAA}_{160})_8$  (◇), and  $(\text{PAA}_{100})_8$  (●)

As seen in Figure 3. 8 the shape of the titration curves is as expected for linear PAA<sup>18, 23, 30</sup> and does not change significantly with increasing arm number or length. However, with increasing arm number (at constant arm length), the titration curves shift to higher  $pH$  values and thus to higher apparent values of  $pK_a$ , taken as the  $pH$  at 50 % neutralization (see Table 3. 3). This is in qualitative agreement with theory.<sup>24</sup> It is due to the higher osmotic pressure inside the stars, caused by counterion confinement (see next section). This leads to a partial reversal of the acid-base reaction, i.e., the formation of uncharged  $-\text{COOH}$  groups within the polyelectrolyte star. As consequence of this process, the  $pH$  value will increase

outside. This effect is believed to be more pronounced for the higher arm numbers and for higher degrees of neutralization, as the osmotic pressure inside the star is increasing with segment density and ionization degree (which is in good approximation equal to  $\alpha$ ).

These titration curve shifts are not just a consequence of increasing the overall molar mass but a consequence of changing the degree of branching. Linear PAA shows almost no titration curve dependence with molecular weight in the range  $2 \cdot 10^3 - 8 \cdot 10^5$  g/mol.<sup>49</sup> We could show by use of stars with the same arm number but different arm lengths (see inset in Figure 3. 8) that with increasing arm length the apparent  $pK_a$  values even decrease. Increasing  $DP_{n,arm}$  decreases the mean segment density within the star and less NaOH is expelled by lowered osmotic pressure.

The results are listed in Table 3. 3.

**Table 3. 3: Apparent  $pK_a$  values of different PAA stars**

	PAA <sub>100</sub>	(PAA <sub>90</sub> ) <sub>5</sub>	(PAA <sub>75</sub> ) <sub>8</sub>	(PAA <sub>100</sub> ) <sub>8</sub>	(PAA <sub>160</sub> ) <sub>8</sub>	(PAA <sub>100</sub> ) <sub>21</sub>
$pK_{a,app}$ <sup>a</sup>	6.22	6.42	6.65	6.55	6.48	6.74

<sup>a</sup> error  $\pm 0.05$ , taken as error in  $pH$  determination

### 3.3.4. Osmometry – Determination of Osmotic Coefficient

The osmotic coefficient describes the amount of released (cationic) counterions in case of (anionic) polyions. We calculated the osmotic coefficient,  $\phi$ , by use of equation 3. 3., where  $\Pi_m$  denotes the measured osmotic pressure and  $\Pi_{cal}$  is the calculated osmotic pressure according to van't Hoff's law.

$$\phi = \frac{\Pi_m}{\Pi_{cal}} = \frac{\Pi_m (\alpha \cdot M_{ANa} + (1 - \alpha) \cdot M_{AA})}{cRT\alpha} \quad 3. 3.$$

The degree of neutralization,  $\alpha$ , is again the number of sodium ions per polymer's repeating unit. Its molar mass is given by the average of the sodium acrylate ( $M_{ANa}$ ) and acrylic acid molar masses ( $M_{AA}$ ) weighted by  $\alpha$ .  $\alpha$  is obtained by comparison of the measured  $pH$  value of a reference solution with the titration curves in Figure 3. 8. The reference solution should have similar concentration as used for the potentiometric titrations.  $c$  is the mass concentration of the polyelectrolyte.

Sodium salts of PAA (NaPA) stars were prepared by use of NaOH. These salts were purified by dialysis to remove low molecular impurities like  $NaHCO_3$ . After two weeks the  $pH$  changed significantly when dialysing 7 g/L (PAA)<sub>x</sub> sodium salt solution adjusted to  $pH$  7 -

8 with NaOH. Resulting in  $pH \sim 5.5$ , the dissociation degree,  $\alpha$ , decreased from 0.6 to 0.25 (see Figure 3. 8). The same principle discussed in context with the titration curves holds true and NaOH, obtained by protolysis of salt of the weak polyacid, is expelled out of the dialysis tube due to high osmotic pressure inside. Carbon dioxide, which can hardly be excluded, has an accelerating effect. This process takes only place for dialysis and not for ultrafiltration as only dialysis provides equilibrium between both sides of the membrane.

Therefore we only investigated star-shaped sodium salts of poly(acrylic acid) with a low ionization degree  $\alpha \cong 0.25$  at different concentrations. The dialysed samples of partially neutralized  $(PAA_{100})_8$  and  $(PAA_{100})_{21}$  show constant osmotic pressure during osmometry in the experiments time frame (30 min).

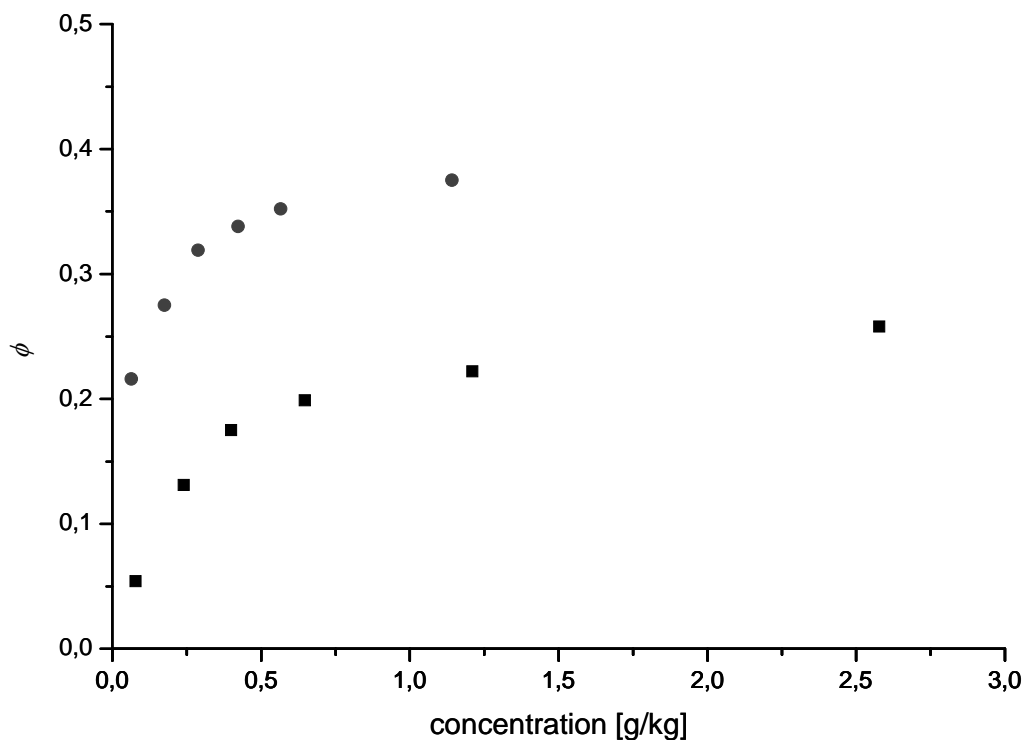


**Figure 3. 9: Osmotic coefficients  $\phi$  of  $(PAA_{100})_{21}$  (■,  $\alpha = 0.24$ ) and  $(PAA_{100})_8$  (●,  $\alpha = 0.25$ ) in dependence of concentration**

We depict in Figure 3. 9 the dilute regime heading towards semi-dilute concentrations. The overlap concentration of  $(PAA_{100})_{21}$  is ca. 4 g/L whereas  $(PAA_{100})_8$  overlaps at ca. 1.5 g/L. The overlap concentrations were calculated as the concentrations at which the stars regarded as spheres with the single arm's contour length as radius (assuming full extension of arms; 250 pm per monomer unit) occupy the total available solution volume. That means these values are lower limits, though stacking factors were not taken into account.

In this context we should be aware that Manning's parameter<sup>5</sup>  $\zeta_M = l_B/b$ , where  $b$  is the average charge to charge distance along the chain and  $l_B$  is the Bjerrum length, is smaller than unity for  $\alpha \sim 0.25$ . Hence, the Manning condensation of counterions along the backbone of the polyelectrolyte chains does not take place ( $\zeta_M < 1$ ). However, we measure an osmotic coefficient  $< 0.4$  which is due to the confinement of counterions within the star.

We find that the osmotic coefficient,  $\phi$ , decreases with increasing arm number (i.e. segment density), which is in qualitative agreement with prediction of theory.<sup>22</sup> For low arm numbers the star polyelectrolyte effect related to the confinement of counterions is not very pronounced, as literature reports typically osmotic coefficients around 0.2 for fully charged linear PAA (NaPA)<sup>16, 20, 50</sup> and around 0.4 for partially charged PAA ( $\alpha \sim 0.25$ ; figure 4 in ref. <sup>16</sup>). At sufficiently high arm number, we do observe the intermediate behaviour between the linear and the brush-like polyelectrolytes. The theory assumes an equidistant charge distribution along the arm's backbone.<sup>22</sup> This may not hold true for our system at low ionization degrees (here:  $\alpha \sim 0.25$ ) and charge annealing can take place leading to a higher charge density on the periphery of the star. This is believed to promote counterion release.

In contrast to previous theoretical work applied on polyelectrolyte brushes<sup>51</sup> the osmotic coefficient increases at higher concentrations. This was also observed by Deserno et al.<sup>52</sup> for rigid rod-like polyelectrolytes. They take the influence of small excess salt concentrations (impurities) into account, which leads to a lowering of the osmotic coefficient.<sup>16, 53</sup> With help of Monte-Carlo simulations, Belloni et al. found similar concentration trends for star-like micelles.<sup>54</sup>

A more systematic theoretical and experimental study for determination of counterion confinement in star-shaped polyelectrolytes will be given in a future publication.

### 3.4. Conclusion

Well defined poly(acrylic acid) stars could be prepared by ATRP of *tert*-butylacrylate with consecutive elimination of isobutylene. Different characterization methods showed that both arm lengths could be adjusted and verified as well the arm number is close to the theoretical value. The titration curves of PAA stars are shifted towards higher *pH* for increasing arm number. This was explained by the increasing segment density and the increasing osmotic pressure inside the stars. For higher arm numbers the osmotic coefficient was considerably lowered as predicted by theory.

**Acknowledgement.** We appreciate the help of Manuela Fink, Günther Jutz, Denise Danz, Xavier André, Sharmila Muthukrishnan, Youyong Xu and S. Wunder during MALDI-ToF MS and GPC measurements respectively. We thank Arben Jusufi for helpful discussions. The financial support by the *Deutsche Forschungsgemeinschaft* within SFB 481 is acknowledged.

### 3.5. References

1. Rau, I. U.; Rehahn, M.; *Acta Polymerica* **1994**, *45*, 3.
2. Holm, C.; Rehahn, M.; Oppermann, W.; Ballauff, M.; *Advances in Polymer Science* **2004**, *166*, 1.
3. Fuoss, R.; Katchalsky, A.; Lifson, S.; *S Proc Natl Acad Sci USA* **1951**, *37*, 579.
4. Imai, N.; Osawa, F.; *Busseiron Kenkyu* **1953**, *No. 46*; *No. 47*, 14.
5. Manning, G. S.; *J Chem Phys* **1969**, *51*, 924.
6. Mori, H.; Chan Seng, D.; Lechner, H.; Zhang, M.; Müller, A. H. E.; *Macromolecules* **2002**, *35*, 9270.
7. Mori, H.; Walther, A.; André, X.; Lanzendörfer, M. G.; Müller, A. H. E.; *Macromolecules* **2004**, *37*, 2054.
8. Bohrisch, J.; Eisenbach, C. D.; Jaeger, W.; Mori, H.; Müller, A. H. E.; Rehahn, M.; Schaller, C.; Traser, S.; Wittmeyer, P.; *Advances in Polymer Science* **2004**, *165*, 1.
9. Ruhe, J.; Ballauff, M.; Biesalski, M.; Dziezok, P.; Gröhn, F.; Johannsmann, D.; Houbenov, N.; Hugenberg, N.; Konradi, R.; Minko, S.; Motornov, M.; Netz, R. R.; Schmidt, M.; Seidel, C.; Stamm, M.; Stephan, T.; Usov, D.; Zhang, H.; *Advances in Polymer Science* **2004**, *165*, 79.
10. Biesalski, M.; Ruhe, J.; *Macromolecules* **1999**, *32*, 2309.
11. Ballauff, M.; In *Polymer Brushes*; Ed. Advincula, R. C.; Wiley-VCH Verlag GmbH & Co. KGaA, Weinheim, Germany, 2004; pp 231
12. Cheng, G.; Böker, A.; Zhang, M.; Krausch, G.; Müller, A. H. E.; *Macromolecules* **2001**, *34*, 6883.
13. Zhang, M.; Breiner, T.; Mori, H.; Müller, A. H. E.; *Polymer* **2003**, *44*, 1449.
14. Guo, X.; Ballauff, M.; *Physical Review E: Statistical, Nonlinear, and Soft Matter Physics* **2001**, *64*, 051406/1.
15. Mei, Y.; Ballauff, M.; *European Physical Journal E: Soft Matter* **2005**, *16*, 341.
16. Katchalsky, A.; *Pure and Applied Chemistry* **1971**, *26*, 327.
17. Das, B.; Guo, X.; Ballauff, M.; *Progress in Colloid & Polymer Science* **2002**, *121*, 34.
18. Kern, W.; *Z physik Chem* **1938**, *A181*, 249.

19. Ise, N.; Okubo, T.; *J Phys Chem* **1967**, *71*, 1287.
20. Kakehashi, R.; Yamazoe, H.; Maeda, H.; *Colloid and Polymer Science* **1998**, *276*, 28.
21. Zhang, B.; Yu, D.; Liu, H.-L.; Hu, Y.; *Polymer* **2002**, *43*, 2975.
22. Jusufi, A.; Likos, C. N.; Löwen, H.; *Journal of Chemical Physics* **2002**, *116*, 11011.
23. Klein Wolterink, J.; Leermakers, F. A. M.; Fleer, G. J.; Koopal, L. K.; Zhulina, E. B.; Borisov, O. V.; *Macromolecules* **1999**, *32*, 2365.
24. Wolterink, J. K.; van Male, J.; Stuart, M. A. C.; Koopal, L. K.; Zhulina, E. B.; Borisov, O. V.; *Macromolecules* **2002**, *35*, 9176.
25. Borisov, O. V.; Zhulina, E. B.; *Journal de Physique II* **1997**, *7*, 449.
26. Borisov, O. V.; Zhulina, E. B.; *European Physical Journal B: Condensed Matter Physics* **1998**, *4*, 205.
27. Likos, C. N.; Hoffmann, N.; Jusufi, A.; Löwen, H.; *J Phys: Condens Matter* **2003**, *15*, 233.
28. Hoffmann, N.; Likos, C. N.; Löwen, H.; *Journal of Chemical Physics* **2004**, *121*.
29. Furukawa, T.; Ishizu, K.; *Macromolecules* **2005**, *38*, 2911.
30. Katchalsky, A.; Gillis, J.; *Recueil des Travaux Chimiques des Pays-Bas et de la Belgique* **1949**, *68*, 879.
31. Borkovec, M.; Koper, G. J. M.; *Berichte der Bunsen-Gesellschaft* **1996**, *100*, 764.
32. de Groot, J.; Koper, G. J. M.; Borkovec, M.; de Bleijser, J.; *Macromolecules* **1998**, *31*, 4182.
33. Borkovec, M.; Koper, G. J. M.; *Macromolecules* **1997**, *30*, 2151.
34. Mays, J. W.; *Polymer Communications* **1990**, *31*, 170.
35. Heinrich, M.; Rawiso, M.; Zilliox, J. G.; Lesieur, P.; Simon, J. P.; *European Physical Journal E: Soft Matter* **2001**, *4*, 131.
36. Held, D.; Müller, A. H. E.; *Macromolecular Symposia* **2000**, *157*, 225.
37. Pitsikalis, M.; Sioula, S.; Pispas, S.; Hadjichristidis, N.; Cook, D. C.; Li, J.; Mays, J. W.; *Journal of Polymer Science, Part A: Polymer Chemistry* **1999**, *37*, 4337.
38. Mengel, C.; Meyer, W. H.; Wegner, G.; *Macromolecular Chemistry and Physics* **2001**, *202*, 1138.
39. Schnitter, M.; Engelking, J.; Heise, A.; Miller, R. D.; Menzel, H.; *Macromolecular Chemistry and Physics* **2000**, *201*, 1504.
40. Moinard, D.; Taton, D.; Gnanou, Y.; Rochas, C.; Borsali, R.; *Macromolecular Chemistry and Physics* **2003**, *204*, 89.

41. Ohno, K.; Haddleton, D. M.; Kukulj, D.; Wong, B.; *Polymer Preprints (American Chemical Society, Division of Polymer Chemistry)* **2000**, *41*, 478.
42. Stenzel-Rosenbaum, M. H.; Davis, T. P.; Chen, V.; Fane, A. G.; *Macromolecules* **2001**, *34*, 5433.
43. Haddleton, D. M.; Edmonds, R.; Heming, A. M.; Kelly, E. J.; Kukulj, D.; *New Journal of Chemistry* **1999**, *23*, 477.
44. Edmonds, R.; Bon, S. A. F.; Haddleton, D. M.; *Polymer Preprints (American Chemical Society, Division of Polymer Chemistry)* **2000**, *41*, 444.
45. Couvreur, L.; Lefay, C.; Belleney, J.; Charleux, B.; Guerret, O.; Magnet, S.; *Macromolecules* **2003**, *36*, 8260.
46. Benoit, H.; Grubisic, Z.; Rempp, P.; Decker, D.; Zilliox, J. G.; *Macromolecules* **1966**, *63*, 1507.
47. Clibbens, D. A.; Nierenstein, M.; *Journal of the Chemical Society, Abstracts* **1915**, *107*, 1491.
48. Van Atta, E.; Zook, H. D.; Elving, P. J.; *Journal of the American Chemical Society* **1954**, *76*, 1185.
49. Kawaguchi, S.; Takahashi, T.; Tajima, H.; Hirose, Y.; Ito, K.; *Polymer Journal (Tokyo)* **1996**, *28*, 735.
50. Ise, N.; *Fortschritte der Hochpolymeren-Forschung* **1971**, *7*, 536.
51. Jusufi, A.; Likos, C. N.; Ballauff, M.; *Colloid and Polymer Science* **2004**, *282*, 910.
52. Deserno, M.; Holm, C.; Blaul, J.; Ballauff, M.; Rehahn, M.; *European Physical Journal E: Soft Matter* **2001**, *5*, 97.
53. Raspaud, E.; da Conceicao, M.; Livolant, F.; *Physical Review Letters* **2000**, *84*, 2533.
54. Belloni, L.; Delsanti, M.; Fontaine, P.; Muller, F.; Guenoun, P.; Mays, J. W.; Boesecke, P.; Alba, M.; *Journal of Chemical Physics* **2003**, *119*, 7560.

## 4. Synthesis and Characterization of Star-Shaped Poly(*N,N*-dimethylaminoethyl methacrylate) and Its Quaternized Ammonium Salts

*Felix A. Plamper<sup>a</sup>, Alexander Schmalz<sup>a</sup>, Evis Penott-Chang<sup>a</sup>, Markus Drechsler<sup>a</sup>,  
Arben Jusufi<sup>b</sup>, Matthias Ballauff<sup>b</sup>, Axel H. E. Müller<sup>a,\*</sup>*

<sup>a</sup>Makromolekulare Chemie II, <sup>b</sup>Physikalische Chemie I, and Bayreuther Zentrum für Kolloide und Grenzflächen, Universität Bayreuth, D-95440 Bayreuth, Germany..

**Published in *Macromolecules* 2007, 40, p.5689.**

**ABSTRACT:** We report on the synthesis and characterization of star-shaped strong polyelectrolytes and their precursor stars with up to 24 arms. To achieve this we polymerized 2-(*N,N*-dimethylamino)ethyl methacrylate (DMAEMA) by atom transfer radical polymerization employing a core-first attempt. Sugar-based scaffolds as well as silsesquioxane nanoparticles were used as oligofunctional initiators. Subsequent quaternization of the obtained poly(DMAEMA) stars yielded star-shaped poly{[2-(methacryloyloxy)ethyl] trimethylammonium iodide} (PMETAI). The initiation site efficiency was determined both by molecular weight measurements of the cleaved arms and by a statistical method after partial destruction of the inorganic core. The rather low efficiency of the initiation sites (30 to 75 %) leads to a moderate arm number distribution of the prepared polyelectrolyte stars. As expected, the hydrodynamic radii of these polyelectrolyte stars decrease with increasing ionic strength. However, if the ionic strength was adjusted with NaI instead of NaCl, pronounced ion-specific effects were observed; the star polyelectrolyte first strongly shrinks with increasing salt concentration and becomes insoluble at about 0.5 M NaI (“salting out”). Still higher concentrations of NaI lead to a re-dissolution and a re-swelling of the star polyelectrolyte (“salting in”). The measured osmotic coefficients are low and decrease with increasing arm number from  $\phi \sim 0.12$  for a 3-arm star down to  $\phi \sim 0.04$  for an 18-arm star, confirming the expected strong counterion confinement within these objects with high charge density.

## 4.1. Introduction

Polymers, in particular polyelectrolytes, with non-linear topologies behave differently in many aspects compared to their linear counterparts. For example the counterions of a star-shaped polyelectrolyte and of densely grafted polyelectrolyte brushes are strongly confined within the macroion as opposed to linear architecture.<sup>1-3</sup> Hence the osmotic coefficient,  $\phi$ , which is defined as the ratio of measured osmotic pressure to the ideal one is therefore lower than for linear polyelectrolytes.<sup>2</sup> Recent work on the osmotic coefficient of spherical polyelectrolyte brushes<sup>4</sup> demonstrated that  $\phi$  measured in strictly salt-free systems is only of the order of a few percent and hence much lower than the value of 0.2 to 0.3 found for highly charged linear chains.<sup>5</sup> This is in full accord with recent theoretical deductions,<sup>6</sup> which suggest that the confinement of counterions should increase with increasing mutual interaction of the polyelectrolyte chains. In case of polyelectrolyte stars this reasoning leads to the prediction that the osmotic coefficient should decrease with increasing arm number.<sup>3</sup>

While the confinement of counterions within spherical polyelectrolyte brushes seems to be a well-studied problem by now, information on polyelectrolyte stars is scarce. Recently, we showed that star-shaped poly(acrylic acid) with a rather low degree of neutralization exhibits indeed the expected decrease of the osmotic coefficient with increasing arm number.<sup>7</sup> However, the degree of neutralization of these *annealed* (weak) star polyelectrolytes was low ( $\alpha \sim 0.25$ ) and reliable data suitable for a comparison with theory<sup>3</sup> could only be obtained for higher arm numbers. Here we wish to pursue this work by studying a *quenched* polyelectrolyte star, that is, a star polymer set up by strong polyelectrolyte chains whose charge density along the backbone is independent of the *pH*. This also alleviates the necessity to adjust a rather high *pH* value for a high degree of neutralization which may degrade the cores of the star polymers through hydrolysis.

The first syntheses leading to cationic/protonizable star-shaped polyelectrolytes were achieved by polymerization of vinylpyridine.<sup>8, 9</sup> Heteroarm stars with long poly(2-vinylpyridine) (P2VP) and short polystyrene arms were made by microgel formation of short polystyrene chains with a difunctional monomer and polymerization of P2VP from the microgel bearing a large number of active sites.<sup>10</sup> A similar route was taken for the preparation of poly(*N,N*-dimethylaminoethyl methacrylate) (PDMAEMA) stars by group transfer polymerization.<sup>11-13</sup> These arm-first methods with difunctional monomers led to fairly large arm numbers, albeit with broad arm number distributions (e.g.  $PDI_{app} > 1.6$ ).<sup>12</sup> In addition, a fraction of linear precursor polymer remains unreacted and therefore is not

incorporated in the star.<sup>11</sup> The core-first method circumvents this problem when a defined initiator with a high initiation site efficiency is used. Cyclodextrin- and other sugar-based initiators are widely used scaffolds for this purpose and were also used by us for the synthesis of star-shaped poly(acrylic acid) by atom transfer radical polymerization (ATRP).<sup>7, 14, 15</sup> ATRP with multifunctional initiator also has been used for the synthesis of both weak and strong cationic polyelectrolyte stars. Partially functionalized  $\beta$ -cyclodextrin was used to form the core of PDMAEMA arms (arm number up to 4.5).<sup>16</sup> The use of quaternized DMAEMA as monomer in aqueous solution directly yields strong polyelectrolytes. However the limited solubility of a fully functionalized  $\beta$ -cyclodextrin initiator in water led to rather broad molecular weight distributions and fairly unsatisfactory control of the molecular weights (molecular weights were up to two times higher than expected).<sup>17</sup>

In this paper we report the synthesis of well-defined PDMAEMA stars with high arm numbers (up to 24) by ATRP using multifunctional initiators. Quaternization transforms these weak polyelectrolytes into well-characterized strong polyelectrolyte stars. Since the amino groups are much more accessible, PDMAEMA has a higher quaternization efficiency than P2VP.<sup>18-21</sup> DMAEMA is easier to handle than the corresponding acrylate (DMAEA), especially under ATRP conditions. This is reflected, e.g., by the fact that only one publication is available for ATRP of the latter monomer<sup>22</sup> while there are many for DMAEMA.<sup>23-29</sup> Although the molecular weights for linear PDMAEA can be adjusted quite well (initiation efficiencies between 0.6 to 0.9), the molecular weight distributions are rather broad (*PDI* between 1.4 to 2.0). The substitution of the chain-end halogen by the amine groups of monomer and polymer was given as one possible reason.<sup>22</sup> This effect is less dominant for the sterically hindered PDMAEMA chain-end.

In order to achieve high arm numbers, we used our recently developed initiator, based on a (diglycidylamino)propyl-functional silsesquioxane.<sup>30</sup> Compared to the sugar-based initiators this initiator leads to a higher number of initiation sites per molecule (number-average ca. 58) but exhibits only a small size (diameter around 3 nm). The drawback of this initiator is its finite polydispersity (*PDI*  $\approx$  1.2) which is due to a mixture of different cage sizes of the silsesquioxane core. To the best of our knowledge this is the first report of a hybrid star polyelectrolyte system having a high number of arms. Previous work was related to the synthesis of stars with eight arms employing a regular octahedral silsesquioxane core.<sup>31-34</sup> The goal of the present work is a comprehensive characterization of these systems in dilute aqueous solution by osmometry and dynamic light scattering and a comparison of these results to the predictions of theory.

In subsequent publications we will report on the interaction of these stars with multivalent counterions<sup>35</sup> and their LCST behavior.<sup>36</sup>

## 4.2. Experimental Section

**Materials:** Anisole, ethyl- $\alpha$ -bromoisobutyrate, *N,N,N',N'',N''',N''''*-hexamethyltriethylenetetraamine (HMTETA), copper bromide (CuBr, CuBr<sub>2</sub>), methyl iodide, 1,4-dioxane, trans-3-indolacrylic acid (IAA), trimethylsilyldiazomethane were purchased from Aldrich, whereas tetrahydrofuran (THF) and hydrochloric acid (HCl) were delivered from Riedel-de Haën. Acetone, sodium hydroxide (NaOH) and hydrofluoric acid (HF) were bought from Merck. All chemicals were purchased in *pro analysi* (p.a.) quality. Deuterated chloroform (CDCl<sub>3</sub>) and heavy water (D<sub>2</sub>O) were delivered from Deutero, Kastellaun, Germany. These chemicals were used as delivered (except CuBr, which was treated with pure acetic acid and filtered to remove traces of Cu(II) compounds). *N,N*-Dimethylaminoethyl methacrylate was donated by RohMax, Darmstadt, and filtered over an alumina-B column before use. The synthesis of the initiators with 5, 8, 21 and 58 initiation sites is described in our previous publications.<sup>7, 30</sup> For dialysis we used regenerated cellulose membranes (either ZelluTrans with *MWCO* 4000 – 6000 Da from Roth, Karlsruhe, or Spectra/Pore 7 with *MWCO* 1000 Da).

**Synthesis of star-shaped poly(*N,N*-dimethylaminoethyl methacrylate):** In a typical reaction the monomer *N,N*-dimethylaminoethyl methacrylate (45.7 g, 290 mmol), the solvent anisole (150g), copper(I)bromide (CuBr, 143 mg, 1.0 mmol) and copper(II)bromide (CuBr<sub>2</sub>, 45 mg, 0.2 mmol) were deoxygenated by purging with nitrogen for 15 min. The solution was heated, under stirring, to 60 °C, yielding a clear, brownish solution. The ligand *N,N,N',N'',N''',N''''*-hexamethyltriethylenetetraamine (270 mg, 1.2 mmol) and the initiator (e.g. 235 mg silsesquioxane-based initiator<sup>30</sup>, 1.16 mmol initiation sites) were dissolved in 5 mL of anisole and purged with nitrogen (15 min). The transfer of the initiator solution to the reaction vessel was performed with a syringe, ensuring as little as possible contact with air. When injecting the initiator/ligand solution, the polymerization mixture immediately turns green. At appropriate time intervals samples were drawn with the help of syringes and the conversion was monitored by <sup>1</sup>H-NMR spectroscopy, comparing the integrals over the signals of the monomeric, unsaturated methylene group (close to 5.6 and 6.2 ppm) with the integrals over the polymeric, methacrylic  $\alpha$ -methyl protons (0.6 – 1.3 ppm). Two polymers with different arm lengths were obtained from each batch by withdrawing a part of the reaction

solution at a desired conversion. This was performed with help of a syringe under nitrogen counterflow. For example sample 58A (100 mL of polymerization mixture) was drawn after 675 min at 21% conversion for the polymerization using the silsesquioxane-based initiator. For the workup the viscous mixtures were diluted with ~ 200 mL THF (or acetone) and then passed through a silica column. Hereby copper salt traces were retained. After reconcentration on the rotational evaporator the polymer was dropwise precipitated into 2 L of cyclohexane / hexane mixtures (volume ratio was 1:2 for polymer 58A). The precipitated polymer was dissolved in dioxane (4 wt.%; 100 g dioxane), dialyzed against dioxane for two days (Roth membrane, regenerated cellulose, *MWCO* 4000-6000 Da) and finally freeze-dried from this dioxane solution in the absence of light (to yield e.g. 4 g of polymer 58A). Direct light exposure and air contact were omitted by storage under nitrogen and below 4 °C. The experimental conditions are given in Table 4. 1. The notations of the polymers are given in the same table together with the expected, theoretical arm length.

**Table 4. 1: Experimental conditions for the synthesis of poly(dimethylaminoethyl methacrylate) (PDMAEMA) stars<sup>a</sup>**

Run no. <sup>b</sup>	[DMAEMA] <sub>0</sub> (mol/L)	<i>t</i> (min)	conversion, <i>x<sub>p</sub></i> <sup>c</sup>	Calculated arm length <sup>d</sup>
5A	1.4	175	0.25	63
5E	1.4	485	0.47	118
8A	1.4	175	0.29	73
8E	1.4	485	0.47	118
21A	1.4	420	0.30	75
21E	1.4	1455	0.50	125
58A	1.3	675	0.21	53
58E	1.3	2820	0.41	100

<sup>a</sup> *T* = 60 °C, [DMAEMA]<sub>0</sub>/[HMTETA]/[Inisite]<sub>0</sub>/[CuBr]/[CuBr<sub>2</sub>] = 250:1:1:0.8:0.2., <sup>b</sup> the number denotes the targeted number of arms, A and E denote short and long arms, respectively, <sup>c</sup> measured by NMR spectroscopy, <sup>d</sup> assuming that all initiator functions have initiated

#### **Synthesis of star-shaped poly{[2-(methacryloyloxy)ethyl] trimethylammonium iodide}:**

For quaternization, PDMAEMA was dissolved in acetone (2 wt. %; e.g. 3 g polymer 58A – 0.02 mol amino groups - in 150 g). Methyl iodide (here 4 g, 0.03 mol) was added at room temperature at a molar ratio of 1.5 compared to amino groups. Although the solution became turbid after 10 min the mixture was kept stirring overnight to ensure quantitative conversion. Acetone was decanted and the polymer was washed several times with acetone (each 20 mL). Then 5 g quaternized polymer were dissolved in 100 mL water and dialyzed against pure

water for two days (Roth membrane, regenerated cellulose, *MWCO* 4000-6000 Da) and finally freeze-dried.

**Polymer Characterization:** *<sup>1</sup>H NMR spectroscopy:* A Bruker Avance (250 MHz) spectrometer was used. The solvent was either D<sub>2</sub>O or CDCl<sub>3</sub>. Simulations were performed with ACD/HNMR and ACD/CNMR Predictor Ver.3.00.

*Gel Permeation Chromatography (GPC):* Apparent molecular weight distributions and their averages of PDMAEMA stars were characterized by GPC using THF with 0.25 wt.% tetrabutylammonium bromide (TBAB) as eluent at a flow rate of 0.5 mL/min at room temperature (calibration with polystyrene standards). The setup was equipped with four columns (length 30 cm, diameter 0.8 cm, 5 μm PL-Gel, pore sizes 100, 10<sup>3</sup>, 10<sup>4</sup>, 10<sup>5</sup> Å) and an RI detector.

*Asymmetric Flow Field-Flow Fractionation (AF-FFF)* for the determination of the molecular weight distribution of the quaternized PDMAEMA was accomplished on a Postnova HRFFF-10000 system equipped with RI and multi-angle light scattering (Wyatt EOS, λ = 682 nm) detectors; dimension of the channel: 0.35 mm; cutoff molecular weight of the membrane 5 kDa; injection volume: 100 μL; constant cross-flow gradient: 1.5 mL/min within 30 min; laminar flow out: 0.6 mL/min; eluent: water with 25 mM sodium nitrate NaNO<sub>3</sub> and 0.2 g/L sodium azide NaN<sub>3</sub>; sample concentration: 0.7 g/L. For determination of the refractive index increment one sample (5 mL of a 1.76 g/L solution of quaternized star 58A in eluent) was dialyzed against 150 mL of eluent for two days (with help of micro dialyzer QuixSep, Roth, Germany, and Spectra/Por 7 membrane, *MWCO* 1000) and then diluted with dialysate to obtain different concentrations. The refractive index increment for that sample was determined as  $dn/dc = 0.1089 \pm 0.0003$  mL/g on a WGE Dr. Bures DnDc-2010 (λ = 620 nm) refractometer at room temperature.

*Static light scattering (SLS)* was performed on a Wyatt EOS (λ = 682 nm) multi-angle light scattering detector, operated in batch mode with acetone as solvent at room temperature (some SLS measurements were performed on a Sofica goniometer using a He-Ne laser). The high sensitivity of the detector enabled us to use very dilute concentrations (in the range of 10<sup>-2</sup> to 10<sup>-1</sup> g/L). The data were evaluated with the Wyatt ASTRA software, version 4.73.04. All samples were filtered before injection (PTFE filter, 0.45 μm). The refractive index increment was measured with differential refractometer DnDc-2010 (WGE Dr. Bures, λ = 620 nm) and Differential Refractometer Software Ver. 3.24 (Brookhaven Instruments). For

samples 21A to 58E the refractive index increment in acetone was determined as  $dn/dc = 0.133 \pm 0.02$  mL/g (no change of  $dn/dc$  was observed for those high molecular weight stars within the experimental error). For samples 5A to 8E  $dn/dc$  was measured as  $0.139 \pm 0.04$  mL/g.

*Dynamic light scattering (DLS)*: For the determination of hydrodynamic radius DLS was performed on an ALV DLS/SLS CGS-8FW compact goniometer system with an ALV 5000/E correlator and a He-Ne laser ( $\lambda = 632.8$  nm). Prior to the light scattering measurements (correlation times approximately 300 s depending on signal strength) the sample solutions were filtered using Millipore Nylon filters with a pore size of 0.45  $\mu\text{m}$ . The measured intensity correlation functions were subjected to CONTIN analysis. Apparent hydrodynamic radii of star-shaped polymers were calculated according to the Stokes-Einstein equation, using the viscosity of water. The viscosities of NaCl solutions ( $c \geq 0.2$  M) were determined with an Ubbelohde viscometer (Schott, 53610 I), taking the increased densities into account.

*Cryogenic Transmission Electron Microscopy (cryo-TEM)*: The sample was prepared by dissolving 10 mg of quaternized PDMAEMA in 0.5 mL 1 M NaCl and inserting it into a stiff dialysis cell (micro dialyzer QuixSep) in order to keep the concentration of polymer constant. Dialysis took two days against pure water. A drop of the sample was put on an untreated bare copper TEM grid (600 mesh, Science Services, München, Germany), where most of the liquid was removed with blotting paper, leaving a thin film stretched over the grid holes. The specimens were instantly shock-vitrified by rapid immersion into liquid ethane and cooled to approximately 90 K by liquid nitrogen in a temperature-controlled freezing unit (Zeiss Cryobox, Zeiss NTS GmbH, Oberkochen, Germany). The temperature was monitored and kept constant in the chamber during all the sample preparation steps. After freezing the specimens, the remaining ethane was removed using blotting paper. The specimen was inserted into a cryo-transfer holder (CT3500, Gatan, München, Germany) and transferred to a Zeiss EM922 EF-TEM. Examinations were carried out at temperatures around 90 K at an acceleration voltage of 200 kV. Zero-loss filtered images ( $\Delta E = 0$  eV) were taken under reduced dose conditions (100-1000 electrons/nm<sup>2</sup>). All images were registered digitally by a bottom-mounted CCD camera system (Ultrascan 1000, Gatan) combined and processed with a digital imaging processing system (Gatan Digital Micrograph 3.9 for GMS 1.4).

*Osmometry*: A membrane osmometer (Gonotec Osmomat 090) with regenerated cellulose membrane (Millipore, PLAC 076 10, *NMWL*: 1000) was used for the determination of the osmotic coefficient. Solutions of PMETA1 (10 g/L) were dialyzed against pure water and

diluted to obtain the samples. Solid content determination by freeze drying and vacuum oven (40 °C) gave the final concentration after dialysis. The cell was kept at 30 °C. To rinse the measurement cell with the new sample approximately 0.7 mL of sample solution were injected three times. The measured osmotic pressure  $\Pi_m$  was converted to the osmotic coefficient  $\phi$ , which is defined by the ratio  $\Pi_m$  to the ideal osmotic pressure  $\Pi_{cal}$  of all counterions according to van't Hoff's law (eq. (1)).<sup>2, 5, 7</sup>

$$\phi = \frac{\Pi_m}{\Pi_{cal}} \quad 4.1.$$

For the determination of the number-average molecular weight in THF we used a regenerated cellulose two-layer membrane with *MWCO* 20000 (Gonotec). Several concentrations were injected and  $\Pi_m/c$  was extrapolated to vanishing concentrations.

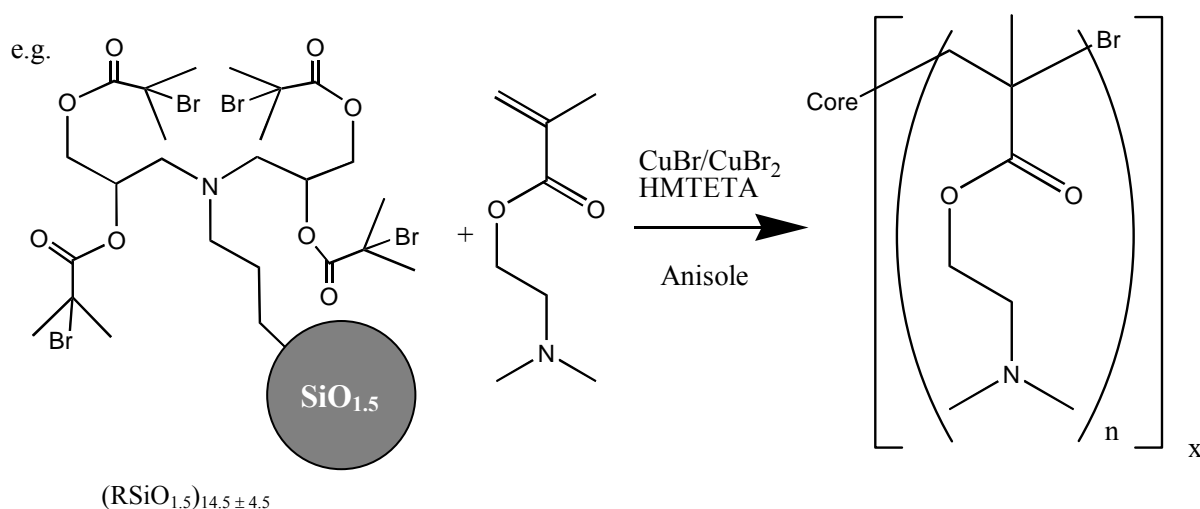
*Elemental Analysis* was performed by the Mikroanalytisches Laboratorium Ilse Beetz in Kronach, Germany.

### 4.3. Results and Discussion

#### 4.3.1 Synthesis of Star-Shaped Poly(*N,N*-dimethylaminoethyl methacrylate)

We performed the synthesis of star-shaped PDMAEMA by atom transfer radical polymerization employing oligofunctional initiators with 2-bromoisobutyryl initiating fragments, with copper bromide CuBr as catalyst and *N,N,N',N'',N''',N''''*-hexamethyltriethylenetetramine as a strong ligand in anisole as solvent (Scheme 4. 1).<sup>24</sup> To minimize the concentration of free radicals and hence reduce termination we added CuBr<sub>2</sub> as a retarder.

**Scheme 4. 1:** Strategy for the synthesis of poly(dimethylaminoethyl methacrylate) (PDMAEMA) stars with initiator example



In addition to initiators based on glucose (5 functions), saccharose (8 functions) or  $\beta$ -cyclodextrin (21 functions),<sup>7</sup> we employed a silsesquioxane-based initiator with ca. 58 functions, which has already been used for the synthesis of star-shaped glycopolymers and hybrid poly(acrylic acid) stars with inorganic core (Scheme 4. 1).<sup>30</sup>

The kinetics of those polymerizations depends on the number of initiating sites. Details are reported in the Supporting Information (chapter 4. 5). By withdrawing samples at different conversions we obtained a range of polymers with different arm numbers and arm lengths. The notation is shown in Table 4. 1. From ratio of monomer to initiating site concentrations and conversion we calculated the theoretical arm lengths by assuming that initiation site efficiency equals unity (see Table 4. 1). Since the monomer is quite bulky, the initiation site efficiency was expected to be below unity, leading to less, but longer arms. However, the overall number-average molecular weight,  $M_n$ , does not change (see Table 4. 2), given that each initiator molecule initiates at least once and chain transfer and chain-chain coupling can be excluded.

**Molecular Characterization.** We performed gel permeation chromatography (GPC) in THF with 0.25 wt. % tetrabutylammonium bromide (TBAB) to minimize the adsorption of the amino-containing polymer on the column. Typical eluograms are given in Figure 4. 1. The apparent molecular weight averages and polydispersity indexes (calibration with linear PS) are given in Table 4. 2.

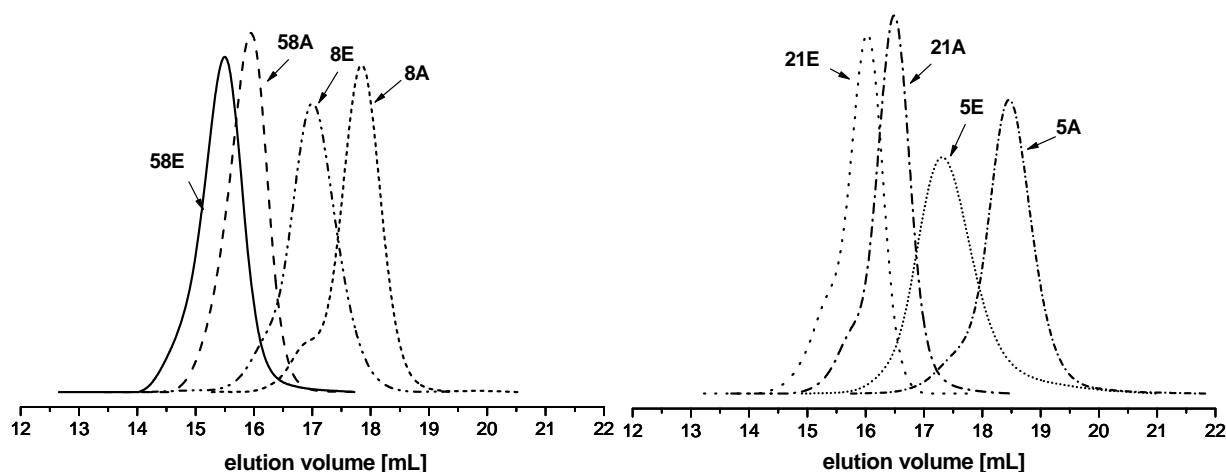


**Figure 4. 1:** Gel Permeation Chromatography eluograms of poly(dimethylaminoethyl methacrylate) stars with tetrahydrofuran (+ 0.25 wt.% tetrabutylammonium bromide) as eluent

**Table 4. 2: Molecular weight averages (in g/mol) of poly(dimethylaminoethyl methacrylate) stars determined by different methods**

<b>Samp le</b>	$10^{-3}M_{n,calc}^a$	$10^{-3}M_{n,exp}^b$	$10^{-3} \cdot M_{n,app}^c$ ( $PDI_{app}$ )	$10^{-3} \cdot M_w^d$ ( $\langle R_g^2 \rangle_z^{0.5}$ [nm])	$PDI^e$
<b>5A</b>	<b>51</b>	<b>56</b>	<b>42 (1.13)</b>	<b>62 (-)</b>	<b>1.22</b>
<b>5E</b>	<b>94</b>	<b>97</b>	<b>74 (1.21)</b>	<b>103 (-)</b>	<b>1.10</b>
<b>8A</b>	<b>93</b>	<b>99</b>	<b>67 (1.09)</b>	<b>117 (-)</b>	<b>1.26</b>
<b>8E</b>	<b>150</b>	<b>155</b>	<b>108 (1.14)</b>	<b>155 (-)</b>	<b>1.03</b>
<b>21A</b>	<b>250</b>	<b>-</b>	<b>162 (1.11)</b>	<b>300 (-)</b>	<b>1.20</b>
<b>21E</b>	<b>430</b>	<b>-</b>	<b>248 (1.18)</b>	<b>560 (23)</b>	<b>1.30</b>
<b>58A</b>	<b>490</b>	<b>500</b>	<b>253 (1.12)</b>	<b>690 (17)</b>	<b>1.41</b>
<b>58E</b>	<b>950</b>	<b>950</b>	<b>371 (1.24)</b>	<b>1360 (29)</b>	<b>1.43</b>

<sup>a</sup> number-average molecular weight ( $M_n$ ) calculated from conversion  $x_{p,NMR}$  ( $M_n = M_{DMAEMA} \cdot x_{p,NMR} \cdot [DMAEMA]_0 / [initiator\ molecule]_0$ ); <sup>b</sup> experimental  $M_n$  determined by membrane osmometry in THF for 5A to 8E and by elemental analysis for 58A/58E; <sup>c</sup> apparent  $M_n$  determined by gel permeation chromatography with linear poly(styrene) standards; <sup>d</sup> weight-average molecular weight ( $M_w$ ) and root of z-average of mean-squared radius of gyration ( $R_g$ ) determined by static light scattering (SLS) in acetone; <sup>e</sup> polydispersity index ( $PDI$ ) determined by ratio of  $M_w$  (SLS) and  $M_n$  (conversion)

In Figure 4. 1 we observe the expected increase of the hydrodynamic volume with increasing arm length as well with increasing arm number. In the case of the sugar-based stars a small fraction of star-star coupling is observed as a small shoulder on the low elution volume side of the eluogram. In contrast, almost no shoulder is found for the PDMAEMA stars with high arm numbers. This might be due to the decreased radical concentration in the synthesis of silsesquioxane-based stars (lower polymerization rate, see Supporting Information). The polydispersity of the silsesquioxane initiator might also obscure the visibility of coupled products. The apparent polydispersity of the stars, which mainly resembles the polydispersity in hydrodynamic radius, increases with conversion in all cases (see Table 4. 2). This might reflect some termination reactions like disproportionation or star-star coupling reactions by either combination of chain end radicals or the attack of amines on the chain end halogen (see also Supporting Information). Both effects should be the more pronounced the better the stars can interpenetrate.

The absolute number-average molecular weights,  $M_n$ , of the stars with lower arm numbers was determined by membrane osmometry in THF (Table 4. 2). For the stars with silsesquioxane core the determination of  $M_n$  was performed by elemental analysis, comparing the silicon and bromine contents, which originated from the initiator, with the nitrogen content of the monomer units (see Table 4. 6, Supporting Information). The obtained values are close to the expected values, which we calculated from conversion. This means that conversions determination by NMR, osmometry and elemental analysis are reliable methods for the determination of  $M_n$  of those PDMAEMA stars.

To determine the real polydispersity of the stars, we performed static light scattering experiments in very dilute acetone solutions of PDMAEMA on a multi-angle light scattering detector. One example of an obtained Zimm-Plot is given in Figure 4. 2. All results are listed in Table 4. 2. The polydispersity index is calculated as the ratio of  $M_w$ , determined by SLS, to  $M_n$ , determined by conversion. Since both values have inherent errors, the error in the *PDI* is larger than that obtained by GPC, but it is not as systematic. GPC of multi-arm stars suffers from the problem that the hydrodynamic volume does not depend as strongly on the arm number as on the arm length.<sup>37</sup>

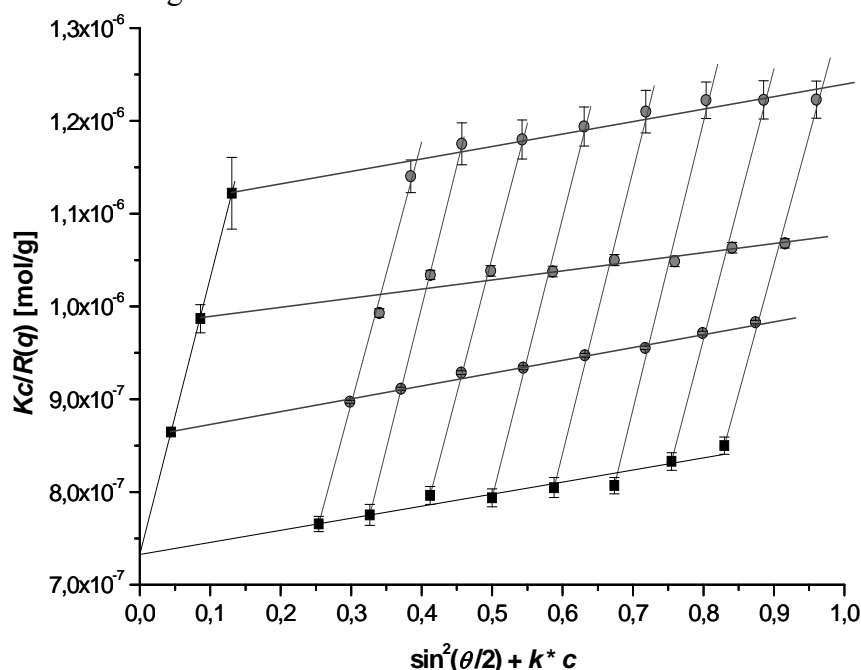


**Figure 4. 2:** Zimm-plot of poly(dimethylaminoethyl methacrylate) star 58E in acetone at 25 °C ( $k = 2$  L/g; concentration  $c = 0.022$  g/L,  $0.043$  g/L and  $0.066$  g/L)

As seen in Table 4. 2 silsesquioxane-based stars have higher polydispersity than the sugar-based stars. One should keep in mind that the initiator is polydisperse ( $PDI = 1.2$ ). The increase in polydispersity as compared to the initiators indicates an additional arm number distribution due slow initiation.<sup>38</sup> Polydispersity due to arm-length variation is rather

negligible, as implied by Schulz's coupling theorem.<sup>39</sup> Though the apparent polydispersity by GPC increases during polymerization in all cases it is striking that the polydispersities appear to decrease with conversion for the stars with low arm numbers.

### 4.3.2. Quaternization of PDMAEMA Stars

In order to obtain strong polyelectrolyte stars, the pendant amino groups were quaternized with methyl iodide, leading to poly{[2-(methacryloyloxy)ethyl] trimethylammonium iodide} (PMETAI). The completeness of quaternization was verified by elemental analysis, <sup>1</sup>H-NMR (Figure 4. 9, Supporting Information) and by Asymmetric Flow Field-Flow Fractionation (AF-FFF) with multi-angle light scattering detector (Figure 4. 3),

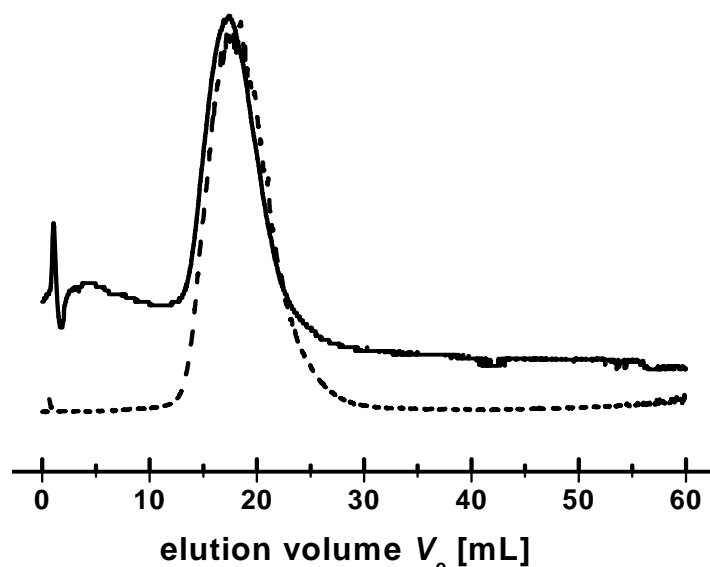


Figure 4. 3: Field-Flow Fractionation (AF-FFF) eluogram of quaternized star 58 A in water (0.7 g/L; 25 mM NaNO<sub>3</sub>, 0.2 g/L NaN<sub>3</sub>; solid line: RI detector; dashed line: multi angle light scattering (MALS) detector at 90°)

The distribution stays monomodal after quaternization. The obtained weight-average molecular weight,  $M_w$ , from the multi angle light scattering detector is  $1.5 \cdot 10^6$  g/mol which is consistent with the expected  $M_w$  of  $1.3 \cdot 10^6$  g/mol. The polydispersity obtained by AF-FFF-MALS is underestimated ( $PDI = 1.1$ ) which might be a result of the poor separation of star-like molecules with an arm-number distribution. The change in molecular weight is only weakly reproduced in a change of hydrodynamic volume as also seen in GPC, where we obtained almost the same apparent polydispersity.

### 4.3.3. Determination of Initiation Site Efficiency

The arms of the quaternized PDMAEMA were detached from the core by classical ester hydrolysis in concentrated NaOH. The resulting linear PMAA was analyzed by aqueous GPC

and additionally esterified to PMMA, which was analyzed by GPC and MALDI-ToF mass spectrometry. The details of procedure and analysis are given in the Supporting Information and the results are listed in Table 4. 3.

**Table 4. 3: Number-average degrees of polymerization of the cleaved arms and their polydispersities (in brackets; both obtained by different methods), initiation site efficiencies,  $f_i$ , derived there from (*bold italics*) and the approximate formulas derived from the averages of initiation site efficiencies.**

method	5A	5E	8A	8E
conversion <sup>a</sup>	63; <i>1.00</i>	118; <i>1.00</i>	73; <i>1.00</i>	118; <i>1.00</i>
GPC of lin. PMAA <sup>b</sup>	101 (1.37); <i>0.62</i>	169 (1.32); <i>0.70</i>	113 (1.40); <i>0.65</i>	169 (1.34); <i>0.70</i>
GPC of lin. PMMA <sup>c</sup>	102 (1.09); <i>0.62</i>	162 (1.13); <i>0.73</i>	116 (1.09); <i>0.63</i>	167 (1.12); <i>0.71</i>
MALDI of PMMA <sup>d</sup>	104 (1.15); <i>0.61</i>	154 (1.15); <i>0.77</i>	99 (1.17); <i>0.73</i>	171 (1.13); <i>0.69</i>
average	<i>0.62</i>	<i>0.73</i>	<i>0.67</i>	<i>0.70</i>
formula <sup>e</sup>	(PDMAEMA <sub>100</sub> ) <sub>3.1</sub>	(PDMAEMA <sub>160</sub> ) <sub>3.7</sub>	(PDMAEMA <sub>110</sub> ) <sub>5.4</sub>	(PDMAEMA <sub>170</sub> ) <sub>5.6</sub>

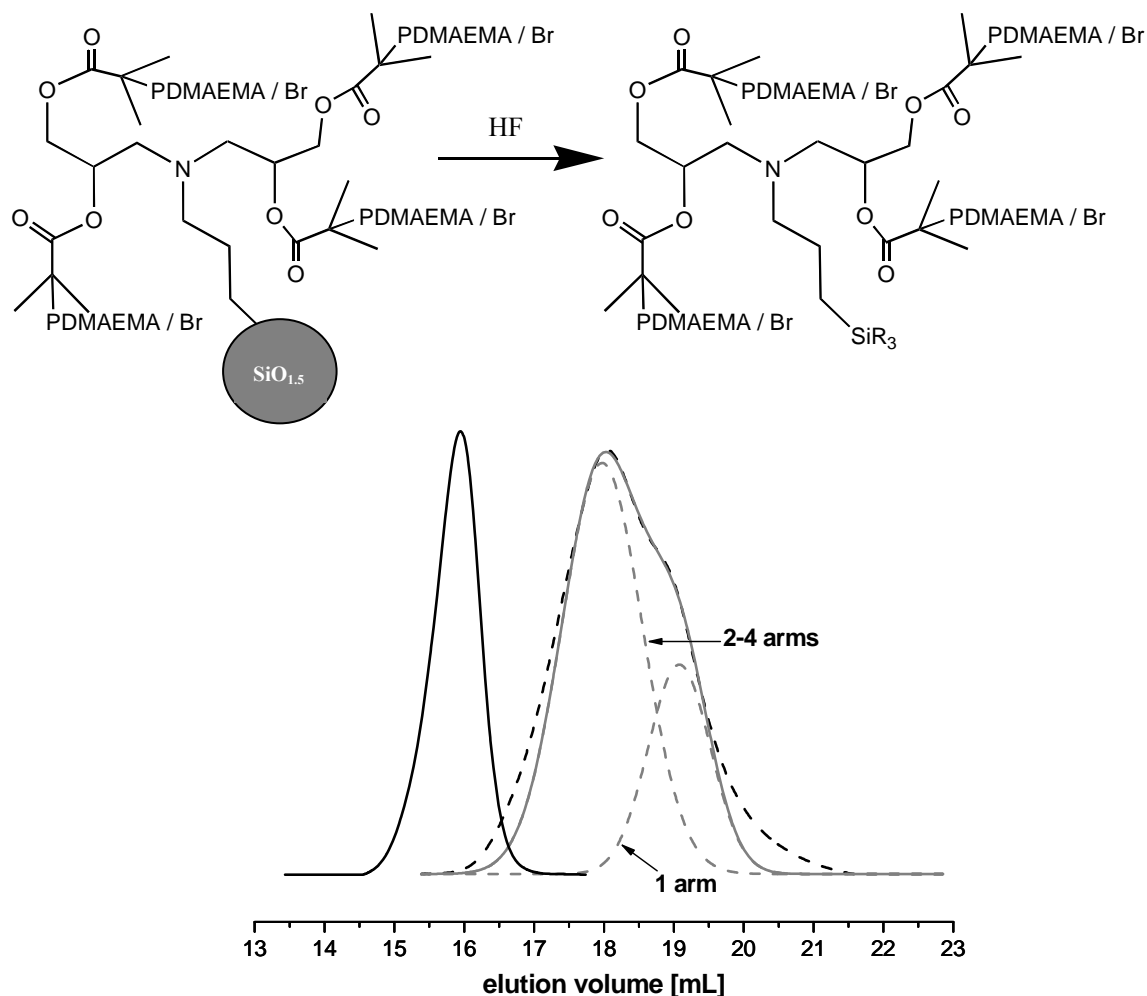
  

method	21A	21E	58A	58E
conversion <sup>a</sup>	75; <i>1.00</i>	125; <i>1.00</i>	53; <i>1.00</i>	100; <i>1.00</i>
GPC of lin. PMAA <sup>b</sup>	173 (1.32); <i>0.43</i>	264 (1.33); <i>0.47</i>	173 (1.38); <i>0.31</i>	238 (1.45); <i>0.42</i>
GPC of lin. PMMA <sup>c</sup>	147 (1.16); <i>0.51</i>	223 (1.31); <i>0.56</i>	161 (1.21); <i>0.33</i>	242 (1.31); <i>0.41</i>
MALDI of PMMA <sup>d</sup>	177 (1.07); <i>0.42</i>	(385 (1.06); <i>0.32</i> )	188 (1.08); <i>0.28</i>	233 (1.05); <i>0.43</i>
average	<i>0.45</i>	<i>0.51</i>	<i>0.31</i>	<i>0.42</i>
formula <sup>e</sup>	(PDMAEMA <sub>170</sub> ) <sub>9.5</sub>	(PDMAEMA <sub>240</sub> ) <sub>11</sub>	(PDMAEMA <sub>170</sub> ) <sub>18</sub>	(PDMAEMA <sub>240</sub> ) <sub>24</sub>

<sup>a</sup> expected degree of polymerization  $P_n$  obtained by conversion  $x_{p,NMR}$  and monomer to initiator ratio ( $P_n = x_{p,NMR} \cdot [DMAEMA]_0/[initiator]_0$ ); <sup>b</sup>  $P_n$  obtained by gel permeation chromatography (GPC) of corresponding poly(methacrylic acid) (PMAA) with water as eluent; <sup>c</sup> GPC of corresponding poly(methyl methacrylate) (PMMA) with tetrahydrofuran as eluent; <sup>d</sup> obtained by matrix assisted laser desorption ionization time of flight (MALDI-ToF) mass spectrometry of corresponding PMMA arms; <sup>e</sup> structure of poly(dimethylaminoethyl methacrylate) stars (PDMAEMA<sub>n</sub>)<sub>x</sub>; n = number-average degree of polymerization per arm; x = number-average arm number

In addition to the classical method one can estimate the initiation site efficiency of the silsesquioxane-based stars by cleaving off segments with four former initiation sites. These are linked via silicon atoms to the silsesquioxane core and can be released by treatment with hydrofluoric acid (Scheme 4. 2).

**Scheme 4. 2: Destruction of the core of silsesquioxane-based stars (R assigns F or OH)**



**Figure 4. 4: Gel permeation chromatography eluograms of poly(dimethylaminoethyl methacrylate) (PDMAEMA) star 58A (—) and its single fragments, obtained by HF treatment of core (-----), and (in grey) the deconvolution of the PDMAEMA star fragments by a double Gaussian fit (—) with its single constituents (-----).**

<sup>1</sup>H-NMR does not give any indication of ester cleavage as the integrals over the signals are the same before and after HF treatment and dialysis, whereas GPC (in THF with TBAB) reveals 100 % scission (Figure 4. 4). Although one would expect a quadrimodal distribution, showing fragments with one, two, three and four arms, the limited GPC resolution only provided a bimodal distribution. Thus, we performed a double Gaussian fit in the distinct region of the eluogram. Furthermore the tailing indicates that the low molecular fraction

(including the low molecular residual) is linear PDMAEMA with only one arm, as the tailing strongly resembles the trace of linear PMMA (former PDMAEMA arms; not shown). The high molecular weight fraction comprises all segments with higher arm numbers. Assuming Bernoullian statistics, which implies independent occurrence of single initiation processes, we can now make a further rough estimation of the initiation site efficiency. In order to compare the expected probability of having segments with  $x$  arms with the response of the mass-sensitive RI-detector one needs to multiply the probability with  $x$ . By trial and error we estimated the initiation site efficiency to be  $p = 0.33$  (Table 4. 4), which coincides nicely with the initiation site efficiency obtained by classical cleavage,  $f_i = 0.31$ . This value fits best the ratio of RI response integrals  $A$  in GPC,  $A(2-4 \text{ arms}) / A(\text{one arm}) = 0.7 / 0.3 = 2.3$ .

**Table 4. 4: Bernoullian probabilities of finding detached stars with  $x$  arms out of maximum four**

$x$	probability calculation	mole fraction, $n(x)$ for $p = 0.33$	weight fraction $w(x) = x \cdot n(x)$
0	$(1-p)^4$	0.202	0
1	$(1-p)^3 \cdot p \cdot 4$	0.397	0.300
2	$(1-p)^2 \cdot p^2 \cdot 6$	0.293	0.444
3	$(1-p) \cdot p^3 \cdot 4$	0.096	0.219
4	$p^4$	0.012	0.036

}  $\Sigma = 0.70$

The same procedure was attempted for 58 E. However as the initiator has a higher initiation site efficiency in that case, the ratio of fragments with only one arm is rather small and, due to GPC's limited resolution for fragments with higher arm number and longer arms, fitting was not feasible. Besides the limited resolution of the GPC, the same hydrodynamic volume can be expected for segments with many short arms and segments with a few long arms. Due to slow initiation both types of segments might be present in our sample and aggravate the analysis since both types of segments overlap in the GPC eluogram.

Another drawback of the new method is the assumption of purely independent initiation processes. We cannot exclude that after one initiation site has initiated, the probability to

initiate the surrounding initiation sites has decreased due to decreased accessibility. This is not taken into account by Bernoullian statistics.

#### 4.3.4. Hydrodynamic Behavior

We performed dynamic light scattering (DLS) measurements on the uncharged PDMAEMA stars in acetone at concentrations below the overlap concentration (0.4 g/L at 25°C except 21E, 58A and 58E: 0.2 g/L) and on the quaternized stars (PMETAI) in aqueous salt solutions. The intensity autocorrelation function of star-shaped PDMAEMA was determined for different scattering angles. A linear dependence of the decay rates,  $\Gamma$ , on the squared length of scattering vector,  $q^2$ , was found in all cases, indicating a purely diffusive process of spherical star polymers.

**Table 4. 5: Dynamic light scattering (DLS) results of the poly(dimethylaminoethyl methacrylate) stars in acetone<sup>a</sup> and the structure-sensitive parameter,  $\rho$ , calculated using the radius of gyration  $\langle R_g^2 \rangle_z^{0.5}$  from Table 4. 2**

	<b>5A</b> (PDMAEMA <sub>100</sub> ) <sub>3.1</sub>	<b>5E</b> (PDMAEMA <sub>160</sub> ) <sub>3.7</sub>	<b>8A</b> (PDMAEMA <sub>110</sub> ) <sub>5.4</sub>	<b>8E</b> (PDMAEMA <sub>170</sub> ) <sub>5.6</sub>
$\langle R_h \rangle_z$ [nm] <sup>b</sup>	4.7	6.1	6.0	7.4
$\langle R_h \rangle_w / \langle R_h \rangle_n$ <sup>c</sup>	1.22	1.36	1.12	1.20
	<b>21A</b> (PDMAEMA <sub>170</sub> ) <sub>9.5</sub>	<b>21E</b> (PDMAEMA <sub>240</sub> ) <sub>11</sub>	<b>58A</b> (PDMAEMA <sub>170</sub> ) <sub>18</sub>	<b>58E</b> (PDMAEMA <sub>240</sub> ) <sub>24</sub>
$\langle R_h \rangle_z$ [nm] <sup>b</sup>	8.7	14.7	13.5	19.9
$\langle R_h \rangle_w / \langle R_h \rangle_n$ <sup>c</sup>	1.08	1.20	1.13	1.31
$\rho = \langle R_h \rangle_z / \langle R_g^2 \rangle_z^{0.5}$	-	1.5	1.3	1.5

<sup>a</sup> concentration 0.4 g/L at 25 °C, except 21E, 58A and 58E: 0.2 g/L; <sup>b</sup> z-average hydrodynamic radius  $R_h$  obtained by CONTIN analysis; <sup>c</sup> polydispersity in hydrodynamic radius obtained by weight- and number-average hydrodynamic radius according to CONTIN analysis

The hydrodynamic radii of some PDMEMA stars, obtained by CONTIN analysis at 90°, are summarized in Table 4. 5. The polydispersity, as seen from this analysis, increases with

the arm length (i.e increasing conversion). This coincides with the apparent polydispersities seen in conventional GPC (Table 4. 2) which reflect the distribution of hydrodynamic volumes.

The observed structure-sensitive parameters,  $\rho = \langle R_h \rangle_z / \langle R_g^2 \rangle_z^{0.5}$ , are typical for star-like structures. Burchard's derivation<sup>40</sup> leads to  $\rho = 1.30$  and  $1.37$  for stars with 24 and 11 polydisperse arms, respectively, at  $\theta$ -conditions. Since our measurements were performed in a good solvent, these theoretical ratios should increase, matching our experimental parameters.

The dependence of the hydrodynamic radius,  $R_h$ , of the star-shaped quaternized PDMAEMA 58A, (PMETA<sub>I170</sub>)<sub>18</sub>, on ionic strength was also investigated by DLS ( $c = 0.3$  g/L, 24 °C, 90°). For very low salt concentrations the intensity-weighted decay rate distributions (after CONTIN treatment of the intensity autocorrelation curves) tend to broaden, most probably due to increasing inter-particle interactions, e.g. slow modes.

For the determination of the hydrodynamic radii, according to the Stokes-Einstein equation, the viscosities of NaCl and NaI solutions were measured and taken into account. At low ionic strength ( $c_{\text{NaX}} < 0.01$  M) we found  $R_h \sim 24$  nm, which is about 56% of the contour length of a single chain ( $L_c = 0.25$  nm  $\times$   $DP_{n,\text{arm}} = 42.5$  nm), indicating a considerable stretching due to Coulombic repulsion and high osmotic pressure inside the star. Figure 4. 5 shows a pronounced drop in hydrodynamic radius with increasing salt concentration, indicating the expected contraction of the polyelectrolyte arms due to electrostatic and osmotic screening (diminishing the high net osmotic pressure within the star). The hydrodynamic radius in the fully salted case ( $R_h \sim 15$  nm at 4.6 M NaCl) is in good agreement with that of the uncharged PDMAEMA star 58A in acetone ( $R_h \sim 14$  nm).

Figure 4. 5 also demonstrates that these cationic star polyelectrolytes exhibit a salting-out and a salting-in effect as observed previously for cationic spherical<sup>41</sup> and planar brushes.<sup>42</sup> Using NaI instead of NaCl leads to the same hydrodynamic radius at low salt concentration but to marked differences starting from  $c \sim 0.1$  M. At 0.5 M NaI the system enters a two-phase region but at 1 M NaI a salting-in occurs. This collapse transition in a single star-like molecule is under further investigation.

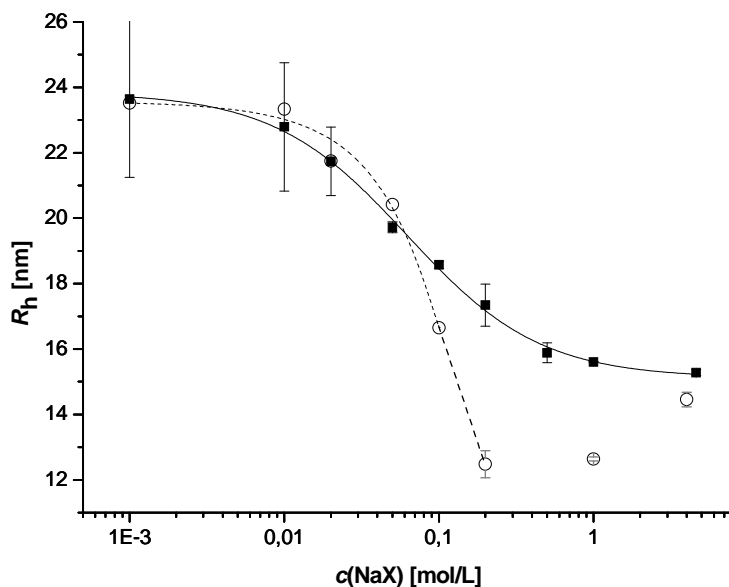
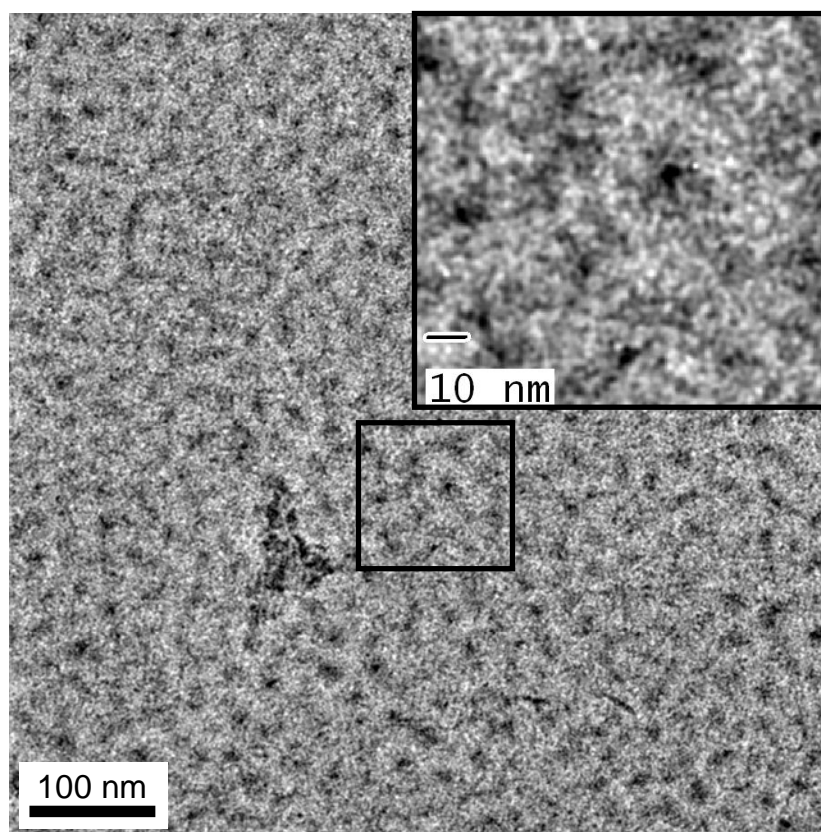


Figure 4. 5: Dependence of the hydrodynamic radius of star-shaped quaternized poly(dimethylaminoethyl methacrylate) 58A, (PMETA<sub>I170</sub>)<sub>18</sub>, with ionic strength; squares: NaCl; circles: NaI. The lines are guides for the eye.

#### 4.3.5. Cryogenic Transmission Electron Microscopy

Finally we characterized the quaternized PDMAEMA star 58A, (PMETA<sub>I170</sub>)<sub>18</sub>, by cryo-TEM. The star polymer was dissolved in 1 M NaCl and dialyzed against pure water which leads to a partial exchange of iodide ions. Distinct structures are seen in Figure 4. 6. In some cases the silsesquioxane cores are apparent as dark spots with a diameter in the range of 3 nm (insert). According to Fourier transformation the mean distance between the particle centers is around 27 nm, i.e. above the overlap concentration (hydrodynamic diameter,  $2R_h \approx 48$  nm). Still we observe some fading shades around the core, which might be attributed to the radially decreasing segment density. Due to the slow initiation during polymerization the segment density around the core is higher than in the case of uniform arms.



**Figure 4. 6:** Cryogenic transmission electron microscopy (cryo-TEM) image of a 2 wt. % solution of quaternized poly(dimethylaminoethyl methacrylate) 58A, (PMETA<sub>170</sub>)<sub>18</sub>, in water (the iodide counterion was partly exchanged by chloride during dialysis); insert: zoom of marked region

#### 4.3.6. Osmotic Coefficients

Recently we published the osmotic behavior of star-shaped poly(acrylic acid) (PAA) with rather low degree of neutralization.<sup>7</sup> Here we present the osmotic coefficient of fully charged, quaternized PDMAEMA stars. Figure 4. 7 shows that the osmotic coefficients decrease with increasing arm number and decreasing arm length. In both cases the segment density and thus the charge density and thus the counterion confinement increase.<sup>3</sup> Figure 4. 7 (right hand side) compares (PAA<sub>100</sub>)<sub>21</sub> and (PMETA<sub>170</sub>)<sub>18</sub>, both having comparable arm numbers and arm lengths but different charge densities. We directly see that increasing charge density leads to larger counterion confinement, as predicted by theory.<sup>3</sup>

For (PMETA<sub>170</sub>)<sub>18</sub> (58A), we also investigated the concentration dependence. We see again an increase of the osmotic coefficient with concentration, though the rise is not as large as for the PAA stars. However, the observed concentration dependence is in contrast to theory<sup>3</sup> as was already discussed for the PAA stars.<sup>7</sup> Nevertheless, both theory and experiment give values in the same order of magnitude. Some deviations might arise due to the polydisperse nature of our stars and due to possible ion-specific interactions. The differences between the

concentration dependences might also stem from the fact that the theory regards all counterions outside the star to have equal osmotic activity even though the counterions in the close vicinity experience a strong electrostatic field, diminishing their activity. Increasing concentration can give a contribution to a higher activity of those counterions since the decreasing distance between the stars alters the net electrostatic field. In theory the entropic contribution of the counterions leads to an increased number of free counterions in respect to decreasing concentration. Nevertheless we can conclude that more than 90 % of the counterions are entrapped within the investigated quenched polyelectrolyte star 58A. This is in full agreement with theory.

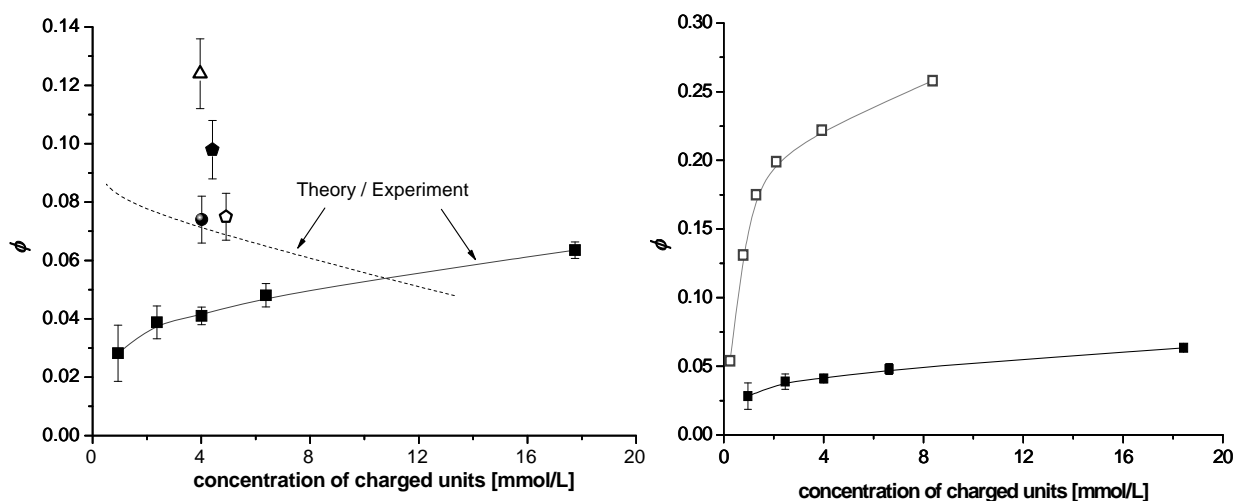


Figure 4. 7: Osmotic coefficients,  $\Phi$ , of star-shaped poly{[2-(methacryloyloxy)ethyl] trimethylammonium iodide} (PMETAIs)<sub>18</sub> (58A, ■), (PMETAIs)<sub>9.5</sub> (21A, ●), (PMETAIs)<sub>5.4</sub> (8A, ◇), (PMETAIs)<sub>5.6</sub> (8E, ◆), and (PMETAIs)<sub>3.1</sub> (5A, △). Dashed line: theoretical dependence for a fully ionized star with 18 arms and degree of polymerization of single arm  $DP_{\text{arm}} = 170$ . Right hand side: comparison of (PMETAIs)<sub>18</sub> with poly(acrylic acid) star (PAA<sub>100</sub>)<sub>21</sub> with degree of neutralization,  $\alpha = 0.24$ .<sup>7</sup>

## 4.4. Conclusions

Star-shaped PDMAEMAs and their quaternized analogues, PMETAIs, were successfully synthesized by the core-first method employing ATRP. The architecture of the initiating system together with the polymerization features lead to polymer stars with a moderate arm number and arm size distribution due to slow initiation. The initiation site efficiency was determined by two different cleaving procedures: cleaving off all of the arms and detaching star-like fragments. The obtained star-shaped strong polyelectrolytes show the expected decrease in hydrodynamic radius with increasing ionic strength. For iodide counterions a salting-out/salting-in effect is observed. Up to 97 % of counterions are confined inside the star, as determined by osmometry in salt-free solution. The confinement increases with increasing arm number and decreasing arm length. However, again there is a discrepancy

between the experimentally observed and theoretically calculated concentration dependence of the osmotic coefficients, which needs further elaboration.

## 4.5. Supporting Information

### Kinetics of ATRP of DMAEMA with multifunctional initiators

The time dependence of conversion during the polymerization was followed by  $^1\text{H-NMR}$  spectroscopy. Figure 4. 1 shows a first-order kinetic plot of the polymerizations of DMAEMA. The polymerization employing the initiator with five initiating functions shows an almost linear dependence in the semi-logarithmic plot whereas the polymerizations with 21- and 58-functional initiator do not exhibit first-order kinetics, in contrast to other reports for the synthesis of linear PDMAEMA.<sup>24, 28</sup> Also, when plotting  $-\ln(1-x_p)$  against  $t^{2/3}$  according to Fischer's theory<sup>43</sup>, no straight line was obtained. The deceleration of the polymerizations can only partly be explained by termination reactions since there is a pronounced trend towards slower polymerization for stars with higher arm numbers. Star-like polyamines seem to be more efficient in complexing the catalyst, thus reducing the available amount of  $\text{CuBr}$ , due to the increased segment density in the stars.

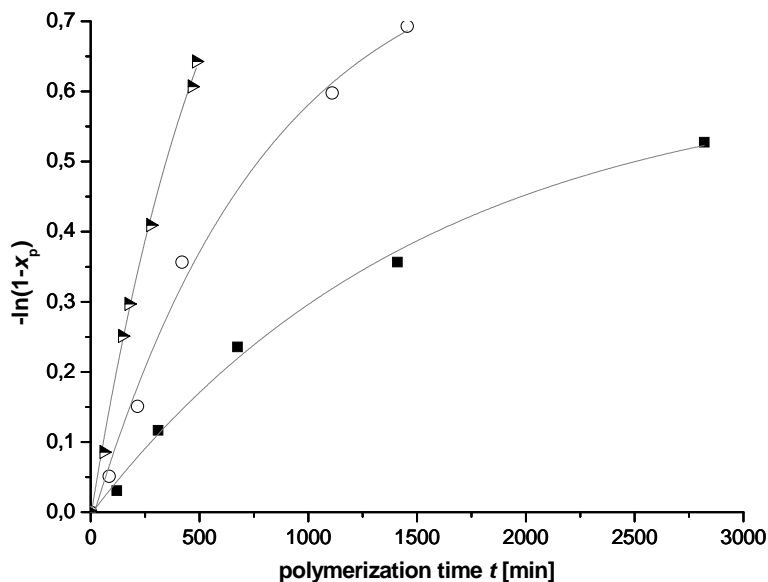


Figure 4. 8: First-order kinetic plots for the atom transfer radical polymerization of dimethylaminoethyl methacrylate (DMAEMA) using an initiator with 5 (▶), 21 (○), or 58 initiation sites (■) at 60 °C in anisole (75 wt.%). ( $[\text{DMAEMA}] : [\text{Inisite}] : [\text{CuBr}] : [\text{CuBr}_2] : [\text{HMTETA}] \approx 250 : 1 : 0.8 : 0.2 : 1$ ).

As shown in Table 4. 3 (main text) the initiation site efficiency decreases with the number of functions, lowering the concentration of active species. Another contribution to the diminution of the radical concentration during polymerization might be the possible

substitution of the chain-end halogen by ubiquitous amines.<sup>22</sup> Due to our long polymerization times this reaction might gain importance. The rather fast polymerizations in literature<sup>24, 28</sup> do not show this effect.

### Elemental Analysis of Silsesquioxane-Based Stars

**Table 4. 6: Elemental analysis of the silicon containing poly(dimethylaminoethyl methacrylate) stars and the theoretical arm length  $DP_{n,theo}(\text{arm})$  calculated therefrom (assuming initiation site efficiency  $f_i = 1$  and no transfer)**

			<b>Si</b>	<b>N</b>	<b>Br</b>	$DP_{n,theo,Br}(\text{arm})^a$	$DP_{n,theo,Si}(\text{arm})^b$
			(wt. %)	(wt. %)	(wt. %)		
<b>58A</b>	(calculated conversion)	from	<b>0.081</b>	<b>8.73</b>	<b>0.92</b>	<b>53</b>	<b>53</b>
<b>58A</b>	(experimental)		<b>0.08</b>	<b>8.67</b>	<b>0.90</b>	<b>55</b>	<b>54</b>
<b>58E</b>	(calculated conversion)	from	<b>0.044</b>	<b>8.81</b>	<b>0.50</b>	<b>100</b>	<b>100</b>
<b>58E</b>	(experimental)		<b>0.04</b>	<b>8.87</b>	<b>0.52</b>	<b>97</b>	<b>110</b>

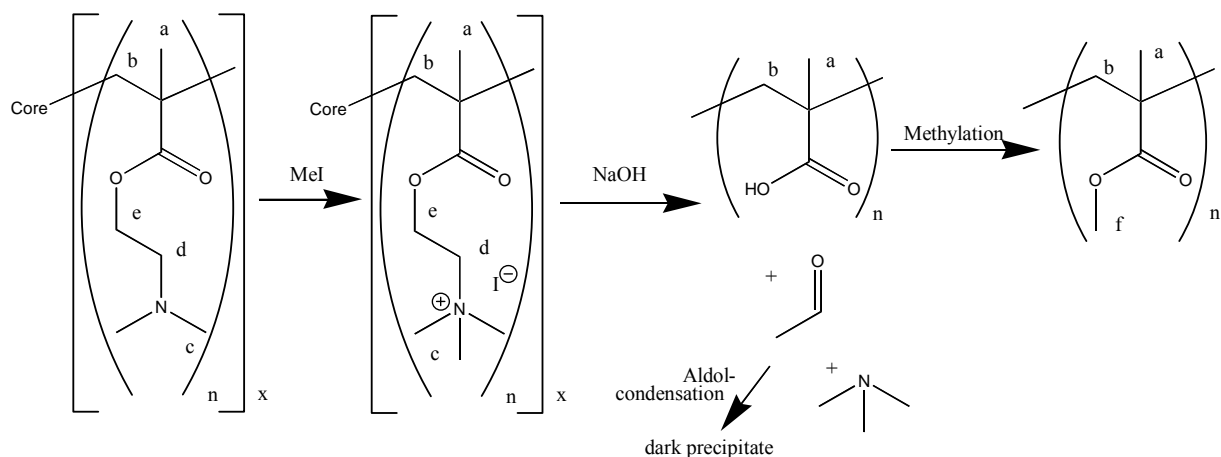
<sup>a</sup> derived from the ratio of the molar amounts of N and Br,  $n(\text{N})/n(\text{Br})$ ; <sup>b</sup> derived from the corrected ratio of the molar amounts of N and Si,  $0.25n(\text{N})/n(\text{Si})$

The results are listed in Table 4. 6. Interestingly the bromine content does not deviate from the expected values, within the experimental error, even for polymer 58E with the longer arms. This might give one hint that the major termination reaction during polymerization is the substitution of the end-chain bromine with ubiquitous amines. This reaction leads to quaternary amines on the chain end; to achieve charge compensation the bromide needs to remain in the sample even after removal of copper bromide salts.

### Determination of initiation site efficiency.

In order to determine the true arm numbers and arm lengths one needs to cleave the arms off the core. Therefore, the quaternized PDMAEMA (= PMETAI) was heated for several days in concentrated, aqueous sodium hydroxide solution (see Scheme 4. 3) to completely detach all amino groups from the polymer (in order to eliminate adsorption during GPC analysis).

Scheme 4. 3: Chemical modifications for determination of initiation site efficiency



During this procedure several reactions take place. Hofmann elimination occurs as detected by the trimethylamine smell. After the ester of the former *N,N*-dimethylaminoethanol has been cleaved the developed acetaldehyde can undergo aldol condensation reactions leading to a dark precipitate. The solution contains neutralized linear poly(methacrylic acid) (PMAA), which can be separated by dialysis after acidification and measured by aqueous GPC. To perform GPC in THF we methylated the PMAA to poly(methyl methacrylate) (PMMA).<sup>7, 44</sup> The conversions of all steps were checked by <sup>1</sup>H-NMR spectroscopy (Figure 4. 9).

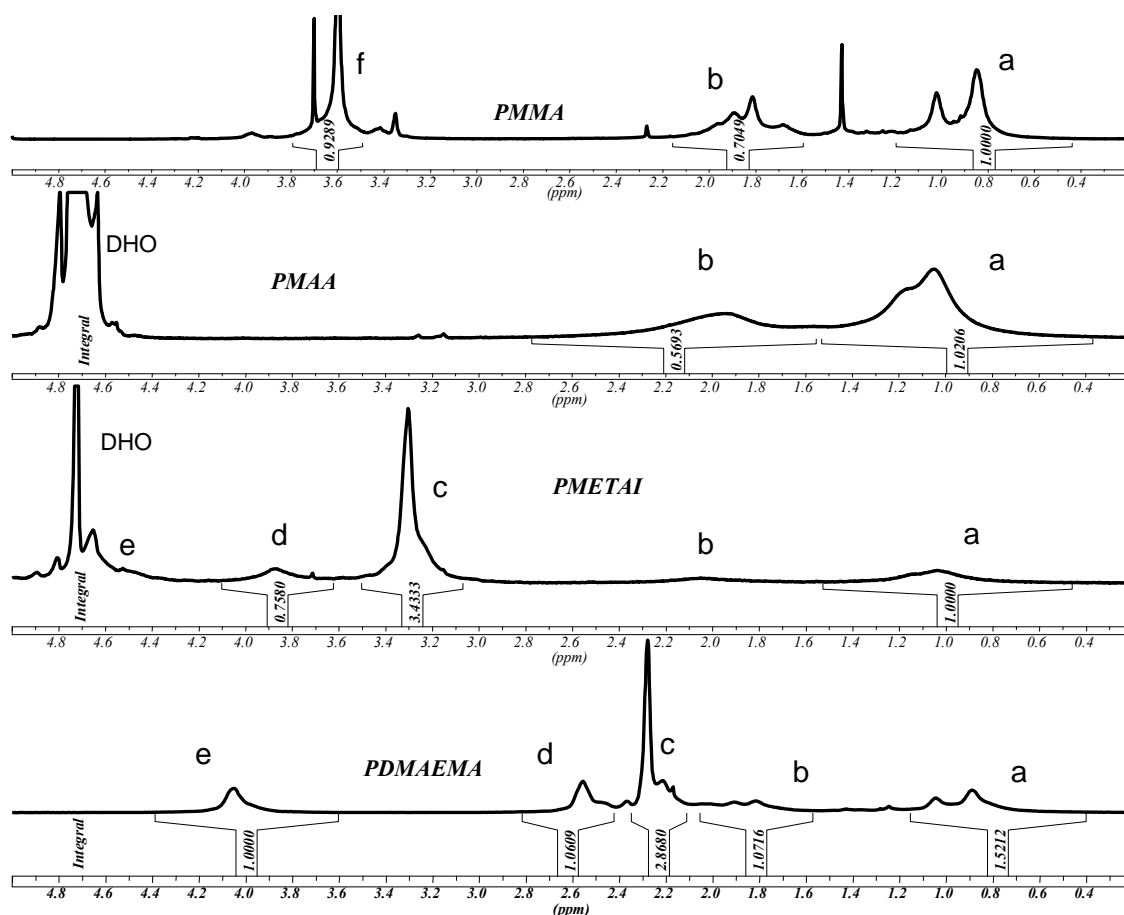


**Figure 4. 9:** <sup>1</sup>H-NMR of all chemical modification steps (in D<sub>2</sub>O and CDCl<sub>3</sub>; here PDMAEMA 58A and its respective products). The assignments are given in Scheme 4. 3.

We see that after quaternization the methyl protons on the amino group shift to higher ppm values, whereas after ester cleavage the trimethylammonium signal almost completely disappears. The methylation again gives the methyl ester signal with 90% conversion (side reactions were discussed in our previous publication<sup>7</sup>).

The obtained degrees of polymerization and polydispersities according to GPC analysis of both linear PMAA (Figure 4. 10) and PMMA (Figure 4. 11) and according to MALDI-ToF mass spectrometry (Figure 4. 12) of linear PMMA are given in Table 4. 3 of the main text.

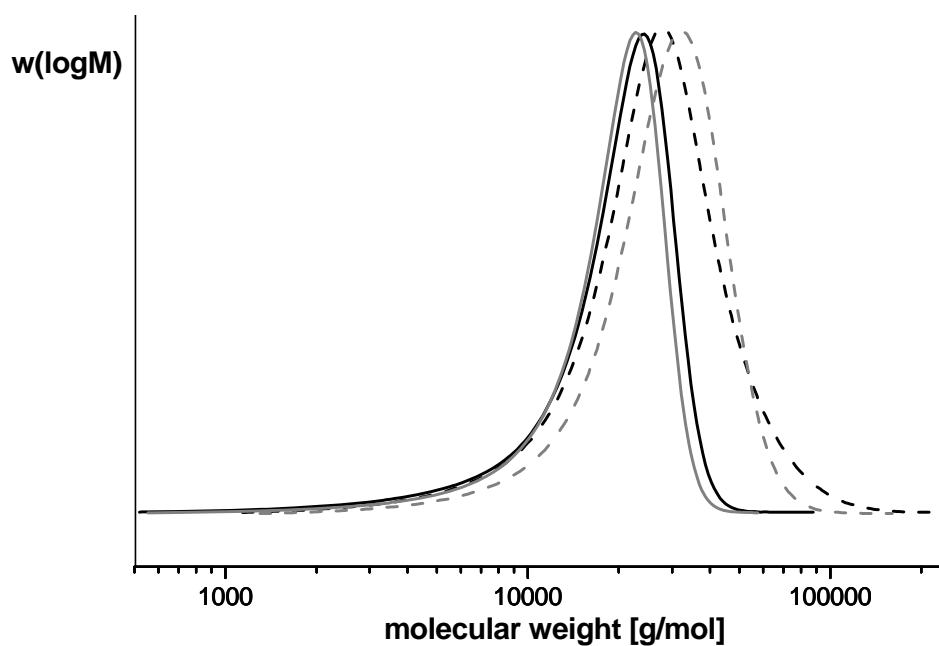


Figure 4. 10: Molecular weight distributions of cleaved-off poly(methacrylic acid) (PMAA) in aqueous gel permeation chromatography (GPC) according to refractive index signals (RI); grey: 21A and 21E (dashed), black: 58A and 58E (dashed).

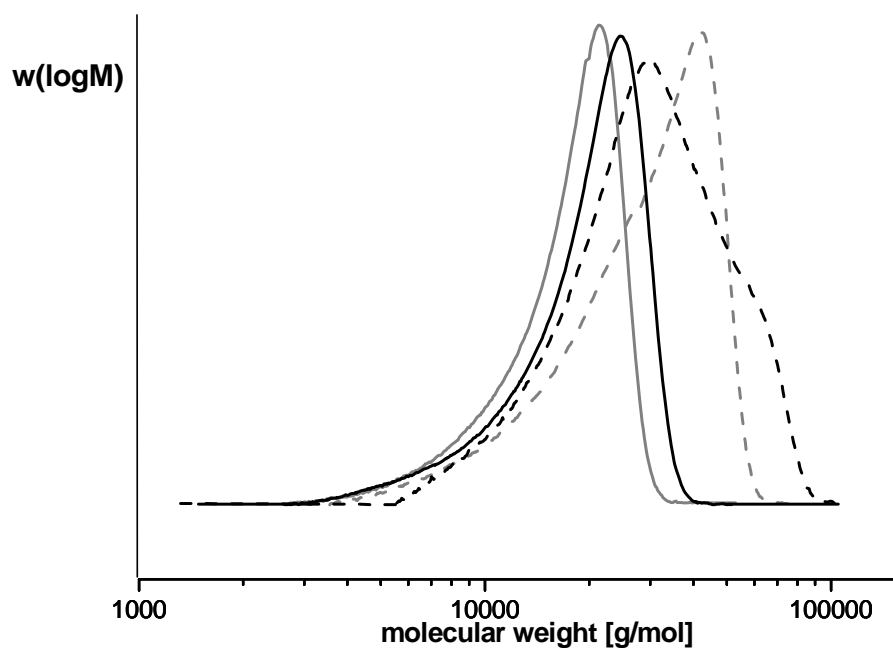
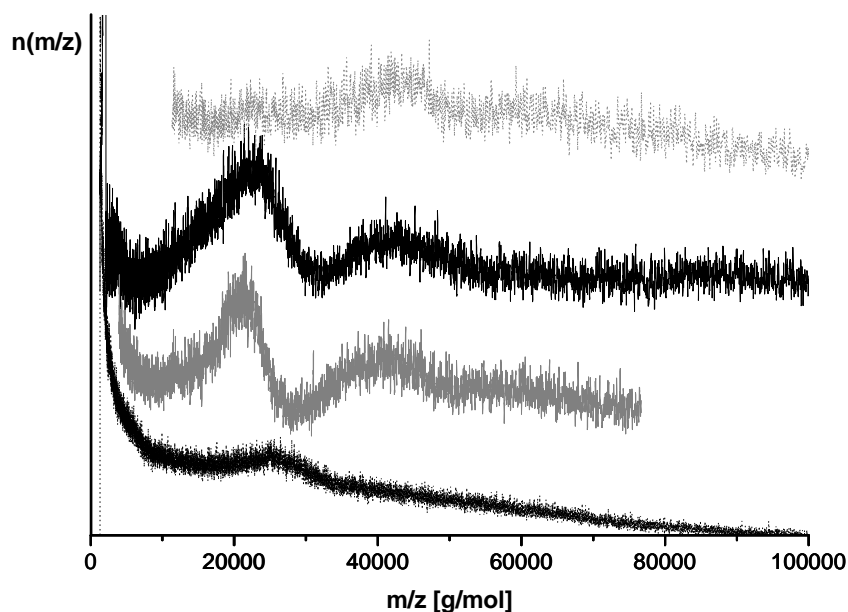


Figure 4. 11: Molecular weight distributions of poly(methyl methacrylate) (PMMA) arms in gel permeation chromatography with tetrahydrofuran as eluent (same notation as in Figure 4. 10; RI signal).



**Figure 4. 12:** Mass spectra (MALDI-ToF) of poly(methyl methacrylate) (PMMA) arms (same notation as in Figure 4. 10).

In aqueous GPC we only get monomodal distributions. Additionally these are broader than in THF-GPC which is typical for our aqueous GPC setup. One PMMA sample gives a bimodal distribution in THF-GPC, which might indicate some incomplete detachment of the star from the core. In both cases we directly see some tailing which is likely caused by slow initiation during polymerization. GPC shows polydispersities close to the limiting value<sup>38, 45</sup> of 1.33 due to slow initiation in particular for the heavier stars. To exclude adsorption on the column due to some undetached amino groups we tried to perform MALDI-ToF mass spectrometry of linear PMMA. Here we obtained sometimes badly resolved spectra with considerably lower polydispersities (Figure 4. 12). We see often peaks with double molecular weight, which might be due to some aggregates formed during ionization. The  $M_n$  values derived from the low molecular peaks are mostly consistent with the values obtained by GPC. As MALDI might discriminate different molecular weight fractions in the sample, we do not stress the polydispersities obtained by mass spectrometry.

## Experimental

**Cleavage of arms by alkaline hydrolysis<sup>7</sup>:** Within a PE vial 100 mg of quaternized PDMAEMA star were suspended in 2 mL of concentrated aqueous NaOH and thermostated for 5 days at 90 °C. When after one hour at 90 °C the solution did not clear up some drops of water were added. After 5 days the smell of trimethylamine could be observed and a dark

precipitate was sometimes found. The cool mixture was carefully filtered (PTFE syringe filter) and the filtrate was carefully brought to low pH by addition of concentrated HCl. This solution was then freeze-dried on the vacuum line to remove excess HCl in order not to harm the membrane in the following aqueous dialysis (Millipore SpectraPore 7 MWCO 1000). Hereby most of the low molecular salts were separated. To be sure that the product, poly(methacrylic acid) (PMAA), was fully protonated, the steps addition of HCl to freeze drying were repeated to obtain roughly 30 mg of PMAA.  $^1\text{H-NMR}$  in  $\text{D}_2\text{O}$  was used to check the conversion of the ester cleavage and aqueous GPC was used to check the conversion of the cleavage of arms.

**Methylation of PMAA**<sup>7, 44</sup>: 10 mg of PMAA were dissolved in 0.1 mL water and 2 mL THF. If the mixture was not totally soluble water was added in small steps. Under stirring and at room temperature a 2 M trimethylsilyldiazomethane solution in dimethylether was added dropwise until the yellow color stayed longer than one hour. If the solubility of the developing poly(methyl methacrylate) (PMMA) was exceeded additional THF was added. The methylated PMAA was again dialysed against pure THF (Spectra/Por 7 MWCO 1000) and finally freeze-dried from dioxane to obtain approximately 10 mg of PMMA. The degree of methylation was again verified by  $^1\text{H-NMR}$  in chloroform.

**Release of star-like segments by treatment with HF (Experimental):**

Within a polyethylene vial 30 mg of a silsesquioxane based PDMAEMA star were dissolved in 4 mL of water and 1 mL of aqueous HF (48 wt.%) and kept at room temperature for 6 h. Finally the mixture was carefully titrated with concentrated, aqueous NaOH solution until  $\text{pH} = 13$ . Due to the heat of neutralization the LCST polymer precipitated. The precipitated polymer was dialyzed against pure water (Spectra/Por 7 MWCO 1000) and freeze-dried. The intactness of the PDMAEMA backbone after HF-treatment was confirmed by  $^1\text{H-NMR}$  in chloroform.

**Polymer Characterization: MALDI ToF Mass Spectrometry:** MS was performed in linear mode on a Bruker Daltonics Reflex 3 with  $\text{N}_2$  laser (337 nm) at a 20 kV acceleration voltage. We used trans-3-indolacrylic acid (IAA) as matrix (mass ratio IAA : polymer = 10 : 1) for molecular weight determination of PMMA polymers. For PMMA the molecular weight of the repeating unit  $M_r$  was assessed to 104 g/mol to reflect partial methylene insertion into the methyl ester moieties.<sup>7</sup>

*Gel Permeation Chromatography:* For PMMA a conventional THF-phase GPC system was used to obtain molecular weights, used in determining the initiation site efficiency. GPC

system I; column set: 5  $\mu\text{m}$  PSS SDV gel,  $10^2$ ,  $10^3$ ,  $10^4$ ,  $10^5$  Å, 30 cm each; injection volume 20  $\mu\text{l}$  of a 2 mg/ml solution; RI and UV detectors. Narrow PMMA standards (PSS, Mainz) were used for the calibration of the column set I. The extracted number-average molecular weight,  $M_n$ , was used to determine the degree of polymerization of one arm,  $DP_{n,\text{arm}}$ , by dividing  $M_n$  by the molar mass of the polymer's repeating unit. The third setup was an aqueous GPC (internal standard ethylene glycol; additives: 0.1 M  $\text{NaN}_3$ , 0.01 M  $\text{NaH}_2\text{PO}_4$ ), which gave the molecular weight of PMAA (PMAA standards, PSS, Mainz). Column set: two 8 mm PL Aquagel-OH columns (mixed and 30 Å), operated at 35°C. RI-detector.

**ACKNOWLEDGEMENT:** This work was supported by the *Deutsche Forschungsgemeinschaft* within SFB 481 and by the *Fonds der Chemischen Industrie*. We thank Manuela Schumacher, Cornelia Rettig and Denise Danz for the MALDI-ToF MS measurements, Youyong Xu, Sabine Wunder, Daniela Kropp and Klaus Kreger for GPC measurements, Markus Burkhardt and Markus Ruppel for their help during SLS/DLS measurements and Andrew Ah Toy for proof-reading the manuscript.

## 4.6. References

1. Pincus, P. *Macromolecules* **1991**, *24*, 2912.
2. Jusufi, A.; Likos, C. N.; Lowen, H. *Physical review letters* **2002**, *88*, 018301.
3. Jusufi, A.; Likos, C. N.; Löwen, H. *Journal of Chemical Physics* **2002**, *116*, 11011.
4. Das, B.; Guo, X.; Ballauff, M. *Progress in Colloid & Polymer Science* **2002**, *121*, 34.
5. Deserno, M.; Holm, C.; Blaul, J.; Ballauff, M.; Rehahn, M. *European Physical Journal E: Soft Matter* **2001**, *5*, 97.
6. Jusufi, A.; Likos, C. N.; Ballauff, M. *Colloid and Polymer Science* **2004**, *282*, 910.
7. Plamper, F. A.; Becker, H.; Lanzendörfer, M.; Patel, M.; Wittemann, A.; Ballauff, M.; Müller, A. H. E. *Macromolecular Chemistry and Physics* **2005**, *206*, 1813.
8. Zilliox, J. G.; Rempp, P.; Parrod, J. *Journal of Polymer Science, Polymer Symposia* **1968**, *22*, 145.
9. Luxton, A. R.; Quig, A.; Delvaux, M. J.; Fetters, L. J. *Polymer* **1978**, *19*, 1320.
10. Tsitsilianis, C.; Voulgaris, D. *Macromolecular Chemistry and Physics* **1997**, *198*, 997.
11. Simmons, M. R.; Yamasaki, E. N.; Patrickios, C. S. *Polymer* **2000**, *41*, 8523.
12. Vamvakaki, M.; Patrickios, C. S. *Chemistry of Materials* **2002**, *14*, 1630.
13. Georgiou, T. K.; Vamvakaki, M.; Phylactou, L. A.; Patrickios, C. S. *Biomacromolecules* **2005**, *6*, 2990.

14. Haddleton, D. M.; Edmonds, R.; Heming, A. M.; Kelly, E. J.; Kukulj, D. *New Journal of Chemistry* **1999**, *23*, 477.
15. Ohno, K.; Wong, B.; Haddleton, D. M. *Journal of Polymer Science, Part A: Polymer Chemistry* **2001**, *39*, 2206.
16. Hu, H.; Fan, X.; Huang, Y. *Gaofenzi Xuebao* **2004**, *6*, 805.
17. Li, J.; Xiao, H.; Kim, Y. S.; Lowe, T. L. *Journal of Polymer Science, Part A: Polymer Chemistry* **2005**, *43*, 6345.
18. Strauss, U. P.; Layton, L. H. *Journal of Physical Chemistry* **1953**, *57*, 352.
19. Frere, Y.; Gramain, P. *Macromolecules* **1992**, *25*, 3184.
20. Chovino, C.; Gramain, P. *Macromolecules* **1998**, *31*, 7111.
21. Bicak, N.; Gazi, M. *Journal of Macromolecular Science, Pure and Applied Chemistry* **2003**, *A40*, 585.
22. Zeng, F.; Shen, Y.; Zhu, S. *Macromolecular Rapid Communications* **2002**, *23*, 1113.
23. Xia, J.; Johnson, T.; Gaynor, S. G.; Matyjaszewski, K.; DeSimone, J. *Macromolecules* **1999**, *32*, 4802.
24. Zeng, F.; Shen, Y.; Zhu, S.; Pelton, R. *Macromolecules* **2000**, *33*, 1628.
25. Fang, Z.; Kennedy, J. P. *Journal of Polymer Science, Part A: Polymer Chemistry* **2002**, *40*, 3679.
26. Lee Sang, B.; Russell Alan, J.; Matyjaszewski, K. *Biomacromolecules* **2003**, *4*, 1386.
27. Zheng, G.; Stoeber, H. D. H. *Macromolecules* **2003**, *36*, 7439.
28. Mao, B.; Gan, L.-H.; Gan, Y.-Y.; Li, X.; Ravi, P.; Tam, K.-C. *Journal of Polymer Science, Part A: Polymer Chemistry* **2004**, *42*, 5161.
29. Lee, H.-i.; Pietrasik, J.; Matyjaszewski, K. *Macromolecules* **2006**, *39*, 3914.
30. Muthukrishnan, S.; Plamper, F.; Mori, H.; Müller, A. H. E. *Macromolecules* **2005**, *38*, 10631.
31. Majoros, I.; Marsalko, T. M.; Kennedy, J. P. *Polymer Bulletin* **1997**, *38*, 15.
32. Costa, R. O. R.; Vasconcelos, W. L.; Tamaki, R.; Laine, R. M. *Macromolecules* **2001**, *34*, 5398.
33. Costa, R. O. R.; Vasconcelos, W. L.; Laine, R. M. *Materials Research (Sao Carlos, Brazil)* **2002**, *5*, 247.
34. Mengel, C.; Meyer, W. H.; Wegner, G. *Macromolecular Chemistry and Physics* **2001**, *202*, 1138.
35. Plamper, F. A.; Walther, A.; Müller, A. H. E.; Ballauff, M. *Nano Letters* **2007**, *7*, 167.

36. Plamper, F. A.; Ruppel, M.; Schmalz, A.; Borisov, O.; Ballauff, M.; Müller, A. H. E. *Macromolecules* **2007**, submitted.
37. Daoud, M.; Cotton, J. P. *Journal de Physique* **1982**, *43*, 531.
38. Gold, L. *Journal of Chemical Physics* **1958**, *28*, 91.
39. Schulz, G. V. *Z. Phys. Chem. (Leipzig)* **1939**, *B43*, 25.
40. Burchard, W.; Schmidt, M.; Stockmayer, W. H. *Macromolecules* **1980**, *13*, 1265.
41. Mei, Y.; Ballauff, M. *European Physical Journal E: Soft Matter* **2005**, *16*, 341.
42. Biesalski, M.; Johannsmann, D.; Ruhe, J. *The Journal of chemical physics* **2004**, *120*, 8807.
43. Fischer, H. *Journal of Polymer Science, Part A: Polymer Chemistry* **1999**, *37*, 1885.
44. Couvreur, L.; Lefay, C.; Belleney, J.; Charleux, B.; Guerret, O.; Magnet, S. *Macromolecules* **2003**, *36*, 8260.
45. Matyjaszewski, K. *Journal of Physical Organic Chemistry* **1995**, *8*, 197.

## 5. Nanoblossoms: Light-Induced Conformational Changes of Cationic Polyelectrolyte Stars in Presence of Multivalent Counterions

*Felix A. Plamper,<sup>a</sup> Andreas Walther,<sup>a</sup> Axel H. E. Müller,<sup>a,\*</sup> Matthias Ballauff<sup>b,\*</sup>*

<sup>a</sup>Makromolekulare Chemie II, <sup>b</sup>Physikalische Chemie I, and Bayreuther Zentrum für Kolloide und Grenzflächen, Universität Bayreuth, D-95440 Bayreuth, Germany

**Published in *Nano Letters* 2007, 7, p.167.**

**ABSTRACT:** We analyze the structure of star-shaped polyelectrolytes in the presence of di- and trivalent counterions and we use the gained knowledge to manipulate the polyelectrolyte's conformation by light. Applying dynamic light scattering and atomic force microscopy we demonstrate that at constant ionic strength the arms of the cationic polyelectrolyte retract when adding multivalent counterions. Adding trivalent hexacyanocobaltate(III) ions leads to a collapse of the polyelectrolyte star even at low concentrations. This is shown by analysis of the star polyelectrolytes in solution as well as in the adsorbed state on mica surfaces. Considerably higher salt concentrations are necessary to obtain the same contraction of the polyelectrolyte star if the divalent tetracyanonickelate(II) ions are used. Sufficiently high multivalent counterion concentration leads finally to the precipitation of the polymer from the solution. We demonstrate that we can switch a polyelectrolyte star from the collapsed to the expanded state by transforming the trivalent hexacyanocobaltate(III) ions into a mixture of mono- and divalent ions by UV light. Thus, these collapsed stars react to light like "nanoblossoms". Moreover, polyelectrolyte stars precipitated through addition of the trivalent hexacyanocobaltate(III) ions can be redissolved by irradiation with light (photoinduced dissolution). Hence, the conformation and interaction of star polyelectrolytes can be switched by light. Possible applications of this novel way of manipulating polymers are discussed.

## 5.1. Introduction

Strong polyelectrolytes are highly charged polymeric macroions.<sup>1,2</sup> Its number of charges, which are usually placed on each repeating unit along the polymer chain, is irrespective to *pH*. Dispersed in water or solvents with high dielectric constant the counterions of the polyelectrolyte will partly dissociate from the polyion. A certain fraction, however, will be closely correlated to the macroion because of its high electric field. For linear polyelectrolytes, this strong binding of counterions has been termed counterion condensation and can be determined directly by the much reduced osmotic activity of the counterions.<sup>3</sup> For more complicated architectures as e.g. star polyelectrolytes or layers of densely grafted polyelectrolytes (polyelectrolyte brushes) this correlation has been predicted to be much stronger leading to a confinement of the order of 90%.<sup>4-7</sup> This strong correlation of the counterions to the macroion in dilute aqueous solution must lead to a marked osmotic pressure within the macroion.<sup>5,6,8,9</sup> As a consequence of this, the arms of the polyelectrolyte star must be strongly stretched. If salt is added to the solution, the electrostatic interaction is more and more screened. Hence, at sufficiently high salt concentration, the stretching of the arms of the star polyelectrolyte will be greatly diminished and the conformation of the macroion should be comparable to the solution structure of uncharged star polymers.<sup>10</sup> This behavior can be directly compared to the well-studied case of polyelectrolyte brushes where long polyelectrolyte chains are densely grafted to planar or spherical surfaces.<sup>11,12</sup>

Replacing monovalent counterions by e.g. trivalent ones should lead to a marked decrease of the osmotic pressure. As a consequence of this, polyelectrolyte stars should collapse in solutions of multivalent counterions, again in direct analogy to the collapse of polyelectrolyte brushes when replacing monovalent counterions by higher valent counterions.<sup>13</sup> To the authors' best knowledge, no experimental work has been published on star polyelectrolytes in presence of trivalent counterions. Practically all available experimental studies refer to systems having monovalent counterions.

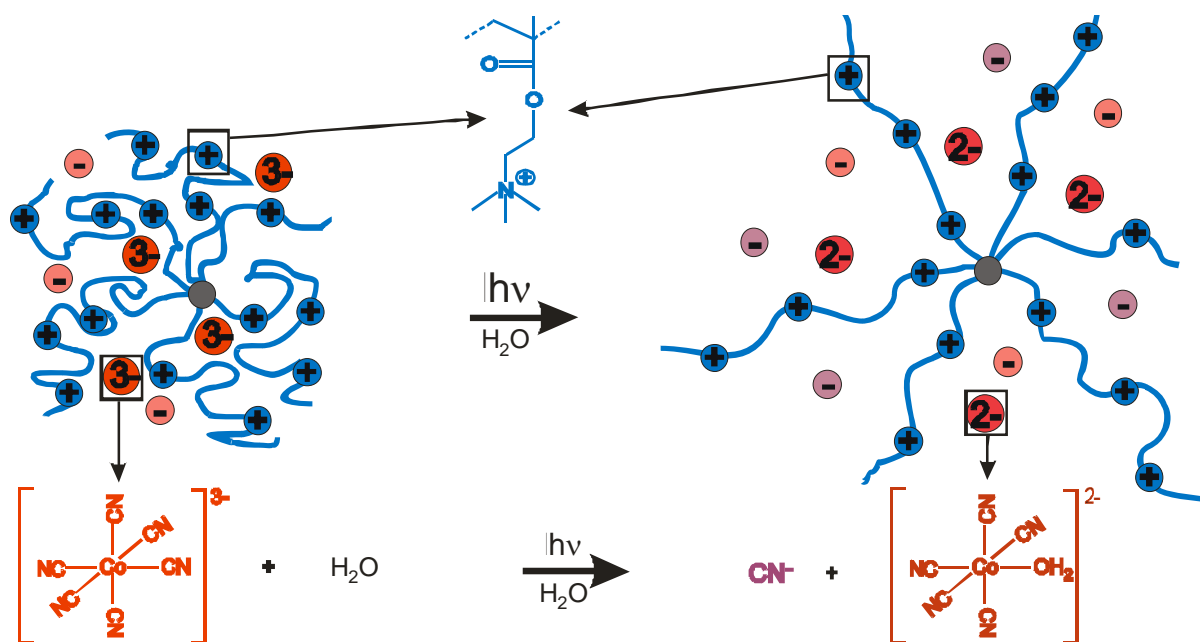


Figure 5. 1: Scheme of the structure of the polyelectrolyte star and the photochemical reaction (photoaquation) leading from trivalent to divalent ions

Here we present the first analysis of star polyelectrolytes<sup>10</sup> in presence of di- and trivalent counterions. We show that the conformation of star polyelectrolytes in aqueous solution can be manipulated by UV-light: Using the photochemical reaction of hexacyanocobaltate(III)  $[\text{Co}(\text{CN})_6]^{3-}$ , trivalent counterions are irreversibly converted into divalent ones (Figure 5. 1).<sup>14, 15</sup> In this way the number of counterions is raised significantly in order to balance the charge of the macroion. We demonstrate that this effect can be used to induce the transition of star polyelectrolytes from a collapsed to a stretched state through a photochemical reaction. In this way we present a novel way of manipulating single molecules in solution by light.

## 5.2. Experimental Section

**Materials:** The synthesis and characterization of cationic polyelectrolyte stars were reported in an earlier publication.<sup>10</sup> Here we used a star-shaped poly{[2-(methacryloyloxy)ethyl] trimethylammonium iodide} (PMETAI) with an arm number  $f_n = 18$  (number average; PDI in arm number distribution  $\approx 1.4$ ) and a number-average degree of polymerization per arm  $P_n(\text{arm}) = 170$  (PDI of arms = 1.2). In our previous publication the non-quaternized precursor was denominated as 58A. The formula of the star polymer is assigned as  $(\text{PMETAI}_{170})_{18}$ . Potassium hexacyanocobaltate(III)  $\text{K}_3[\text{Co}(\text{CN})_6]$  was purchased by Aldrich, whereas potassium tetracyanonickelate(II)  $\text{K}_2[\text{Ni}(\text{CN})_4]$  was purchased from ABCR and used as received.

**Sample Preparation:** The samples for DLS measurement were prepared by slow addition (titration rates from 0.008 mL/min to 0.15 mL/min; added volume increment around 0.02 mL) of freshly prepared aqueous  $K_3[Co(CN)_6]$  (0.0167 M) or  $K_2[Ni(CN)_4]$  (0.0333 mol/L) solutions to a polyelectrolyte solution (100ml) of 0.5 g/L (PMETAI<sub>170</sub>)<sub>18</sub>) with the same ionic strength (adjusted with NaCl; here 0.1 N) as the metalate solutions. For this purpose we used a titrator (Titrand 809, Metrohm, Herisau, Switzerland) equipped with a turbidity sensor (wavelength = 523 nm, Spectrosense, Metrohm). The same setup was also used for turbidimetric titrations (without any sample removal). We assumed negligible dilution during addition of metalate solution, as only up to three ml were added to a starting volume of 100ml. The samples were kept at room temperature for about one day, then they were filtered in a flow box for measurements by dynamic light scattering. Exposure to direct sunlight was avoided.

**Dynamic light scattering (DLS)** was performed at 24° C using an ALV DLS/SLS CGS-8FW compact goniometer system with an ALV 5000/E correlator and a He-Ne laser ( $\lambda = 632.8$  nm; Peters ALV, Langen, Germany). The intensity fluctuations were detected at 90°. By means of CONTIN analysis of the intensity autocorrelation functions the intensity weighted hydrodynamic radii were derived from the collective diffusion coefficients by the Stokes-Einstein relation. Prior to the light scattering measurements the sample solutions were filtered using Millipore Nylon filters with a pore size of 0.45  $\mu$ m.

**Atomic Force Microscopy (AFM):** For sample preparation the polyelectrolyte was first dissolved in a 0.1 N NaCl aqueous solution (0.5 g/L (PMETAI<sub>170</sub>)<sub>18</sub>). For the samples with trivalent counterions additionally 0.37 mmol/L  $[Co(CN)_6]^{3-}$  were present. All samples were dialyzed against pure water, then diluted by factor 100 with pure water and finally deposited onto freshly cleaved Mica by spin coating at 2000 rpm. A multimode AFM instrument (Digital Instruments, Santa Barbara, CA) was operated in tapping mode using an E-Scanner. SuperSharpSilicon SFM-Sensors (SSS-NCHR-10, Nanosensors) with a typical tip radius of 2 nm, spring constant of 10 – 130 N/m, and resonance frequency of 204 - 497 kHz were used for imaging. All measurements were performed at very soft tapping conditions to minimize structural changes of the previously deposited star-shaped polymers. The images were acquired at settings when it was just possible to obtain a meaningful height image by decreasing the amplitude set-point (ca. 1.9 V, depending on the individual measurement and setup), leading to tapping conditions where the SFM tip just touches the substrate sufficiently. Additionally, the imaging was done at very low scan speeds (0.1 – 1 Hz) to minimize lateral forces exerted by the SFM tip to the sample. These parameters correspond to very soft SFM

tapping conditions, minimize scan artefacts and lead to the most reliable height data. Off-line data processing was done using the Nanoscope software 6.12r1.

The mixtures were irradiated using a Honle UVAHAND 250<sub>H1/BL</sub> lamp (310 W), operated with black light filter, which transmits light of wavelengths between 310 and 400 nm. IR radiation was diminished with a water flow filter. The samples were placed 7 cm away from the lamps surface. No special care was taken for the transmittance of the glassware used (small glass vials, VWR, and cuvettes of standard glass).

## 5.3. Results and Discussion

### 5.3.1. Collapse of Polyelectrolyte Stars Induced by Multivalent Counterions

Figure 5. 1 displays the structure of the cationic star polymer used in this study. The star-shaped polyelectrolyte, whose formula was assigned as (PMETAI<sub>170</sub>)<sub>18</sub>, bears 18 arms (number average) and a number-average degree of polymerization per arm of 170. The details of the synthesis and characterization of these systems have been given elsewhere.<sup>10</sup>

As for the counterions we chose cyanometalates with high complexation equilibrium constants,  $K_c$  ( $\log K_c$  in the range of 30), like the quadratic planar tetracyanonickelate(II) ( $[\text{Ni}(\text{CN})_4]^{2-}$ ) and octahedral hexacyanocobaltate(III) ( $[\text{Co}(\text{CN})_6]^{3-}$ ). Both do not change structure at moderate  $p\text{H}$ -values. Only the cobaltate is able to undergo photoaquation (i.e. exchange of cyano ligand with water) when irradiated with UV-light (see Figure 5. 1).<sup>14, 15</sup> This effect will be used for a photochemical switching of the star polyelectrolytes in solution as already sketched in Figure 5. 1.

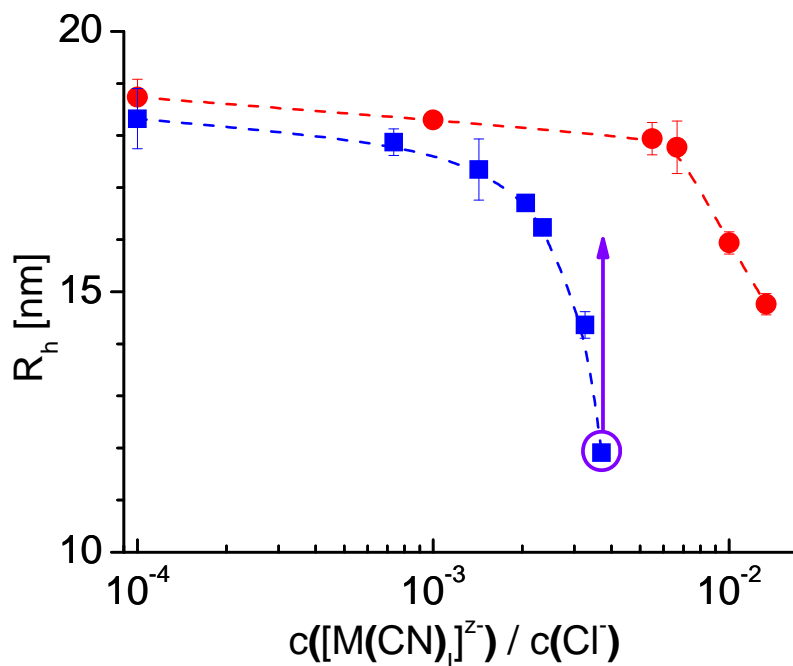


**Figure 5. 2:** Change of the hydrodynamic radius of the cationic star polyelectrolyte (0.5 g/L of (PMETA<sub>170</sub>)<sub>18</sub>) in dilute aqueous solutions with same ionic strength (0.1 N NaCl) but different ratios of mono- to multivalent salt; circles: titrated with 0.033 mol/L divalent  $K_2[Ni(CN)_4]$ ; squares: titrated with 0.0167 mol/L trivalent  $K_3[Co(CN)_6]$ ; the arrow demonstrates the principle of photostretching (see Figure 5. 4); the dashed lines are a guide to the eye

We first discuss the overall dimensions of the star polyelectrolyte in dilute aqueous solution. Figure 5. 2 displays the hydrodynamic radius of the star polyelectrolyte when monovalent salt is gradually replaced by divalent or by trivalent salt. Note that the ionic strength was kept constant at 0.1 mol/L in all cases. If only the Debye length would be the decisive parameter, the hydrodynamic radius would not change with increasing cyanometalate concentration. However, there is a strong exchange of the monovalent counterions by a smaller number of the multivalent ones.<sup>13</sup> This leads to a pronounced drop in osmotic pressure within the star and to a partial retraction of the arms. Hence, the overall dimensions of the star polyelectrolytes in solution are expected to become considerably smaller as seen from the decrease of the hydrodynamic radius.

The influence of counterion charge at constant ionic strength is depicted in Figure 5. 2. For both the divalent as well as for the trivalent counterions, a marked decrease of the overall dimensions is seen, as expected. In particular, a rather small fraction of trivalent counterions is already sufficient to lead to a collapse of the star polyelectrolyte in solution. The divalent tetracyanonickelate(II) ( $[Ni(CN)_4]^{2-}$ ) counterion, however, needs a higher counterion concentration for a marked decrease of the dimensions as compared to trivalent counterions, e.g.  $[Co(CN)_6]^{3-}$ . Since divalent counterions bear a lower charge the charge compensation and ion exchange takes place at higher counterion concentration. At sufficiently high counterion

concentrations both systems enter a two-phase region, yielding a polyelectrolyte-rich gel-like precipitate and a virtually polymer-free aqueous phase. The onset of precipitation for the system used for Figure 5. 2 occurs, as obtained by turbidimetric titration, at a concentration of trivalent counterions about  $4 \cdot 10^{-4}$  mol/L (i.e.  $c([\text{Co}(\text{CN})_6]^{3-}) / c(\text{Cl}^-) \approx 4 \cdot 10^{-3}$ ). Precipitation starts close to the point where the number of nominal charges of the polyelectrolyte star is matched with the number of charges originating the added trivalent counterions. Thus the large majority of the trivalent counterions is expected to be located inside the collapsed stars. But as soon as most of the star's charges are compensated with trivalent counterions, net attractive forces between the polymers prevail since excess counterions are able to bridge different stars. A similar observation has already been made for spherical polyelectrolyte brushes in presence of trivalent counterions.<sup>13</sup>

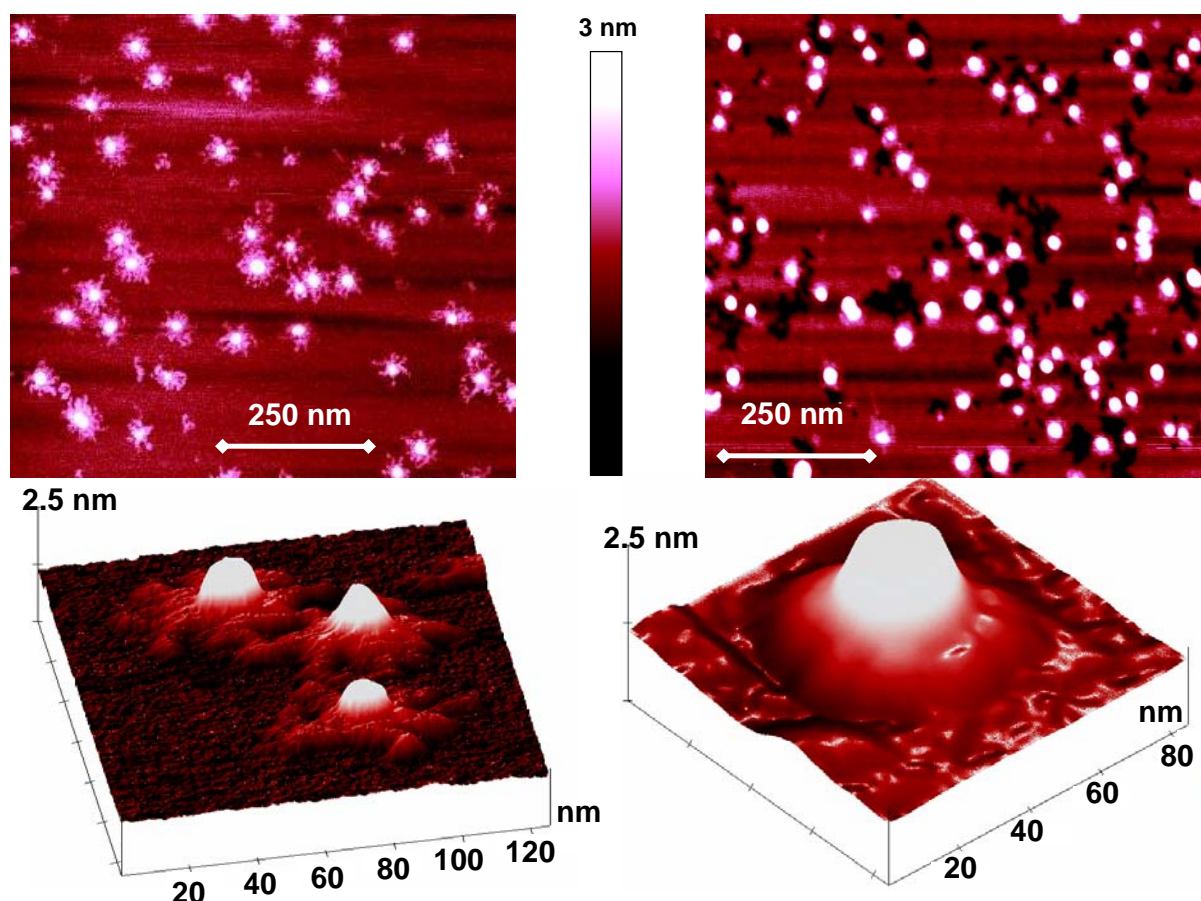


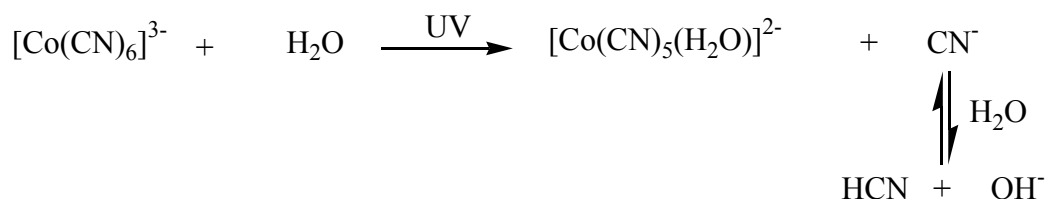
**Figure 5. 3:** AFM height images of spin-coated solutions of  $(\text{PMETA I}_{170})_{18}$  ( $\sim 0.005$  g/L) on mica (left hand side: without added trivalent counterion, dialysed against pure water from 0.1 N NaCl solution; right hand side: dialysed against pure water from 0.1 N NaCl and  $3.7 \cdot 10^{-4}$  mol/L  $[\text{Co}(\text{CN})_6]^{3-}$ ); bottom: enlarged 3D-representations.

The marked collapse of cationic star polyelectrolytes in solution when replacing mono- by multivalent counterions can also be demonstrated by the study of the interaction of these

polyelectrolytes with solid surfaces. Atomic Force Microscopy (AFM) is the method of choice as has been demonstrated in early work on spherical polyelectrolyte brushes<sup>16</sup> and on charged dendrimers.<sup>17</sup> On the left-hand side of Figure 5. 3 we see adsorbed (PMETA<sub>I170</sub>)<sub>18</sub> without trivalent counterions. The cores of the stars (height around 2.5 nm) and its arms or several arms are clearly visible. Occasionally some single polymer chains or some triarm stars are visible. It is not clear if this fraction is already present in the sample or if those fragments develop due to adsorption effects on mica (no evidence of detached fragments was found in a previous study<sup>10</sup>). The right hand side of Figure 5. 3 displays the image of the same star polyelectrolyte in presence of [Co(CN)<sub>6</sub>]<sup>3-</sup>. Now the arms only appear as a corona around the core, which assumes a globular shape. No single arms can be seen anymore as is expected for a collapsed conformation of the polyelectrolyte star. Before deposition of the samples on mica, excess salt was removed by dialysis in both cases. This helps to avoid the formation of salt crystals on the surface, which hampers the visibility of the stars. Due to the strong interaction of the trivalent counterions with the branched polyelectrolyte, the multivalent counterions are preferentially confined within the star and thus not removed by dialysis, as seen in Figure 5. 3.

### 5.3.2. Photostretching of Polyelectrolyte Stars

We finally turn to the photo-switching of the conformation of the polyelectrolyte stars in solution. Figure 5. 2 demonstrates that at constant concentration of multivalent counterions the degree of contraction depends sensitively on the valency of the counterions. Hence, changing the valency of the counterion by an external stimulus from trivalent to divalent should lead to a marked increase of the overall dimensions. The trivalent hexacyanocobaltate(III) counterion can be changed to a mixture of divalent aquapentacyanocobaltate(III) and monovalent cyanide ions by the so-called photoaquation of the cyanocobaltate.<sup>14, 15</sup>



To demonstrate the photo-switching of star polyelectrolytes by change of the valency of the counterions, we adjust the concentration of the trivalent hexacyanocobaltate(III) counterions in order to achieve a collapsed state (indicated by encircled sample in Figure 5. 2). Shining UV light on this solution, the hydrodynamic radius  $R_h$  is indeed increasing as is seen from

Figure 5. 4. Like the petals of a flower the arms can be stretched again by illumination as the trivalent counterions are transformed to divalent counterions. In this way the star polyelectrolytes can be viewed upon as “nanoblossoms”. Note that the decrease in ionic strength due to transformation of trivalent to divalent counterions is negligible because of the excess of NaCl that determines the ionic strength.

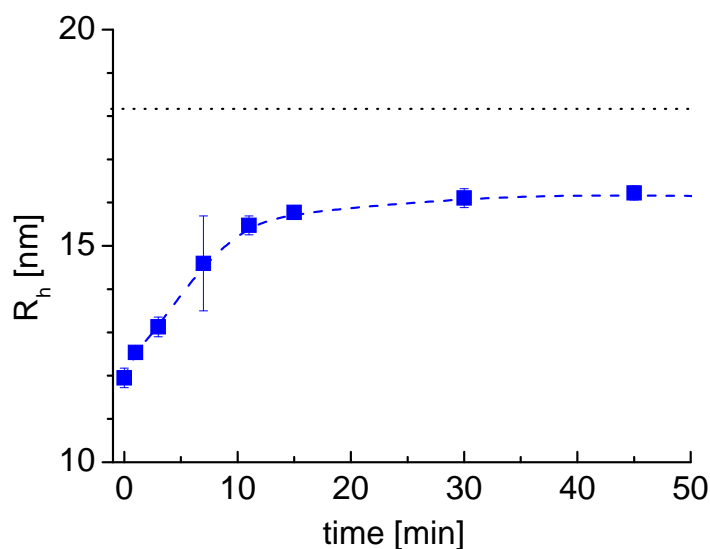


**Figure 5. 4: Photoinduced stretching measured by DLS of 0.5 g/L (PMETA<sub>I</sub>)<sub>18</sub> in 0.1 N NaCl in presence of  $3.7 \cdot 10^{-4}$  mol/L  $K_3[Co(CN)_6]$  in dependence of illumination time; the dotted line depicts the hydrodynamic radius of (PMETA<sub>I</sub>)<sub>18</sub> in 0.1 N NaCl with  $3.7 \cdot 10^{-4}$  mol/L divalent  $[Ni(CN)_4]^{2-}$ .**

Figure 5. 4 shows that the final state expected for total conversion of the trivalent ions to divalent ones cannot be reached (18 nm; see Figure 5. 2) even after prolonged irradiation. After longer irradiation  $R_h$  starts to decrease again which may be traced back to the cleavage of the cores of the stars. Photoaquation produces hydroxide ions directly inside the star by the protonation of cyanide which may cleave off the arms.

### 5.3.3. Photodissolution of Polyelectrolyte Stars

The same mechanism as described for photostretching can be used for photoinduced dissolution. In order to demonstrate this, mixtures of 0.5 g/L (PMETA<sub>I</sub>)<sub>18</sub> in 0.1 N NaCl and  $5.9 \cdot 10^{-4}$  mol/L  $K_3[Co(CN)_6]$  were prepared by direct mixing. A precipitate of aggregated counterion-polyelectrolyte complexes was immediately formed as one is already in the two-phase region for trivalent counterions. The amount of trivalent cobaltate was adjusted that way that after complete conversion to divalent cobaltate one would still expect almost uncollapsed polyelectrolyte stars (see Figure 5. 2). On the way to those uncollapsed polyelectrolytes the aggregation disappears by UV-irradiation. This was seen by complete redissolution of the precipitate after 45 min UV-irradiation, while the mixture turns slightly

yellow due to  $[\text{Co}(\text{CN})_5\text{H}_2\text{O}]^{2-}$ . Figure 5. 5 shows photographs of the mixture before and after partial photodissolution.



**Figure 5. 5:** left hand side: mixture of 0.5 g/L  $(\text{PMETA}_{170})_{18}$  in 0.1 N NaCl and  $5.9 \cdot 10^{-4}$  mol/L  $\text{K}_3[\text{Co}(\text{CN})_6]$  one day after mixing (precipitate has settled along the walls of the glass vial); center: same mixture with mask; right hand side: after 25 min UV-irradiation mask was wiped away and photo-undissolved complex was left behind

Those effects described in this paper might be used and optimized for applications like the use in waterborne photoresists. Especially the compact structure of the star-polymers could lead to defined patterns in lithography. In principle, the photo-manipulation of polyelectrolytes can be applied to all branched polyelectrolyte architectures. Thus the photoinduced expansion of polyelectrolyte chains grafted on e.g. latex particles could lead to photofreezing of a concentrated latex suspension. Therefore the viscosity of polyelectrolyte solutions can be manipulated by light. These effects will be of interest in our future research.

## 5.4. Conclusion

We demonstrate a novel way to manipulate the conformation of polyelectrolytes by changing the charge of counterions by light. Further we present the first study on the collapse of star polyelectrolytes in presence of di- and trivalent ions. The pronounced shrinkage of the dimensions of the cationic polyelectrolyte star in presence of di- and trivalent counterions could directly be observed by DLS and AFM. Star polyelectrolytes collapsed by the trivalent hexacyanocobaltate(III) ions can be re-opened again by UV-light (“nanoblossoms”). We demonstrated that this transition is due to the photoaquation reaction transforming the trivalent hexacyanocobaltate(III) ions into a mixture of the divalent aquapentacyanocobaltate(III) and monovalent cyanide ions. Possible applications of this photo-switching could be related for example to photoresists or systems with light-responsive viscosity.

**ACKNOWLEDGMENT** This work was supported by Deutsche Forschungsgemeinschaft (DFG) within SFB 481 and by Fond der Chemischen Industrie (FCI). We acknowledge Alexander Schmalz for his help in finding the photoactive complex, Yu Mei, Manuela Schumacher, Markus Ruppel and Markus Burkhardt for the help with dynamic light scattering and photography and Frauke Pfeiffer for her help with the UV lamp.

## 5.5. References

1. Katchalsky, A. *Pure Appl. Chem.* **1971**, *26*, 327.
2. Mandel, M. *Encycl. Polym. Sci. Eng.* **1987**, *11*, 739.
3. Manning, G. S. *J. Chem. Phys.* **1969**, *51*, 924.
4. Pincus, P. *Macromolecules* **1991**, *24*, 2912.
5. Jusufi, A.; Likos, C. N.; Lowen, H. *Phys. Rev. Lett.* **2002**, *88*, 018301.
6. Jusufi, A.; Likos, C. N.; Löwen, H. *J. Chem. Phys.* **2002**, *116*, 11011.
7. Borisov, O. V.; Zhulina, E. B. *Eur. Phys. J. B* **1998**, *4*, 205.
8. Guo, X.; Ballauff, M. *Phys. Rev. E: Statistical, Nonlinear, and Soft Matter Physics* **2001**, *64*, 051406.
9. Plamper, F. A.; Becker, H.; Lanzendörfer, M.; Patel, M.; Wittemann, A.; Ballauff, M.; Müller, A. H. E. *Macromol. Chem. Phys.* **2005**, *206*, 1813.
10. Plamper, F.; Schmalz, A.; Penott-Chang, E.; Jusufi, A.; Ballauff, M.; Müller, A. *Macromolecules* **2007**, ASAP.
11. Rühle, J.; Ballauff, M.; Biesalski, M.; Dziezok, P.; Gröhn, F.; Johannsmann, D.; Houbenov, N.; Hugenberg, N.; Konradi, R.; Minko, S.; Motornov, M.; Netz, R. R.; Schmidt, M.; Seidel, C.; Stamm, M.; Stephan, T.; Usov, D.; Zhang, H. *Advances in Polymer Science* **2004**, *165*, 79.
12. Advincula, R. C.; Brittain, W. J.; Caster, K. C.; Rühle, J., *Polymer Brushes*. Wiley VCH: Weinheim, 2004.
13. Mei, Y.; Lauterbach, K.; Hoffmann, M.; Borisov, O.; Ballauff, M.; Jusufi, A. *Phys. Rev. Lett* **2006**, *97*, 158301.
14. MacDiarmid, A. G.; Hall, N. F. *J. Am. Chem. Soc.* **1953**, *75*, 5204.
15. Wrighton, M.; Hammond, G. S.; Gray, H. B. *J. Am. Chem. Soc.* **1971**, *93*, 5254.
16. Mei, Y.; Wittemann, A.; Sharma, G.; Ballauff, M.; Koch, T.; Gliemann, H.; Horbach, J.; Schimmel, T. *Macromolecules* **2003**, *36*, 3452.
17. Pericet-Camara, R.; Papastavrou, G.; Borkovec, M. *Langmuir* **2004**, *20*, 3264.

## 6. Tuning the Thermoresponsive Properties of Weak Polyelectrolytes: Aqueous Solutions of Star-Shaped and Linear Poly(*N,N*-dimethylaminoethyl methacrylate)

*Felix A. Plamper<sup>a</sup>, Markus Ruppel<sup>a</sup>, Alexander Schmalz<sup>a</sup>,  
Oleg Borisov<sup>c</sup>, Matthias Ballauff<sup>b,\*</sup>, Axel H. E. Müller<sup>a,\*</sup>*

<sup>a</sup>Makromolekulare Chemie II, <sup>b</sup>Physikalische Chemie I, and Bayreuther Zentrum für Kolloide und Grenzflächen, Universität Bayreuth, D-95440 Bayreuth, Germany,

<sup>c</sup>Institut Pluridisciplinaire de Recherche sur l'Environnement et les Matériaux, UMR 5254 CNRS/UPPA, 64053 Pau, France

**Published in *Macromolecules* 2007, 40, p.8361.**

**ABSTRACT:** We investigated the thermoresponsive behavior of aqueous solutions of star-shaped and linear poly(*N,N*-dimethylaminoethyl methacrylate) (PDMAEMA). The observed cloud points strongly decrease with increasing *pH* of the solution. This is explained by a weak charging of the star polymers with decreasing *pH*. A significant decrease of the cloud points with increasing molecular weight for high *pH*, i.e. for the almost uncharged state, was found to be virtually independent of the arm number and arm length. These findings are explained by classical Flory-Huggins theory. The increase of cloudpoints upon charging is captured by introduction of an effective degree of polymerization. Polymers with shorter arms show slightly higher cloud points at low *pH* than polymers with longer arms. The intramolecular segment density also influences the observed apparent  $pK_b$  values, leading to higher values for stars with higher arm numbers.

## 6.1. Introduction

Thermoresponsive polymers, which show a pronounced change in their solvation at a certain temperature, caused much attention in former research. Especially thermoresponsive polymers, which are water-soluble, are of interest in respect to applications under physiological conditions.<sup>1-5</sup> These polymers show partial solubility in a certain temperature range, whereas full solubility is accomplished outside the temperature range. Hereby the binodal line separates the one-phase region from the two-phase region. A maximum in the coexistence curve accounts for the upper critical solution temperature (UCST), whereas a minimum in the binodal represents the lower critical solution temperature (LCST). For LCST polymers, the phase separation at higher temperatures is owing to an entropy loss due to ordering of solvent molecules around the polymer segments.

The cloud points (single point on the binodal) of thermosensitive polymer solutions are believed to be influenced by the architecture of the polymer.<sup>6</sup> Theoretical considerations predicted a stabilization against phase separation by branching.<sup>7-9</sup> For an organo-soluble star-like polymer (polystyrene in cyclohexane), there is an experimental evidence that the one-phase region becomes extended upon an increase in the degree of branching (lowering of the UCST).<sup>10, 11</sup> However, experimental data do not give a uniform picture for water-soluble LCST polymers.

One of the most prominent LCST polymers is poly(*N*-isopropylacrylamide) (PNIPAAm) which usually shows a LCST around 32 °C in water.<sup>12, 13</sup> Though there is still some controversy regarding the molecular weight dependence of the LCST,<sup>14, 15</sup> PNIPAAm is regarded to belong to the so-called class II of LCST polymers (according to Berghmans' classification).<sup>16, 17</sup> That means the observed LCST is hardly dependent on the molar mass of the polymer. Architecture has negligible effect as well, since star-shaped PNIPAAm does not change its LCST compared to linear polymer.<sup>18</sup> Exceptions are given by polymers with hydrophobic/hydrophilic endgroups<sup>14, 19, 20</sup> and polymers with a high number of arms (high arm number prevents macroscopic demixing under microscopic collapse).<sup>17, 21</sup> Also other architectures of PNIPAAm show the transition to bad solvent conditions around 32 °C (e.g. spherical brushes).<sup>22, 23</sup>

Another example of LCST-polymers is poly(*N,N*-dimethylaminoethyl methacrylate) (PDMAEMA). However, the cloud points of the latter polymer reported in literature vary from 14 °C to 50 °C in pure water (46 °C in pH 7 buffer).<sup>24-28</sup> This gives some indication of a class I LCST behavior (LCST depends on molecular weight). Patrickios and coworkers

investigated the thermoresponsive properties of PDMAEMA stars, which were prepared by the arm-first method. Thus they have larger hydrophobic cores.<sup>29</sup> They report that the cloud point in pure water does not depend much on the arm number (a change from 29 °C for a star with 24 arms to 34 °C for a star with 50 arms was observed). PDMAEMA brushes were prepared by Matyjaszewski et al.<sup>30</sup> They copolymerized a minor amount of a light-sensitive azobenzene monomer to investigate the observed cloud points in dependence of illumination. The brushes with *cis*-azobenzene units did not show any macroscopic demixing, whereas the brush with *trans*-azobenzene units showed a moderate decrease in transmission at rather high concentration (1 wt. %). These examples imply the conclusion that macroscopic phase separation is hampered for thermoresponsive polymers with higher branching and/or segment densities. The result that phase separation is prevented for PNIPAAm brushes or PNIPAAm stars with high arm number supports this conclusion.<sup>21-23</sup> One possible reason is given in the review of Aseyev et al.<sup>17</sup> Aggregation is kinetically prevented for even linear polymers especially at low particle concentrations due to vitrification of the intermediate colloidal globules.

The introduction of charges leads to an additional, effective stabilization of macromolecules in solution against aggregation and phase separation. PDMAEMA is a useful polymer to study the effects of charges on the LCST, since it is a weak cationic polyelectrolyte. The thermoresponsive properties of the polybase PDMAEMA can then be altered by slight changes in *pH* and salinity as well. *pH* and salinity do not show pronounced effects for the neutral PNIPAAm unless incorporation of ionizable groups introduces *pH* sensitivity.<sup>31-34</sup> These modified, linear PNIPAAm polymers were studied to demonstrate the increase of the cloud points by varying the degree of ionization.

The effect of ionic charges on phase separation in polymer solution has been amply studied theoretically. Vasilevskaya et al. demonstrated that incorporation of a small fraction of permanently charged monomer units in the chain enhances the solubility and weakens the tendency to macroscopic phase separation (precipitation) due to an additional contribution of translational entropy of the counterions.<sup>35</sup> Khokhlov et al. demonstrated that the effect of weak charges can be captured to first approximation by an effective degree of polymerization  $1/DP_{eff} = 1/DP + \alpha'$  where  $\alpha'$  is the degree of dissociation. Bokias et al. have generalized the approach of Khokhlov et al. and proposed a model of “migrating charges” to explain the effect of incorporation of *pH* sensitive monomer units on the LCST of the modified PNIPAAm.<sup>33</sup> Although the latter model does not account correctly for ionization equilibrium in both dilute and concentrated polymer phases in buffered solution, it does capture the

dominant effect of increasing contribution of translation entropy of the counterions upon increasing ionization provoked by the  $pH$  variation. Borue and Erukhimovich demonstrated that solutions of weakly charged polyelectrolytes exhibit a microphase separation instead of precipitation upon a decrease in the solvent strength below the  $\theta$ -point.<sup>36</sup>

Therefore we report on the investigation of the thermoresponsive properties of a well defined set of star-shaped PDMAEMA. The polymers were prepared by the core-first method yielding stars with up to 24 arms and rather low polydispersity (absolute  $PDI \leq 1.43$ ). In contrast, PDMAEMA stars made by arm-first methods usually exhibit higher polydispersities (e.g.  $PDI_{app} > 1.6$ ),<sup>37</sup> possess a rather large hydrophobic core and possess possibly hydrophobic initiator moieties attached at the periphery. These effects might alter the LCST behavior. The results are compared to those obtained with linear polymers. For details of synthesis and characterization we refer to an earlier paper.<sup>38</sup> The present work aims at a systematic investigation of the LCST behavior of PDMAEMA. In particular, the influence of charges on the demixing temperature is studied and compared to the model of Khokhlov et al. in a semi-quantitative manner.

## 6.2. Experimental Section

The synthesis and characterization of star-shaped PDMAEMA by ATRP using CuBr/HMTETA in anisole are described in a previous paper.<sup>38</sup> Linear PDMAEMA 1A and 1B were prepared according to the same recipe using ethyl- $\alpha$ -bromoisobutyrate (EBIB) as initiator. The numbers in our nomenclature (1, 5, 8, 21, and 58) assign the relative number of initiation sites of the (multifunctional) initiators used for the synthesis of the (star-shaped) polymers. The letters differentiate between different batches (A, B, etc.). Longer PDMAEMA (1C, 1D) was synthesized by conventional radical polymerization using AIBN (Merck) as initiator. The monomer DMAEMA (Merck) was filtered over basic alumina; the initiator was dissolved in 10 mL of monomer before the mixture was purged with nitrogen to eliminate oxygen. The mixture was placed in oil bath, and after appropriate time, the mixture was cooled.  $^1H$ -NMR spectroscopy (Bruker Avance 250 MHz) was performed to determine conversion.<sup>38</sup> The polymer was precipitated from hexane and finally freeze-dried from dioxane. The conditions used for the polymerizations are listed in Table 6. 1. The characterization of all linear PDMAEMA was performed in the same way as described before.<sup>38</sup> the polymers were converted to poly(methacrylic acid) and poly(methyl methacrylate) to achieve meaningful determination of the molecular weights by Gel

Permeation Chromatography (GPC) and sometimes by matrix assisted laser desorption ionization time-of-flight (MALDI-ToF) mass spectrometry. The results are listed in Table 6. 2. The formulas of all polymers used are listed in Table 6. 3. ((PDMAEMA<sub>n</sub>)<sub>x</sub>; n = number-average degree of polymerization per arm; x = number-average arm number).

**Table 6. 1: Experimental conditions for the synthesis of linear PDMAEMA<sup>a</sup>**

sample	[DMAEMA] <sub>0</sub> (mol/L)	[Initiator] <sub>0</sub> (mmol/L)	[CuBr] (mmol/L)	[CuBr <sub>2</sub> ] (mmol/L)	t (min)	conversion, x <sub>p</sub> <sup>d</sup>
<b>1A</b>	1.4 <sup>e</sup>	5.8 <sup>b</sup>	4.9	1.0	180	0.26
<b>1B</b>	1.4 <sup>e</sup>	5.8 <sup>b</sup>	4.9	1.0	600	0.38
<b>1C</b>	5.9 <sup>f</sup>	10 <sup>c</sup>	-	-	20	0.08
<b>1D</b>	5.9 <sup>f</sup>	1 <sup>c</sup>	-	-	120	0.16

<sup>a</sup>T = 60°C; <sup>b</sup>initiator: ethyl- $\alpha$ -bromoisobutyrate EBIB; <sup>c</sup>initiator azobisisobutyronitrile (AIBN); <sup>d</sup>determined by NMR; <sup>e</sup>solvent: anisole; <sup>f</sup>performed in bulk;

**Table 6. 2: Number-average degrees of polymerization of linear PDMAEMA and polydispersities (in brackets; both obtained by different methods), initiation site efficiencies,  $f_i$ , derived therefrom (bold, italics) and the resulting formulas: PDMAEMA<sub>n</sub> (n equals number-average degree of polymerization)**

	1A	1B	1C	1D
GPC of lin. PMAA	126 (1.18); <b><i>0.52</i></b>	155 (1.23); <b><i>0.62</i></b>	1590 (6.5)	1740 (5.3)
GPC of lin. PMMA	105 (1.06); <b><i>0.62</i></b>	134 (1.10); <b><i>0.72</i></b>	1270 (1.9)	1470 (1.8)
MALDI of PMMA	100(1.10); <b><i>0.65</i></b>	115 (1.16); <b><i>0.83</i></b>	-	-
Average	<b><i>0.60</i></b>	<b><i>0.72</i></b>	-	-
approx. formula	PDMAEMA <sub>108</sub>	PDMAEMA <sub>133</sub>	PDMAEMA <sub>1400</sub>	PDMAEMA <sub>1600</sub>

The determination of the cloud points was achieved by turbidity measurements using a titrator (Titrand 809, Metrohm, Herisau, Switzerland) equipped with a turbidity sensor ( $\lambda_0 = 523$  nm, Spectrosense, Metrohm). In addition, a temperature sensor (Pt 1000, Metrohm) and a pH-sensor (micro pH glass electrode, Metrohm) were used. The temperature program (1K / min) was run by a thermostat (LAUDA RE 306 and Wintherm\_Plus software), using a home-made thermostatable vessel. All aqueous solutions were prepared either from Millipore water

or buffer ( $pH = 10$ : boric acid buffer Titrinorm, VWR;  $pH = 9$ : boric acid buffer 9461, Merck;  $pH = 8$ : boric acid buffer CertiPUR, Merck;  $pH = 7$ : phosphate buffer 82571, Fluka; ionic strength of all buffers in the order of 0.05 mol/L) by vigorous stirring. The solutions were degassed by applying vacuum (50 - 100 mbar) for 15 min at room temperature to minimize bubble formation during heating. The solutions were measured under nitrogen for measurements without buffer. We defined the cloud point as the intercept of the tangents at the onset of turbidity (Figure 6. 1). The potentiometric titrations (titer 0.1 N HCl 0.06 mL/min) were performed under similar conditions, using the same  $pH$ -electrode (connected to a separation amplifier). But instead of a turbidity sensor a conductivity sensor (712 Conductometer, Metrohm) was used to determine the equivalence point of the titration (intercept of tangents in the conductivity curve).

We took only freshly prepared solutions for the titrations and for all turbidity measurements. This helps to obtain reliable data, since a shift of cloud points to higher temperatures was observed during turbidity measurements when using several heating and cooling cycles (see Figure 6. 8 in Supporting Information).

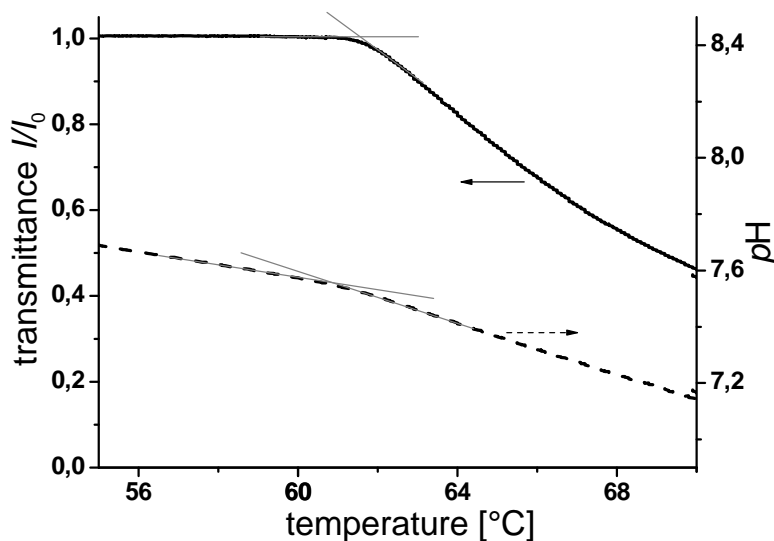


Figure 6. 1: Determination of cloud points  $T_{cl}$  (extraction of cloud point from the turbidity data and comparison with cloud point obtained by  $pH$ -measurement; here: 0.1 g/L 1A PDMAEMA<sub>108</sub> in pure water).

### 6.3. Results and Discussion

In this contribution we investigate the cloud points of aqueous solutions of star-shaped poly(dimethylaminoethyl methacrylate) (PDMAEMA) in dependence of arm number, arm length and  $pH$ . For this reason we performed turbidity measurements applying a temperature ramp and defined the cloud point as the intercept of the tangents at the onset of turbidity. The  $pH$  dependence with temperature in buffer-free solutions shows a kink very close to this

temperature (Figure 6. 1). This indicates that the intra- and intermolecular aggregation leads to an increase in the local density of polymer and therefore hinders ionization of the aminogroups. The initial slope of the  $pH$  curve is mainly determined by the change of the protonation equilibrium along with the change in the solubilizing abilities of water with temperature (electrode potential was corrected with respective temperature to obtain current  $pH$ ). The protonation equilibrium is also altered by the degree of branching as seen in potentiometric titrations (Figure 6. 2 and Figure 6. 7 of Supporting Information) and as expected by theory.<sup>39</sup>

### 6.3.1. Titration Behavior of Star-Shaped PDMAEMA

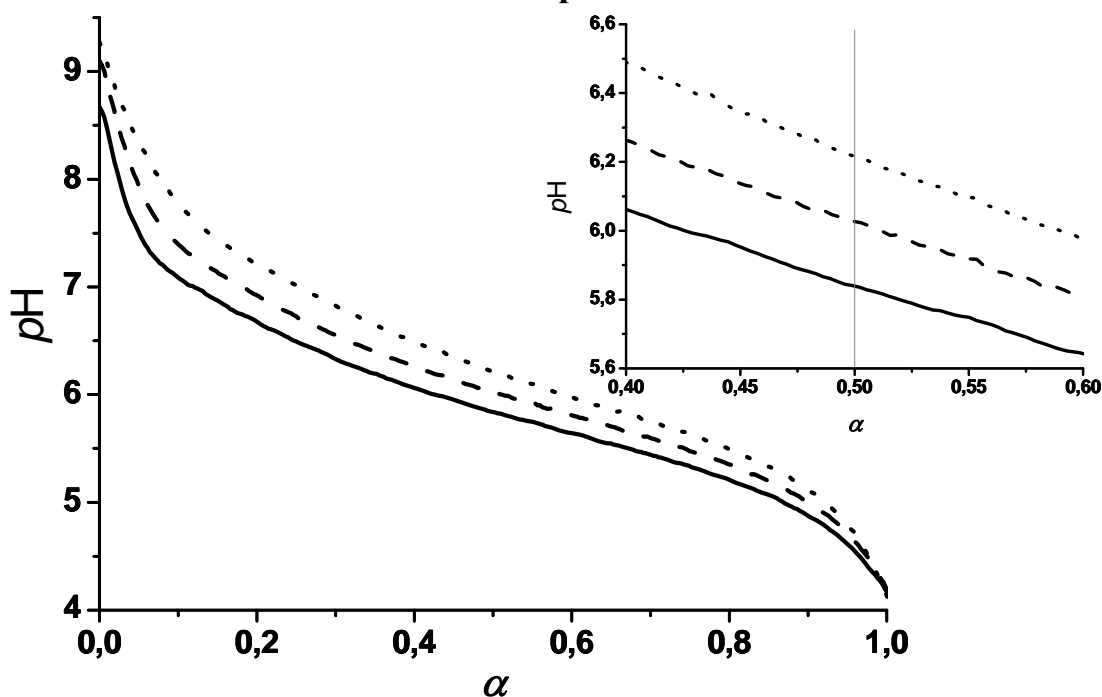


**Figure 6. 2:** Titration curves of star-shaped PDMAEMA in Millipore water with 0.1 n HCl in dependence of degree of neutralization  $\alpha$  (1.0 g/L; 24 °C; ..... 1A PDMAEMA<sub>108</sub>, ---- 8A (PDMAEMA<sub>110</sub>)<sub>5.4s</sub>, — 58A (PDMAEMA<sub>170</sub>)<sub>18</sub>). The inset shows an enlarged portion of the graph around half neutralization.

The titration curves are shifted to lower  $pH$  values for higher arm numbers but similar arm length (e.g. compare 1A, 8A). That means that the apparent  $pK_{b,app}$  increases with higher branching (see Table 6. 3).  $pK_{b,app} = -\log[OH^-]_{\alpha=0.5}$  is determined as  $pK_w - pH_{\alpha=0.5}$ , where  $pK_w$  is the negative decadic logarithm of the equilibrium constant of the autodissociation of water  $K_w$ . This result is consistent with former results found with help of star-shaped poly(acrylic acid).<sup>40</sup> For this polyacid, the apparent  $pK_a$  increased with increasing branching. This was explained by the high concentration of counterions inside the branched structure, which hampers the deprotonation of the weak polyacid at the same degree of neutralization.

Analogously our polybase keeps a certain amount of HCl for its own microscopic Donnan equilibrium. An increasing part of the added HCl does not contribute to the protonation of the amino groups, when the branching increases. This is again due to the increasing osmotic pressure inside the star, which opposes the protonation. For the dependence of the apparent  $pK_b$  on the arm length see Chapter 6. 5 and previous publication.<sup>40</sup>

### 6.3.2. Thermoresponsive Properties of Star-Shaped PDMAEMA

Because of the considerable drop of  $pH$  during heating in pure water (Figure 6. 1) and the anticipated effect of the  $pH$  on the LCST behaviour, we primarily investigated the cloud points of the star-shaped polymers in buffer solution. This keeps the  $pH$  more constant over the whole temperature range. However at the same time the ionic strength is increased ( $\sim 0.05$  mol/L) due to salt present in the buffer solution.

We performed most of the measurements at a concentration of 0.1 g/L (each 25 mL of freshly prepared PDMAEMA solutions) in order to save polymer. There is a concentration dependence of the cloud points as expected (we move along the binodal which has the minimum in the LCST). It leads to a shift of the phase boundary to lower temperatures with increasing concentration (0.1 g/L - 1.0 g/L; see Table 6. 3). The effect is more pronounced for linear polymer. But since the effect is in the order of a few Kelvin in the investigated concentration range, we continue most of the measurements with 0.1 g/L. This is in all cases below the overlap concentration.

The cloud points at 0.1 g/L are represented in Figure 6. 3 in dependence of molecular weight and  $pH$  (see also Figure 6. 4).

We start the discussion at high  $pH$  ( $\geq 9$ ), where the stars are almost uncharged. Here the cloud points decrease monotonously with increasing molecular weight irrespective of arm length and arm number. Therefore all cloud points seem to fit one “master curve”.

According to Flory-Huggins theory for linear polymers the critical temperature (here  $T_{cl}$ ) depends on the degree of polymerization,  $DP$ , in the following way:<sup>41</sup>

$$\frac{1}{T_{cl}} = \frac{1}{\theta} + \frac{1}{\theta\psi} \left( \frac{1}{2 \cdot DP} + \frac{1}{\sqrt{DP}} \right) \quad 6.1.$$

$\theta$  is the theta temperature, and  $\psi$  accounts for the sign of the temperature dependence of the Flory-Huggins parameter  $\chi$ . In the case of LCST polymers  $\psi < 0$ . In a strict sense, equation 6.1. holds only true for the critical volume fraction. However, for the rather high molecular weights the critical volume fraction is expected to be of the order of the polymer volume

fractions used here. Moreover, we only aim at a semi-quantitative approach that elucidates the general trends.

**Table 6. 3: Cloud points  $T_c$  of PDMAEMA under different conditions (1.0 g/L; italics: 0.1 g/L) and  $pK_{b,app}$  (bold;  $pK_{a,app}$  measured at  $pH$  at  $\alpha = 0.5$ , 1.0 g/L in pure water, and converted into  $pK_{a,app}$  using  $pK_{a,app} + pK_{b,app} = 14$ )**

	<i>pH = 7</i>	<i>pH = 8</i>	<i>pH = 9</i>	<i>pH = 10</i>	<b><math>pK_{b,app}</math></b>
<b>1A PDMAEMA<sub>108</sub></b>	76.0; 79.9	53.0; 56.5	42.3; 46.9	38.7; 44.4	<b>7.78</b>
<b>1B PDMAEMA<sub>133</sub></b>	78.7	54.4	43.0	40.5	<b>7.78</b>
<b>1C PDMAEMA<sub>1400</sub></b>	77.6	-	-	28.9	-
<b>1D PDMAEMA<sub>1600</sub></b>	77.7	-	-	25.0	-
<b>5A (PDMAEMA<sub>100</sub>)<sub>3.1</sub></b>	78.0	51.3	40.0	36.0	<b>7.94</b>
<b>5E (PDMAEMA<sub>160</sub>)<sub>3.7</sub></b>	77.0	50.0	36.9	32.6	<b>7.98</b>
<b>8A (PDMAEMA<sub>110</sub>)<sub>5.4</sub></b>	77.6	50.0	36.9	32.9	<b>7.98</b>
<b>8E (PDMAEMA<sub>170</sub>)<sub>5.6</sub></b>	77.6	49.3	35.1	31.0	<b>7.98</b>
<b>21A (PDMAEMA<sub>170</sub>)<sub>9.5</sub></b>	80.0	49.1	33.7	29.3	-
<b>21E (PDMAEMA<sub>240</sub>)<sub>11</sub></b>	78.0	48.7	32.7	28.0	<b>8.05</b>
<b>58A (PDMAEMA<sub>170</sub>)<sub>18</sub></b>	78.7	49.1	31.1; 32.6	27.8	<b>8.16</b>
<b>58E (PDMAEMA<sub>240</sub>)<sub>24</sub></b>	78.7	48.7	31.5	25.8	<b>8.11</b>

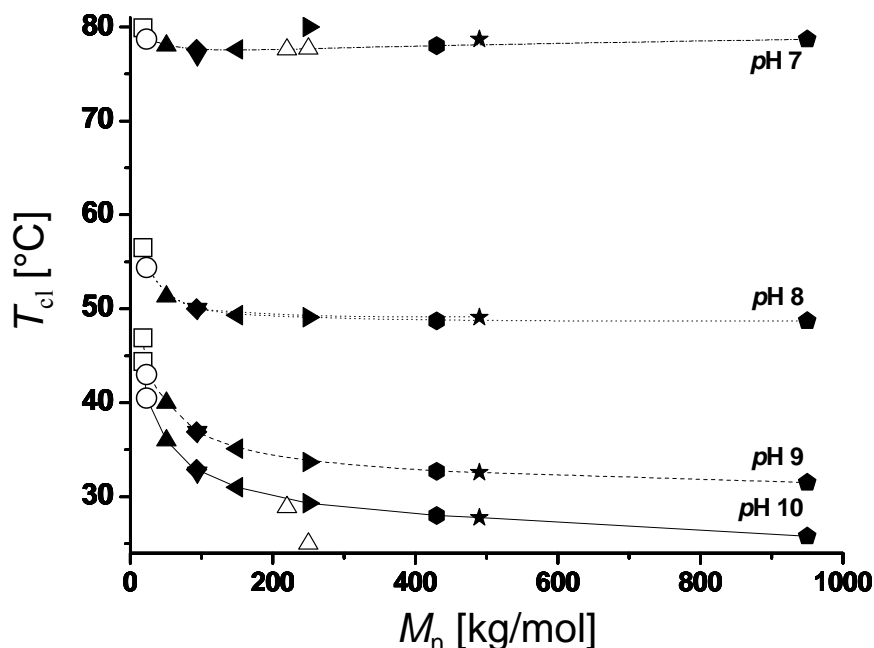


**Figure 6. 3:** Cloud points,  $T_{cl}$ , at 0.1 g/L of linear and star-shaped PDMAEMA in dependence of molecular weight,  $M_n$ , ( $\square$ : PDMAEMA<sub>108</sub>;  $\circ$ : PDMAEMA<sub>133</sub>;  $\blacktriangle$ : (PDMAEMA<sub>100</sub>)<sub>3.1</sub>;  $\blacktriangledown$ : (PDMAEMA<sub>160</sub>)<sub>3.7</sub>;  $\blacklozenge$ : (PDMAEMA<sub>110</sub>)<sub>5.4</sub>;  $\blacktriangleleft$ : (PDMAEMA<sub>170</sub>)<sub>5.6</sub>;  $\blacktriangleright$ : (PDMAEMA<sub>170</sub>)<sub>9.5</sub>;  $\bullet$ : (PDMAEMA<sub>240</sub>)<sub>11</sub>;  $\star$ : (PDMAEMA<sub>170</sub>)<sub>18</sub>;  $\blacklozenge$ : (PDMAEMA<sub>240</sub>)<sub>24</sub>;  $\triangle$ : PDMAEMA<sub>1400</sub> and PDMAEMA<sub>1600</sub> prepared by free radical polymerization); the lines are a guide to the eye

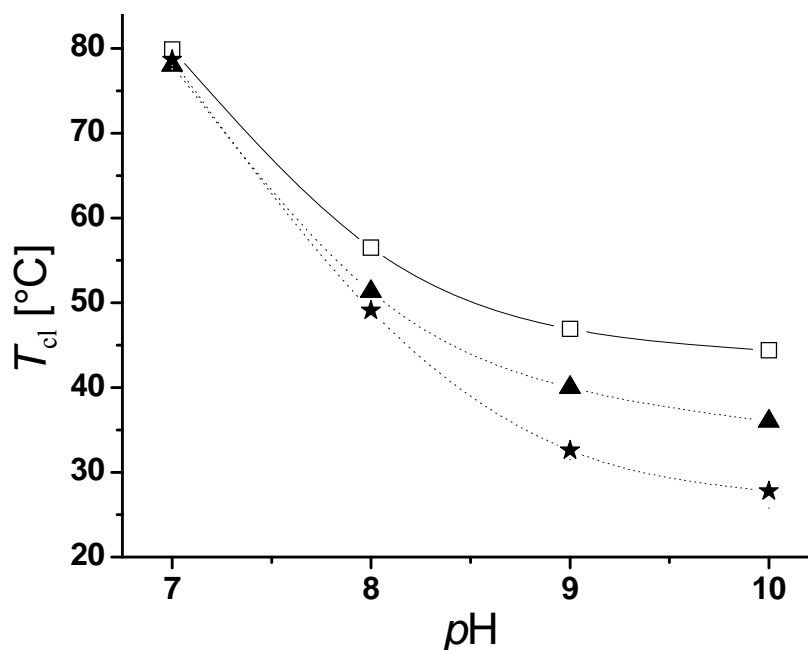


**Figure 6. 4:** Cloud points  $T_{cl}$  at 0.1 g/L of linear and star-shaped PDMAEMA in dependence of  $pH$  (for symbol assignment see Figure 6. 3)

Figure 6. 5. demonstrates that the cloud points of the star-shaped polymers lie on one straight line for  $pH = 9$  and  $pH = 10$ , respectively, in good approximation. Slight deviations are only seen for the short linear samples. Otherwise architecture has only a negligible influence on the phase separation of the polymers studied here. Possible endgroup effects are

coupled directly to architecture as the number of endgroups increases with arm number and decreases with arm length. Also they are not observed here and we assume that the bromine atom at the terminus does not have a significant effect on the polarity. Molecular weight alone determines the observed cloud points at constant high  $pH$ . Therefore PDMAEMA acts like an LCST polymer of class I in high  $pH$  buffer solutions.<sup>17</sup> Even linear PDMAEMA with a rather high molecular weight (samples 1C and 1D, prepared by free radical polymerization) does not deviate much from the curve in Figure 6. 3. One reason for the deviation of sample 1C and 1D might be the rather high polydispersity resulting from conventional radical polymerization. In conclusion, the Flory approach in terms of a temperature-dependent  $\chi$  parameter seems to well describe the thermoresponsive behavior of PDMAEMA at high  $pH$ . This is in contrast to various alternative models (two-state model, n-cluster model etc)<sup>42, 43</sup> proposed to describe the LCST behaviour of non-ionic polymers in aqueous solutions, like e.g. poly(ethylene oxide).<sup>44</sup>

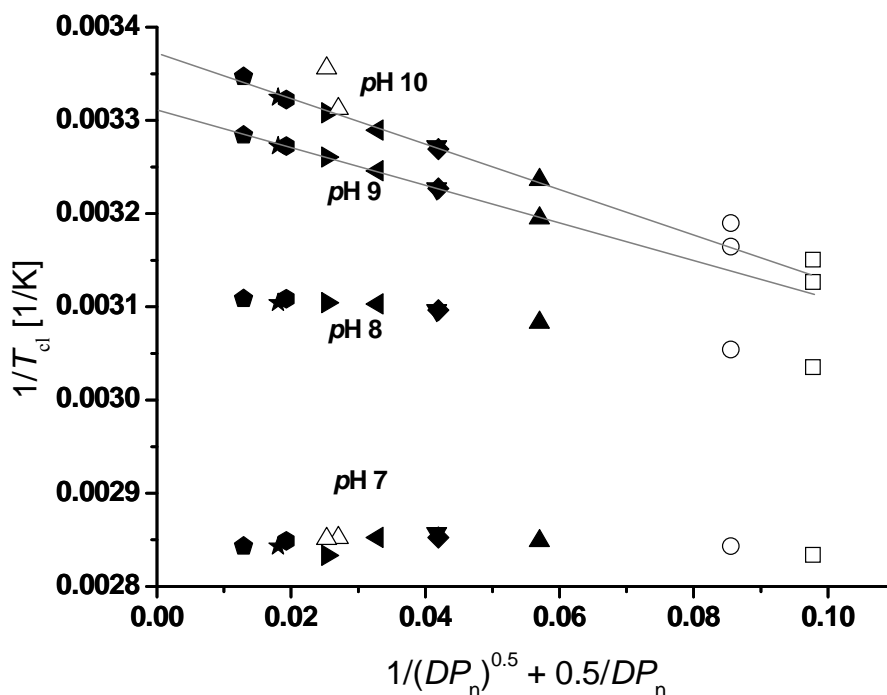


**Figure 6. 5:** Plot of inverse cloud points according to Flory theory (equation 6.1.) using the number-average degree of polymerization  $DP_n$  (for symbol assignment see Figure 6. 3)

At decreasing  $pH$  the PDMAEMA stars will be more and more charged (degree of neutralization  $\alpha \sim 0.05$  for  $pH = 8$  and  $\alpha \sim 0.11 - 0.25$  for  $pH = 7$ ). This is also reflected in the shift of the phase boundary to higher temperatures as expected.<sup>33, 45</sup> Already at  $pH = 8$  the cloud points increased by more than 10 K. In addition, the cloud points do not fit to one monotonous “master curve” any more. This behavior is even more pronounced at  $pH = 7$ . Furthermore, the cloud points are now located in a rather narrow window between 77 and 80 °C, i.e. they are nearly independent of  $DP$ .

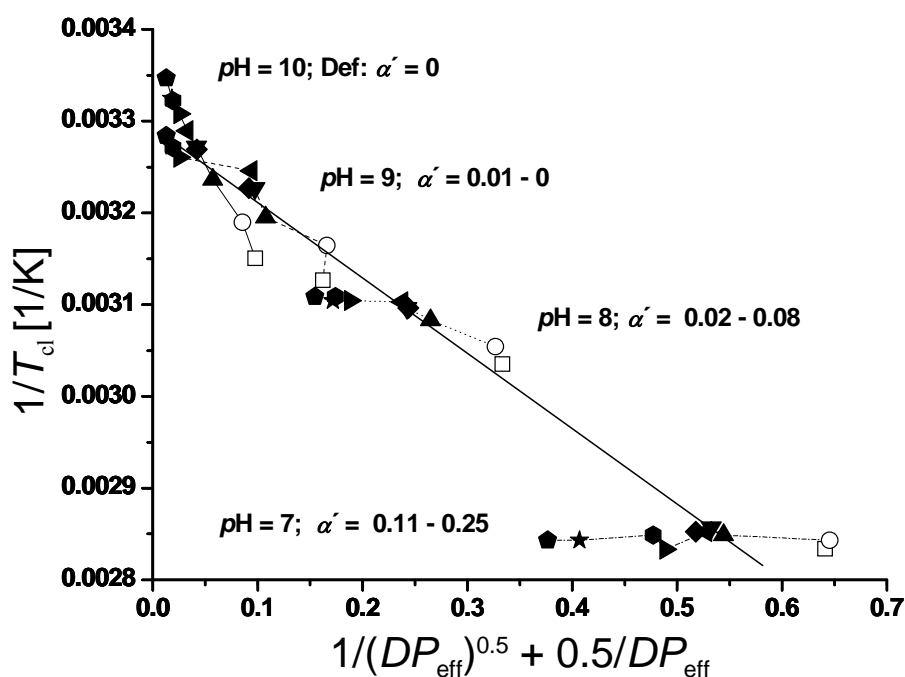


Figure 6. 6: Cloud point data plotted according to equation 6.1. after introduction of the effective degree of polymerization (equation 6.2.); for symbol assignment see Figure 6. 3.

We now take into account the charging (effect of counterions) by introducing the Khokhlov concept of the “effective degree of polymerization”,<sup>33, 46</sup>

$$DP_{eff} = \left( \frac{1}{DP} + \alpha' \right)^{-1} \quad 6.2.$$

where  $\alpha'$  equals the degree of ionization. Then we can linearize the set of our cloud point data. The data points gather around one straight line when taking  $\alpha$  (degree of neutralization) instead of  $\alpha'$  from Figure 6. 2 (and Figure 6. 7 in Supporting Information). However, at low degrees of neutralization the true degree of ionization deviates from  $\alpha$ . This is obvious since the polymer is slightly charged ( $\alpha' \neq 0$ ) even without any added acid ( $\alpha = 0$ ) as seen on the basic pH of PDMAEMA solutions without buffer. The inherent salt in the buffers can alter additionally the protonation equilibrium, but even by these approximations the overall trend seems to be well-captured as seen in Figure 6. 6. We remark that for  $\alpha' \cdot DP \gg 1$ ,  $DP_{eff} \approx 1/\alpha'$ , i.e. it does not virtually depend on the actual degree of polymerization. This is in good agreement with the flattening of the LCST dependence on the  $DP$  at pH 7 and 8.

Some deviations from the master curve at high pH are caused by the small but existent charging of the polymer. A contribution to the deviations at low pH might be attributed to the architecture and the resulting counterion confinement. Moreover, at low pH the charge density (ionization) starts to have an influence on the observed cloud point. This is also seen

in Figure 6. 3: especially the polymers with shorter arms (e.g. 21A and 58A) show slightly higher cloud points exceeding the anticipated curve for the polymers with longer arms (e.g. 21E and 58E). Though higher segment density has a limited opposing effect on the ionization in salt- and buffer-free solution (see Figure 6. 2), the increased segment density for the polymers with shorter arms leads also to an increased charge density. This may facilitate the solubility in water especially in salted and buffered solutions, where the salt-dominance regime is approached. Then the degree of ionization of monomer units is controlled by the  $pH$  imposed by the buffer solution and is virtually independent on the degree of branching.

As shown, we always get macroscopic demixing even at low concentrations of PDMAEMA in buffer solution. Therefore, the arm number seems to be too low to prevent macroscopic phase separation as seen on PNIPAAm stars with high arm number.<sup>21</sup> However we do not observe macroscopic phase separation at even higher concentrations in pure water for stars with more than 9 arms. In weak polyelectrolyte brushes<sup>47</sup> micelles of polystyrene-block-poly(methacrylic acid)<sup>48</sup> and in micelles of poly(*n*-butyl acrylate)-block-poly(acrylic acid)<sup>49</sup> a fraction of arms collapses and forms a virtually non-ionized core, whereas the other arms form an extended ionized corona. Thus, in analogy we expect that at a  $pH$  close to  $pK_a$  a decrease in solvent strength leads to intra-molecular phase separation in star-like  $pH$  sensitive polyelectrolytes. This more strongly charged corona may efficiently prevent stars from aggregation above the LCST. This electro-steric stabilization plays the dominant role in the salt-free case. These results will be an issue of a future publication.

## 6.4. Conclusions

We can conclude that the cloud points of PDMAEMA in buffer solutions can be easily tuned by changing the  $pH$ , molecular weight and concentration. At high  $pH$  the architecture has no dominant influence on the observed cloud points. At intermediate  $pH$  it has only a minor influence of the order of a few Kelvins. Our results indicate that phase separation in PDMAEMA solutions induced by an increase in temperature can be satisfactorily described following the classical Flory approach in terms of a temperature-dependent  $\chi$  parameter.

## 6.5. Supporting Information

### Potentiometric Titration

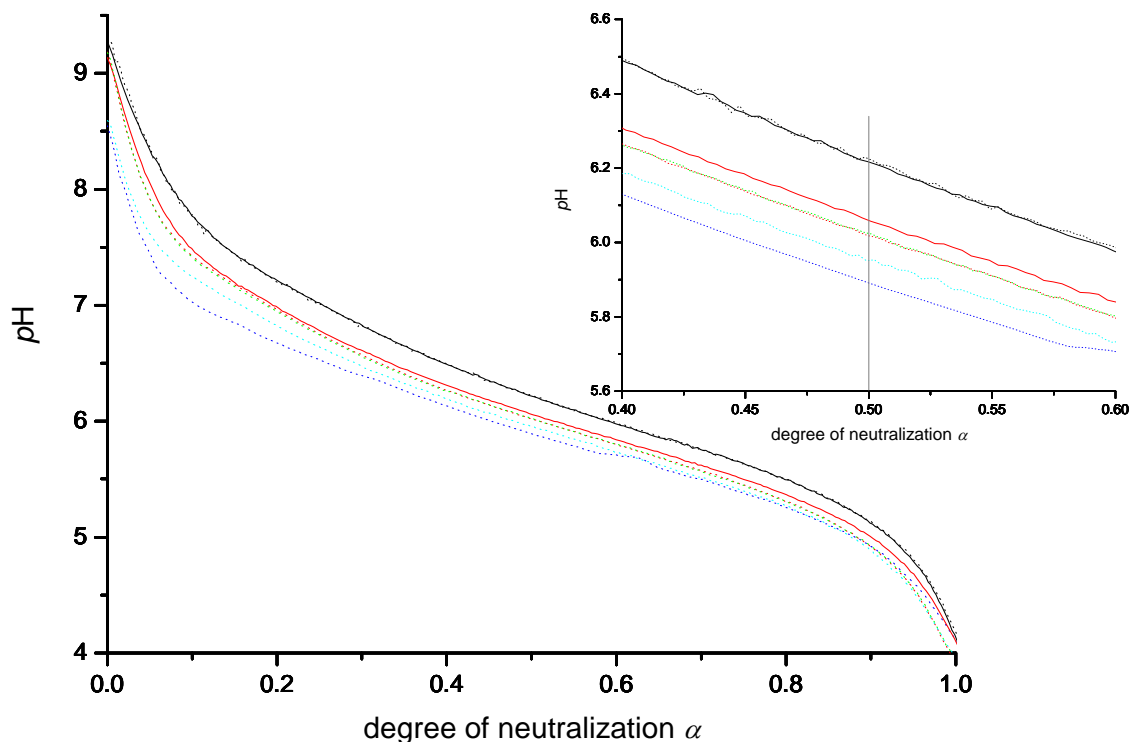
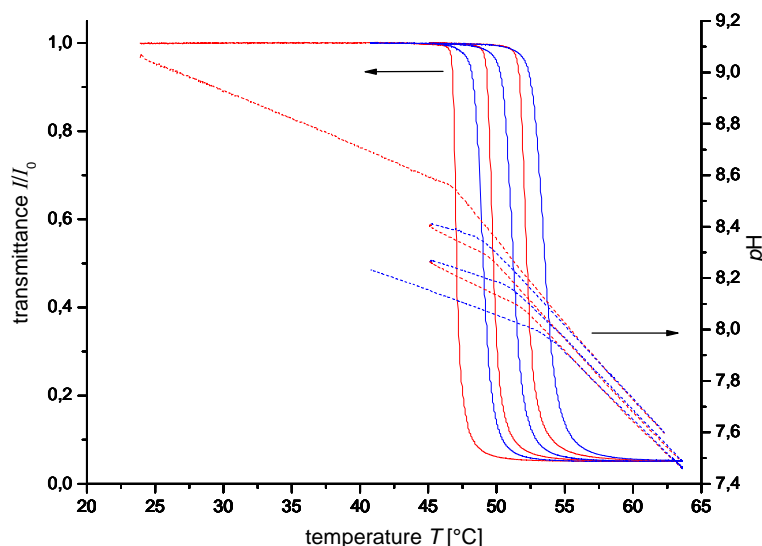


Figure 6. 7: Titration behavior of star-shaped PDMAEMA in Millipore water with 0.1 n HCl (1.0 g/L; 24 °C; — 1A PDMAEMA<sub>108</sub>, ..... 1B PDMAEMA<sub>133</sub>, — 5A (PDMAEMA<sub>100</sub>)<sub>3.1</sub>, ..... 5E (PDMAEMA<sub>160</sub>)<sub>3.7</sub>, ..... 8E (PDMAEMA<sub>170</sub>)<sub>5.6</sub>, ..... 21E (PDMAEMA<sub>240</sub>)<sub>11</sub>, ..... 58E (PDMAEMA<sub>240</sub>)<sub>24</sub>)

The dependence of the apparent  $pK_b$  with constant arm number but increasing arm length is not that apparent in Figure 6. 7, as we did not obtain any pair of stars with constant arm number. When comparing 58A and 58E we observe the higher  $pK_b$  for 58A. The longer the arms the lower is the segment density and the osmotic pressure inside the star is decreased.

#### Stability of PDMAEMA solutions:

We took only freshly prepared solutions for the titrations and for all turbidity measurements. This helps to obtain reliable data, since a shift of cloud points to higher temperatures was observed during turbidity measurements when using several heating and cooling cycles (see Figure 6. 8). One reason might be the slow autocatalytic hydrolysis of the ester moieties. This is also seen in the  $pH$ -change at the same temperature after several cycles. Though we could not see any clear evidence of hydrolytic damage of polymer 1A PDMAEMA<sub>108</sub> by NMR (after one month in 1 g/L aqueous solution and after dialysis to get rid of low molecular side products), already small changes in the system might cause major effects.



**Figure 6. 8:** Effect of heating cooling cycles on the cloud point (full lines) and  $pH$  of an aqueous solution of PDMAEMA<sub>108</sub> (1g/L; heating rate 1K/min, cooling rate 20 K/h; heating red, cooling blue)

**ACKNOWLEDGMENT:** We thank Andreas Walther for discussion and Deutsche Forschungsgemeinschaft (DFG; SFB 481) and Fond der Chemischen Industrie (FCI) for financial support.

## 6.6. References

1. Twaites, B. R.; de las Heras Alarcon, C.; Cunliffe, D.; Lavigne, M.; Pennadam, S.; Smith, J. R.; Gorecki, D. C.; Alexander, C. *Journal of Controlled Release* **2004**, *97*, 551.
2. Pennadam, S. S.; Ellis, J. S.; Lavigne, M. D.; Gorecki, D. C.; Davies, M. C.; Alexander, C. *Langmuir* **2007**, *23*, 41.
3. Kwon, I. K.; Matsuda, T. *Biomaterials* **2006**, *27*, 986.
4. Carter, S.; Rimmer, S.; Rutkaite, R.; Swanson, L.; Fairclough, J. P. A.; Sturdy, A.; Webb, M. *Biomacromolecules* **2006**, *7*, 1124.
5. Wei, H.; Zhang, X.; Cheng, C.; Cheng, S.-X.; Zhuo, R.-X. *Biomaterials* **2007**, *28*, 99.
6. Russell, T. P.; Fetters, L. J.; Clark, J. C.; Bauer, B. J.; Han, C. C. *Macromolecules* **1990**, *23*, 654.
7. Zhulina, E. B.; Borisov, O. V.; Birshtein, T. M. *Vysokomolekulyarnye Soedineniya, Seriya A* **1988**, *30*, 774.
8. Garas, G.; Kosmas, M. *Macromolecules* **1994**, *27*, 6671.

9. Francois, J.; Beaudoin, E.; Borisov, O. *Langmuir* **2003**, *19*, 10011.
10. Numasawa, N.; Okada, M. *Polymer Journal (Tokyo)* **1999**, *31*, 99.
11. Shmakov, S. L. *Polymer* **2001**, *43*, 1491.
12. Taylor, L. D.; Cerankowski, L. D. *Journal of Polymer Science, Polymer Chemistry Edition* **1975**, *13*, 2551.
13. Schild, H. G. *Progress in Polymer Science* **1992**, *17*, 163.
14. Xia, Y.; Burke, N. A. D.; Stöver, H. D. H. *Macromolecules* **2006**, *39*, 2275.
15. Xia, Y.; Yin, X.; Burke, N. A. D.; Stöver, H. D. H. *Macromolecules* **2005**, *38*, 5937.
16. Meeussen, F.; Nies, E.; Berghmans, H.; Verbrugghe, S.; Goethals, E.; Du Prez, F. *Polymer* **2000**, *41*, 8597
17. Aseyev, V. O.; Tenhu, H.; Winnik, F. M. *Advances in Polymer Science* **2006**, *196*, (Conformation-Dependent Design of Sequences in Copolymers II), 1.
18. Zheng, Q.; Pan, C.-Y. *European Polymer Journal* **2006**, *42*, 807.
19. Plummer, R.; Hill, D. J. T.; Whittaker, A. K. *Macromolecules* **2006**, *39*, 8379.
20. Schilli, C. M.; Müller, A. H. E.; Rizzardo, E.; Thang, S. H., RAFT Polymers: Novel Precursors for Polymer-Protein Conjugates. In *Advances in Controlled/Living Radical Polymerization*; Matyjaszewski, K., Ed. ACS Symposium Series 854; American Chemical Society: Washington, DC, **2003**; p 603.
21. Luo, S.; Xu, J.; Zhu, Z.; Wu, C.; Liu, S. *Journal of Physical Chemistry B* **2006**, *110*, 9132.
22. Lu, Y.; Wittemann, A.; Ballauff, M.; Drechsler, M. *Macromolecular Rapid Communications* **2006**, *27*, 1137.
23. Deike, I.; Ballauff, M.; Willenbacher, N.; Weiss, A. *Journal of Rheology (New York, NY, United States)* **2001**, *45*, 709.
24. Cho, S. H.; Jhon, M. S.; Yuk, S. H.; Lee, H. B. *Journal of Polymer Science, Part B: Polymer Physics* **1997**, *35*, 595.
25. Liu, Q.; Yu, Z.; Ni, P. *Colloid and Polymer Science* **2004**, *282*, 387.
26. Bütün, V.; Armes, S. P.; Billingham, N. C. *Polymer* **2001**, *42*, 5993.
27. Burillo, G.; Bucio, E.; Arenas, E.; Lopez, G. P. *Macromolecular Materials and Engineering* **2007**, *292*, 214.
28. Fournier, D.; Hoogenboom, R.; Thijs, H. M. L.; Paulus, R. M.; Schubert, U. S. *Macromolecules* **2007**, *40*, 915.
29. Georgiou, T. K.; Vamvakaki, M.; Patrickios, C. S.; Yamasaki, E. N.; Phylactou, L. A. *Biomacromolecules* **2004**, *5*, 2221.

30. Lee, H.-i.; Pietrasik, J.; Matyjaszewski, K. *Macromolecules* **2006**, *39*, 3914.
31. Pei, Y.; Chen, J.; Yang, L.; Shi, L.; Tao, Q.; Hui, B.; Li, J. *Journal of biomaterials science. Polymer edition* **2004**, *15*, 585.
32. Erbil, C.; Akpinar, F. D.; Uyanik, N. *Macromolecular Chemistry and Physics* **1999**, *200*, 2448.
33. Bokias, G.; Vasilevskaya, V. V.; Iliopoulos, I.; Hourdet, D.; Khokhlov, A. R. *Macromolecules* **2000**, *33*, 9757.
34. Yoo, M. H.; Sung, Y. K.; Cho, C. S.; Lee, Y. M. *Polymer* **1997**, *38*, 2759.
35. Grosberg, A. Y.; Khokhlov, A. R., *Statistical Physics of Macromolecules*. **1994**; p 350.
36. Borue, V. Y.; Erukhimovich, I. Y. *Macromolecules* **1988**, *21*, 3240.
37. Vamvakaki, M.; Patrickios, C. S. *Chemistry of Materials* **2002**, *14*, 1630.
38. Plamper, F.; Schmalz, A.; Penott-Chang, E.; Jusufi, A.; Ballauff, M.; Müller, A. *Macromolecules* **2007**, *40*, 5689.
39. Wolterink, J. K.; van Male, J.; Stuart, M. A. C.; Koopal, L. K.; Zhulina, E. B.; Borisov, O. V. *Macromolecules* **2002**, *35*, 9176.
40. Plamper, F. A.; Becker, H.; Lanzendörfer, M.; Patel, M.; Wittemann, A.; Ballauff, M.; Müller, A. H. E. *Macromolecular Chemistry and Physics* **2005**, *206*, 1813.
41. Shultz, A. R.; Flory, P. J. *Journal of the American Chemical Society* **1952**, *74*, 4760-7.
42. Sevick, E. M. *Macromolecules* **1998**, *31*, 3361.
43. De Gennes, P. G. *C. R. Acad. Sci., Ser. Iib* **1991**, *313*, 1117.
44. Halperin, A. *European Physical Journal B: Condensed Matter Physics* **1998**, *3*, 359.
45. Kudlay, A. N.; Erukhimovich, I. Y.; Khokhlov, A. R. *Macromolecules* **2000**, *33*, 5644.
46. De Gennes, P. G. *Scaling Concepts in Polymer Physics*; Cornell University Press, Ithaca, NY, 1979.
47. Pryamitsyn, V. A.; Leermakers, F. A. M.; Fleer, G. J.; Zhulina, E. B. *Macromolecules* **1996**, *29*, 8260.
48. Stepanek, M.; Prochazka, K.; Brown, W. *Langmuir* **2000**, *16*, 2502.
49. Colombani, O.; Ruppel, M.; Burkhardt, M.; Drechsler, M.; Schumacher, M.; Gradzielski, M.; Schweins, R.; Müller, A. H. E. *Macromolecules* **2007**, *40*, 4351.

## 7. Tuning the Thermoresponsiveness of Weak Polyelectrolytes by pH and Light: Lower and Upper Critical-Solution Temperature of Poly(*N,N*-dimethylaminoethyl methacrylate)

*Felix A. Plamper<sup>a</sup>, Alexander Schmalz<sup>a</sup>, Matthias Ballauff<sup>b,\*</sup>, Axel H. E. Müller<sup>a,\*</sup>*

<sup>a</sup>Makromolekulare Chemie II, <sup>b</sup>Physikalische Chemie I, and Bayreuther Zentrum für Kolloide und Grenzflächen, Universität Bayreuth, D-95440 Bayreuth, Germany,

Published in *Journal of the American Chemical Society* 2007, 129, p.14538.

**ABSTRACT:** The presence of multivalent counterions induces an upper critical solution temperature (UCST) in addition to the known lower critical solution temperature (LCST) of poly(*N,N*-dimethylaminoethyl methacrylate) (PDMAEMA). The LCST-type cloud points can be adjusted by *pH* of the buffer, whereas the UCST-type cloud points can be adjusted by the concentration of trivalent counterions. High *pH* favors the LCST-transition, whereas lower *pH* extends the UCST-type miscibility gap at constant concentration of trivalent counterions. By use of hexacyanocobaltate(III) as a trivalent counterion, we can even switch off again the UCST-behavior by UV-illumination (photoinduced dissolution).

## 7.1. Results and Discussion

Thermoresponsive polymers exhibit a change in the solubility upon heating or cooling. Water-soluble polymers often exhibit a lower critical solution temperature (LCST), i.e. phase separation at rising temperatures. Examples are poly(*N*-isopropyl acrylamide) or poly(vinyl methylether).<sup>1,2</sup> In contrast, an upper critical solution temperature (UCST) behavior, that is, demixing on cooling, is often observed for solutions in organic solvents.<sup>3</sup>

There are only a few examples of water-soluble polymers that exhibit both LCST and UCST. Examples are poly(vinyl alcohol)<sup>4</sup> and triblock copolymers of, for example, polyglycidol and poly(propylene oxide).<sup>5</sup> Concentrated poly(vinyl methyl ether) mixtures with water as the minority component show an additional UCST transition below 0 °C.<sup>6</sup> The opposite behavior is reported for poly(ethylene oxide), showing a UCST above the reported LCST (above 100 °C under pressure).<sup>7</sup> However, there is no way to adjust critical temperatures over a wide range.

We recently reported that the LCST-type cloud points of linear and star-shaped PDMAEMA can be easily adjusted by *pH* ( $pK_{a,app} \approx 6$  for the protonated polybase).<sup>8</sup> At high *pH*, when the polymer is almost uncharged (degree of neutralization < 2% at *pH* 9),<sup>8</sup> the cloud points of PDMAEMA behave as for uncharged polymers.<sup>9</sup> At lower *pH*, however, the weak polyelectrolyte PDMAEMA starts to carry charges by protonation, enhancing the solubility in water. Concomitantly the cloud points are shifted to higher temperatures.

Herein we present the the first observation of a UCST behavior of a typical LCST polymer, poly(*N,N*-dimethylaminoethyl methacrylate) (PDMAEMA), in presence of small quantities of trivalent counterions. This behavior is similar to the UCST behavior reported by Jia et al. for micelles consisting of an inner core of protonated poly(2-vinyl pyridine), where the core is connected by redox-sensitive divalent counterions.<sup>10</sup> Moreover, we demonstrate that both LCST and UCST can be adjusted independently over a wide temperature range and the UCST-like cloudpoint can even be manipulated by UV light.

We monitored the cloud points of aqueous solutions of PDMAEMA by turbidimetry (for experimental details see the Supporting Information). In all cases reported here the UCST-type cloud points were lower than the LCST transitions, and a one-phase region intervenes. As seen in Figure 7.1, the UCST-type cloud points appear by adding small amounts of the trivalent counterion hexacyanocobaltate(III)  $[\text{Co}(\text{CN})_6]^{3-}$  as a trivalent counterion. The more trivalent counterions present, the higher the cloud points of the lower miscibility gap. This is found at practically constant ionic strength and constant *pH*. At the same time the LCST-type cloud points are hardly affected by the presence of  $[\text{Co}(\text{CN})_6]^{3-}$ . This behavior is observed for

both linear and star-shaped PDMAEMA. The region of full miscibility is narrowed for star-shaped PDMAEMA (for synthesis see ref. <sup>11</sup>) due to the higher molecular weight compared to the linear polymer.<sup>8</sup> Hence, effects caused by the different architecture of the polymers cannot be excluded.

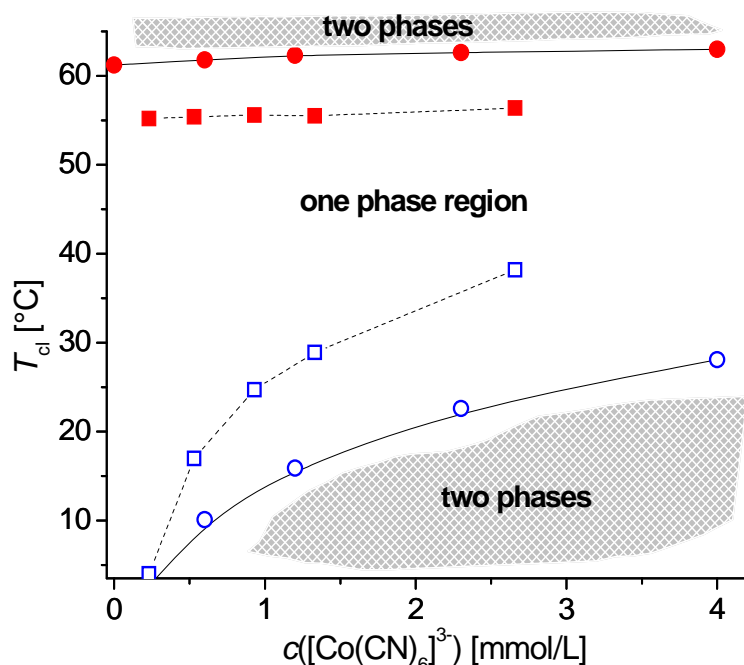
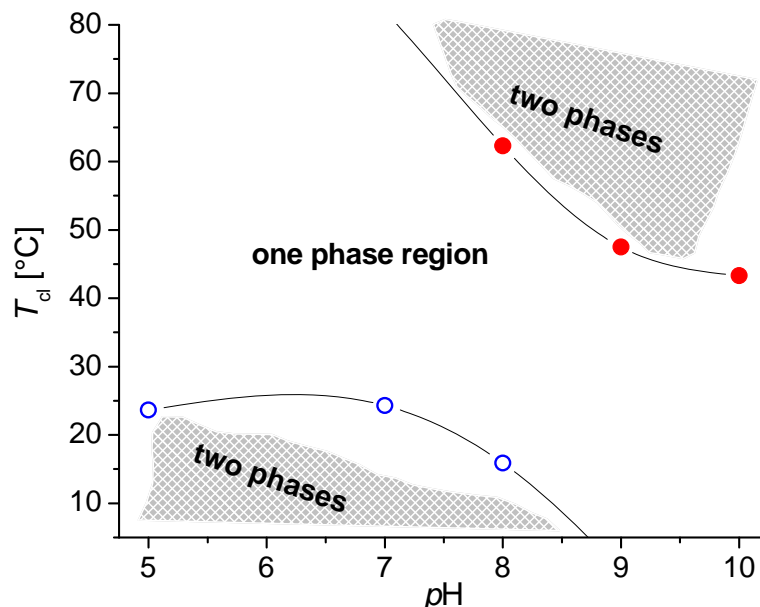


Figure 7.1: Dependence of the cloud points  $T_{cl}$  of aqueous PDMAEMA solutions (0.1 g/L in buffer of  $pH$  8 + 0.1 n NaCl) on the  $[\text{Co}(\text{CN})_6]^{3-}$  concentration (titrated 0.0166 n  $\text{K}_3[\text{Co}(\text{CN})_6]$  into 25 mL PDMAEMA solution) for linear PDMAEMA<sub>100</sub> (circles) and star-shaped (PDMAEMA<sub>170</sub>)<sub>18</sub> (squares); closed symbols assign LCST-type cloud points, open ones refer to cloud points of the UCST-behavior (the lines are a guide to the eye).

As shown earlier, the cloud points of the LCST behavior can be adjusted by the  $pH$  of the buffer.<sup>8</sup> Now the UCST can be adjusted by addition of trivalent counterions (Figure 7.1).

The effect of  $pH$  on both UCST and LCST at constant concentration of counterions and polymer is shown in Figure 7.2. The UCST-type cloud point disappears at high  $pH$ . This is due to the fact that the electrostatic interaction between the almost uncharged polymer and the trivalent ions must vanish at high  $pH$ . This indicates that the electrostatic interaction of counterions with the polymer induces the UCST behavior: the multivalent counterions connect different polymer molecules, leading to precipitation at low temperatures. The interactions weaken and the bridges break at higher temperatures. This could be also one reason for the negligible influence of the trivalent ion on the LCST-type cloud points. On the other hand, the introduction of charges stabilizes the homogeneous phase as shown recently. Hence, the phase behavior seen when introducing trivalent ions results from the competition

of two effects: i) The stabilization of the homogeneous phase by charges, and ii) the destabilization through the bridges introduced by trivalent ions.



**Figure 7.2:** Dependence of the UCST- (open symbols) and LCST-type (full symbols) cloud points on pH (0.1 g/L PDMAEMA<sub>100</sub>; 1.2 mmol/L [Co(CN)<sub>100</sub>]<sup>3-</sup>; 0.1 n NaCl); the lines are a guide to the eye.

However, an excess of the number of trivalent charges compared to those on the polymer was always needed to obtain an UCST behavior. This might be due to the unfavorable equilibrium between multivalent counterions freely dissolved in bulk solution and counterions bridging the weakly charged polyelectrolyte. This is in contrast to the behavior of strongly charged polymer stars in the presence of multivalent counterions.<sup>12</sup>

We have shown earlier that photosensitive counterions [Co(CN)<sub>6</sub>]<sup>3-</sup> can induce a conformational change in polyelectrolyte stars upon illumination besides a change in their solubility.<sup>12</sup> The counterion reduces its valency from trivalent to divalent by ligand exchange after excitation with UV-light (exchange of one cyanide ligand with water).<sup>13</sup> Since the interaction and the bridging abilities of the counterions with the weak polyelectrolyte are very much dependent on the valency, we expect a photo-induced tuning of the UCST (and in less extent of the LCST). In contrast to other more tedious techniques to modify the thermoresponsive properties (e.g. incorporation of light sensitive monomers into the polymer),<sup>14, 15</sup> the present observations demonstrate that the thermosensitive behavior can be switched in a much easier fashion.

Indeed, we are able to switch off the UCST-behavior again by UV illumination as seen in Figure 7.3. The UCST-type cloud point decreases below the accessible temperature range after 45 min of UV illumination (photoinduced dissolution). The divalent [Co(CN)<sub>5</sub>H<sub>2</sub>O]<sup>2-</sup>

ions developed by illumination of the solution are less efficient to bridge the polymer chains. The influence of illumination on the LCST is less pronounced, since multivalent counterions have only a minor effect here (Figure 7.1).

All effects mentioned in this Communication were only observed in buffered solutions containing a considerable amount of salt (ionic strength  $\approx 0.1$  mol/L). The thermoresponsive effects are more complicated in buffer-free solution, since the various parameters cannot be varied independently from each other. In fact, pH increases in the presence of multivalent counterions (counterions stabilize the protonated form of PDMAEMA and act as a cobase). Evidently, a shift of the pH has a considerable influence on the cloud points. Thus, we did not observe an UCST behavior in the absence of buffer. In the absence of additional monovalent ions the electrostatic repulsion of the charged polymer is dominant. However, the LCST-type cloud point is at that stage very much dependent on the concentration of multivalent counterions. This point is in need of further elucidation.

In conclusion, the phase behavior of a weak polyelectrolyte can be changed in a well-defined manner by introducing trivalent counterions: A UCST is induced in addition to the LCST already present. Photoswitching the valency of the counterions from trivalent to divalent can be used to undo this change. Hence, we presented a novel way to change the thermodynamics of polymer solutions by light.

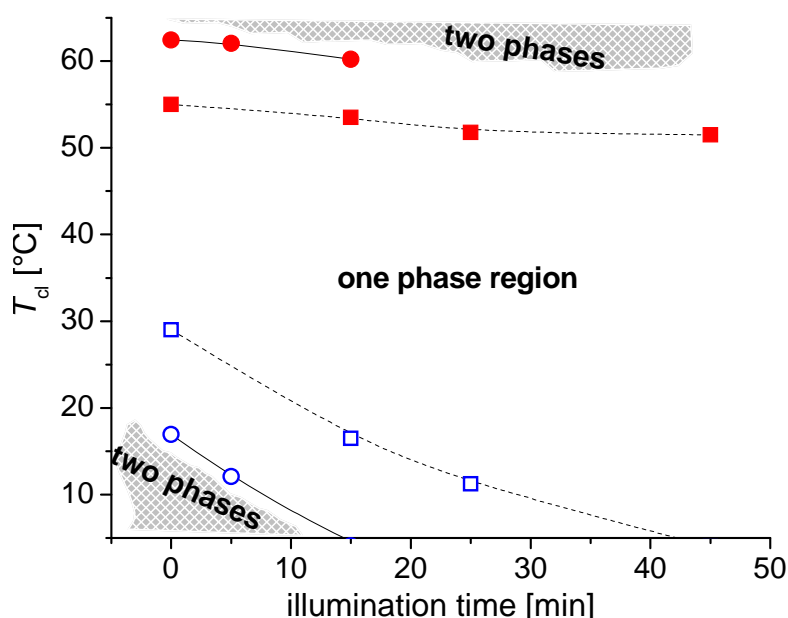


**Figure 7.3:** Tuning of the UCST-type (open symbols) and LCST-type (closed symbols) cloud point by UV-illumination ( $\lambda = 300 - 400$  nm); 0.1 g/L (PDMAEMA<sub>170</sub>)<sub>18</sub> (squares) and PDMAEMA<sub>100</sub> (circles) in pH 8 buffer, 0.1 n NaCl and 1.3 mmol/L [Co(CN)<sub>6</sub>]<sup>3-</sup>; the lines are a guide to the eye.

## 7.2. Supporting Information – Experimental Details

**Materials:** The polymer's preparation and characterization are described in previous papers (i.e. for linear poly(*N,N*-dimethylaminoethyl methacrylate) PDMAEMA<sub>100</sub> and star-shaped (PDMAEMA<sub>170</sub>)<sub>18</sub>).<sup>8, 11</sup> Potassium hexacyanocobaltate(III) K<sub>3</sub>[Co(CN)<sub>6</sub>] and sodium chloride NaCl were purchased from Aldrich. The buffer solutions were delivered by Riedel-de Haën (e.g. pH 8 sodium borate / hydrochloric acid buffer type 33547), Merck (pH 9 boric acid / potassium chloride / sodium hydroxide buffer type 9461) and VWR Titrimorm (pH 7 potassium dihydrogen phosphate / disodium hydrogen phosphate buffer 32 096.291).

**Sample Preparation:** All aqueous solutions were prepared by dissolution of the respective amount of NaCl and PDMAEMA in 25 mL of buffer by vigorous stirring (ionic strength of all buffers in the order of 0.05 mol/L). The NaCl concentrations were set as 0.1 mol/L in order to dominate the ionic strength in relation to the inherent salt of the buffer solutions. A K<sub>3</sub>[Co(CN)<sub>6</sub>] solution of same ionic strength (0.016 mol/L) was titrated to the respective solutions in order to adjust the cobaltate concentration. The prepared solutions were degassed by applying vacuum (50 - 100 mbar) for 15 min at room temperature to minimize bubble formation during heating.

**Cloudpoint Determination:** The determination of the cloud points was achieved by turbidity measurements using a titrator (Titrand 809, Metrohm, Herisau, Switzerland) equipped with a turbidity sensor ( $\lambda_0 = 523$  nm, Spectrosense, Metrohm). In addition, a temperature sensor (Pt 1000, Metrohm) was used. The temperature program (1K / min) was run by a thermostat (LAUDA RE 306 and Wintherm\_Plus software), using a home-made thermostatable vessel. We defined the cloud point as the intercept of the tangents of the transmittance-temperature dependence at the onset of turbidity. All cloud points were obtained from the one-phase region by heating (LCST-type cloud point) or cooling (UCST-type cloud point). The error of determining the cloud points by this method is small, since two independent determinations of the cloud points of the same stock solution gave always the same cloud point, varying just in the first digit after the comma.

### Dependence of cloud points on the PDMAEMA concentration

Additional experiments (see Table 7. 1) demonstrated that the ratio of trivalent counterions to monomer units determines the UCST. If the cobaltate concentration is kept constant and the PDMAEMA concentration increased, the UCST-type cloud point decreases. The relative number of associative interactions decreases compared to the total amount of polymer. If the

ratio of trivalent counterions compared to monomeric units was kept constant, but the polymer concentration was increased by a factor of three, the cloud point increased by ca. 10 K. Therefore the decisive parameter determining the UCST-type cloud points is the ratio of monomer unit concentration compared to the concentration of the trivalent counterions  $[\text{Co}(\text{CN})_6]^{3-}$ .

**Table 7.1:** Cloud points of PDMAEMA<sub>100</sub> (0.1 g/L or 0.3 g/L) in pH 8 buffer (+ 0.1 n NaCl) at different concentrations of polymer and  $[\text{Co}(\text{CN})_6]^{3-}$  (italics: LCST-type cloud point; bold: UCST-type cloud point)

	1.2 mmol/L $[\text{Co}(\text{CN})_6]^{3-}$	3.6 mmol/L $[\text{Co}(\text{CN})_6]^{3-}$
0.1 g/L	<b>15.9</b> , 62.3	-
0.3 g/L	<b>13.3</b> , 60.2	<b>23.6</b> , 61.4

**Acknowledgement.** This work was supported by Deutsche Forschungsgemeinschaft (Grants SFB 481 and Mu896/25-1) and Fonds der Chemischen Industrie (FCI).

### 7.3. References

1. Aseyev, V. O.; Tenhu, H.; Winnik, F. M. *Advances in Polymer Science* **2006**, *196*, (Conformation-Dependent Design of Sequences in Copolymers II), 1.
2. André, X.; Zhang, M.; Müller, A. H. E. *Macromolecular Rapid Communications* **2005**, *26*, 558.
3. Schulz, D. N.; Peiffer, D. G.; Agarwal, P. K.; Larabee, J.; Kaladas, J. J.; Soni, L.; Handwerker, B.; Garner, R. T. *Polymer* **1986**, *27*, 1734.
4. Pae, B. J.; Moon, T. J.; Lee, C. H.; Ko, M. B.; Park, M.; Lim, S.; Kim, J.; Choe, C. R. *Korea Polymer Journal* **1997**, *5*, 126.
5. Halacheva, S.; Rangelov, S.; Tsvetanov, C. *Macromolecules* **2006**, *39*, 6845.
6. Van Durme, K.; Van Assche, G.; Nies, E.; Van Mele, B. *Journal of Physical Chemistry B* **2007**, *111*, 1288.
7. Hammouda, B.; Ho, D.; Kline, S. *Macromolecules* **2002**, *35*, 8578.
8. Plamper, F. A.; Ruppel, M.; Schmalz, A.; Borisov, O.; Ballauff, M.; Müller, A. H. E. *Macromolecules* **2007**, submitted.
9. Shultz, A. R.; Flory, P. J. *Journal of the American Chemical Society* **1952**, *74*, 4760.

10. Jia, X.; Chen, D.; Jiang, M. *Chemical Communications (Cambridge, United Kingdom)* **2006**, *16*, 1736.
11. Plamper, F. A.; Schmalz, A.; Penott-Chang, E.; Drechsler, M.; Jusufi, A.; Ballauff, M.; Müller, A. H. E. *Macromolecules* **2007**, ASAP.
12. Plamper, F. A.; Walther, A.; Müller, A. H. E.; Ballauff, M. *Nano Letters* **2007**, *7*, 167.
13. Wrighton, M.; Hammond, G. S.; Gray, H. B. *Journal of the American Chemical Society* **1971**, *93*, 5254.
14. Lee, H.-i.; Pietrasik, J.; Matyjaszewski, K. *Macromolecules* **2006**, *39*, 3914.
15. Laschewsky, A.; Reka, E. D. *Macromolecular Rapid Communications* **2000**, *21*, 937.

## 8. Summary

Star-shaped polyelectrolytes were prepared by means of atom transfer radical polymerization (ATRP) utilizing the core-first approach. Star-shaped poly(acrylic acid) (PAA) with 5, 8 and 21 arms and different arm lengths was prepared via the corresponding poly(*tert*-butyl acrylate) (PtBA) precursors having a glucose, saccharose or  $\beta$ -cyclodextrin core. Adopting the attempt for preparation of PAA we used the same scaffolds for the preparation of star-shaped poly(dimethylaminoethyl methacrylate) (PDMAEMA). It is a weak cationic polyelectrolyte and it can be easily transformed to a strong one by quantitative quaternization (with methyl iodide) leading to poly{[2-(methacryloyloxy)ethyl] trimethylammonium iodide}, PMETAI. In order to reach high arm number a novel, hybrid silsesquioxane initiator with 58 initiation sites was introduced.

The solution behavior of the obtained PAA stars was analyzed. Potentiometric titrations indicate a decrease of PAA's acidity when increasing the arm number whereas a slight increase of the acidity was observed when increasing the molecular weight by increasing the length of the arms at constant arm number. The results are explained by the higher segment density of samples with short arms and high arm numbers, leading to a pronounced osmotic pressure inside the stars due to the presence of counterions. The osmotic pressure opposes further deprotonation, resulting in a decreased acidity. The osmotic coefficient decreases with increasing arm number, indicating higher counterion confinement within structures with higher branching. The use of strong polyelectrolytes facilitates the determination of the osmotic coefficient. It was seen directly that increasing arm numbers and decreasing arm lengths lead to a decrease of the osmotic coefficient. The osmotic coefficients of the investigated stars are in the range from 0.03 to 0.13, indicating the strong counterion confinement. Theory and experiment meet in the same order of magnitude. However the concentration dependence predicted by theory is not rendered by the experiment.

The size of PMETAI stars in solution was investigated by dynamic light scattering (DLS), showing the expected collapse of the stars with increasing ionic strength. Electrostatic and osmotic screening leads to a retraction of the originally stretched arms, when no additional salt is present. However ion-specific effects lead to a more pronounced shrinkage when sodium chloride was exchanged with sodium iodide.

The considerable osmotic pressure inside the star helps to incorporate multivalent counterions. The ion exchange reduces the number of counterions within the star, simultaneously increasing the translatory entropy of all counterions, since a multiple number of monovalent counterions is released into bulk for one multivalent counterion, which has

been incorporated. The ion exchange leads to a decrease in osmotic pressure inside the star, reducing the strong stretching of the polymer's arms, as seen by DLS. The collapse is more pronounced for counterions of higher valency. The switching of the counterion's charge can therefore lead to smart polyelectrolytes. This was seen for the trivalent, light-sensitive hexacyanocobaltate(III), which by UV illumination transforms to a divalent counterion. Simultaneously the hydrodynamic radius increases upon irradiation.

Finally the thermoresponsive properties of aqueous solutions of star-shaped PDMAEMA were investigated. PDMAEMA is both *pH*-sensitive as temperature-sensitive, showing a miscibility gap at higher temperatures (LCST behavior). PDMAEMA shows a typical Flory-Huggins behavior irrespective to polymers architecture at high *pH* (in buffer), where it is virtually uncharged. Charge density starts to account for the deviations from ideal Flory-Huggins behavior at intermediate *pH*. The presence of multivalent ions leads in buffered solutions of PDMAEMA to the appearance of a miscibility gap at low temperatures (UCST behavior). In salt-free solutions the electrostatic stabilization is especially pronounced for polymers with high arm numbers (having higher charge density). No macroscopic demixing was observed for polymers with more than 9 arms.

## Zusammenfassung

In dieser Arbeit wurden sternförmige Polyelektrolyte mittels Atom Transfer Radical Polymerization (ATRP) hergestellt. Hierzu verwendete man multifunktionelle Initiatoren (Core-first Ansatz). Sternförmige Polyacrylsäure (PAA) mit 5, 8 und 21 Armen wurde aus den entsprechenden Poly-*tert*-butylacrylaten (PtBA) mit jeweils Glucose-, Saccharose- und  $\beta$ -Cyclodextrinkern freigesetzt. Durch geeignete Modifizierung der Synthese von PAA und unter Verwendung der gleichen Initiatoren wurde sternförmiges Polydimethylaminoethylmethacrylat (PDMAEMA) synthetisiert. Es ist ein schwacher, kationischer Polyelektrolyt und kann durch Quaternisierung leicht in den entsprechenden starken Polyelektrolyt verwandelt werden (mit Methyliodid), nämlich Poly{[2-(methacryloyloxy)ethyl] trimethylammonium iodide} (PMETAI). Um höhere Armzahlen zu erreichen, führte man neue Silsesquioxaneinitiatoren mit durchschnittlich 58 Initiationsstellen ein.

Die Lösungseigenschaften der erhaltenen PAA-Sterne wurden in Wasser untersucht. So wurde das Titrationsverhalten mit NaOH bestimmt. Es zeigte sich, dass die apparente Säurestärke der PAA mit zunehmender Armzahl abnimmt. Ein gegenläufiger Effekt wurde bei Erhöhung der Armlänge beobachtet. Dies wird erklärt durch die höhere Segmentdichte bei Proben mit kurzen Armen und hoher Armzahl. Die hohe Segmentdichte führt zu einem erhöhten osmotischen Druck innerhalb des Sterns, der eine weitere Deprotonierung erschwert und somit eine verminderte Säurestärke bedingt. Der osmotische Koeffizient nimmt mit steigender Armzahl ab. Dies deutet auf eine stärkere Gegenionenbindung für verzweigte Strukturen hin. Die Verwendung der starken Polyelektrolyte erleichterte die Bestimmung des osmotischen Koeffizienten. Zunehmende Armzahl und abnehmende Armlänge erniedrigt den osmotischen Koeffizienten, der in den durchgeführten Messungen zwischen 0.03 und 0.13 lag. Damit sind die Gegenionen stark mit dem Polyion korreliert. Diese Ergebnisse wurden mit den Vorhersagen der Theorie verglichen, wobei Theorie und Experiment in der gleichen Größenordnung liegen. Jedoch wird die Konzentrationsabhängigkeit nicht vom Experiment wiedergegeben.

Das Lösungsverhalten der PMETAI Lösungen wurde mittels Dynamische Lichtstreuung (DLS) untersucht. DLS zeigt den erwarteten Kollaps der Sterne mit steigender Ionenstärke. Elektrostatisches und osmotisches Screening führt dabei zu einer Schrumpfung der ursprünglich stark gestreckten Arme. Jedoch können ionenspezifische Effekte einen stärkeren Kollaps bewirken, wie man anhand von NaI anstelle von NaCl zeigen konnte.

Der hohe osmotische Druck innerhalb des Sterns begünstigt die Einlagerung multivalenter Gegenionen. Dieser Ionenaustausch verringert die Gegenionenkonzentration innerhalb des Sterns. Gleichzeitig erhöht sich die Entropie aller Gegenionen, da mehrere einwertige Gegenionen für ein mehrwertiges Gegenion aus dem Stern entlassen werden. Der Ionenaustausch führt zu einer Reduktion des osmotischen Drucks innerhalb des Sterns, wobei die starke Streckung der Polymerarme vermindert wird. Dies konnte anhand DLS gezeigt werden. Die Schrumpfung ist ausgeprägter für höher geladene Gegenionen bei gleicher Gegenionenkonzentration. Daher kann das Schalten der Ladung der Gegenionen zu intelligenten Polyelektrolytsystemen führen. Dies wurde anhand der dreiwertigen, lichtsensitiven Hexacyanocobaltat(III) Gegenionen gezeigt, die sich bei UV-Bestrahlung zu zweiwertigen Gegenionen umwandeln. Gleichzeitig erhöht sich der hydrodynamische Radius infolge der Belichtung.

Schließlich wurden die thermosensitiven Eigenschaften von sternförmigem PDMAEMA in wässriger Lösung untersucht. PDMAEMA ist sowohl *pH*-sensitiv als auch temperatursensitiv. Es zeigt eine Mischungslücke mit Wasser bei erhöhten Temperaturen (LCST-Polymer). In unseren Versuchen bei hohem *pH* zeigt PDMAEMA ein typisches Flory-Huggins Verhalten unabhängig von der Architektur der Sterne. Bei hohem *pH* in Puffer ist PDMAEMA praktisch ungeladen. Bei gemäßigten *pH*-Werten (wiederum in Puffer) spielen Ladungsdichteeffekte für Abweichungen vom idealen Flory-Huggins Verhalten eine Rolle. In gepufferten Lösungen von PDMAEMA wird eine Mischungslücke in Gegenwart von mehrwertigen Gegenionen bei tieferen Temperaturen induziert (UCST-Verhalten). Jedoch führt die elektrostatische Stabilisierung zu einem Ausbleiben von makroskopischer Entmischung in salzfreien Lösungen für Sterne mit hoher Armzahl ( $> 9$  Arme).

## 9. List of Publications

During the course of this thesis the following publications have been prepared

- Plamper, F. A.; Becker, H.; Lanzendörfer, M.; Patel, M.; Wittemann, A.; Ballauff, M.; Müller, A. H. E. “Synthesis, Characterization and Behavior in Aqueous Solution of Star-Shaped Poly(acrylic acid)” *Macromolecular Chemistry and Physics* **2005**, *206*, (18), 1813
- Muthukrishnan, S.; Plamper, F.; Mori, H.; Müller, A. H. E. “Synthesis and Characterization of Glycomethacrylate Hybrid Stars from Silsesquioxane Nanoparticles” *Macromolecules* **2005**, *38*, (26), 10631
- Ballauff, M.; Patel, M.; Rosenfeldt, S.; Dingenouts, N.; Narayanan, T.; Müller, A.; Plamper, F. “Analysis of the Correlation of Counterions to Macroions by Anomalous Small-Angle Scattering” *Pol. Mat. Sci. Eng. Preprints* **2005**, *93*, 232
- Plamper, F. A.; Walther, A.; Müller, A. H. E.; Ballauff, M. “Nanoblossoms: Light-Induced Conformational Changes of Cationic Polyelectrolyte Stars in the Presence of Multivalent Counterions” *Nano Letters* **2007**, *7*, (1), 167
- Plamper, F. A.; Müller, A. H. E.; Ballauff, M. “Nanoblossoms: Photoinduced Stretching and Photoinduced Dissolution of Polycation Stars by Switching the Charge of Counterions” *Pol. Mat. Sci. Eng. Preprints* **2007**, *96*, 799
- Plamper, F.; Schmalz, A.; Penott-Chang, E.; Drechsler, M.; Jusufi, A.; Ballauff, M.; Müller, A. H. E. “Synthesis and Characterization of Star-Shaped Poly(dimethylaminoethyl methacrylate) and its Quaternized Ammonium Salts” *Macromolecules* **2007**, *40*, 5689
- Plamper, F. A.; Ruppel, M.; Schmalz, A.; Borisov, O.; Ballauff, M.; Müller, A. H. E. “Tuning the Thermoresponsive Properties of Weak Polyelectrolytes: Aqueous Solutions of Star-Shaped and Linear Poly(dimethylaminoethyl methacrylate)” *Macromolecules* **2007**, *40*, 8361
- Plamper, F. A.; Schmalz, A.; Ballauff, M.; Müller, A. H. E. “Tuning the Thermoresponsiveness of Weak Polyelectrolytes by pH and Light: Lower and Upper Critical-Solution Temperature of Poly(N,N-dimethylaminoethyl methacrylate)” *Journal of the American Chemical Society* **2007**, *129*, 14538

## 10. Appendix

### 10.1. Appendix to Chapter 2.1, Chapter 3 and Chapter 4 – Preparation of Star-Shaped Polyelectrolytes with Higher Arm Numbers

To increase the number of arms per star, a new initiator with a high number of initiation sites was required. Therefore novel silsesquioxane nanoparticles bearing a high number of hydroxyl functions were prepared.<sup>1</sup> Those particles were moderately polydisperse in terms of molecular weight ( $PDI \sim 1.2$ ). Those nanoparticles were used to prepare initiators with on average 58 initiation sites per molecule. Analysis was based on NMR, IR spectroscopy, elemental analysis and MALDI-ToF MS. The preparation pathway and the development of the mass spectra are depicted in Figure 10. 1 and Figure 10. 2.

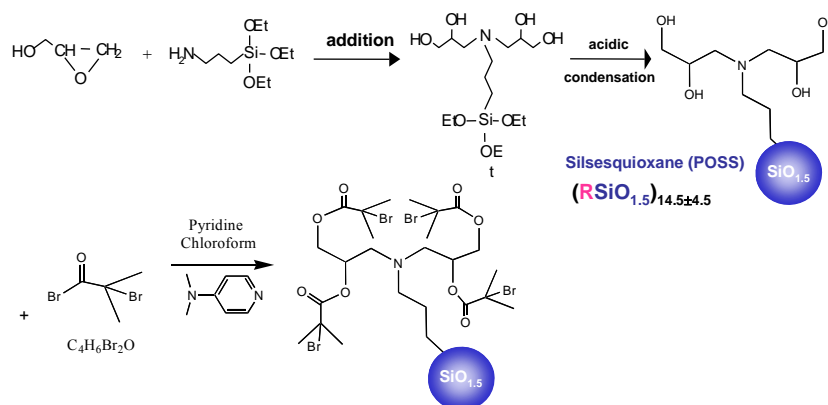


Figure 10. 1: Synthesis of hybrid nanoparticle initiators for ATRP

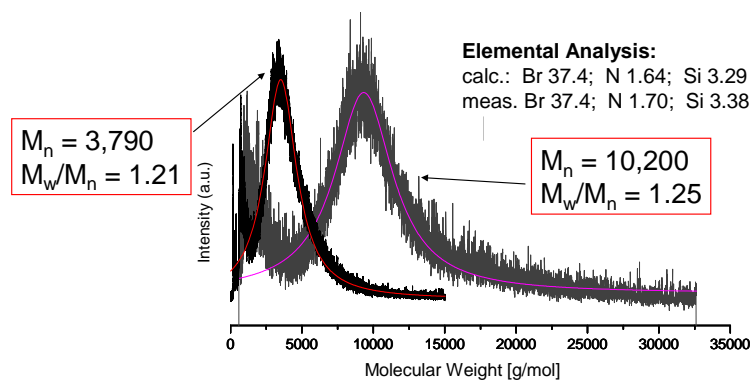
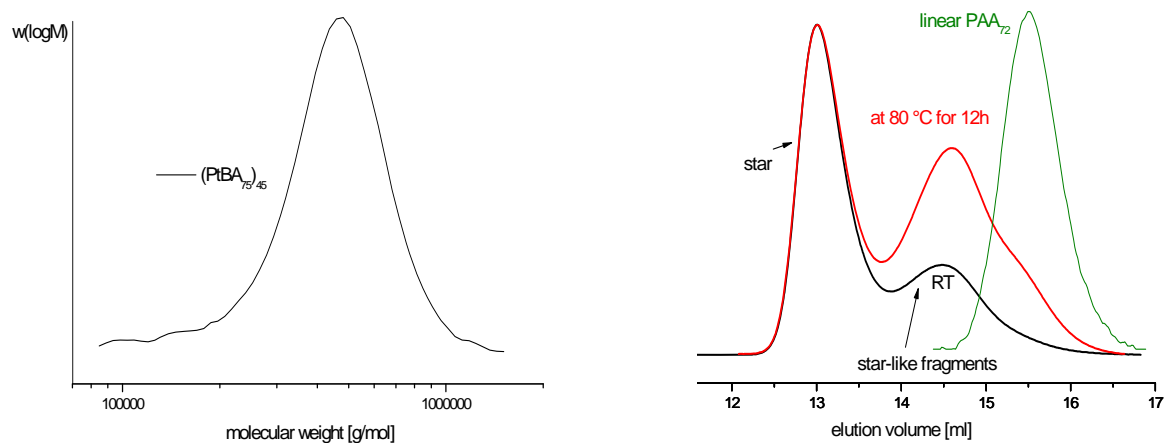


Figure 10. 2: MALDI-ToF mass spectra of both the hydroxyfunctionalized nanoparticles and the initiators derived therefrom

Besides their use in preparation of glyco-stars,<sup>1</sup> they can be used for the synthesis of PtBA with arm number up to 40 (unpublished). The initiation site efficiency was again determined by cleavage of the arms by NaOH after transformation to PAA. The observed lowered initiation site efficiency ( $f_i = 0.7$  instead of  $f_i \sim 1$  for the sugar-based stars) originates from the congestion caused by the high density of initiation sites around the nanoparticle. However the consecutive transformation of PtBA to PAA was always accompanied with destruction of the inorganic core, yielding fragments with up to four arms (Figure 10. 3). This is irrespective to the acid catalyst used for isobutylene elimination (trifluoroacetic acid, toluenesulfonic acid). The stars could be separated by fractionated precipitation (slow condensation of diethylether into a isopropanol solution; not shown here).



**Figure 10. 3:** Molecular weight distribution of  $(PtBA_{75})_{45}$  according to GPC with viscosity detection and comparison of the eluograms of both the detached PAA arms of  $(PtBA_{75})_{45}$  and the crude product after transformation of  $(PtBA_{75})_{45}$  to PAA in aqueous GPC.

$M_n$  and molecular weight distribution of PtBA stars were determined by GPC with viscosity detection. It could be shown that  $M_n(\text{GPC-visco})$  coincides again with the theoretical molecular weight obtained by conversion ( $M_{n,\text{theo}}$ ).

## 10.2. Appendix to Chapter 2.2, Chapter 3 and Chapter 6 – Titration Behavior of Weak Polyelectrolytes

From titration dataset ( $pH$  against degree of neutralization  $\alpha$ ), the apparent  $pK_{a,\text{app}}$  can be calculated ( $pK_{a,\text{app}}$  is the  $pH$  at  $\alpha = 0.5$ ; degree of neutralization  $\sim$  degree of ionization  $\alpha$ ). This macroscopic equilibrium constant includes the electrostatics due to backbone charging, whereas the microscopic equilibrium constant of each acid group remains principally unchanged. Therefore more important and easier to correlate to the structure is  $pK_{a,0}$ . When doing extrapolation ( $\alpha \rightarrow 0$ ) we extract the "non-electrostatic" equilibrium constant  $K_{a,0}$ ,

which is still a macroscopic, laterally averaged value, as we do not regard carboxylic group's position and environment within the star. This is done by<sup>2</sup>

$$K_a = \frac{([S]\alpha + [H^+]) \cdot [H^+]}{[S](1-\alpha) - [H^+]} \quad 10.1$$

[S] is the total acid group concentration before addition of base. The concentration of acid groups before equilibration but after neutralization with base is  $[S](1-\alpha)$ .  $\alpha$  is the degree of neutralization ( $[Na^+]/([COOH]+[COO^-])$ ), which is in good approximation in a wide range of the titration curve equal to the ionization degree  $\alpha'$ . The concentration of carboxylate groups before establishment of equilibrium is therefore  $[S]\alpha$ . The total concentrations change as equilibrium has to be established by equation 10.1. (residual carboxylic groups deprotonate to yield protons and additional carboxylate). Taking the logarithm we can plot  $pK_a$  against  $\alpha$  by use of

$$pK_a = pH + \log([S](1-\alpha) - 10^{-pH}) - \log([S]\alpha + 10^{-pH}) \quad 10.2.$$

Equation 10.2 gives Figure 10.4, which shows the laterally averaged  $pK_a$  in dependence of  $\alpha$ . It is laterally averaged, as the local  $pK_a$  is dependent on the position of the carboxy group within the star.

The  $pK_a$  at  $\alpha = 0$  (no added NaOH) is taken as  $pK_{a,0}$ . The results are plotted on the right hand side of Figure 10.4. We obtain reasonable results as all values lie in the range of the  $pK_a$  of acetic acid ( $pK_a = 4.75$ ) or glutaric acid ( $pK_a = 4.31$ ).

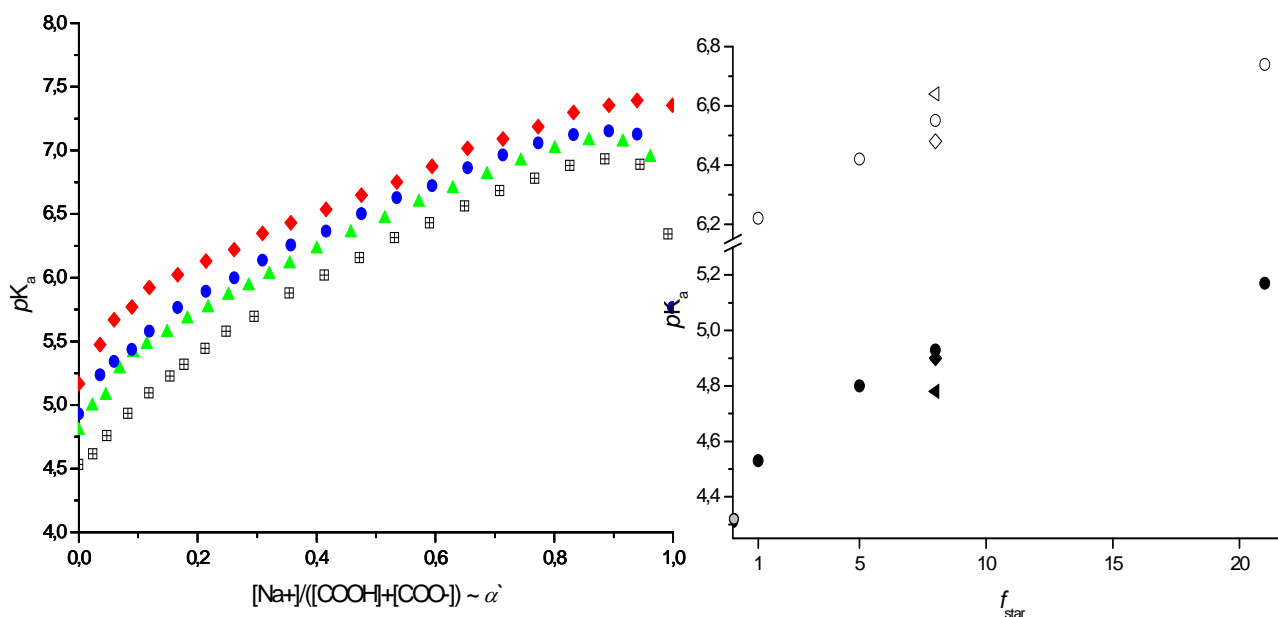
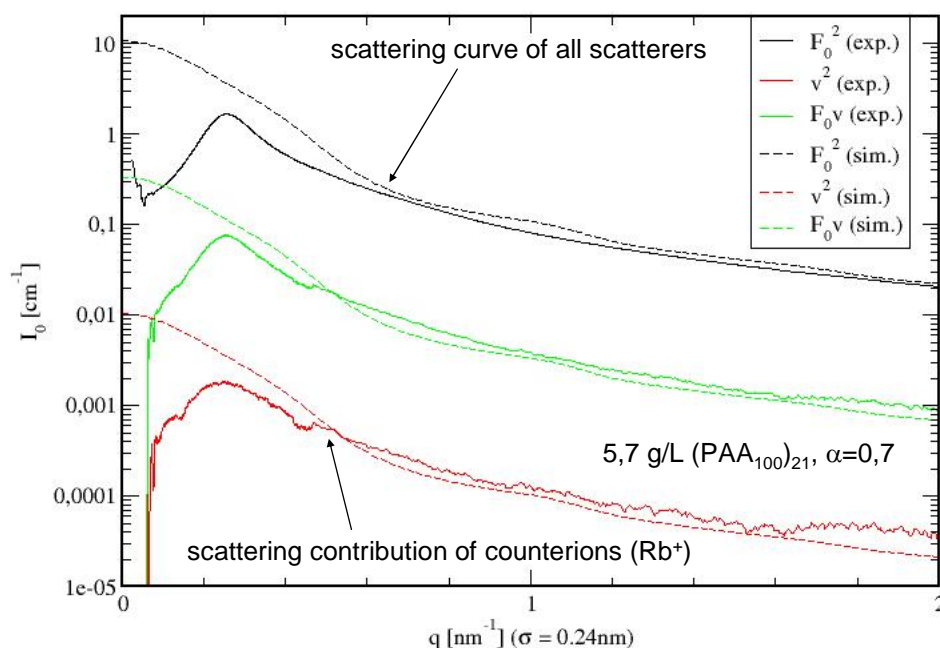


Figure 10.4: Extraction of  $pK_a$  of different  $(PAA_n)_f$  stars (left hand side; notation is the same as in Figure 2.3); Comparison of  $pK_{a,0}$  and  $pK_{a,app}$  in dependence of arm number  $f_{star}$  (right hand side;  $n \approx 75$  ( $\nabla$ );  $n \approx 100$  ( $\circ$ );  $n \approx 160$  ( $\diamond$ );  $\bullet$  depicts the  $pK_a$  of glutaric acid<sup>3</sup>)

One contribution for differences in the observed  $pK_{a,0}$  is also believed to be reflected in differences of local proton and carboxylic group concentrations within the star especially for low degrees of ionization. These different concentrations alter the equilibrium for the deprotonation of the carboxylic groups (Ostwald Dilution Law).<sup>4, 5</sup> At high local carboxy concentrations less carboxy groups dissociate compared to low local carboxy group concentrations.

### 10.3. Appendix to Chapter 2.3, Chapter 3 and Chapter 4 – Counterion Distribution of Star-Shaped Polyelectrolytes

Some stars prepared during this thesis were also investigated by Anomalous Small Angle Scattering (ASAXS), which can be used to extract the scattering contribution of solely the counterions. In continuation the counterion contribution is directly reflected in the scattering curve. As the evaluation was not performed by me, I want just to present a final result.<sup>6</sup>



**Figure 10. 5:** ASAXS analysis of (PAA<sub>100</sub>)<sub>21</sub>; **black:** contribution of all scatterers, **red:** scattering contribution of counterions, **green:** cross-term ( $\alpha \sim 0.7$ ; 5.7 g/L; counterion: Rb<sup>+</sup>; **dashed line:** theory; **solid line:** experiment)

We see that the experimental scattering contributions do adequately correspond to the theoretical one (theory by Arben Jusufi). In addition, the scattering contribution of the Rb<sup>+</sup>-counterions are almost parallel to the scattering curve of all scatterers. This can be explained by the good correlation between the macroion and the counterions. The macroion seems to be decorated with the counterions, which reflects the strong counterion condensation.

These results were confirmed by osmometry. Unfortunately for PAA with higher degrees of neutralization ( $\alpha > 0.3$ ), the osmotic pressure did not stay constant during the measurements. It increased after injection and dropped again after going through a maximum. This was always the case even after extensive ultrafiltration of the PAA salts. Ultrafiltration was used as a purification method, which keeps the degree of neutralization  $\alpha$  more constant during the purification process than dialysis. Dialysis establishes an equilibrium between both sides of the membrane. The same principle is true for osmometry. We saw after extensive dialysis that the degree of neutralization decreased during dialysis, when we started with a PAA solution with  $\alpha \sim 0.6$  (final  $\alpha \sim 0.25$ ).

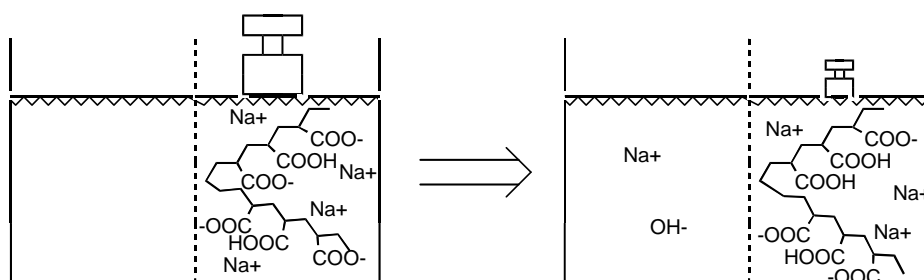


**Figure 10. 6: Principle of the reversal of the acid-base reaction due to high osmotic pressure**

During two weeks of dialysis the  $pH$  decreased in the solution simultaneously lowering the degree of neutralization. This is (at least partly) explained by the establishment of a Donnan equilibrium,<sup>7,8</sup> generated by low molecular salt delivered from the PAA salt by reversal of the acid base equilibrium (NaOH). This can happen since we used a weak polyelectrolyte. Therefore only samples with a low degree of neutralization were available when using dialysis. Those samples also showed constant osmotic pressure during measurement. It is not difficult to derive a theory for the osmotic pressure driven reversal of the acid base reaction. Donnan equilibrium is established, when following equation is fulfilled:<sup>9</sup>

$$[Na^+]_R \cdot [OH^-]_R = [Na^+]_L \cdot [OH^-]_L \quad 10.3$$

$[Na^+]_R$  assigns the sodium concentration on the right hand side of the membrane (where the polyelectrolyte is dissolved). Further conditions are given by the charge neutrality on the left hand side ( $[Na^+]_L = [OH^-]_L$ ) and the known total amount of acid ( $[COOH]_R + [COO^-]_R = c_R$ ). The charge neutrality on the right hand side can be approximated by (at moderate to acidic  $pH$  values  $[OH^-]_R$  is negligible):

$$[Na^+]_R = [COO^-]_R \quad 10.4 \quad \text{with} \quad [COO^-]_R = \frac{c_R}{1 + \frac{K_w}{K_a [OH^-]_R}}$$

since the acid base equilibrium reads as: 
$$\frac{K_a}{K_w} = \frac{[COO^-]_R}{[COOH]_R \cdot [OH^-]_R} \quad 10.5$$

Now  $[OH^-]_R$  can be expressed in terms of  $[Na^+]_R$  and introduced into the Donnan equilibrium:

$$[Na^+]_L^2 = \frac{K_w}{K_a} \cdot \frac{[Na^+]_R^2}{c_R - [Na^+]_R} \quad 10.6$$

The amount of total sodium concentration is known ( $c_R \alpha_0 = [Na^+]_R + [Na^+]_L V_L/V_R$ ).  $V_L$  is the volume on the left side of the membrane and  $\alpha_0$  is the initial degree of neutralization. Therefore we get an expression for  $[Na^+]_L$  in dependence of the volume ratio,  $\alpha_0$ ,  $c_R$  and the equilibrium constant of the acid  $K_a$ :

$$[Na^+]_L^3 + [Na^+]_L^2 \left( \frac{V_R}{V_L} \cdot c_R (1 - \alpha_0) - \frac{K_w}{K_a} \cdot \frac{V_L}{V_R} \right) + [Na^+]_L \cdot 2 \cdot c_R \cdot \alpha_0 \cdot \frac{K_w}{K_a} - c_R^2 \cdot \alpha_0^2 \cdot \frac{K_w}{K_a} \cdot \frac{V_R}{V_L} = 0 \quad 10.7$$

This calculation explains partly the sodium exchange in typical dialysis setups:

**Table 10. 1: Sodium concentrations on the polymerfree ( $[Na^+]_L$ ) and polyelectrolyte side ( $[Na^+]_R$ , initial 0.07 mol/l) in dependence of ratio of volumes on the polymerfree and sample side under conditions of an initial ionization degree  $\alpha_0 = 0.7$  and acidity constant  $K_a = 10^{-5}$  mol/l; the concentration of polymer's repeating unit is  $c_R = 0.1$  mol/l**

$V_L/V_R$	$[Na^+]_L$ [mol/l]	$[Na^+]_R$ [mol/l]	$[Na^+]_R$ loss [%]
100	$12.3 \cdot 10^{-6}$	0.069	1
1000	$9.6 \cdot 10^{-6}$	0.060	14
10000	$3.8 \cdot 10^{-6}$	0.032	54

**Table 10. 2: Sodium concentrations on the polymerfree ( $[Na^+]_L$ ) and polyelectrolyte side ( $[Na^+]_R$ , initial 0.07 mol/l) in dependence of deprotonation constant  $K_a$  of the polymer's acid moiety under conditions of an initial ionization degree  $\alpha_0 = 0.7$  and volume ratio  $V_L/V_R = 100$ ; the concentration of polymer's repeating unit is  $c_R = 0.1$  mol/l**

$K_a$ [mol/l]	$[Na^+]_L$ [mol/l]	$[Na^+]_R$ [mol/l]	$[Na^+]_R$ loss [%]
$10^{-5}$	$12.3 \cdot 10^{-6}$	0.069	1
$10^{-6}$	$36.2 \cdot 10^{-6}$	0.066	5
$10^{-7}$	$96.0 \cdot 10^{-6}$	0.060	14

In contrast ultrafiltrated samples did not establish equilibrium before. They can generate NaOH in obviously sufficient amount during osmometry, which can move across the

membrane. This lowers the net osmotic pressure. Therefore we always took the maximum in the osmotic pressure for the extraction of the osmotic coefficient:

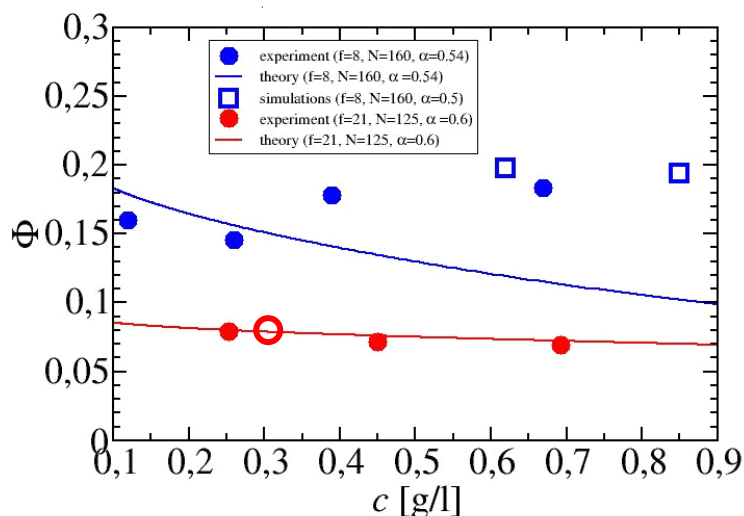


**Figure 10. 7: Osmotic coefficient of (PAA<sub>125</sub>)<sub>21</sub> (red;  $\alpha = 0.6$ ) and (PAA<sub>160</sub>)<sub>8</sub> (blue;  $\alpha = 0.54$ ) in dependence of polymeric salt concentration (counterion Na<sup>+</sup>; solid lines: theory; blue open symbols: simulation; full symbols: experiment; red open symbol helps to compare with data from Figure 10. 8)**

The comparison with theory for (PAA<sub>125</sub>)<sub>21</sub> is truly satisfactory, whereas the simulations better fit the experimental values for (PAA<sub>160</sub>)<sub>8</sub> (simulations and theory by Arben Jusufi). Fluctuations within the star lead to deviations to the theoretical meanfield approach.<sup>10</sup> Those fluctuations are more pronounced for smaller arm numbers. However, these results were not published due to the lack of constant signal during osmometry.

The close agreement at all concentrations between theory and experiment of (PAA<sub>125</sub>)<sub>21</sub> might stem from the expectation that the NaOH release is more pronounced at low concentrations (high  $V_L/V_R$  ratio; see Table 10. 1). This leads temporarily to a higher contribution of NaOH to the osmotic coefficient in diluted solutions. For stars with low  $\alpha$  or quenched polyelectrolyte stars, this effect is absent and the theoretical concentration dependence does not totally match the experimental (see Chapter 2.3)

We compared the osmotic coefficient of the PAA stars with the activity coefficient  $f$  of counterions obtained by potentiometry. We used a sodium sensitive electrode during the titration of the PAA stars with NaOH and compared the potential of the electrode  $U$  at a certain sodium concentration  $c$  with the potential obtained by calibration with sodium acetate at the same sodium concentration.

$$U = U_0 + 0,059V \cdot \log a \quad 10. 8$$

$$U_{analysis} - U_{calibration} = 0.059V \cdot \log \frac{a_{analysis}}{a_{calibration}} = 0.059V \cdot \log \frac{f_{analysis} \cdot c}{f_{calibration} \cdot c} \approx 0.059V \cdot \log f_{analysis} \quad 10.9$$

We obtain the activity coefficient of  $\text{Na}^+$  in presence of the electrical field of the stars in dependence of the degree of neutralization  $\alpha$ . At the beginning of the titration the error of the electrode was high due to cross sensitivity towards protons (no sodium present at the beginning). This was seen on the higher potential of the sample solution compared to the non acidic calibration solution at the beginning of the titration. Therefore we neglect the discussion of the activity coefficient for low  $\alpha$ . We can now compare with the osmotic coefficient for those  $\alpha$ , which were also investigated during osmotic pressure measurements. The concentration was either 0.25 g/L or 0.8 g/L.

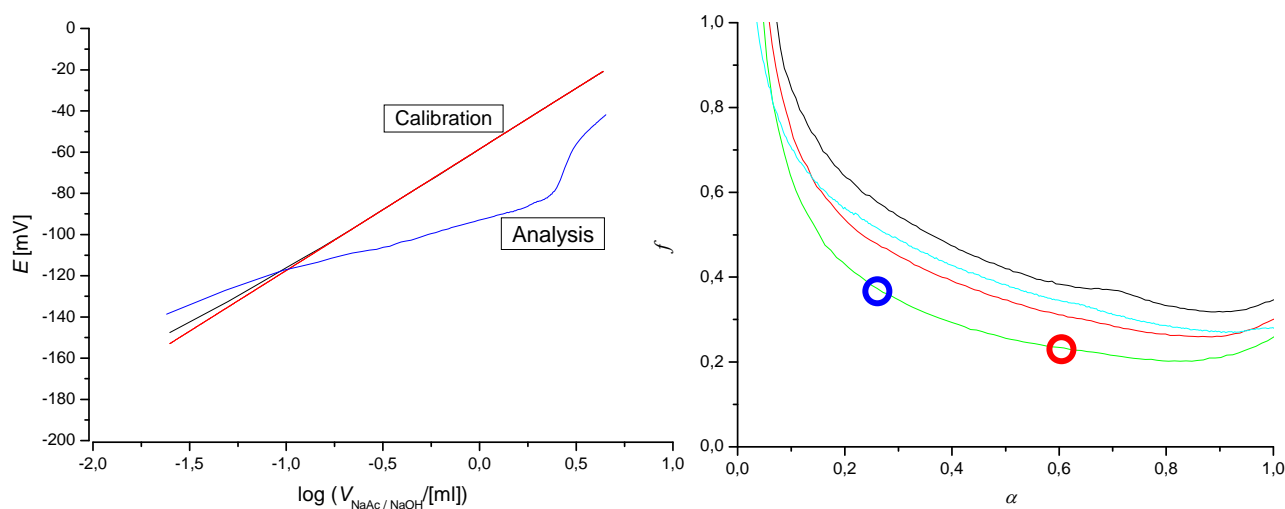


**Figure 10. 8:** Left hand side: principle of measuring the activity by potentiometric titration and help of a sodium selective electrode (polymer membrane electrode 6.0508.100, Metrohm; equivalence point determination by conductometry; calibration: addition of 0.1 n NaAc to 100 mL Millipore water; analysis: addition of 0.1 n NaOH to 100 mL aqueous solution of PAA; titration rate: 0.15 mL/min); right hand side: extracted activity coefficients of  $(\text{PAA}_{100})_{21}$  (green line),  $(\text{PAA}_{100})_5$  (black line),  $(\text{PAA}_{100})_8$  (red; all 0.25 g/L) and  $(\text{PAA}_{100})_8$  (0.8 g/L; blue line) in dependence of degree of neutralization  $\alpha$ ; the open symbols help to compare with data from Figure 10. 7 and Figure 2.5.

Qualitatively the results are identical to the results obtained by osmometry: The larger the arm number the lower the activity of  $\text{Na}^+$ . Also higher concentrated solutions yield higher activity coefficients as seen by osmometry (when having constant osmotic pressure; see Chapter 2.3). The larger the degree of ionization the lower the counterion's activity. However the absolute values of the activity coefficients are by a factor 2-3 higher than the osmotic coefficients, obtained by osmometry. The origin of the differences could be explained by the nontrivial theoretical relation between the osmotic coefficient and the activity coefficient.<sup>11-14</sup> This is counterintuitive, since the osmotic coefficient can be regarded as a kind of activity coefficient, measured just by osmometry. But also additional sources can contribute to the

deviations. For example stars could adsorb on the electrode, increasing the local sodium concentration. Therefore the absolute values of the activity coefficient measured by potentiometry should be taken with care.

## 10.4. Appendix to Chapter 2.4, and Chapter 5 – Interaction of Multivalent Counterions with Polyelectrolyte Stars

Presence of multivalent counterions can lead to a collapse and finally to a phase separation of the stars even at constant ionic strength. This was shown by turbidimetric titrations of (PMETA<sub>I170</sub>)<sub>18</sub> solutions with hexacyanocobaltate(III) ([Co(CN)<sub>6</sub>]<sup>3-</sup>).

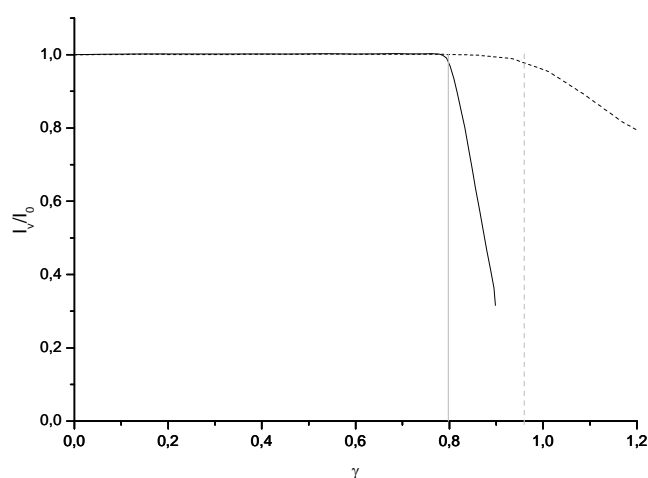


**Figure 10. 9:** Turbidimetric Titration of (PMETA<sub>I180</sub>)<sub>17</sub> (0.5 g/L: black full line; 0,05 g/L: black dashed line) in 0.1 n NaCl solution with 0.0167 n K<sub>3</sub>[Co(CN)<sub>6</sub>] as titer (relative transmitted intensity against charge compensation  $\gamma$  of PE star with trivalent counterions); lines in light grey design the onset of precipitation

We see from Figure 10. 9 that basically the ratio  $\gamma$  of charge concentrations once due to multivalent counterions and due to the macroion ( $\gamma = z \cdot c([\text{M}(\text{CN})_l]^{z-}) / c_{\text{monomerunit}}$ ) determines the interstellar interactions. Close to the point where all charges of the macrocations are compensated by the charges of the trivalent anions the system becomes macroscopically immiscible yielding a phase with high polymer content and an almost polymer free aqueous phase. It seems that there is slight dependence on the macroion's concentration, i.e. at higher star densities the precipitation is facilitated (Figure 10. 9). This might be caused by stronger interactions due to decreased mean interparticle distances.

Figure 10. 9 also implies that the charge compensation ratio defines the conformation of the star-shaped polyelectrolyte in solution. This was investigated by dynamic light scattering usually at 90°. At constant ionic strength the hydrodynamic radius was investigated in

dependence of multivalent counterion concentration. The results are summarized in Figure 10. We directly see that the hydrodynamic radius  $R_h$  decreases with increasing concentration of multivalent counterions though the ionic strength is kept constant for each single run. If only Debye-Hückel law<sup>15</sup> would hold true for this system, the hydrodynamic radius would not change with increasing cyanometalate concentration. But the intrastellar exchange of a considerable part of monovalent counterions with multivalent counterions leads to a pronounced drop in osmotic pressure within the star and to an increase in the counterion's entropy. This is the actual driving force for this transition, seen in the arm's collapse due to lowered osmotic pressure inside the star.

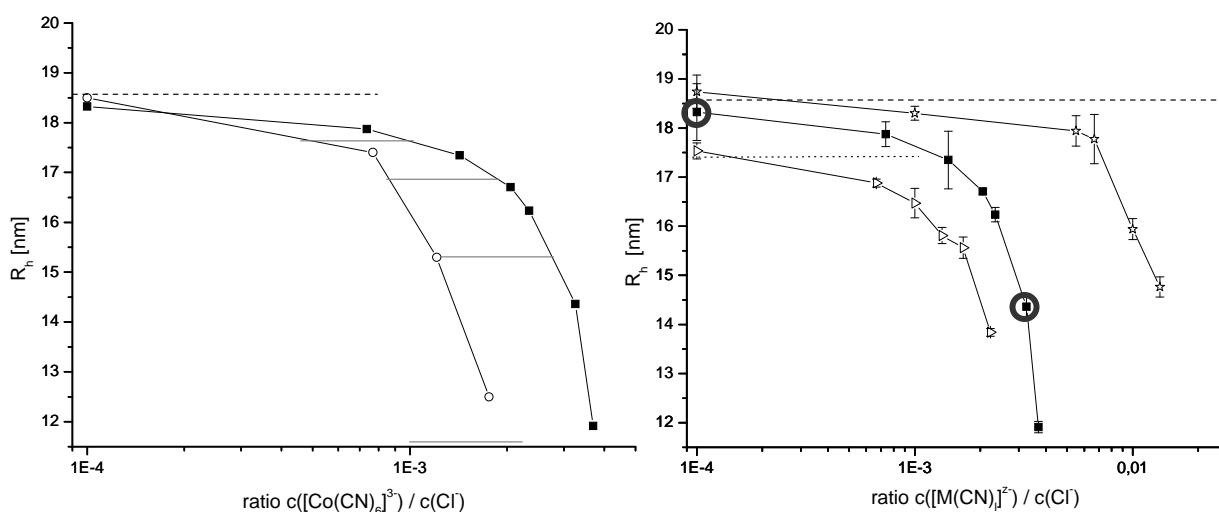


**Figure 10. 10:** Collapse of hydrodynamic radius  $R_h$  of cationic polyelectrolyte star (PMETA<sub>180</sub>)<sub>17</sub> in respect to concentration ratio of multivalent to monovalent counterions; left hand side: polyelectrolyte concentration effect (0.1 n NaCl solution titrated with 0.0167 n  $\text{K}_3[\text{Co}(\text{CN})_6]$ ; ■: 0.5 g/L (PMETA<sub>180</sub>)<sub>17</sub>; ○: 0.2 g/L; the grey bars depict a factor in the concentration ratio of 2.25); right hand side: effect on counterion valency (☆: 0.1 n NaCl solution titrated with 0.033 n  $\text{K}_2[\text{Ni}(\text{CN})_4]$ ; 0.5 g/L of (PMETA<sub>180</sub>)<sub>17</sub>) and ionic strength (▷: 0.2 n NaCl solution titrated with 0.033 n  $\text{K}_3[\text{Co}(\text{CN})_6]$ ; 1.0 g/L of (PMETA<sub>180</sub>)<sub>17</sub>) and for comparison (■: 0.1 n NaCl solution titrated with 0.0167 n  $\text{K}_3[\text{Co}(\text{CN})_6]$ ; 0.5 g/L (PMETA<sub>180</sub>)<sub>17</sub>); dashed lines depict  $R_h$ , measured without multivalent counterions); circles depict the samples which were used for cryo-TEM

On the left hand side of Figure 10. 10 we see the comparison of the collapse curves with different polyelectrolyte concentrations and constant ionic strength. This implies that the majority of the trivalent counterions are incorporated by the cationic star-shaped macroion, as the collapse curves are shifted by almost the factor which is given by the ratio of the two differing polyelectrolyte concentrations (see grey bar in Figure 10. 10). This is consistent with the results of the turbidimetric titration (see Figure 10. 9).

The influence of ionic strength is given on the right hand side of Figure 10. 10. To compare collapse curves with different ionic strengths in the same type of presentation as given in Figure 10. 10, one needs to increase also the polyelectrolyte concentration. The reason: the x-

axis is coupled to the ionic strength, determined by the NaCl concentration. As seen in Figure 10. 10 the collapse seems to take place at slightly lower  $[\text{Co}(\text{CN})_6]^{3-}$ -concentration when the ionic strength is increased. This appears to be contra-intuitive, but since the number density of stars has increased, the bulk volume (volume not occupied by stars) has decreased. This is believed to accelerate the incorporation as the volume for free trivalent counterions is diminished.

The influence of counterions charge at constant ionic strength is also depicted on the right hand side of Figure 10. 10. Usage of tetracyanonickelate(II) ( $[\text{Ni}(\text{CN})_4]^{2-}$ ) as divalent counterion needs a higher counterion concentration for the collapse compared to trivalent counterions ( $[\text{Co}(\text{CN})_6]^{3-}$ ). Since divalent counterions bear lower charge the charge compensation takes place at higher counterion concentration. But when plotting the results of Figure 10. 10 against charge compensation ratio  $\gamma$  it becomes obvious that the collapse still goes on even when the macroions charge has already been compensated by divalent counterions (Figure 10. 11). This is in accordance with molecular dynamics simulations showing that the binding of divalent counterions to a macroion is of intermediate nature.<sup>16</sup> Also this system precipitates at higher divalent counterion concentrations.

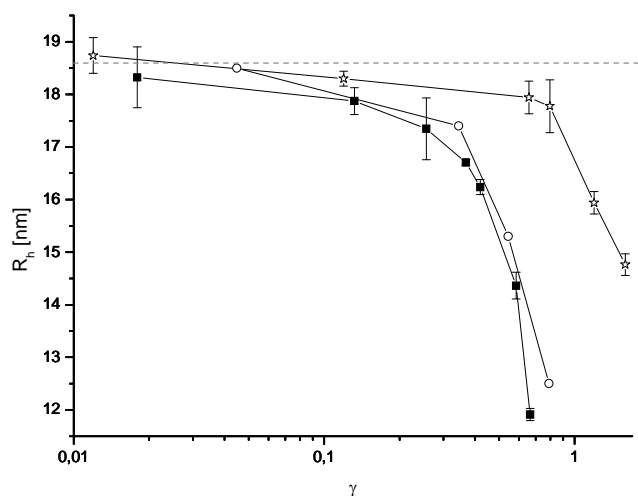


**Figure 10. 11: results of Figure 10. 10 depicted against charge compensation ratio  $\gamma$  (for assignment see Figure 10. 10)**

Cryo-TEM did also reveal differences in the star structures with and without trivalent counterions. Without trivalent counterions, the stars appeared fuzzier, whereas the trivalent counterions lead to a more compact structure. Same was seen by AFM (see chapter 5).

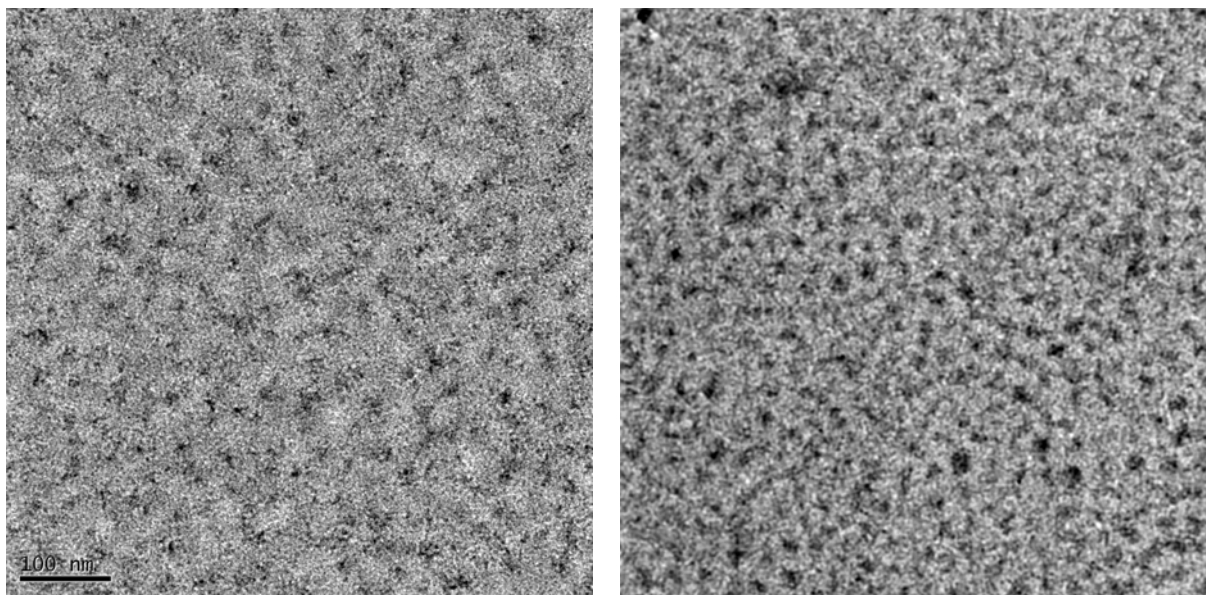


**Figure 10. 12:** Cryo-TEM images of 0.5 g/L (PMETA<sub>180</sub>)<sub>17</sub> in 0.1 n NaCl (left hand side:  $c([\text{Co}(\text{CN})_6]^{3-}) = 1.0 \cdot 10^{-5} \text{ n}$ ; right hand side:  $3.3 \cdot 10^{-4} \text{ n}$ ; scale bar 100 nm)

For the low concentration of trivalent salt the polyelectrolyte star's structure seem to be quite diffuse. One can discern some black dots, which are believed to be the core of the stars (diameter in the range of 3nm; silsesquioxane core) and some shadows around the cores, which corresponds to the decreasing segment density around the star's cores. It is hard to discern the star's diameter. At high concentrations of cobaltate the structures appear much more compact (visible diameter in the range of 20 nm), which is in accordance with the incorporation of the trivalent counterion.

By use of  $[\text{Co}(\text{CN})_6]^{3-}$ , we can reverse this contraction by simple UV-irradiation (chapter 5).<sup>17, 18</sup> Light exchanges one cyano ligand with water and the charge of the counterion is reduced (photoaquation). One counterion is decomposed into two counterions. This leads again to an increase in osmotic pressure inside the star and the star's arms stretch. Due to the resemblance to real flowers we called those stars "nanoblossoms". Figure 2.8. (Chapter 2. 4) shows the hydrodynamic radius after uninterrupted illumination. The intensity weighted size distributions according to CONTIN analysis were then monomodal for most measurements, even if the light scattering experiment was repeated hours later. If one interrupts the illumination (e.g. for DLS measurement) and continues the illumination afterwards a small fraction of aggregates (around 100 nm) appears in the intensity weighted size distributions after 11 min of UV-illumination (and 3 interruptions). Those aggregates were not visible for uninterrupted illumination with same irradiation time. With interruptions the  $R_h$  of the single stars is after 45 min close to the expected 18 nm. But since the aggregates might slightly

influence the  $R_h$  of the single stars during CONTIN analysis and since we do not understand the mechanism of the development of species with long diffusion times, we do not further discuss the interrupted illumination.

Chapter 5 also describes a way of dissolving the polymer-counterion complex by UV-irradiation (see chapter 5 for details). The solution turns slightly turbid after one day by keeping the already photodissolved solution in darkness. A precipitate was observed after one week. The supernatant solutions stayed yellowish but the precipitate can be redissolved by UV illumination. This behavior is not yet understood. Maybe the photoaquation process is slightly reversible slowly producing trivalent counterions after irradiation. However the photoaquation of  $[\text{Co}(\text{CN})_6]^{3-}$  is reported to be irreversible.<sup>17, 18</sup> Also partial hydrolysis of the polymer's quaternary amine moiety by developed hydroxide could lead to an ampholytic polymer with changed solubility.

## **10.5. Appendix to Chapter 2.5, Chapter 6 and Chapter 7 – Thermoresponsive Properties of PDMAEMA**

Having investigated the cloud points in buffer solutions (see chapter 6), we now turn to PDMAEMA in pure Millipore water. Since PDMAEMA is a polybase, the concentration of PDMAEMA strongly influences the  $pH$  of the resulting solution.  $pH$  has a decisive effect on the phase boundary, as seen in Figure 2.9. Thus concentration variation should lead to a more pronounced response on the location of the cloud points than for buffer solutions. Indeed a concentration variation by an order of magnitude can easily lead to a shift of the cloud points by more than 30 K (Table 10. 3). In addition we could only see demixing at a concentration of 0.1 g/L in case of linear PDMAEMA. The star-shaped molecules did not show any phase boundary at that dilute concentration within the experimental window (20°C to 80°C). Therefore we performed most measurements at a concentration of 1.0 g/L.

Having used a  $pH$  sensor during the turbidity measurements of polymer 1A (PDMAEMA<sub>108</sub>), we can determine the  $pH$  at the cloud point and compare it with results in buffer. If the  $pH$  is the only decisive parameter determining the cloud point, the results in Millipore water should coincide with the results in buffer.

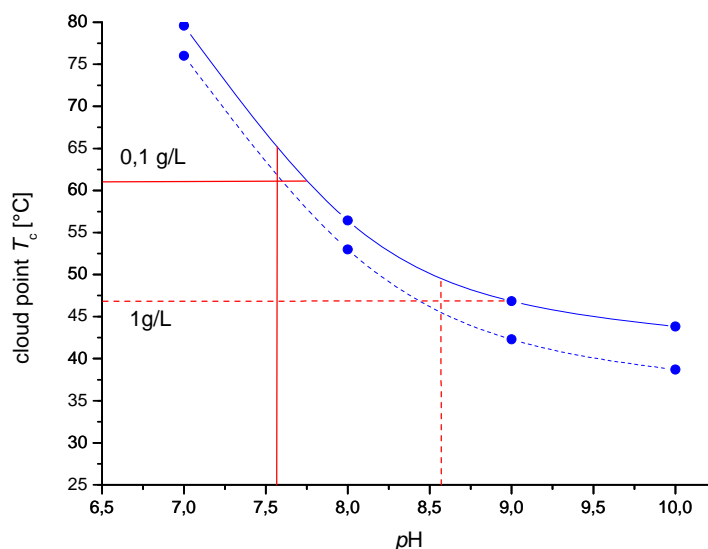


**Figure 10. 13: Comparison of  $pH$  and temperatures at demixing in buffer solutions (blue) and Millipore water (red) of  $(PDMAEMA_{108})_1$  (1A; dashed lines: 1.0 g/L; full lines: 0.1 g/L)**

However, as seen in Figure 10. 13, there are some discrepancies: at low concentration (0.1 g/L) the cloud point in Millipore water is about 4 K lower than the cloud point expected in buffer with the same  $pH$ . At higher concentration (1.0 g/L) the observed cloud point is 1 K higher than expected in buffer solution. Here we see that besides  $pH$  other external parameters might determine the cloud point. For example one should be aware, that the buffer solutions contain additional salt (ionic strength in the order of 0.05 n), though it can not explain the low cloud point in dilute Millipore solution. Closely regarded, the situation in Millipore water is somewhat different compared to buffer solution. As said, in pure water PDMAEMA generates its own hydroxide ions, which determines the  $pH$ . At the same time the polymer gets charged: the higher the  $pH$  at the same concentration, the more the polymer is charged and the less likely is aggregation for the same polymer. In buffer the opposite is true: the higher the  $pH$  the lower is the charging. That means that at the same  $pH$  the charge density is not necessarily the same in buffer and Millipore water and differences arise in the observed cloud point.

We turn back to the cloud point measurements at higher concentrations: at 1.0 g/L we only observed demixing for stars with up to 6 arms (8E  $(PDMAEMA_{170})_{5,6}$ ). For solutions of the polymers 21A, 21E, 58A and 58E the two-phase region was not reached within the experimental temperature range. This is in contrast to measurements performed by Patrickios et al.<sup>19</sup> They report cloud points at moderate temperatures (max. 34 °C) for star-shaped PDMAEMA solutions with an arm number up to 50. This might be due to the star's hydrophobic cores. Surprisingly our other polymers showed cloud points in a rather narrow temperature window (Figure 10. 14). Especially  $(PDMAEMA_{100})_{3,1}$ ,  $(PDMAEMA_{160})_{3,7}$  and  $(PDMAEMA_{110})_{5,4}$  solutions demixed at almost the same temperature (41 °C). Linear

polymers showed a somewhat higher cloud point, whereas the polymer solution of 8E (PDMAEMA<sub>170</sub>)<sub>5,6</sub> stayed more transparent at higher temperatures than for the other polymers with low arm number. Here we might observe the transition to the case where macroscopic demixing does not take place any more (polymers 21A, 21E, 58A and 58E; Figure 10. 15), since the whole transition appears rather broad.

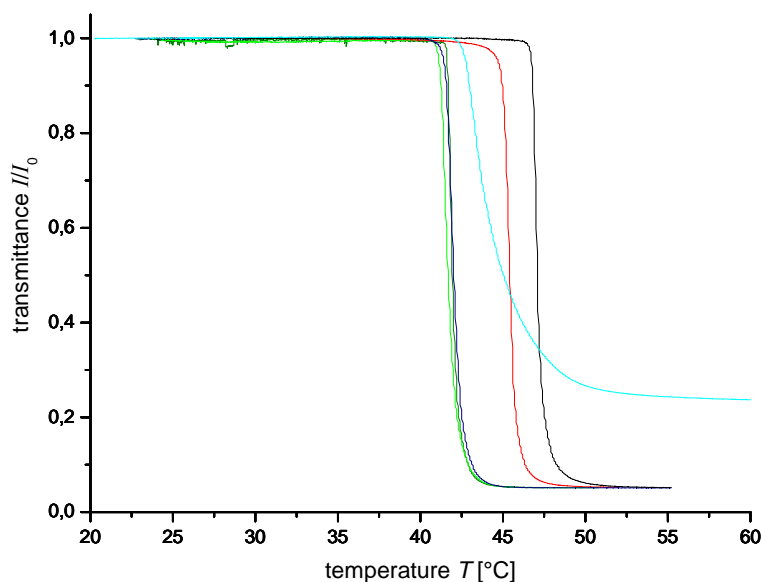


**Figure 10. 14:** Cloud points of PDMAEMA in Millipore water at 1.0 g/L (black: 1A (PDMAEMA<sub>108</sub>)<sub>1</sub>; red: 1B (PDMAEMA<sub>133</sub>)<sub>1</sub>; dark green: 5A (PDMAEMA<sub>100</sub>)<sub>3,1</sub>; bright green: 5B (PDMAEMA<sub>160</sub>)<sub>3,7</sub>; dark blue: 8A (PDMAEMA<sub>110</sub>)<sub>5,4</sub>; bright blue: 8E (PDMAEMA<sub>170</sub>)<sub>5,6</sub>)

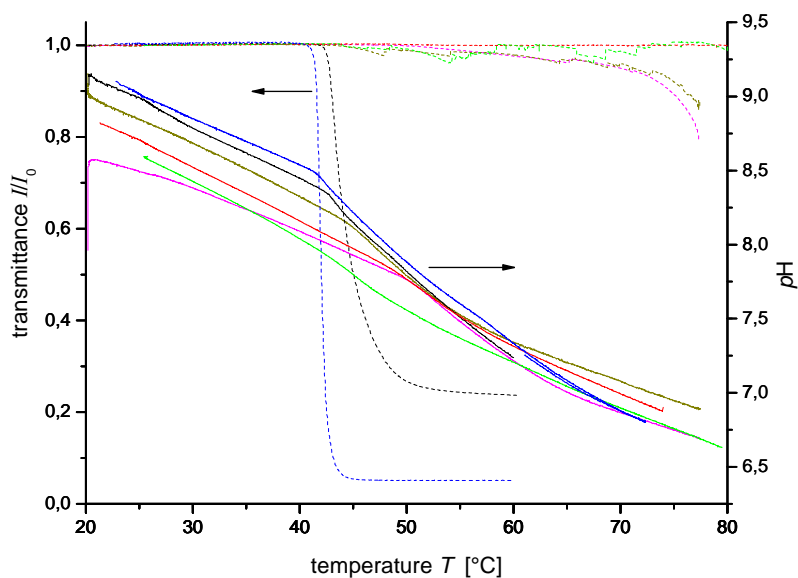


**Figure 10. 15:**  $pH$  dependence with temperature for solutions of 8A (PDMAEMA<sub>110</sub>)<sub>5,4</sub> (blue), 8E (PDMAEMA<sub>170</sub>)<sub>5,6</sub> (black), 21A (PDMAEMA<sub>170</sub>)<sub>9,5</sub> (magenta), 21E (PDMAEMA<sub>240</sub>)<sub>11</sub> (dark yellow), 58A (PDMAEMA<sub>170</sub>)<sub>18</sub> (red) and 58E (PDMAEMA<sub>240</sub>)<sub>24</sub> (green) (full lines; all 1.0 g/L; dashed lines: turbidity results)

By use of a simple  $pH$  sensor we had a first indication that for stars with higher arm number a microscopic collapse takes place in the investigated temperature range despite of the absence of macroscopic demixing (Figure 10. 15). There is a kink in the  $pH$  curve near the

cloud point. This kink was also observed for 58E (PDMAEMA<sub>240</sub>)<sub>24</sub> (43 °C) and is reflected also in a collapse of the stars as seen by dynamic light scattering (DLS; Figure 10. 16). We saw always two processes at different decay rates  $\Gamma = 1/\tau_0$ , as expected for polyelectrolytes without added salt (overlapping bimodal distribution functions after CONTIN analysis; at 25 °C corresponding to hydrodynamic radii of 10 and 50 nm respectively).<sup>20</sup> For both a linear dependence of the decay rates at different angles with the squared length of scattering vector  $q^2$  was obtained, which indicates a diffusive process in both cases. But since the fast mode disappears upon addition of salt (disappearance of slow mode was expected)<sup>21</sup> and therefore we are not able to assign the origin of the two modes, we just plot the inverse of the decay rate of the two processes against temperature (corrected by viscosity; the term  $(\Gamma \cdot \eta)^{-1}$  is directly proportional to the hydrodynamic radius). The decay rates were obtained by fitting the normalized intensity autocorrelation function ( $g^{(2)}(\tau)$ ; 30° to 120°) by two exponential decays ( $g^{(2)}(\tau) = k_1 e^{-2\Gamma_1 \tau} + k_2 e^{-2\Gamma_2 \tau}$ ;  $\tau$  is the lag time,  $\Gamma$  is the decay rate of the corresponding field autocorrelation function  $g^{(1)}(\tau)$ ,  $k$  corresponds to an efficiency factor).

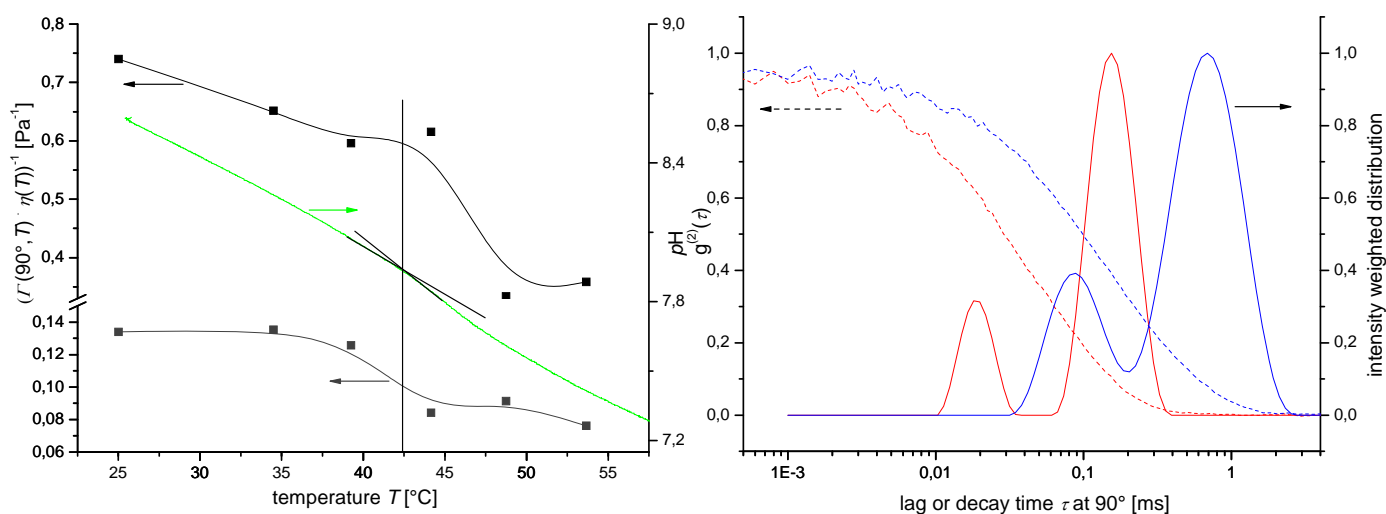


**Figure 10. 16:** Left hand side: comparison of pH dependence and decay rate dependences of two processes obtained by DLS with temperature (corrected with solvent viscosity;  $(\Gamma(90^\circ, T) \cdot \eta(T))^{-1}$  of an aqueous solution of (PDMAEMA<sub>240</sub>)<sub>24</sub> (1.0 g/L); the grey and black lines are a guide to the eye; right hand side: autocorrelation functions  $g^{(2)}(\tau)$  (dashed) and CONTIN plot (solid lines) of the same system at 25 °C (blue line) and 55°C (red) at 90°

We see that the two processes extracted by DLS accelerate in the vicinity of the kink in the pH curve. This is understood in terms of a decrease in the hydrodynamic radius. This collapse of the stars coincides with the change in the accessibility of the amino groups which causes the change in the slope of the pH curve. The slope at high temperatures is not as steep as for real precipitation. This is consistent with a collapse of the arms, but due to glassiness of the obtained colloids,<sup>22</sup> other steric reasons and/or electrostatic reasons aggregation of stars is

prevented. The two phase region was always reached in basic buffer (at even lower concentrations), though pure non electrostatical reasons should have prevented phase separation also there. This implies that the electrostatics play the major role for the stabilization of our polymers. This can also be seen by addition of salt to the aqueous solution. Without salt demixing was not observed for (PDMAEMA<sub>170</sub>)<sub>18</sub> (1.0 g/L solution), but salt screens the electrostatic interactions and the two phase region is accessible (even for 0.1 g/L solution). Already small differences in salt concentration can then have considerable effect on the cloud points as summarized in Table 10. 3.

**Table 10. 3: Cloud points  $T_c$  of PDMAEMA under different conditions (1.0 g/L; italics: 0.1 g/L; \*: broad transition; in brackets: kink in  $pH$  curve, no macroscopic demixing visible)**

cloud points	Millipore	0.5 n NaCl	1.0 n NaCl
<b>1A (PDMAEMA<sub>108</sub>)<sub>1</sub></b>	46.8; <i>61.6</i>	-	-
<b>1B (PDMAEMA<sub>133</sub>)<sub>1</sub></b>	45.0; <i>72.1</i> *	-	-
<b>5A (PDMAEMA<sub>100</sub>)<sub>3.1</sub></b>	41.6	-	-
<b>5E (PDMAEMA<sub>160</sub>)<sub>3.7</sub></b>	41.2	-	-
<b>8A (PDMAEMA<sub>110</sub>)<sub>5.4</sub></b>	41.5	-	-
<b>8E (PDMAEMA<sub>170</sub>)<sub>5.6</sub></b>	42.6	-	-
<b>21A (PDMAEMA<sub>170</sub>)<sub>9.5</sub></b>	(50.3)	-	-
<b>21E (PDMAEMA<sub>240</sub>)<sub>11</sub></b>	(44.7)	-	-
<b>58A (PDMAEMA<sub>170</sub>)<sub>18</sub></b>	(48.9)	<i>55.5</i>	<i>43.7</i>
<b>58E (PDMAEMA<sub>240</sub>)<sub>24</sub></b>	(42.5)	-	-

In contrast, adding salt to a buffer solution of PDMAEMA has an unexpected effect. The cloud points increase with increasing salt concentration, though the charge effect is more and more screened. The screening seems to give less contribution in this case than the change in the protonation equilibria due to salt addition. First the buffer becomes more acidic. It is also known that weak polyelectrolytes get more easily charged in presence of salt (see also Figure 10. 18).<sup>23</sup>

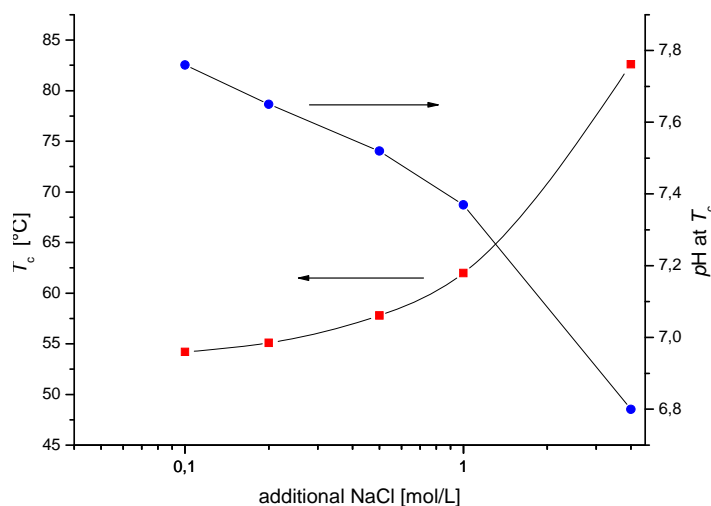


**Figure 10. 17: effect of ionic strength on the cloud points of 0.1 g/L (PDMAEMA<sub>170</sub>)<sub>18</sub> in buffer (originally pH 8) and the effect of salt on the pH**

However, at high ionic strength, the effects of charging implied by the lowered pH should be eliminated by electrostatic screening. One explanation might be the structural change of PDMAEMA upon protonation. The polar N-H bond can give rise to additional H-bonding irrespective to the introduced charge. This promotes solubility even at elevated temperatures.

Finally we investigated the influence of multivalent counterions on the location of the cloud points (here again in buffer free solution). We used thermally stable trivalent hexacyanocobaltate(III) ( $[\text{Co}(\text{CN})_6]^{3-}$ ), which can be transformed by UV-light to a divalent counterion.<sup>18</sup> The multivalent counterions act as cobase in presence of the weak polycation. The effect is more pronounced for branched PDMAEMA. The counterions do not act as a base alone, but they stabilize the protonated ammonium moieties, which leads to an increase in the pH by addition of  $[\text{Co}(\text{CN})_6]^{3-}$ , until the star is saturated (Figure 10. 18). This means that the star becomes a stronger base in presence of multivalent counterions. This was predicted theoretically for weak anionic polyelectrolytes and shown indirectly for ion exchange fibers.<sup>24, 25</sup> It is not just an effect of ionic strength but it arises mainly due to counterion's high valency as seen in Figure 10. 18.

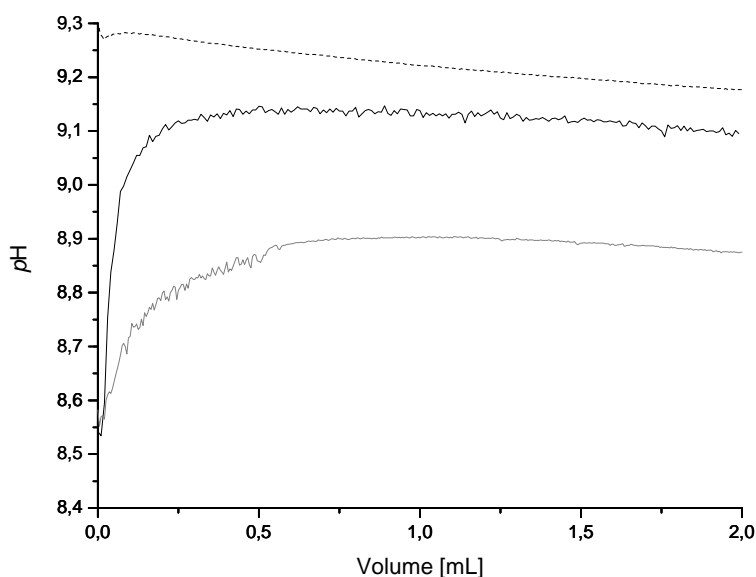


Figure 10. 18:  $pH$  change measured by  $pH$  electrode during titration of 25 mL of 1.0 g/L 58E (PDMAEMA<sub>240</sub>)<sub>24</sub> or 1B (PDMAEMA<sub>133</sub>)<sub>1</sub> (dashed line) with 0.033 n  $K_3[Co(CN)_6]$  (0.06 mL/min); grey: titration of 1.0 g/L (PDMAEMA<sub>240</sub>)<sub>24</sub> with 0.2 n NaCl instead of  $K_3[Co(CN)_6]$

Though the star has now a higher nominal charge compared to the star without trivalent counterions, demixing takes place at lower temperatures for higher salt concentrations. This can be explained by the strong interaction of the trivalent counterions with the polyelectrolyte, which increases the hydrophobicity of the polymer. Ionic strength gives only a minor contribution as seen for a PDMAEMA solution with the same ionic strength adjusted by NaCl than the solution with the highest  $[Co(CN)_6]^{3-}$  concentration (compare black and grey curve in Figure 10. 19).

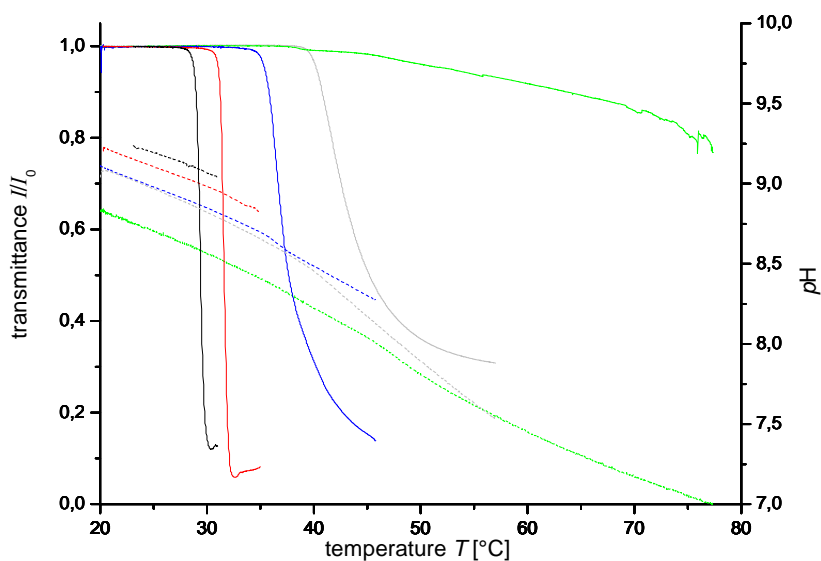


Figure 10. 19: Influence of trivalent counterions on the cloud point of 58E (PDMAEMA<sub>240</sub>)<sub>24</sub> (1.0 g/L; green: 0.026 mmol/L  $[Co(CN)_6]^{3-}$  - 0.02 ml of 0.033 n  $[Co(CN)_6]^{3-}$  added to 25 ml of aqueous PDMAEMA solution; blue: 0.132 mmol/L  $[Co(CN)_6]^{3-}$ ; red: 0.66 mmol/L  $[Co(CN)_6]^{3-}$ ; black: 2.6 mmol/L  $[Co(CN)_6]^{3-}$ ; grey: 16 mmol/L NaCl; dashed lines:  $pH$ ; full lines: turbidity results)

Besides the increase of the onset of turbidity, decreasing cobaltate concentration leads to a less pronounced demixing since the transmittance change is smaller for lower counterion concentration. This indicates the weaker mutual attraction of the polymer stars at higher temperatures for lower concentrations of trivalent salt.

We compared also the phase behavior of linear with star-shaped PDMAEMA in presence of trivalent counterions. The branched structure helps to incorporate the trivalent counterions (Table 10. 4). As expected there is no major change by addition of trivalent counterions to the cloudpoint of a solution of linear PDMAEMA. Only the *pH*-shift after irradiation leads to a decrease in the cloud point due to developed hydroxide (by protonation of  $\text{CN}^-$ ). The cloud points in presence of trivalent salt in bufferfree solution are listed in Table 10. 4.

**Table 10. 4: Cloud points (first decrease in transmission) of PDMAEMA (1.0 g/L) in dependence of  $[\text{Co}(\text{CN})_6]^{3-}$  concentration and comparison with NaCl solution**

cloud points	0.026	0.132	0.66	2.6	16
	mmol/L	mmol/L	mmol/L	mmol/L	mmol/L
	NaCl				
<b>1B (PDMAEMA<sub>133</sub>)<sub>1</sub></b>	-	-	-	45.8	-
<b>58E (PDMAEMA<sub>240</sub>)<sub>24</sub></b>	37.6	35.5	31.2	29.0	39.9

## 10.6. References

1. Muthukrishnan, S.; Plamper, F.; Mori, H.; Müller, A. H. E. *Macromolecules* **2005**, *38*, 10631.
2. Nylén, P.; Wigren, N.; Joppien, G., *Einführung in die Stöchiometrie*. Steinkopff Verlag: Darmstadt, **1991**; p 109.
3. Lide, D. R., *Handbook of Chemistry and Physics*. 71st ed.; CRC Press: **1990**.
4. Ostwald, W. *Z. physik. Chem.* **1888**, *2*, 36.
5. Ostwald, W. *Z. physik. Chem.* **1888**, *2*, 270.
6. Ballauff, M.; Patel, M.; Rosenfeldt, S.; Dingenouts, N.; Narayanan, T.; Plamper, F.; Müller, A. H. E. *Polym. Mater. Sci. Eng.* **2005**, *93*, 232.
7. Donnan, F. G. *Zeitschrift fuer Elektrochemie* **1911**, *17*, 572.
8. Donnan, F. G. *Chem. Rev.* **1924**, *1*, 73.
9. Donnan, F. G. *Journal of Membrane Science* **1995**, *100*, 45.

10. Jusufi, A. *Journal of Chemical Physics* **2006**, *124*, 044908/1.
11. Schreiner, E. *Z. physik. Chem.* **1924**, *111*, 415.
12. Bjerrum, N. *Zeitschrift fuer Elektrochemie und Angewandte Physikalische Chemie* **1918**, *24*, 321.
13. Bjerrum, N. *Z. physik. Chem.* **1923**, *104*, 406.
14. Cantelo, R. C. *Journal of Physical Chemistry* **1929**, *33*, 627.
15. Debye, P.; Huckel, E. *Physik. Z.* **1923**, *24*, 185.
16. Spohr, E.; Hribar, B.; Vlachy, V. *Journal of Physical Chemistry B* **2002**, *106*, 2343.
17. MacDiarmid, A. G.; Hall, N. F. *Journal of the American Chemical Society* **1953**, *75*, 5204.
18. Wrighton, M.; Hammond, G. S.; Gray, H. B. *Journal of the American Chemical Society* **1971**, *93*, 5254.
19. Couderc-Azouani, S.; Sidhu, J.; Georgiou, T. K.; Charalambous, D. C.; Vamvakaki, M.; Patrickios, C. S.; Bloor, D. M.; Penfold, J.; Holzwarth, J. F.; Wyn-Jones, E. *Langmuir* **2004**, *20*, 6458.
20. Sedlak, M.; Konak, C.; Stepanek, P.; Jakes, J. *Polymer* **1990**, *31*, 253.
21. Förster, S.; Schmidt, M.; Antonietti, M. *Polymer* **1990**, *31*, 781.
22. Aseyev, V. O.; Tenhu, H.; Winnik, F. M. *Advances in Polymer Science* **2006**, *196*, (Conformation-Dependent Design of Sequences in Copolymers II), 1.
23. Guo, X.; Ballauff, M. *Physical Review E: Statistical, Nonlinear, and Soft Matter Physics* **2001**, *64*, 051406/1.
24. Mafe, S.; Garcia-Morales, V.; Ramirez, P. *Chemical Physics* **2004**, *296*, 29.
25. Jaskari, T.; Vuorio, M.; Kontturi, K.; Manzanares, J. A.; Hirvonen, J. *Journal of Controlled Release* **2001**, *70*, 219.

## Glossary

$a$	activity	$g$	autocorrelation function
$A_2$	second virial coefficient	$G$	free enthalpy
AFFF	asymmetric field-flow fractionation	GPC	gel permeation chromatography
AFM	atom force microscopy	$H$	enthalpy
AIBN	azobisisobutyronitrile	HMTETA	1,1,4,7,10,10-hexamethyltriethylene-tetraamine
ATRP	atom transfer radical polymerization	$[\eta]$	intrinsic viscosity
$\alpha$	Kuhn-Mark-Houwink coefficient, degree of neutralization, polarizability	$\eta_{\text{red}}, \eta_{\text{sp}}$	reduced, specific viscosity
$\alpha'$	degree of dissociation	$\theta$	theta temperature, scattering angle
$b$	distance between charges	$I$	ionic strength, intensity
$c$	concentration	IAA	indolylacrylic acid
$\gamma$	charge compensation by multivalent counterions	$k$	Boltzmann constant
$\Gamma$	decay rate	$K$	Kuhn-Mark-Houwink-coefficient, equilibrium constant
$D$	diffusion coefficient	$l_b$	Bjerrum length
DLS	dynamic light scattering	$L_c$	contour length
DMAEMA	<i>N,N</i> -dimethylaminoethyl methacrylate	LCST	lower critical solution temperature
$DP_{(\text{arm})}$	degree of polymerization (per arm)	$\lambda$	wavelength
$DP_{\text{eff}}$	effective degree of polymerization	$m$	mass
DT	degenerative transfer	MALDI	matrix assisted laser desorption/ionization
$e$	elemental charge	MALS	multi angle light scattering
EBIB	ethyl- $\alpha$ -bromoisobutyrate	MeOH	methanol
$\varepsilon$	dielectricity constant, interaction energy	min	minute
$\zeta_M$	Manning's parameter	$M_n / M_w$	number-average / weight average molecular weight
$f$	activity coefficient	MS	mass spectrometry
$F$	Faraday constant, free energy	$\mu$	chemical potential
$f_i$	initiation site efficiency	$n$	molar concentration, refractive index
$f_{\text{star}}$	arm number	$N_A$	Avogadro's number
(FT-) IR	(Fourier-transform) infrared	NaOH	sodium hydroxide

NMP	nitroxide mediated polymerization	s	singlet
		$S$	entropy
NMR	nuclear magnetic resonance	SLS	static light scattering
$N_{st}$	number of stars	$S(\theta)$	structure factor
$n_x$	concentration	$\sigma_{LJ}$	monomer radius
$\xi_M$	Manning parameter	$\varsigma$	local charge density
$p$	pressure, probability	$t$	time
$\Pi$	osmotic pressure	tBA	<i>tert</i> -butyl acrylate
p.a.	pro analysis	$T_{cl}$	cloud point
PAA	poly(acrylic acid)	TEM	transmission electron microscopy
$PDI$	polydispersity	THF	tetrahydrofuran
PDMAEMA	poly( <i>N,N</i> -dimethylaminoethyl methacrylate)	ToF	time-of-flight
PMA	poly(methyl acrylate)	$\tau$	lag time, decay time
PMAA	poly(methacrylic acid)	$U$	electrostatic energy, voltage
PMETAI	poly{[2-(methacryloyloxy)ethyl] trimethylammonium iodide}	UCST	upper critical solution temperature
PMDETA	<i>N,N,N',N',N''</i> -pentamethyl-diethylentriamin	UV	ultraviolet light
PMMA	poly(methyl methacrylate)	$\nu$	Flory parameter of excluded volume
PNIPAAm	poly( <i>N</i> -isopropyl acrylamide)	$\phi$	osmotic coefficient
PtBA	poly( <i>tert</i> -butylacrylat)	$\Phi$	Flory-Fox parameter
$P(\theta)$	form factor	$\varphi$	volume fraction
$q$	charge, length of the scattering vector	$V$	volume
$Q$	charge	$V_e$	elution volume
$\rho$	number density, structure sensitive parameter	$V_h$	hydrodynamic volume
$R$	gas constant, radius	$w$	weight fraction
RAFT	reversible addition-fragmentation chain transfer	$x$	molar fraction, length
$R_g$	radius of gyration	$x_p$	conversion
$R_h$	hydrodynamic radius	$\chi$	Flory Huggins interaction parameter
RI	refractive index	$\psi$	electrostatic potential, coefficient for temperature dependence of $\chi$
$R(\theta)$	Raleigh ratio	$z$	number of charges
RT	room temperature	$z_M$	average distance to charged monomers
$R_w$	radius of the Wigner-Seitz cell	$[\ ]$	concentration

## Acknowledgement

I would like to thank all people, who have contributed to this thesis. I owe my special gratitude to Prof. Axel H. E. Müller and Prof. Matthias Ballauff, who gave me the opportunity to work on a very interesting topic. I'm especially grateful to Prof. Müller, who took always his time for fruitful discussions and guidance. I really appreciate that this was also the case even when he was very busy. His patience is outstanding and this contributed very much to a very nice working atmosphere. Without this atmosphere making my Ph.D. work would have been much harder. I thank him also for the many corrections during the reviewing of my manuscripts. He had the courage to submit to *Nano Letters*.

I also want to thank Prof. Ballauff for the nice collaboration. He gave the initiation of this Ph.D. project. I'm especially grateful for his encouragement. He gave the incentive to work on multivalent counterions. At the same time I'm really thankful to all people of his department of Physikalische Chemie I (PCI). They were really helpful during all the measurements performed in PCI. I thank especially Arben Jusufi for many discussions about the comparison of theory/simulation and experiment. I'm also grateful towards Sabine Rosenfeldt, Mushtaq Patel, Björn Haupt and Sreenath Bolisetty. They invested a lot of time during the X-ray scattering experiments.

I surely do not want to forget all the people in the department Macromolekulare Chemie II (MCII). Holger Schmalz, Andreas Walther, Markus Burkhardt, Anja Goldmann, Saikat Mandal, Youyong Xu, Jiayin Yuan, Pierre Millard, Stefan Reinicke, Alexander Schmalz, Felix Schacher, Manuela Schumacher, Evis Penott-Chang, Jeannine Rockser, Karina Möller, Xavier André, Denise Dantz, Sabine Wunder, Cornelia Rettig, Harald Becker, Günther Jutz, Annette Krökel, Gaby Cantea, Chih-Cheng Peng, Gaby Rösner-Oliver and many more helped me in many small and big things even though I was sometimes reluctant in helping them. Special thanks to Markus Ruppel, Sergey Nosov and Girish Behera for the lab 797 connection. For financial support I do appreciate the funding of both Deutsche Forschungsgemeinschaft (DFG) within Sonderforschungsbereich 481 (SFB 481) and Fonds der Chemischen Industrie (FCI). I am very grateful for their generous support, which provided conditions to concentrate on the research.

I owe thousand thanks to my beloved family. Without the loving and encouraging care of my wife Carolin, this thesis would have been almost impossible to master. Carolin's and Milena's patience provided precious time to perform this work. I surely do not want to forget the encouragement of my parents and my parents in law. I am thankful that they always supported me in many different ways. At the same time I thank all of my friends for their support. They acquiesced, when time was sometimes scarce.

Finally I want to thank my God and Saviour. He is the real reason. Without Him, this thesis would never have become true. I thank him for teaching me confidence. He does not disappoint even during hard times.



---

## **Erklärung**

Die vorliegende Arbeit wurde von mir selbstständig verfasst und ich habe dabei keine anderen als die angegebenen Hilfsmittel und Quellen benutzt.

Ferner habe ich nicht versucht, anderweitig mit oder ohne Erfolg eine Dissertation einzureichen oder mich der Doktorprüfung zu unterziehen.

Bayreuth, den 11.07.2007

Felix Plamper